

SCALABLE NESTED OPTIMIZATION FOR DEEP LEARNING

by

Jonathan Peter Lorraine

A thesis submitted in conformity with the requirements
for the degree of Doctor of Philosophy

Department of Computer Science
University of Toronto

Scalable Nested Optimization for Deep Learning

Jonathan Peter Lorraine

Doctor of Philosophy

Department of Computer Science

University of Toronto

2023

Abstract

Gradient-based optimization has been critical to the success of machine learning, updating a single set of parameters to minimize a single loss. A growing number of applications rely on a generalization of this, where we have a bilevel or nested optimization of which subsets of parameters update on different objectives nested inside each other. We focus on motivating examples of hyperparameter optimization and generative adversarial networks. However, naïvely applying classical methods often fails when we look at solving these nested problems on a large scale. In this thesis, we build tools for nested optimization that scale to deep learning setups.

- In Chapter 2, we provide an explicit, differentiable approximation to how neural network weights best-respond – or optimize – for their loss. We train a hypernetwork that takes in hyperparameters and outputs neural network weights. We use this hypernetwork for hyperparameter optimization.
- In Chapter 3, we explore an algorithm that implicitly approximates the neural network weights best-response, using the implicit function theorem. We apply this to hyperparameter optimization, showing we can tune as many hyperparameters as neural network weights.
- In Chapter 4, we augment simultaneous gradient descent to mitigate rotational dynamics. We do this by generalizing gradient descent with momentum to have a complex-valued momentum while retaining real-valued parameter updates.
- In Chapter 5, we generalize strategies for finding diverse solutions in single-objective optimization to finding diverse solutions in setups where multiple agents optimize for their own objective. We do this by taking the Ridge-rider algorithm and generalizing their branching criteria to occur at bifurcations using connections to Lyapunov exponents.

Acknowledgements

I extend my deepest gratitude to my advisor, David, whose influence has been nothing short of transformative. My experience under your mentorship has been educational and a source of personal growth, making my Ph.D. a wonderful journey. The environment you cultivated was rich with engaging research, unwavering support, and kindness. You taught me how to be a researcher, maintain high standards, communicate effectively, and everything else. I will greatly miss brainstorming ideas on your whiteboard. I am sincerely thankful for your impact on my life and career, and I aspire to provide similar guidance and support to others, just as you have done for me.

A big thank you to Roger Grosse and Nisarg Shah, the members of my supervisory committee, for their guidance and support throughout this journey. Your advice and wisdom have profoundly shaped my research and broader academic perspective. Roger, thank you for your exceptional detail-oriented approach, patience, and wide-ranging insights you made through our collaborations. I also want to thank my external reviewers, Zico Kolter and Murat Erdogdu for their efforts in this process.

I had the great privilege of working with various mentors during my internships. Jakob Foerster, thank you for supporting my first internship and showing me how to approach complex problems in a way that I will carry to my future endeavors. Mehadi Hassen, thank you for helping build the foundations of my engineering skills to carry out research in production. A special thanks to James Lucas for not only fulfilling but greatly surpassing the role of a mentor. Your job advice, strategic guidance on research agendas, and friendship have been a cornerstone of my success.

I am immensely grateful to all my coauthors for the opportunity to work with brilliant, insightful, and enjoyable colleagues. My sincere thanks to Paul Vicol for our many fruitful collaborations. I also want to give a big thanks to my other co-authors: David Acuna, Kevin Xie, Xiaohui Zeng, George Adam, Matthew MacKay, Safwan Hossain, Jack Parker-Holder, Aldo Pacchiano, Luke Metz, Tal Kachman, Aniruddh Raghu, Simon Kornblith, Matthew McDermott, Jack Richter-Powell, Brandon Amos, Fabian Pedregosa, Nihesh Anderson, Chansoo Lee, Quentin De Laroussilhe, Chen-Hsuan Lin, Towaki Takikawa, Nicholas Sharp, Tsung-Yi Lin, Ming-Yu Liu, Derek Lim, Haggai Maron, Marc Law, Michael Zhang, Nishkrit Desai, Juhan Bae, Jimmy Ba, Wu Lin, Nikhil Mehta, Steve Masson, Ramanathan Arunchalam, Zaid Pervaiz Bhat, Arun George Zakhariah, and Dmitry Krass.

I extend my gratitude to the pivotal institutions in my PhD journey. The University of Toronto, The Vector Institute, Facebook, Google, and NVIDIA - each has provided support, resources, and opportunities that have greatly enriched my academic experience. In addition, a special thanks to the Toronto AI Lab for creating an exceptional environment. I extend my heartfelt appreciation to Sanja Fidler for her pivotal role in organizing and leading this vibrant community.

Mom and Dad, you have been the bedrock of my success, consistently promoting the value of education and providing an environment where learning and curiosity could flourish. Your sacrifices, guidance, and encouragement have been the driving forces behind my achievements. To my mother, thank you for your endless patience, nurturing spirit, and the confidence you instilled in me. To my father, thank you for your wisdom, resilience, and the invaluable life lessons that have shaped my character. You both have ensured my success and taught me the importance of perseverance and curiosity. I am forever grateful for everything you have done and continue to do.

To all of my other wonderful friends in Toronto, I cannot express enough gratitude for the support and joy you brought to my life during my PhD journey. Thank you for being the anchor that kept me sane amid the whirlwind of academia. Your presence has been a constant reminder of the world beyond research. Thank you to Moeen, Hashir, Marius, Jack, Mousa, Aly, Jaideep, Andy, Carson, Ewan, Shoaib, Calypso, Peter, Dan, Gareth, Luis, Samuel, Tahsin, and Mahrukh.

Alex, you were with me on my very first day of university, and I deeply wish you could have seen this journey to its end. The void that you left is irreplaceable. Thank you, Alex, for the shared moments; I will always cherish our memories.

Contents

1	Introduction	1
1.1	Thesis Outline	2
1.2	Summary of Publications	3
1.2.1	Research Used in Thesis	3
1.2.2	Non-thesis Research	4
2	Hyperparameter Optimization Through Hypernetworks	6
2.1	Introduction	6
2.2	Training a network to output optimal weights	8
2.2.1	Advantages of hypernetwork-based optimization	9
2.2.2	Limitations of hypernetwork-based optimization	9
2.2.3	Jointly training parameters and hyperparameters	11
2.3	Related Work	12
2.4	Experiments	13
2.4.1	Learning a global best-response	13
2.4.2	Learning a local best-response	13
2.4.3	Hyper-training and unrolled optimization	13
2.4.4	Optimizing with deeper networks	14
2.4.5	Estimating weights versus estimating loss	15
2.5	Conclusions and Future Work	15
3	Optimizing Millions of Hyperparameters by Implicit Differentiation	17
3.1	Introduction	17
3.2	Overview of Proposed Algorithm	19
3.2.1	Proposed Algorithms	21
3.3	Related Work	21
3.4	Method	23
3.4.1	Hyperparameter Optimization is Pure-Response	23
3.4.2	The Relationship Between Unrolled Optimization and the IFT	24
3.4.3	Scope and Limitations	25
3.5	Experiments	25
3.5.1	Approximate Inversion Algorithms	25
3.5.2	Overfitting a Small Validation Set	27
3.5.3	Dataset Distillation	27

3.5.4	Learned Data Augmentation	28
3.5.5	RNN Hyperparameter Optimization	28
3.5.6	Effects of Many Hyperparameters	30
3.6	Conclusion	31
4	Complex Momentum for Optimization in Games	33
4.1	Introduction	33
4.2	Background	35
4.2.1	Game Formulations	35
4.2.2	Limitations of Existing Methods	36
4.2.3	Coming up with our Method	37
4.3	Complex Momentum	37
4.3.1	Dynamics of Complex Momentum	38
4.3.2	What about Acceleration?	41
4.3.3	Implementing Complex Momentum	42
4.3.4	Scope and Limitations	42
4.4	Experiments	42
4.4.1	Optimization in Purely Adversarial Games	42
4.4.2	Adversarialnesses Effect on Convergence	43
4.4.3	Training GANs on 2D Distributions	45
4.4.4	Training BigGAN with a Complex Adam	45
4.4.5	A Practical Initial Guess for the Momentum’s Argument	46
4.5	Related Work	46
4.6	Conclusion	47
5	Lyapunov Exponents for Diversity in Differentiable Games	49
5.1	Introduction	49
5.2	Background	51
5.2.1	Ridge Rider (RR)	51
5.2.2	Optimization in Games	51
5.3	Methods for Generalizing RR	52
5.3.1	Connecting Diversity and Bifurcations	52
5.3.2	Lyapunov Exponents for Bifurcations	53
5.4	Proposed Algorithms	54
5.4.1	Branching Optimization Tree Searches	55
5.4.2	Generalized Ridge Rider (GRR)	57
5.4.3	Comparing GRR and RR	58
5.5	Experimental Setting	58
5.6	Experimental Results	60
5.6.1	Diagnostic Experiments	60
5.6.2	Scaling the Results	61
5.7	Conclusion	64

6	Discussion and Concluding Remarks	65
6.1	Summary of Chapters	65
6.2	Limitations and Future Directions	66
6.2.1	Hyperparameter Optimization Through Hypernetworks	66
6.2.2	Optimizing Millions of Hyperparameters by Implicit Differentiation	66
6.2.3	Complex Momentum for Optimization in Games	67
6.2.4	Lyapunov Exponents for Diversity in Differentiable Games	67
A	Optimizing Millions of Hyperparameters by Implicit Differentiation	69
A.1	Extended Background	69
A.2	Extended Related Work	70
A.3	Implicit Function Theorem	72
A.4	Proofs	72
A.5	Experiments	74
A.5.1	Overfitting a Small Validation Set	74
A.5.2	Dataset Distillation	74
A.5.3	Learned Data Augmentation	75
A.5.4	RNN Hyperparameter Optimization	75
B	Complex Momentum for Optimization in Games	77
B.1	Supporting Results	77
B.1.1	Theorem 3 Proof Sketch	79
B.1.2	Characterizing the Augmented Dynamics Eigenvalues	80
B.1.3	Convergence Bounds	81
B.2	Algorithms	83
B.2.1	Complex Momentum in PyTorch	84
B.3	Experiments	85
B.3.1	Computing Infrastructure and Runtime	85
B.3.2	Optimization in Purely Adversarial Games	85
B.3.3	Adversarialnesses Effect on Convergence	85
B.3.4	Training GANs on 2D Distributions	85
C	Lyapunov Exponents for Diversity in Differentiable Games	92
C.1	Related Work	92
C.2	Proposed Algorithms	95
C.2.1	Branching Optimization Tree Searches	95
C.3	Experiments	95
C.3.1	Test Problems	95

List of Figures

2.1	Compute graph for hyperparameter optimization with hypernetworks	7
2.2	Hypernetwork validation loss visualization	7
2.3	Inner and outer loss approximation visualization	8
2.4	Trained hypernetwork on locally sampled hyperparameters	11
2.5	Hypernetwork optimization curves	12
2.6	Validation loss approximation distributions	14
3.1	Gradient-based hyperparameter optimization overview	18
3.2	Hypergradient computation overview	20
3.3	Neumann matrix inverse approximations quantitative comparison	26
3.4	Inverse Hessian approximation visualizations	26
3.5	Overfitting CIFAR-10 with many hyperparameters	27
3.6	Distilled datasets for CIFAR-10, MNIST, and CIFAR-100	28
3.7	Learned data augmentations	29
3.8	Overfitting hyperparameters on LSTMs	30
3.9	Validation split sizes and overfitting capacity visualization	32
4.1	Complex momentum in Jax	35
4.2	The complex buffers dependence on gradient history	39
4.3	Heatmap of convergence rate over optimizer parameters for complex momentum	39
4.4	Complex momentum on a Dirac GAN	41
4.5	Complex momentum bilinear convergence rates	43
4.6	Complex momentum convergence in eigenspaces	44
4.7	Log-polar eigenspace visualization for GANs	48
5.1	Lyapunov exponent visualization	53
5.2	Phase portrait of common methods on the IPD	55
5.3	Visualization of branching optimization tree search	56
5.4	Branching at different bifurcation types	56
5.5	Gradient descent on the 1-step maximum Lyapunov exponent	59
5.6	Optimization of a maximum 10-step Lyapunov exponent	61
5.7	Lyapunov exponent heatmap on toy problems	62
A.1	Overfitting validation data	75
A.2	The complete dataset distillation for CIFAR-100	76

B.1	Compute graphs for momentum variants	83
B.2	Spectrum of the augmented learning dynamics for complex momentum	86
B.3	Dirac GAN convergence rates for optimizer parameters	86
B.4	GAN eigenvalue spectrum during training	87
B.5	BigGAN heatmaps of performance with complex momentum	88
B.6	Learned mixture of Gaussians samples	88
B.7	Class-conditional BigGAN samples	89
B.8	BigGAN grid search results	89
B.9	BigGAN inception scores during training	90
C.1	Phase portrait for standard methods on various problems	96
C.2	Different direction estimation strategies in 10-step Lyapunov exponent calculation	97
C.3	Visualizing Lyapunov exponent calculations for various step numbers	97
C.4	Contrasting Lyapunov exponent calculations between LOLA and simSGD	98
C.5	Visualizing the impact of optimization algorithm parameters on the Lyapunov exponent	99
C.6	Using Lyapunov exponents on single objective optimization problems	100
C.7	Lyapunov exponent of the logistic map	100
C.8	Lyapunov exponents and Lyapunov entropy visualization	101
C.9	Ground truth samples for our mixture of Gaussians	102
C.10	Lyapunov exponent heatmaps on various toy problems	102
C.11	Comparing optimization for various numbers of Lyapunov exponents	103
C.12	Comparing optimization for different Lyapunov exponent losses	104
C.13	Optimization with multi-step Lyapunov exponents	105

List of Tables

3.1	Overviewing methods to approximate hypergradients	22
3.2	Gradient based hyperparameter optimization cost comparison	22
3.3	Accuracy of different inverse approximations	29
3.4	Comparing hyperparameter optimization methods for LSTM training	31
4.1	BigGAN inception scores with complex momentum	46
5.1	Comparing strategies for finding diverse solutions to the iterated prisoner’s dilemma	63
5.2	Comparing HVP evaluations required to reach various accuracies	63
5.3	Quantitative results for Lyapunov exponent calculation on GANs	64
A.1	Notation For Optimizing Millions of Hyperparameters by Implicit Differentiation . .	71
B.1	Notation for Complex Momentum for Optimization in Games	91
C.1	Notation for Lyapunov Exponents for Diversity in Differentiable Games	93

List of Algorithms

1	Standard cross-validation with stochastic optimization	10
2	Optimization of hypernetwork, then hyperparameters	10
3	Joint optimization of hypernetwork and hyperparameters	10
4	Gradient-based hyperparameter optimization for $\lambda^*, \mathbf{w}^*(\lambda^*)$	21
5	Hypergradient computation	21
6	Neumann approximation of vector-inverse-Hessian product	21
7	Simultaneous update complex momentum	38
8	Complex Adam variant without momentum bias-correction	45
9	Aggregated momentum	83
10	Recurrently linked momentum	84
11	Complex momentum	84
12	Complex momentum with only real values	84
13	Branching optimization tree search	95

Chapter 1

Introduction

Motivating single-objective optimization in machine learning: In recent years, machine learning has emerged as a transformative force in numerous scientific and industrial domains, profoundly impacting everything from computer-vision, to natural language processing, to personalized medicine. Large neural networks have become a foundational workhorse for using machine learning to advance these fields. Central to this revolution has been the advancement of gradient-based optimization techniques, which have effectively trained increasingly large and complex neural network architectures. However, the traditional focus on optimizing a single set of parameters for a singular objective increasingly gives way to more nuanced paradigms.

Motivating the generalized nested optimization paradigm in machine learning: A growing number of applications require learning with subsets of parameters updating on different objectives. Important examples are hyperparameter optimization (Maclaurin et al., 2015a; Andrychowicz et al., 2016; Fu et al., 2016; Shaban et al., 2019), GANs (Goodfellow et al., 2014), actor-critic models (Pfau and Vinyals, 2016), curriculum learning (Baker et al., 2019; Balduzzi et al., 2019; Sukhbaatar et al., 2018), adversarial examples (Bose et al., 2020; Yuan et al., 2019), learning models (Rajeswaran et al., 2020; Abachi et al., 2020; Nikishin et al., 2021), domain adversarial adaptation (Acuna et al., 2021), neural architecture search (Elsken et al., 2019), and meta-learning (Finn et al., 2017; Ren et al., 2018a, 2020). This thesis focuses on motivating examples of hyperparameter optimization and GANs. Furthermore, we will call a setup with more than one objective a *game*, call optimization here *learning in games*, and each subset of parameters with their respective losses will be called a *player*.

Introducing nested optimization more formally: Consider 2-player games¹—with players denoted by A and B —where each player minimizes their loss $\mathcal{L}_A, \mathcal{L}_B$ with their parameters θ_A, θ_B . We work with setups where the objectives are nested inside of each other – so-called Stackelberg games or bilevel optimization (Von Stackelberg, 1952) – whose solutions can be defined as:

$$\begin{aligned}\theta_A^* &= \underset{\theta_A}{\operatorname{argmin}} \mathcal{L}_A(\theta_A, \theta_B^*(\theta_A)), \\ \theta_B^*(\theta_A) &= \underset{\theta_B}{\operatorname{argmin}} \mathcal{L}_B(\theta_A, \theta_B)\end{aligned}\tag{1.1}$$

¹See our non-thesis research in Raghu et al. (2020) for an example with more players.

Here, $\theta_B^*(\theta_A)$ denotes player B 's best-response function, which says how their optimal parameters change as a function of the other players' parameters. In general, the inner and outer optimization can have multiple solutions – see [Vicol et al. \(2022a\)](#) – giving rise to a best-response set instead of a function. However, for most of the thesis, we focus on the setup with unique solutions, except in Chapter 5, where we look at methods to find multiple valid solutions.

Existing nested optimization approaches and their limitations: The overarching goal of this thesis is to efficiently find solutions (θ_A^*, θ_B^*) when our parameters θ_A and θ_B are approaching the size of modern neural network parameters. We may be able to approximately find θ_A^* efficiently if we can do gradient-based optimization on:

$$\mathcal{L}_A^*(\theta_A) = \mathcal{L}_A(\theta_A, \theta_B^*(\theta_A)) \quad (1.2)$$

Optimizing this objective would require computing the *hypergradient* $\frac{\partial \mathcal{L}_A^*}{\partial \theta_A}$:

$$\underbrace{\frac{\partial \mathcal{L}_A^*(\theta_A)}{\partial \theta_A}}_{\text{hypergradient}} = \left(\frac{\partial \mathcal{L}_A}{\partial \theta_A} + \frac{\partial \mathcal{L}_A}{\partial \theta_B} \frac{\partial \theta_B^*}{\partial \theta_A} \right) \Big|_{\theta_A, \theta_B^*(\theta_A)} = \underbrace{\frac{\partial \mathcal{L}_A(\theta_A, \theta_B^*(\theta_A))}{\partial \theta_A}}_{\text{direct gradient}} + \underbrace{\frac{\partial \mathcal{L}_A(\theta_A, \theta_B^*(\theta_A))}{\partial \theta_B^*(\theta_A)}}_{\text{indirect gradient}} \times \underbrace{\frac{\partial \theta_B^*(\theta_A)}{\partial \theta_A}}_{\text{best-response Jacobian}} \quad (1.3)$$

Unfortunately, this often requires $\frac{\partial \theta_B^*}{\partial \theta_A}$, but $\theta_B^*(\theta_A)$ and its Jacobian are typically intractable, as they require exact evaluation and differentiation through optimization. An alternative strategy is simultaneous/alternating gradient descent, where each player does gradient descent on their own objectives – $\frac{\partial \mathcal{L}_A}{\partial \theta_A}$ and $\frac{\partial \mathcal{L}_B}{\partial \theta_B}$ respectively. However, strategies like this can fail. For example, because a gradient is identically zero as in hyperparameter optimization or because of rotational dynamics ([Berard et al., 2019](#)) as in GANs. Black-box methods like random-search or Bayesian Optimization ([Moćkus, 1975](#); [Snoek et al., 2012](#)) circumvent gradient calculations but are ineffective for high-dimensional problems – e.g., greater than 100 dimensions. Specifically, we want the ability to optimize high-dimensional problems prevalent in machine learning.

1.1 Thesis Outline

In the Chapters 2 and 3, we explore approximations for the best-response $\theta_B^*(\theta_A)$ and its Jacobian $\frac{\partial \theta_B^*}{\partial \theta_A}$, which are applied to hyperparameter optimization. In Chapter 4, we instead look at augmenting the gradient dynamics to avoid rotational dynamics, without approximating $\frac{\partial \theta_B^*}{\partial \theta_A}$, which is applied to GANs. Finally, we look at generalizing a branching single-objective optimization algorithm that finds multiple solutions to set-ups with multiple objectives.

- In Chapter 2, we explicitly approximate the best-response function $\theta_B^*(\theta_A)$ with a hypernetwork which we differentiate through for optimization. Our method collapses the nested optimization of model weights and hyperparameters into a joint stochastic optimization. We do this via amortized optimization with hypernetworks, which output approximately optimal weights as a function of hyperparameters. We compare this with standard hyperparameter optimization and demonstrate its use in tuning hundreds to thousands of hyperparameters.

- In Chapter 3 we approximate the best-response Jacobian $\frac{\partial \theta_B^*}{\partial \theta_A}$ using the implicit function theorem (IFT), which we then use for optimization. We propose an inexpensive gradient-based hyperparameter optimization algorithm that combines the IFT with efficient inverse Hessian approximations. We present results on the relationship between IFT and differentiation through optimization, which motivates our algorithm. We use the proposed approach to train modern network architectures with millions of weights and *millions of hyperparameters*. We learn a data-augmentation network—where every weight is a hyperparameter tuned for validation performance—that outputs augmented training examples; we learn a distilled dataset where every feature in each data point is a hyperparameter; and we tune millions of regularization hyperparameters. Jointly tuning weights and hyperparameters with our approach is only a few times more costly in memory and compute than standard training.
- In Chapter 4, we augment simultaneous gradient descent to mitigate the rotational dynamics. We generalize gradient descent with momentum for optimization in differentiable games to have complex-valued momentum. We give theoretical motivation for our method by proving convergence on bilinear zero-sum games for simultaneous and alternating updates. Our method gives real-valued parameter updates, making it a drop-in replacement for standard optimizers. We empirically demonstrate that complex-valued momentum can improve convergence in realistic adversarial games—like generative adversarial networks—by showing that we find better solutions with an almost identical computational cost. We also show a practical complex-valued Adam variant, which we use to train BigGAN to improve inception scores on CIFAR-10.
- Ridge Rider (RR) is an algorithm to find diverse solutions in optimization problems by following eigenvectors of the Hessian (“ridges”). RR is designed for conservative gradient systems (i.e., settings involving a single loss function), where it branches at saddles — easy-to-find bifurcation points. In Chapter 5, we generalize this idea to nonconservative dynamics from gradient optimization on multiple objectives by proposing a method – denoted Generalized Ridge Rider (GRR) – for finding arbitrary bifurcation points. We give theoretical motivation for our method by leveraging machinery from the field of dynamical systems. We construct novel toy problems where we visualize new phenomena while giving insight into high-dimensional problems of interest. Finally, we evaluate our method by finding diverse solutions to the iterated prisoners’ dilemma and relevant machine learning problems, including generative adversarial networks.

1.2 Summary of Publications

1.2.1 Research Used in Thesis

The contents of Chapter 2 consist of research ideas and results taken from:

Lorraine, Jonathan, and David Duvenaud. “Stochastic hyperparameter optimization through hypernetworks” 31st Conference on Neural Information Processing Systems (NIPS 2017), Workshop on Meta-learning. Long Beach, USA. 2017.

The contents of Chapter 3 consist of research ideas and results taken from:

Lorraine, Jonathan, Paul Vicol, and David Duvenaud. “Optimizing millions of hyperparameters by implicit differentiation.” International Conference on Artificial Intelligence and Statistics (AISTATS). PMLR, 2020.

The contents of Chapter 4 consist of research ideas and results taken from:

Lorraine, Jonathan, David Acuna, Paul Vicol, and David Duvenaud. “Complex momentum for optimization in games.” In International Conference on Artificial Intelligence and Statistics (AISTATS). PMLR, 2022.

The contents of Chapter 5 consist of research ideas and results taken from:

Lorraine, Jonathan, Paul Vicol, Jack Parker-Holder, Tal Kachman, Luke Metz, and Jakob Foerster. “Lyapunov Exponents for Diversity in Differentiable Games.” In Proceedings of the 21st International Conference on Autonomous Agents and Multiagent Systems (AAMAS). 2022.

1.2.2 Non-thesis Research

Publications I have worked during my Ph.D. and are excluded from this thesis include [Mehta et al. \(2024a,b\)](#); [Bae et al. \(2024\)](#); [Xie et al. \(2024\)](#); [Lim et al. \(2024, 2023\)](#); [Zhang et al. \(2023a,b\)](#); [Lorraine et al. \(2023a,b, 2022a\)](#); [Vicol et al. \(2022a,b, 2021\)](#); [Richter-Powell et al. \(2021\)](#); [Raghu et al. \(2021a,b\)](#); [Lorraine and Hossain \(2019\)](#); [MacKay et al. \(2019a,b\)](#); [Adam and Lorraine \(2019\)](#).

Mehta, Nikhil, Jonathan Lorraine, Steve Masson, Ramanathan Arunachalam, Zaid Pervaiz Bhat, James Lucas, Arun George Zachariah. “Improving Hyperparameter Optimization with Checkpointed Model Weights.” In Submission to Advances in Neural Information Processing Systems (NeurIPS), 2024.

Bae, Juhan, Wu Lin, Jonathan Lorraine, Roger Grosse. “Training Data Attribution via Approximate Unrolled Differentiation.” In Submission to Advances in Neural Information Processing Systems (NeurIPS), 2024.

Xie, Kevin, Jonathan Lorraine, Tianshi Cao, Jun Gao, James Lucas, Antonio Torralba, Sanja Fidler, Xiaohui Zeng. “LATTE3D: Large-scale Amortized Text-To-Enhanced3D Synthesis.” In Submission to The European Conference on Computer Vision (ECCV), 2024.

Lim, Derek, Haggai Maron, Marc T. Law, Jonathan Lorraine, and James Lucas. “Graph Metanetworks for Processing Diverse Neural Architectures.” The International Conference on Learning Representations (ICLR), 2024.

Zhang, Michael, Nishkrit Desai, Juhan Bae, Jonathan Lorraine, and Jimmy Ba. “Using Large Language Models for Hyperparameter Optimization.” Advances in Neural Information Processing Systems (NeurIPS), 2023 Foundation Models for Decision Making Workshop.

Lorraine, Jonathan, Kevin Xie, Xiaohui Zeng, Chen-Hsuan Lin, Towaki Takikawa, Nicholas Sharp, Tsung-Yi Lin, Ming-Yu Liu, Sanja Fidler, and James Lucas. “ATT3D: Amortized Text-to-3D Object Synthesis.” In Proceedings of the International Conference on Computer Vision (ICCV), 2023.

Lorraine, Jonathan, Nihesh Anderson, Chansoo Lee, Quentin De Laroussilhe, and Mehadi Hassen. “Task Selection for AutoML System Evaluation.” arXiv:2208.12754 (2022).

Vicol, Paul, Jonathan Lorraine, Fabian Pedregosa, David Duvenaud, and Roger B. Grosse. “On Implicit Bias in Overparameterized Bilevel Optimization.” In International Conference on Machine Learning (ICML), pp. 22234-22259. PMLR, 2022.

Richter-Powell, Jack, Jonathan Lorraine, and Brandon Amos. “Input Convex Gradient Networks.” Advances in Neural Information Processing Systems (NeurIPS) Optimal Transport and Machine Learning (OTML) Workshop, November 2021.

Raghu, Aniruddh, Jonathan Lorraine, Simon Kornblith, Matthew McDermott, and David K. Duvenaud. “Meta-Learning to Improve Pre-Training.” Advances in Neural Information Processing Systems 34 (NeurIPS) 2021: 23231-23244.

Lorraine, Jonathan, and Safwan Hossain. “JacNet: Learning Functions with Structured Jacobians.” In International Conference on Machine Learning Invertible (ICML), 2019 Neural Nets and Normalizing Flows (INNF) Workshop.

Mackay, Matthew, Paul Vicol, Jonathan Lorraine, David Duvenaud, and Roger Grosse. “Self-Tuning Networks: Bilevel Optimization of Hyperparameters using Structured Best-Response Functions.” In International Conference on Learning Representations (ICLR). 2018.

Adam, George, and Jonathan Lorraine. “Understanding Neural Architecture Search Techniques.” arXiv:1904.00438 (2019).

Chapter 2

Hyperparameter Optimization Through Hypernetworks

Machine learning models often nest optimization of model weights within the optimization of hyperparameters. We give a method to collapse this nested optimization into joint stochastic optimization of weights and hyperparameters. We train a neural (hyper)network to output optimized weights as a function of hyperparameters. We compare this method to standard hyperparameter optimization methods and demonstrate its effectiveness in tuning thousands of hyperparameters.

Context for this Work

This was my first paper, guided to a workshop submission and then a technical report by David. All material in this chapter comes from [Lorraine and Duvenaud \(2017\)](#). We had a follow-up paper, Self-Tuning Networks ([MacKay et al., 2019a](#)), led by Matthew MacKay and Paul Vicol, which improves many aspects of this work. There, we build more scalable hypernetwork architectures, a better parameterization of the distribution of hyperparameters for training the hypernetwork, tuning hyperparameters of larger-scale networks in varying modalities, a wide variety of hyperparameters are optimized, and we demonstrate practical benefits from the method. Further improvements are in the follow-up of Δ -STN ([Bae and Grosse, 2020](#)).

2.1 Introduction

Model selection and hyperparameter tuning are significant bottlenecks in the design of predictive models. Hyperparameter optimization is a nested optimization, which can be viewed as a special case of Equation 1.1. Here, the inner optimization finds the neural network’s weights \mathbf{w} that minimize the training loss \mathcal{L}_T given hyperparameters $\boldsymbol{\lambda}$. The outer optimization chooses $\boldsymbol{\lambda}$ to reduce the validation loss with the best-responding weights \mathcal{L}_V^* :

$$\boldsymbol{\lambda}^* = \underset{\boldsymbol{\lambda}}{\operatorname{argmin}} \mathcal{L}_V^*(\boldsymbol{\lambda}) \text{ where} \tag{2.1}$$

$$\mathcal{L}_V^*(\boldsymbol{\lambda}) = \mathcal{L}_V(\boldsymbol{\lambda}, \mathbf{w}^*(\boldsymbol{\lambda})) \text{ and } \mathbf{w}^*(\boldsymbol{\lambda}) = \underset{\mathbf{w}}{\operatorname{argmin}} \mathcal{L}_T(\boldsymbol{\lambda}, \mathbf{w}) \tag{2.2}$$

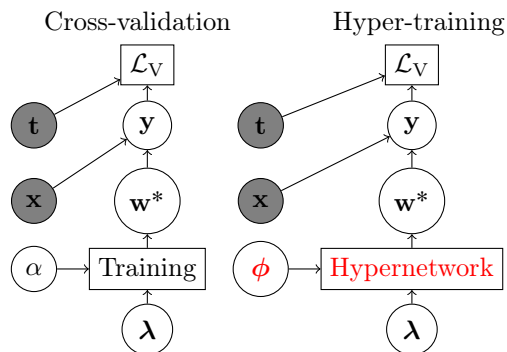


Figure 2.1: *Left*: A typical computational graph for cross-validation, where α are the optimizer parameters, and λ are training loss hyperparameters. It is expensive to differentiate throughout the training procedure. *Right*: The proposed computational graph with our changes in red, where ϕ are the hypernetwork parameters. We can differentiate cheaply through the hypernetwork to optimize the validation loss \mathcal{L}_V with respect to hyperparameters λ . We use x , t , and y to refer to a data point, a label, and a prediction.

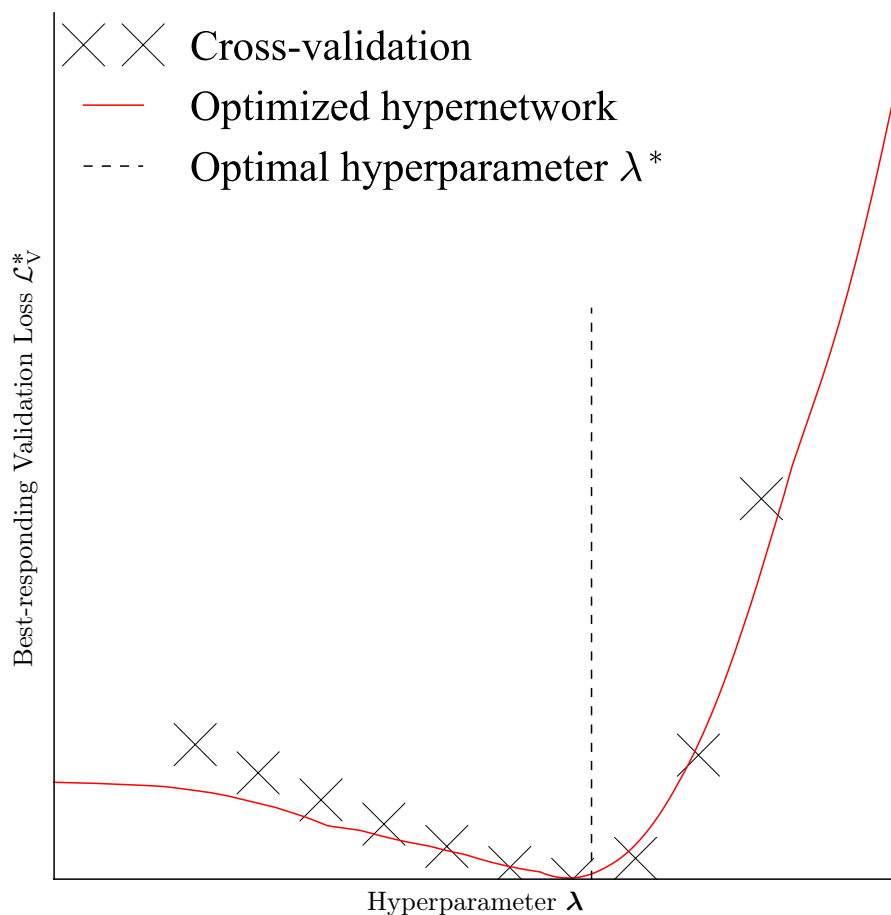


Figure 2.2: The validation loss of a neural net is estimated by cross-validation (crosses) or a hypernetwork (line), which outputs 7850-dimensional network weights. Cross-validation requires optimizing from scratch each time. The hypernetwork can be used as a proxy to cheaply evaluate the best-responding validation loss \mathcal{L}_V^* .

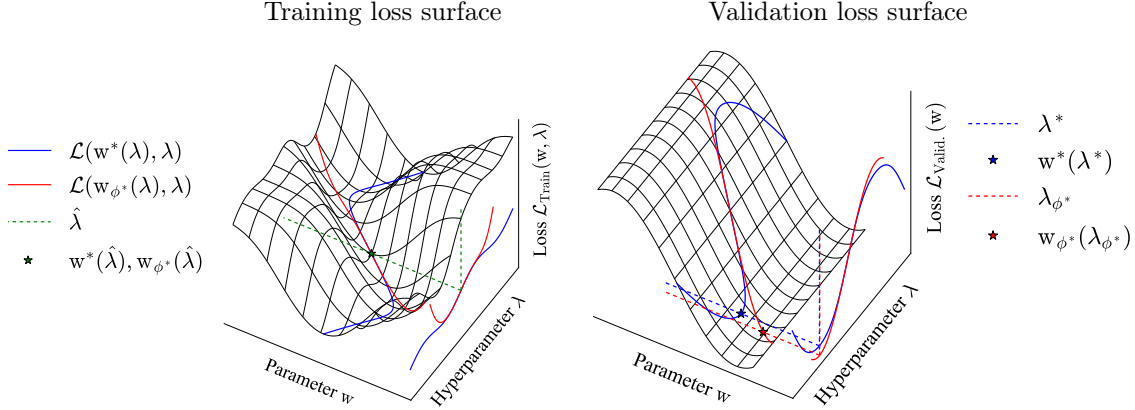


Figure 2.3: A visualization of exact (blue) and approximate (red) optimal weights as a function of hyperparameters. The approximately optimal weights \mathbf{w}_{ϕ^*} are produced by a linear model fit at $\hat{\lambda}$. The true optimal hyperparameter is λ^* , while the hyperparameter minimizing the hypernetwork-approximated validation loss is λ_{ϕ^*} .

Standard practice in machine learning solves Equation 2.1 by gradient-free optimization of hyperparameters, such as grid or random search. Each set of hyperparameters is evaluated by reinitializing the weights and training the model to completion. Retraining a model from scratch is wasteful if the hyperparameters change by a small amount. Some approaches, such as Hyperband (Li et al., 2016) and freeze-thaw Bayesian optimization (Swersky et al., 2014), resume model training but often scale poorly beyond 10 to 20 dimensions. How can we avoid retraining from scratch each time? Well, the optimal parameters \mathbf{w} are a function of the hyperparameters λ :

$$\mathbf{w}^*(\lambda) = \underset{\mathbf{w}}{\operatorname{argmin}} \mathcal{L}_{\text{T}}(\mathbf{w}, \lambda) \quad (2.3)$$

We propose to *learn this function*.¹ Specifically, we train a neural network that takes hyperparameters as input and outputs an approximately optimal set of weights. This formulation provides two main benefits. First, we can train the hypernetwork to convergence using stochastic gradient descent without training any particular model to completion. Second, differentiating through the hypernetwork allows us to optimize hyperparameters with stochastic gradient-based optimization.

2.2 Training a network to output optimal weights

Given some hyperparameters, how can we teach a hypernetwork (Ha et al., 2016) to produce approximately optimal weights for another neural network? At each iteration, we ask a hypernetwork with parameters ϕ to input hyperparameters λ and to output a set of weights: $\mathbf{w}_{\phi}(\lambda)$. Instead of updating the weights \mathbf{w} using the training loss gradient $\partial \mathcal{L}_{\text{T}}(\mathbf{w}) / \partial \mathbf{w}$, we update the hypernetwork weights ϕ using the chain rule: $\frac{\partial \mathcal{L}_{\text{T}}(\mathbf{w}_{\phi})}{\partial \mathbf{w}_{\phi}} \frac{\partial \mathbf{w}_{\phi}}{\partial \phi}$. At convergence, we want our hypernetwork to match the best-response function closely: $\mathbf{w}_{\phi}(\lambda) \approx \mathbf{w}^*(\lambda)$. This formulation allows us to optimize the hyperparameters λ using our hypernetwork-learned function as a surrogate best-response. We call this method *hyper-training* and contrast it with standard training methods.

¹This notation implies \mathbf{w} has a unique solution, which is used for simplicity but is not generally true. See Vicol et al. (2022a) for an investigation of the consequences of this in hyperparameter optimization.

Our method is related to the concurrent work of [Brock et al. \(2017\)](#), whose SMASH algorithm also approximates optimal weights as a function of model architectures to perform a gradient-free search over discrete model structures. They only estimate the performance of various model architectures while we additionally compute gradients for the hypernetwork input.

We further extend this idea by formulating an algorithm to jointly optimize the hypernetwork and hyperparameters. Joint optimization of parameters and hyperparameters addresses one of SMASH’s main weaknesses: the hypernetwork must be very large to learn approximately optimal weights for many different settings. During joint optimization, the hypernetwork only needs to model approximately optimal weights for the neighborhood around the current hyperparameters, allowing us to use even linear hypernetworks.

2.2.1 Advantages of hypernetwork-based optimization

Hyper-training is a method to learn a mapping from hyperparameters to validation loss that is differentiable and inexpensive to evaluate. Alternatively, model-based hyperparameter schemes, like Bayesian optimization (e.g., [Snoek et al. \(2012\)](#)) build a model of the validation loss as a function of hyperparameters. This approach has several disadvantages compared to hyper-training.

First, obtaining data for standard Bayesian optimization requires optimizing models from initialization for each set of hyperparameters. In contrast, hyper-training never needs to optimize any one model fully, removing choices like how many models to train and for how long. Second, standard Bayesian optimization treats the best-responding validation loss as a black-box function. In contrast, hyper-training takes advantage of the fact that validation loss is a known, differentiable function, which can be evaluated stochastically by sampling points from the validation set. This can have a better generalization for learning hyperparameter to validation loss than directly fitting the loss using a Gaussian process (e.g., [Rasmussen and Williams \(2006\)](#)), as in [Figure 2.6](#).

2.2.2 Limitations of hypernetwork-based optimization

We apply this method to unconstrained continuous bilevel optimization problems with a differentiable inner and outer loss function. But what kind of parameters can be optimized by our approach? Hyperparameters typically fall into two broad categories: (1) parameters that change the set of locally optimal points, like regularization parameters or architectural choices, and (2) parameters that affect the choice of locally optimal point and the rate we converge to them, like optimization hyperparameters such as learning rates. Hyper-training does not have inner optimization parameters because there is no internal training loop, so we cannot optimize these. We must still choose the optimization parameters for the fused optimization loop. In principle, hyper-training can handle continuous relaxations of discrete hyperparameters, which we further explore in non-thesis research of [MacKay et al. \(2019a\)](#).

A clear difficulty of this approach is that hypernetworks can require several times as many parameters as the original model. For example, training a fully connected hypernetwork with 1 hidden layer of H units to output D parameters requires at least $D \times H$ hypernetwork parameters. To partially address this problem, in [Section 2.2.3](#), we propose an algorithm that trains only a linear model that maps hyperparameters to model weights. We further explore better alternatives in non-thesis research of [MacKay et al. \(2019a\)](#).

Another limitation is that our approach only proposes making local changes to the hyperparameters and does not do global optimization or uncertainty-based exploration. Finally, choosing the training distribution of hyperparameters $p(\boldsymbol{\lambda})$ is not obvious. If we do not sample a sufficient range of hyperparameters, the estimated gradient of the validation loss with respect to the hyperparameters may be inaccurate. We discuss several approaches to this problem in Section 2.2.3, and further explore this in non-thesis research of MacKay et al. (2019a).

Algorithm 1 Standard cross-validation with stochastic optimization

```

1: for  $i = 1, \dots, T_{\text{outer}}$  do
2:   Initialize elementary parameters  $\mathbf{w}$ 
3:    $\boldsymbol{\lambda} = \text{hyperopt} \left( \boldsymbol{\lambda}^{(1:i)}, \mathcal{L}_V \left( \boldsymbol{\lambda}^{(1:i)}, \mathbf{w}^{(1:i)} \right) \right)$ 
4:   while  $T_{\text{inner}}$  steps do
5:      $\mathbf{x} \sim \text{Training data}$ 
6:      $\mathbf{w} -= \alpha \nabla_{\mathbf{w}} \mathcal{L}_T(\boldsymbol{\lambda}, \mathbf{w}, \mathbf{x})$ 
7:   end while
8:    $\boldsymbol{\lambda}^i, \mathbf{w}^i = \boldsymbol{\lambda}, \mathbf{w}$ 
9: end for
10:  $i = \underset{i}{\operatorname{argmin}} \mathcal{L}_V \left( \boldsymbol{\lambda}^{(i)}, \mathbf{w}^{(i)}, \mathbf{x} \right)$ 
11: return  $\boldsymbol{\lambda}^{(i)}, \mathbf{w}^{(i)}$ , potentially re-training  $\mathbf{w}$  with  $\boldsymbol{\lambda}^{(i)}$  on all data

```

Algorithm 2 Optimization of hypernetwork, then hyperparameters

```

1: Initialize hypernetwork  $\phi$ 
2: Initialize hyperparameters  $\hat{\boldsymbol{\lambda}}$ 
3: for  $T_{\text{hypernetwork}}$  steps do
4:    $\mathbf{x} \sim \text{Training data}, \boldsymbol{\lambda} \sim \mathbf{p}(\boldsymbol{\lambda})$ 
5:    $\phi -= \alpha \nabla_{\phi} \mathcal{L}_T(\boldsymbol{\lambda}, \mathbf{w}_{\phi}(\boldsymbol{\lambda}), \mathbf{x})$ 
6: end for
7: for  $T_{\text{hyperparameter}}$  steps do
8:    $\mathbf{x} \sim \text{Validation data}$ 
9:    $\hat{\boldsymbol{\lambda}} -= \beta \nabla_{\hat{\boldsymbol{\lambda}}} \mathcal{L}_V \left( \hat{\boldsymbol{\lambda}}, \mathbf{w}_{\phi}(\hat{\boldsymbol{\lambda}}), \mathbf{x} \right)$ 
10: end for
11: return  $\hat{\boldsymbol{\lambda}}, \mathbf{w}_{\phi}(\hat{\boldsymbol{\lambda}})$ 

```

Algorithm 3 Joint optimization of hypernetwork and hyperparameters

```

1: Initialize hypernetwork  $\phi$ 
2: Initialize hyperparameters  $\hat{\boldsymbol{\lambda}}$ 
3: loop
4:    $\mathbf{x} \sim \text{Training data}, \boldsymbol{\lambda} \sim p(\boldsymbol{\lambda} | \hat{\boldsymbol{\lambda}})$ 
5:    $\phi -= \alpha \nabla_{\phi} \mathcal{L}_T(\boldsymbol{\lambda}, \mathbf{w}_{\phi}(\boldsymbol{\lambda}), \mathbf{x})$ 
6:    $\mathbf{x} \sim \text{Validation data}$ 
7:    $\hat{\boldsymbol{\lambda}} -= \beta \nabla_{\hat{\boldsymbol{\lambda}}} \mathcal{L}_V \left( \hat{\boldsymbol{\lambda}}, \mathbf{w}_{\phi}(\hat{\boldsymbol{\lambda}}), \mathbf{x} \right)$ 
8: end loop
9: return  $\hat{\boldsymbol{\lambda}}, \mathbf{w}_{\phi}(\hat{\boldsymbol{\lambda}})$ 

```

In Algorithms 1, 2, and 3, we compare standard hyperparameter optimization, our global algorithm, and our joint algorithm, respectively. Here, hyperopt refers to a generic hyperparameter optimization, and we abuse notation, making the loss dependence on sampled data \mathbf{x} explicit. Notably, instead of updating the weights \mathbf{w} using the loss gradient $\nabla_{\mathbf{w}}\mathcal{L}$, we update the hypernetwork ϕ and hyperparameters λ , which we use for gradient-based hyperparameter optimization.

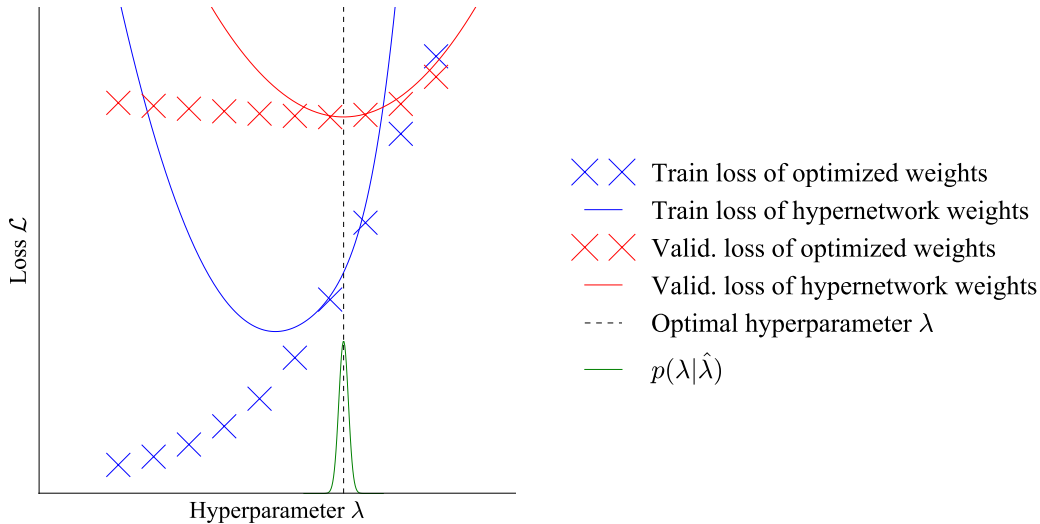


Figure 2.4: Training and validation losses of a neural network are estimated by cross-validation (crosses) or a linear hypernetwork (lines). The hypernetwork’s limited capacity makes it only accurate where the hyperparameter distribution puts mass.

2.2.3 Jointly training parameters and hyperparameters

In practice, we should choose a distribution of hyperparameters for training the hypernet $p(\lambda)$ that places most of its mass on promising hyperparameter values. It may not be possible to learn a best-response for all hyperparameters due to limited hypernetwork capacity. Thus, we propose Algorithm 3, which only tries to match a best-response locally. We introduce a “current” hyperparameter $\hat{\lambda}$, updated each iteration. We define a conditional hyperparameter distribution, $p(\lambda|\hat{\lambda})$, which only puts the mass close to $\hat{\lambda}$.

Algorithm 3 combines both phases of Algorithm 2. Instead of training a hypernetwork to output weights for any hyperparameter and then optimizing the hyperparameters, Algorithm 3 only samples hyperparameters near the current $\hat{\lambda}$. So, the hypernetwork only needs to estimate weights for a concentrated set of hyperparameters. There is an extra cost to retrain the hypernetwork on each hyperparameter $\hat{\lambda}$ update. The locally trained hypernetwork is used for gradients to update $\hat{\lambda}$.

How simple can we make the hypernetwork and still obtain useful gradients to optimize hyperparameters? Consider the case in our experiments where the hypernetwork is a linear function of the hyperparameters and the conditional hyperparameter distribution is $p(\lambda|\hat{\lambda}) = \mathcal{N}(\hat{\lambda}, \sigma I)$ for some small σ . This hypernetwork learns a tangent hyperplane to a best-response function and only needs minor adjustments at each step if the hyperparameter updates are small. We can further restrict the capacity of a linear hypernetwork by factorizing its weights, effectively adding a bottleneck layer with a linear activation and a small number of hidden units.

2.3 Related Work

Here, we briefly review the gradient-free and gradient-based methods we compare to in our experiments. Our work complements the SMASH algorithm of Brock et al. (2017), with Section 2.2 discussing our differences. We are both special cases of amortized optimization methods, which use learning to predict solutions when we repeatedly solve instances of the same problem (Amos, 2022). The idea of weight generation given a context vector has been used in multiple areas (Requeima et al., 2019; Ratzlaff and Fuxin, 2019; Pilault et al., 2020; Tay et al., 2020; Rusu et al., 2018).

Gradient-free Hyperparameter Optimization: Various gradient-free hyperparameter optimization methods – not scalable to this regime – are detailed in Appendix Section A.2. Model-free approaches use only trial and error to explore the hyperparameter space. Simple model-free approaches applied to hyperparameter optimization include grid and random search (Bergstra and Bengio, 2012), or more sophisticated methods like Hyperband (Li et al., 2016) combine bandit approaches with modeling the learning procedure. Model-based approaches build a surrogate function, like Bayesian optimization (Moćkus, 1975; Snoek et al., 2012), which we use as a baseline in our experiments, implemented by Snoek et al. (2019). Evolutionary methods (Alexandropoulos et al., 2019) are similar to our method, such as population-based training (Jaderberg et al., 2017), which maintains a set of networks instead of using a hypernetwork.

Gradient-based Hyperparameter Optimization: Notably, we compare to differentiating through optimization, which Domke (2012) proposes, Maclaurin et al. (2015a) scales to differentiating through learning procedures in deep learning, and is implemented by Franceschi et al. (2017). More gradient-based methods are discussed in Chapter 3, Section 3.3 where we compare with them.

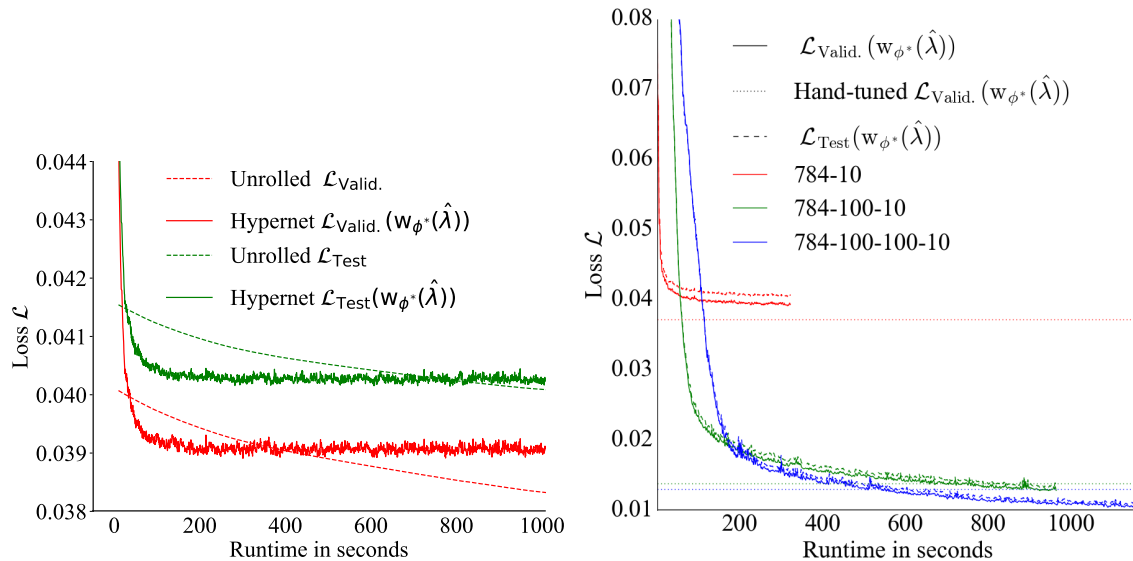


Figure 2.5: Validation and test losses during hyperparameter optimization with a separate ℓ_2 weight decay applied to each weight in the model. Thus, models with more parameters have more hyperparameters. *Left:* We solve the 7850-dimensional hyperparameter optimization problem with a linear network and multiple algorithms. Hypernetwork-based optimization converges to a suboptimal solution faster than unrolled optimization from Maclaurin et al. (2015a). *Right:* Hyper-training is applied to different layer configurations in the model.

2.4 Experiments

Our experiments examine the standard example of stochastic gradient-based optimization of neural networks with a weight regularization penalty. In all experiments, Algorithms 2 or 3 are used to optimize the weights on MNIST (LeCun et al., 1998) with a ℓ_2 weight decay penalty weighted by $\exp(\lambda)$. Unless otherwise specified, all hidden units in the hypernetwork have ReLU activation (Nair and Hinton, 2010). Autograd (Maclaurin et al., 2015b) was used to compute all derivatives. The mini-batch samples 2 sets of hyperparameters and up to 1000 training data points for each experiment. We use Adam (Kingma and Ba, 2014) to train the hypernetwork and hyperparameters with a step size of 0.0001, and $(\beta_1, \beta_2) = (.9, .999)$.

2.4.1 Learning a global best-response

Our first experiment, shown in Figure 2.2, demonstrates learning a global approximation to a best-response function using Algorithm 2. To simplify visualization of the regularization loss, we use 10 training data points to exacerbate overfitting. We compare the performance of the weights output by the hypernetwork with those trained by standard cross-validation (Algorithm 1). The elementary weights were randomly initialized for each hyperparameter choice. When training the hypernetwork, the hyperparameters were sampled from a broad Gaussian distribution: $p(\lambda) = \mathcal{N}(0, 1.5)$. The hypernetwork has 50 hidden units. **Takeaway:** The minimum of the best-response in Figure 2.2 is close to the real minimum of the validation loss, which shows that a hypernetwork can approximate a global best-response function in small problems.

2.4.2 Learning a local best-response

Figure 2.4 shows the same experiment as Figure 2.2, except using Algorithm 3. The fused updates result in finding a best-response approximation whose minimum is the actual minimum faster than in the prior experiment. The conditional hyperparameter distribution is given by $p(\lambda|\hat{\lambda}) = \mathcal{N}(\hat{\lambda}, 0.00001\mathbf{I})$. Here, the hypernetwork is a linear model. Again, the minimum of the best-response at the end of training minimizes the validation loss. **Takeaway:** Using only a locally trained linear best-response function can give sufficient gradient information to optimize hyperparameters while being less computationally expensive than learning a global best-response.

2.4.3 Hyper-training and unrolled optimization

We train models with a separate ℓ_2 weight decay applied to each weight in a one-layer model to compare hyper-training with other gradient-based hyperparameter optimization methods. The conditional hyperparameter distribution and optimizer for the hypernetwork and hyperparameters are the same as in the prior experiments. Here, we use a hypernetwork with 10 hidden units. Figure 2.5, top, shows that Algorithm 3 converges more quickly than the unrolled reverse-mode optimization implemented by Franceschi et al. (2017). Hyper-training overfits validation data less than unrolling but reaches sub-optimal solutions – perhaps because of limitations on how many hyperparameters can be sampled for each update. Standard Bayesian optimization cannot be scaled to this many hyperparameters. **Takeaway:** Algorithm 3 can efficiently partially optimize thousands of hyperparameters. But, unrolled optimization performed better asymptotically.

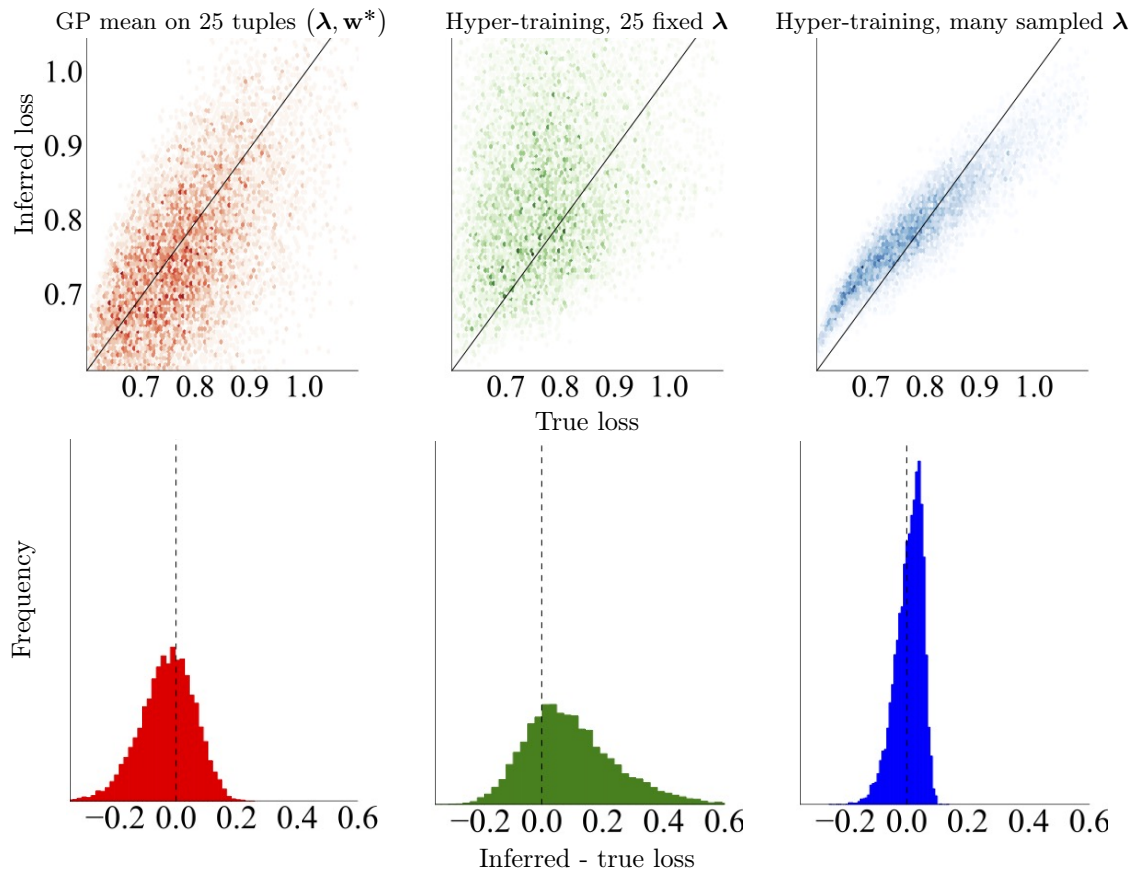


Figure 2.6: Comparing three approaches to inferring the best-responding validation loss. *First column: A Gaussian process*, fit to 25 hyperparameters, and the corresponding validation losses. *Second column: A hypernetwork that fits the same 25 hyperparameters* and the corresponding optimized weights. *Third column: Our proposed method, a hypernetwork trained with stochastically sampled hyperparameters*. *Top row: The distribution of inferred and true losses*. The diagonal black line is where the predicted loss equals the true loss. *Bottom row: The distribution of differences between inferred and true losses*. The Gaussian process more often under-predicts the true loss, while the hypernetwork trained on the same data tends to over-predict it. **Takeaway: Our method, in blue** has a distribution more concentrated around 0, showing that it estimates the best-responding validation loss most accurately, and this performance is from seeing many more different hyperparameters during optimization. In particular, **our method** uses the same amount of compute as training the 25 models used to fit the Gaussian process.

2.4.4 Optimizing with deeper networks

To see if we can optimize deeper networks with hyper-training, we optimize models with 1, 2, and 3 layers and a separate ℓ_2 weight decay applied to each weight. The conditional hyperparameter distribution and optimizer for the hypernetwork and hyperparameters are the same as in the prior experiment. Again, we select a hypernetwork with 10 hidden units. Figure 2.5, bottom, shows that Algorithm 3 can scale to networks with multiple hidden layers and outperform hand-tuned settings. Adding more layers improves model performance with lower training, validation, and test losses, indicating that using a separate weight decay on each weight could be useful for generalization. The follow-up work of MacKay et al. (2019a) compares other architectures, such as recurrent or convolutional networks, on various other hyperparameter choices.

2.4.5 Estimating weights versus estimating loss

Our approach differs from Bayesian optimization, which attempts to model the validation loss of optimized weights directly, where we try to learn to predict optimal weights. In this experiment, we begin to unravel the reason for the better performance of our method. Is it because of a better inductive bias or because our way can see more hyperparameter settings during optimization?

First, we constructed a hyper-training set: We optimized 25 sets of weights to completion, given randomly sampled hyperparameters. We chose 25 samples because that is the regime in which we expect Gaussian process-based approaches to have the largest advantage. We constructed an unseen set of 10 215 (optimized weight, hyperparameter) tuples generated similarly. **We then fit a Gaussian process (GP)** regression model with an RBF kernel from sklearn on the validation loss data. **A hypernetwork is fit to the same set of hyperparameters and data.** Finally, **we optimize another hypernetwork using Algorithm 2** for the same amount of time as building the GP training set. The two hypernetworks are linear models with the same optimizer parameters as prior experiments.

Figure 2.6 shows the distribution of prediction errors for these three models. The Gaussian process tends to underestimate the loss. The hypernetwork trained with the same small fixed set of examples tends to overestimate loss. We conjecture that this is due to the hypernetwork producing bad weights in regions without enough training data. Because the hypernetwork must provide actual weights to predict the validation loss, poorly fit regions can overestimate the loss \mathcal{L}_V^* . Finally, the hypernetwork trained with Algorithm 2 produces errors tightly centered around 0. **Takeaway:** A hypernetwork can learn more accurate surrogate functions than a GP for equal compute budgets because it views (noisy) evaluations of many more points.

2.5 Conclusions and Future Work

This chapter addressed the tuning of hyperparameters using gradient-based optimization by replacing the training optimization loop with a differentiable hypernetwork. We also presented a simple and more scalable method that jointly optimizes hyperparameters and hypernetwork weights, allowing our method to work with manageable-sized hypernetworks. Experimentally, we showed that hypernetworks could provide a better inductive bias for hyperparameter optimization than Gaussian processes that fit the validation loss. There are many ways to extend the proposed methods, with more examples in Section 6.2. For example, the hypernetwork could consist of several optimization iterations as an easily differentiated fine-tuning step. Hypernetworks could be incorporated into meta-learning schemes, such as MAML (Finn et al., 2017), which finds weights that perform various tasks after unrolling gradient descent. We also note that optimizing thousands of hyperparameters raises the question of *hyper-regularization*, or regularization of hyperparameters.

A key limitation of this work is that it does not scale to ultra-large hyperparameter regimes, where we have as many hyperparameters as neural network parameters for large networks. In the following chapter, we look at methods that scale to this regime.

Acknowledgments

We thank Matthew MacKay, Dougal Maclaurin, Daniel Flam-Shepard, Daniel Roy, and Jack Klys for helpful discussions.

My Contributions Towards this Paper As it Pertains to the Thesis

This was my first paper and was shepherded into a submission under the close guidance of David Duvenaud, for which I will forever be grateful. I proposed the idea while David helped code up initial versions of this in Autograd, which I fleshed out into our experiments. I also wrote most of the paper with much assistance from David. This paper has an updated arXiv version ([Lorraine and Duvenaud, 2018](#)) and an older workshop version ([Lorraine and Duvenaud, 2017](#)).

Chapter 3

Optimizing Millions of Hyperparameters by Implicit Differentiation

We propose an inexpensive, gradient-based hyperparameter optimization algorithm that combines the implicit function theorem (IFT) with efficient inverse Hessian approximations. We present results on the relationship between IFT and differentiation through optimization, motivating our algorithm. We use our approach to train modern network architectures with millions of weights and *millions of hyperparameters*. Specifically, we learn a data-augmentation network—where every weight is a hyperparameter tuned for validation performance—that outputs augmented training examples; we learn a distilled dataset where every feature in each data point is a hyperparameter; and we tune millions of regularization hyperparameters. Jointly tuning weights and hyperparameters with our approach is only a few times more costly in memory and compute than standard training.

3.1 Introduction

Neural network generalization to unseen data crucially depends on hyperparameter choice. Hyperparameter optimization (HO) has a rich history (Schmidhuber, 1987; Bengio, 2000), and has recently achieved successful scaling due to gradient-based optimizers (Domke, 2012; Maclaurin et al., 2015a; Franceschi et al., 2017, 2018; Shaban et al., 2019; Finn et al., 2017; Rajeswaran et al., 2019; Liu et al., 2018; Grefenstette et al., 2019; Mehra and Hamm, 2019). There are dozens of regularization techniques to combine in deep learning, and each may have multiple hyperparameters (Kukačka et al., 2017). If we can scale hyperparameter optimization to have as many—or more—hyperparameters as parameters, various exciting regularization strategies exist to investigate. For example, we could learn a distilled dataset with a hyperparameter for every feature of each input (Maclaurin et al., 2015a; Wang et al., 2018), weights on each loss term (Ren et al., 2018b; Kim and Choi, 2018; Zhang et al., 2019a), or augmentation on each input (Cubuk et al., 2018; Xie et al., 2019).

When the hyperparameters are low-dimensional—e.g., 1-5 dimensions—simple methods, like random search, work; however, these break down for medium-dimensional hyperparameter optimization—e.g., 5-100 dimensions. We may use more scalable algorithms like Bayesian optimization (Moćkus, 1975; Snoek et al., 2012; Kandasamy et al., 2019), but this often breaks down for high-dimensional hyperparameter optimization—e.g., >100 dimensions. Hypernetwork-based approaches, as in Chapter 2, scale further (~ 1000 dimensions), but break down when approaching the scale of modern neural networks. We can solve high-dimensional hyperparameter optimization problems locally with gradient-based optimizers, but this is difficult because we must differentiate through the optimized weights as a function of the hyperparameters. Formally, we must approximate the Jacobian of the best-response function of the parameters to the hyperparameters.

We leverage the Implicit Function Theorem (IFT) to compute the optimized validation loss gradient with respect to the hyperparameters, hereafter denoted the *hypergradient*. The IFT requires inverting the training Hessian for the neural network weights, which is infeasible for modern, deep networks. Thus, we propose an approximate inverse, motivated by a link to unrolled differentiation (Domke, 2012) that scales to Hessians of large neural networks, is more stable than conjugate gradient (Liao et al., 2018; Shaban et al., 2019), and only requires a constant amount of memory.

Finally, when fitting many parameters, the amount of data can limit generalization. There are *ad hoc* rules for partitioning data into training and validation sets—e.g., using 10% for validation. Practitioners often re-train their models from scratch on the combined training and validation partitions with optimized hyperparameters, which can provide marginal test-time performance increases. We verify empirically that standard partitioning and retraining procedures perform well when fitting a few hyperparameters but break down when fitting many. When fitting many hyperparameters, we may need a large validation partition, which makes retraining our model with optimized hyperparameters vital for strong test performance.

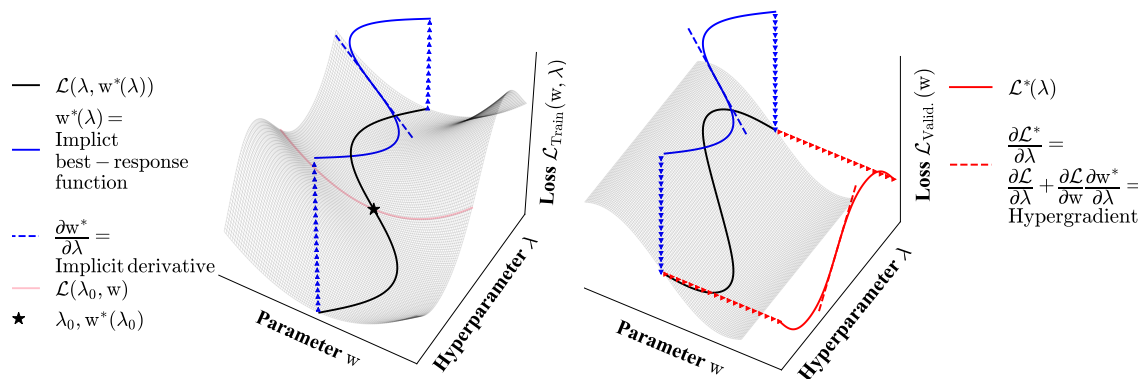


Figure 3.1: Overview of gradient-based hyperparameter optimization. *Left*: a training loss manifold; *Right*: a validation loss manifold. The implicit function $\mathbf{w}^*(\boldsymbol{\lambda})$ is the best-response of the weights to the hyperparameters and shown in blue projected onto the $(\boldsymbol{\lambda}, \mathbf{w})$ -plane. We obtain our desired objective function $\mathcal{L}_V^*(\boldsymbol{\lambda})$ when the best-response gives the network weights in the validation loss, shown projected on the hyperparameter axis in red. The validation loss does not depend directly on the hyperparameters, as is typical in hyperparameter optimization. Instead, the hyperparameters only affect the validation loss by changing the weights’ response. We show the best-response Jacobian in blue and the hypergradient in red.

Contributions

- We motivate existing inverse Hessian approximation algorithms by connecting them to iterative optimization algorithms.
- We scale IFT-based hyperparameter optimization to large neural architectures, including AlexNet and LSTM-based language models.
- We demonstrate several uses for fitting hyperparameters almost as easily as weights, including per-parameter regularization, data distillation, and learned data augmentation methods.
- We explore how training-validation splits should change when tuning many hyperparameters.

3.2 Overview of Proposed Algorithm

There are four essential components to understanding our proposed algorithm. Further background is provided in Appendix A.1, and the notation is shown in Table A.1.

1. Hyperparameter optimization is nested optimization: \mathcal{L}_T and \mathcal{L}_V denote the training and validation losses, \mathbf{w} the neural network weights, and $\boldsymbol{\lambda}$ the hyperparameters. We aim to find optimal hyperparameters $\boldsymbol{\lambda}^*$ such that the neural network minimizes the validation loss after training:

$$\boldsymbol{\lambda}^* = \underset{\boldsymbol{\lambda}}{\operatorname{argmin}} \mathcal{L}_V^*(\boldsymbol{\lambda}) \text{ where} \quad (3.1)$$

$$\mathcal{L}_V^*(\boldsymbol{\lambda}) = \mathcal{L}_V(\boldsymbol{\lambda}, \mathbf{w}^*(\boldsymbol{\lambda})) \text{ and } \mathbf{w}^*(\boldsymbol{\lambda}) = \underset{\mathbf{w}}{\operatorname{argmin}} \mathcal{L}_T(\boldsymbol{\lambda}, \mathbf{w}) \quad (3.2)$$

As in Chapter 2, our implicit function $\mathbf{w}^*(\boldsymbol{\lambda})$ is the *best-response* of the weights to the hyperparameters, and our desired objective is the best-responding validation loss \mathcal{L}_V^* in red. Again, for simplicity, we assume unique solutions to argmin , and refer to non-thesis research of Vicol et al. (2022a) for analysis in the non-unique setup.

2. Hypergradients have two terms: For gradient-based hyperparameter optimization we want the hypergradient $\frac{\partial \mathcal{L}_V^*(\boldsymbol{\lambda})}{\partial \boldsymbol{\lambda}}$, which decomposes into:

$$\underbrace{\frac{\partial \mathcal{L}_V^*(\boldsymbol{\lambda})}{\partial \boldsymbol{\lambda}}}_{\text{hypergradient}} = \left(\frac{\partial \mathcal{L}_V}{\partial \boldsymbol{\lambda}} + \frac{\partial \mathcal{L}_V}{\partial \mathbf{w}} \frac{\partial \mathbf{w}^*}{\partial \boldsymbol{\lambda}} \right) \Bigg|_{\boldsymbol{\lambda}, \mathbf{w}^*(\boldsymbol{\lambda})} = \underbrace{\frac{\partial \mathcal{L}_V(\boldsymbol{\lambda}, \mathbf{w}^*(\boldsymbol{\lambda}))}{\partial \boldsymbol{\lambda}}}_{\text{hyperparam direct grad.}} + \overbrace{\frac{\partial \mathcal{L}_V(\boldsymbol{\lambda}, \mathbf{w}^*(\boldsymbol{\lambda}))}{\partial \mathbf{w}^*(\boldsymbol{\lambda})} \times \frac{\partial \mathbf{w}^*(\boldsymbol{\lambda})}{\partial \boldsymbol{\lambda}}}_{\text{hyperparam indirect grad.}} \quad (3.3)$$

The **direct gradient** is easy to compute. However, the indirect gradient is difficult to compute because we must account for how the optimal weights change for the hyperparameters (i.e., $\frac{\partial \mathbf{w}^*(\boldsymbol{\lambda})}{\partial \boldsymbol{\lambda}}$). In hyperparameter optimization the **direct gradient** is often identically 0, necessitating an approximation of the indirect gradient to make any progress (visualized in Figure 3.1). In Chapter 4, we look at algorithms that do not require **response Jacobians** for setups where the **direct gradient** is non-zero.

$$\begin{aligned}
 \underbrace{\frac{\partial \mathcal{L}_V^*}{\partial \lambda}}_{\text{red}} &= \underbrace{\frac{\partial \mathcal{L}_V}{\partial \lambda}}_{\text{green}} + \underbrace{\frac{\partial \mathcal{L}_V}{\partial \mathbf{w}}}_{\text{white}} \underbrace{\frac{\partial \mathbf{w}^*}{\partial \lambda}}_{\text{blue}} \\
 &= \underbrace{\frac{\partial \mathcal{L}_V}{\partial \lambda}}_{\text{green}} + \underbrace{\frac{\partial \mathcal{L}_V}{\partial \mathbf{w}}}_{\text{white}} \underbrace{\left[-\left[\frac{\partial^2 \mathcal{L}_T}{\partial \mathbf{w} \partial \mathbf{w}^\top}\right]^{-1}\right]}_{\text{magenta}} \underbrace{\frac{\partial^2 \mathcal{L}_T}{\partial \mathbf{w} \partial \lambda^\top}}_{\text{white}} \\
 &= \underbrace{\frac{\partial \mathcal{L}_V}{\partial \lambda}}_{\text{green}} + \underbrace{\frac{\partial \mathcal{L}_V}{\partial \mathbf{w}} \times \left[-\left[\frac{\partial^2 \mathcal{L}_T}{\partial \mathbf{w} \partial \mathbf{w}^\top}\right]^{-1}\right]}_{\text{orange}} \underbrace{\frac{\partial^2 \mathcal{L}_T}{\partial \mathbf{w} \partial \lambda^\top}}_{\text{white}} \\
 &\hspace{10em} \text{vector-Jacobian product}
 \end{aligned}$$

Figure 3.2: We visualize the hypergradient computation, which can be performed efficiently using vector-Jacobian products if provided a cheap approximation to the **vector-inverse-Hessian product**.

3. We can estimate the implicit best-response with the IFT: We approximate the **best-response Jacobian**—how the optimal weights change with respect to the hyperparameters—using the IFT (Theorem 1). We present the complete statement in Appendix A.3, but highlight the key assumptions and results here.

Theorem 1 (Cauchy, Implicit Function Theorem). *If for some (λ', \mathbf{w}') , $\frac{\partial \mathcal{L}_T}{\partial \mathbf{w}} \Big|_{\lambda', \mathbf{w}'} = 0$ and regularity conditions are satisfied, then surrounding (λ', \mathbf{w}') there is a function $\mathbf{w}^*(\lambda)$ such that $\frac{\partial \mathcal{L}_T}{\partial \mathbf{w}} \Big|_{\lambda, \mathbf{w}^*(\lambda)} = 0$ and we have:*

$$\frac{\partial \mathbf{w}^*}{\partial \lambda} \Big|_{\lambda'} = - \underbrace{\left[\frac{\partial^2 \mathcal{L}_T}{\partial \mathbf{w} \partial \mathbf{w}^\top}\right]^{-1}}_{\text{training Hessian}} \times \underbrace{\frac{\partial^2 \mathcal{L}_T}{\partial \mathbf{w} \partial \lambda^\top}}_{\text{training mixed partials}} \Big|_{\lambda', \mathbf{w}^*(\lambda')} \quad (3.4)$$

The condition $\frac{\partial \mathcal{L}_T}{\partial \mathbf{w}} \Big|_{\lambda', \mathbf{w}'} = 0$ is equivalent to λ', \mathbf{w}' being a fixed point of the training gradient field. Since $\mathbf{w}^*(\lambda')$ is a fixed point of the training gradient field, we can leverage the IFT to evaluate the **best-response Jacobian** locally. We only have access to an approximation of the true best-response—denoted $\widehat{\mathbf{w}}^*$ —which we can find with gradient descent.

4. Tractable inverse Hessian approximations: To exactly invert a general $m \times m$ Hessian, we often require $\mathcal{O}(m^3)$ operations, which is intractable for the matrix in Equation 3.4 for modern neural networks. We can efficiently approximate the inverse with the Neumann series:

$$\left[\frac{\partial^2 \mathcal{L}_T}{\partial \mathbf{w} \partial \mathbf{w}^\top}\right]^{-1} = \lim_{i \rightarrow \infty} \alpha \sum_{j=0}^i \left[\mathbf{I} - \alpha \frac{\partial^2 \mathcal{L}_T}{\partial \mathbf{w} \partial \mathbf{w}^\top}\right]^j \quad (3.5)$$

In our exposition, we assume that $\alpha = 1$ for simplicity, but in practice, we reuse the learning rate for the inner optimization. In Section 3.4, we show that unrolling differentiation for i steps around locally optimal weights \mathbf{w}^* is equivalent to approximating the inverse with the first i terms in the Neumann series. We then show how to make this approximation without instantiating any matrices using efficient vector-Hessian products (Pearlmutter, 1994).

Algorithm 4 Gradient-based hyperparameter optimization for $\lambda^*, \mathbf{w}^* (\lambda^*)$

```

1: Initialize hyperparameters  $\lambda'$  and weights  $\mathbf{w}'$ 
2: while not converged do
3:   for  $k = 1 \dots N$  do
4:      $\mathbf{w}' \leftarrow \mathbf{w}' - \alpha \cdot \frac{\partial \mathcal{L}_T}{\partial \mathbf{w}} \Big|_{\lambda', \mathbf{w}'}$ 
5:   end for
6:    $\lambda' \leftarrow \text{hypergradient}(\mathcal{L}_V, \mathcal{L}_T, \lambda', \mathbf{w}')$ 
7: end while
8: return  $\lambda', \mathbf{w}'$ 

```

▷ $\lambda^*, \mathbf{w}^* (\lambda^*)$ from **Equation 3.1**

Algorithm 5 $\text{hypergradient}(\mathcal{L}_V, \mathcal{L}_T, \lambda', \mathbf{w}')$

```

1:  $\mathbf{v}_1 = \frac{\partial \mathcal{L}_V}{\partial \mathbf{w}} \Big|_{\lambda', \mathbf{w}'}$ 
2:  $\mathbf{v}_2 = \text{approxInverseHVP}(\mathbf{v}_1, \frac{\partial \mathcal{L}_T}{\partial \mathbf{w}})$ 
3:  $\mathbf{v}_3 = \text{grad}(\frac{\partial \mathcal{L}_T}{\partial \mathbf{w}}, \lambda, \text{grad\_outputs} = \mathbf{v}_2)$ 
4: return  $\frac{\partial \mathcal{L}_V}{\partial \lambda} \Big|_{\lambda', \mathbf{w}'} - \mathbf{v}_3$ 

```

▷ Return to **Algorithm 4**

Algorithm 6 $\text{approxInverseHVP}(\mathbf{v}, \mathbf{f})$: Neumann approximation of vector-inverse-Hessian $\mathbf{v} \left[\frac{\partial \mathbf{f}}{\partial \mathbf{w}} \right]^{-1}$

```

1: Initialize sum  $\mathbf{p} = \mathbf{v}$ 
2: for  $j = 1 \dots i$  do
3:    $\mathbf{v} \leftarrow \mathbf{v} - \alpha \cdot \text{grad}(\mathbf{f}, \mathbf{w}, \text{grad\_outputs} = \mathbf{v})$ 
4:    $\mathbf{p} \leftarrow \mathbf{p} + \mathbf{v}$ 
5: end for
6: return  $\alpha \mathbf{p}$ 

```

▷ Return to **Algorithm 5**.

3.2.1 Proposed Algorithms

We outline our method in Algorithms 4, 5, and 6, where α denotes the learning rate. Algorithm 6 is also shown in Liao et al. (2018) and is a special case of algorithms from Christianson (1998). We visualize the hypergradient computation in Figure 3.2.

3.3 Related Work

Implicit Function Theorem. The IFT has been used for optimization in nested optimization problems (Ochs et al., 2015; Wang et al., 2019a; Lee et al., 2019), backpropagating through arbitrarily long RNNs (Liao et al., 2018), k -fold cross-validation (Beirami et al., 2017), and influence functions (Koh and Liang, 2017). Early work applied the IFT to regularization by explicitly computing the Hessian (or Gauss-Newton) inverse (Larsen et al., 1996; Bengio, 2000). In Luketina et al. (2016), the identity matrix approximates the IFT’s inverse Hessian. HOAG (Pedregosa, 2016) uses conjugate gradient (CG) to approximately invert the Hessian and provides convergence results given tolerances on the optimal parameter and inverse. In iMAML (Rajeswaran et al., 2019), a center to the weights is fit to perform on multiple tasks, where we fit to perform on the validation loss. In DEQ (Bai et al., 2019), implicit differentiation is used to add differentiable fixed-point methods to neural network architectures. We use a Neumann approximation for the inverse Hessian instead of CG (Pedregosa, 2016; Rajeswaran et al., 2019) or the identity.

Method	Steps	Eval.	Hypergradient Approximation
Exact IFT	∞	$\mathbf{w}^*(\boldsymbol{\lambda})$	$\frac{\partial \mathcal{L}_V}{\partial \boldsymbol{\lambda}} - \frac{\partial \mathcal{L}_V}{\partial \mathbf{w}} \times \left[\frac{\partial^2 \mathcal{L}_T}{\partial \mathbf{w} \partial \mathbf{w}^\top} \right]^{-1} \frac{\partial^2 \mathcal{L}_T}{\partial \mathbf{w} \partial \boldsymbol{\lambda}^\top} \Big _{\mathbf{w}^*(\boldsymbol{\lambda})}$
Unrolled Diff.	i	\mathbf{w}_0	$\frac{\partial \mathcal{L}_V}{\partial \boldsymbol{\lambda}} - \frac{\partial \mathcal{L}_V}{\partial \mathbf{w}} \times \sum_{j \leq i} \left[\prod_{k < j} \mathbf{I} - \frac{\partial^2 \mathcal{L}_T}{\partial \mathbf{w} \partial \mathbf{w}^\top} \Big _{\mathbf{w}_{i-k}} \right] \frac{\partial^2 \mathcal{L}_T}{\partial \mathbf{w} \partial \boldsymbol{\lambda}^\top} \Big _{\mathbf{w}_{i-j}}$
L -Step Truncated Unrolled Diff.	i	\mathbf{w}_L	$\frac{\partial \mathcal{L}_V}{\partial \boldsymbol{\lambda}} - \frac{\partial \mathcal{L}_V}{\partial \mathbf{w}} \times \sum_{L \leq j \leq i} \left[\prod_{k < j} \mathbf{I} - \frac{\partial^2 \mathcal{L}_T}{\partial \mathbf{w} \partial \mathbf{w}^\top} \Big _{\mathbf{w}_{i-k}} \right] \frac{\partial^2 \mathcal{L}_T}{\partial \mathbf{w} \partial \boldsymbol{\lambda}^\top} \Big _{\mathbf{w}_{i-j}}$
Larsen et al. (1996)	∞	$\widehat{\mathbf{w}}^*(\boldsymbol{\lambda})$	$\frac{\partial \mathcal{L}_V}{\partial \boldsymbol{\lambda}} - \frac{\partial \mathcal{L}_V}{\partial \mathbf{w}} \times \left[\frac{\partial \mathcal{L}_T}{\partial \mathbf{w}} \frac{\partial \mathcal{L}_T}{\partial \mathbf{w}^\top} \right]^{-1} \frac{\partial^2 \mathcal{L}_T}{\partial \mathbf{w} \partial \boldsymbol{\lambda}^\top} \Big _{\widehat{\mathbf{w}}^*(\boldsymbol{\lambda})}$
Bengio (2000)	∞	$\widehat{\mathbf{w}}^*(\boldsymbol{\lambda})$	$\frac{\partial \mathcal{L}_V}{\partial \boldsymbol{\lambda}} - \frac{\partial \mathcal{L}_V}{\partial \mathbf{w}} \times \left[\frac{\partial^2 \mathcal{L}_T}{\partial \mathbf{w} \partial \mathbf{w}^\top} \right]^{-1} \frac{\partial^2 \mathcal{L}_T}{\partial \mathbf{w} \partial \boldsymbol{\lambda}^\top} \Big _{\widehat{\mathbf{w}}^*(\boldsymbol{\lambda})}$
$T_1 - T_2$	1	$\widehat{\mathbf{w}}^*(\boldsymbol{\lambda})$	$\frac{\partial \mathcal{L}_V}{\partial \boldsymbol{\lambda}} - \frac{\partial \mathcal{L}_V}{\partial \mathbf{w}} \times \left[\mathbf{I} \right]^{-1} \frac{\partial^2 \mathcal{L}_T}{\partial \mathbf{w} \partial \boldsymbol{\lambda}^\top} \Big _{\widehat{\mathbf{w}}^*(\boldsymbol{\lambda})}$
Ours	i	$\widehat{\mathbf{w}}^*(\boldsymbol{\lambda})$	$\frac{\partial \mathcal{L}_V}{\partial \boldsymbol{\lambda}} - \frac{\partial \mathcal{L}_V}{\partial \mathbf{w}} \times \left(\sum_{j \leq i} \left[\mathbf{I} - \frac{\partial^2 \mathcal{L}_T}{\partial \mathbf{w} \partial \mathbf{w}^\top} \right]^j \right) \frac{\partial^2 \mathcal{L}_T}{\partial \mathbf{w} \partial \boldsymbol{\lambda}^\top} \Big _{\widehat{\mathbf{w}}^*(\boldsymbol{\lambda})}$
Conjugate Gradient (CG) \approx	-	$\widehat{\mathbf{w}}^*(\boldsymbol{\lambda})$	$\frac{\partial \mathcal{L}_V}{\partial \boldsymbol{\lambda}} - \left(\underset{\mathbf{x}}{\operatorname{argmin}} \left\ \mathbf{x} \frac{\partial^2 \mathcal{L}_T}{\partial \mathbf{w} \partial \mathbf{w}^\top} - \frac{\partial \mathcal{L}_V}{\partial \mathbf{w}} \right\ \right) \frac{\partial^2 \mathcal{L}_T}{\partial \mathbf{w} \partial \boldsymbol{\lambda}^\top} \Big _{\widehat{\mathbf{w}}^*(\boldsymbol{\lambda})}$
Hypernetwork	-	-	$\frac{\partial \mathcal{L}_V}{\partial \boldsymbol{\lambda}} + \frac{\partial \mathcal{L}_V}{\partial \mathbf{w}} \times \frac{\partial \mathbf{w}_\phi^*}{\partial \boldsymbol{\lambda}}$ where $\mathbf{w}_\phi^*(\boldsymbol{\lambda}) = \underset{\phi}{\operatorname{argmin}} \mathcal{L}_T(\boldsymbol{\lambda}, \mathbf{w}_\phi(\boldsymbol{\lambda}))$
Bayesian Optimization	-	-	$\frac{\partial \mathbb{E}[\mathcal{L}_V^*]}{\partial \boldsymbol{\lambda}}$ where $\mathcal{L}_V^* \sim \text{Gaussian-Process}(\{\boldsymbol{\lambda}_i, \mathcal{L}_V(\boldsymbol{\lambda}_i, \mathbf{w}^*(\boldsymbol{\lambda}_i))\})$

Table 3.1: An overview of methods to approximate hypergradients. Some methods can be viewed as using an approximate inverse in the IFT or differentiating through optimization at an evaluation point. Here, $\widehat{\mathbf{w}}^*(\boldsymbol{\lambda})$ approximates the best-response at a fixed $\boldsymbol{\lambda}$, often found with gradient descent.

Method	Memory Cost
Differentiation through Optimization (Domke, 2012; Maclaurin et al., 2015a)	$\mathcal{O}(PI + H)$
Linear Hypernetwork (Lorraine and Duvenaud, 2017)	$\mathcal{O}(PH)$
Self-Tuning Nets (STN) (MacKay et al., 2019a)	$\mathcal{O}((P + H)K)$
Neumann/CG IFT	$\mathcal{O}(P + H)$

Table 3.2: Gradient-based methods for hyperparameter optimization. Differentiation through optimization scales with the number of unrolled iterations I ; the STN scales with bottleneck size K , while our method only scales with the weight and hyperparameter sizes P and H .

Approximate inversion algorithms. CG is difficult to scale to modern, deep neural networks. We use a Neumann inverse approximation, which is a more stable alternative to CG in neural networks (Liao et al., 2018; Shaban et al., 2019) and useful in stochastic settings (Agarwal et al., 2017). The stability is motivated by connections between the Neumann series and unrolled differentiation (Shaban et al., 2019). Alternatively, we could use prior knowledge about the neural network structure to aid in the inversion—e.g., as with KFAC (Martens and Grosse, 2015). Approximating the Hessian with the Gauss-Newton matrix or the Fisher information matrix (Larsen et al., 1996) is possible. Various works use an identity approximation to the inverse, which is equivalent to 1-step unrolled differentiation (Luketina et al., 2016; Ren et al., 2018b; Balaji et al., 2018; Liu et al., 2018; Finn et al., 2017; Shavitt and Segal, 2018; Nichol et al., 2018; Mescheder et al., 2017).

Unrolled differentiation for hyperparameter optimization. A key difficulty in nested optimization is approximating how the optimized inner parameters (i.e., neural network weights) change with respect to the outer parameters (i.e., hyperparameters). We often optimize the inner parameters with gradient descent so that we can differentiate through this optimization. Differentiation through optimization has been applied to nested optimization problems by Domke (2012), was scaled to hyperparameter optimization for neural networks by Maclaurin et al. (2015a), and has been applied to various applications, such as learning optimizers (Andrychowicz et al., 2016). Franceschi et al. (2018) provides convergence results for this class of algorithms, while Franceschi et al. (2017) discusses forward- and reverse-mode variants.

As the number of gradient steps we backpropagate through increases, so does the memory and computational cost. Often, gradient descent does not exactly minimize our objective after a finite number of steps, but only approaches a local minimum. Thus, we may have to unroll the optimization infeasibly far to see how the hyperparameters affect the local minima. Unrolling a small number of steps can be crucial for performance but may induce bias (Wu et al., 2018). Shaban et al. (2019) discusses connections between unrolling and the IFT and proposes to unroll only the last L -steps. DrMAD (Fu et al., 2016) proposes an interpolation scheme for the optimization to save memory.

We compare the hypergradient approximations in Table 3.1 and the memory costs of gradient-based hyperparameter optimization methods in Table 3.2. We survey gradient-free hyperparameter optimization in Appendix A.2.

3.4 Method

In this section, we discuss how hyperparameter optimization is a uniquely challenging nested optimization problem and how to combine the benefits of the IFT and unrolled differentiation.

3.4.1 Hyperparameter Optimization is Pure-Response

Equation 3.3 shows that the hypergradient decomposes into a *direct* and *indirect gradient*. The bottleneck in hypergradient computation is usually finding the indirect gradient because we must consider how the optimized parameters vary for the hyperparameters. A simple optimization approach is to neglect the indirect gradient and only use the *direct gradient*. This can be useful in zero-sum games like GANs (Goodfellow et al., 2014) because they always have a non-zero direct term.

However, using only the *direct gradient* does not work in general games (Balduzzi et al., 2018). In particular, it does not work for hyperparameter optimization because the *direct gradient* is identically 0 when the hyperparameters λ only influence the validation loss by changing the optimized weights $\mathbf{w}^*(\lambda)$. For example, if we use regularization like weight decay when computing the training loss but not the validation loss, then the *direct gradient* is always 0.

If the *direct gradient* is identically 0, we call the game *pure-response*. Pure-response games are difficult nested optimization problems for gradient-based methods because we cannot simply use the *direct gradient* like in simultaneous SGD. So, we must approximate the indirect gradient.

3.4.2 The Relationship Between Unrolled Optimization and the IFT

Here, we (a) introduce the recurrence relation that arises when we unroll SGD optimization, (b) give a formula for the derivative of the recurrence, and (c) establish conditions for the recurrence to converge. Notably, we show that the fixed points of the recurrence recover the IFT solution. We use these results to motivate a computationally tractable approximation scheme to the IFT solution. Proofs of all the results are in Appendix A.4. Unrolling SGD optimization at an initialization \mathbf{w}_0 gives us the recurrence:

$$\mathbf{w}_{i+1}(\boldsymbol{\lambda}) = \mathbf{F}(\boldsymbol{\lambda}, \mathbf{w}_i) = \mathbf{w}_i(\boldsymbol{\lambda}) - \alpha \frac{\partial \mathcal{L}_{\mathcal{T}}(\boldsymbol{\lambda}, \mathbf{w}_i(\boldsymbol{\lambda}))}{\partial \mathbf{w}} \quad (3.6)$$

We provide a formula for the derivative of the recurrence, to show that it converges to the IFT under some conditions.

Lemma. *Given the recurrence from unrolling SGD optimization in Equation 3.6, we have:*

$$\frac{\partial \mathbf{w}_{i+1}}{\partial \boldsymbol{\lambda}} = -\alpha \sum_{j \leq i} \left[\prod_{k < j} \mathbf{I} - \alpha \frac{\partial^2 \mathcal{L}_{\mathcal{T}}}{\partial \mathbf{w} \partial \mathbf{w}^{\top}} \Big|_{\boldsymbol{\lambda}, \mathbf{w}_{i-k}(\boldsymbol{\lambda})} \right] \frac{\partial^2 \mathcal{L}_{\mathcal{T}}}{\partial \mathbf{w} \partial \boldsymbol{\lambda}^{\top}} \Big|_{\boldsymbol{\lambda}, \mathbf{w}_{i-j}(\boldsymbol{\lambda})} \quad (3.7)$$

This recurrence converges to a fixed point if the Jacobian of the fixed-point operator $\frac{\partial \mathbf{F}}{\partial \mathbf{w}} = \mathbf{I} - \alpha \frac{\partial^2 \mathcal{L}_{\mathcal{T}}}{\partial \mathbf{w} \partial \mathbf{w}^{\top}}$ is contractive by the Banach Fixed-Point Theorem (Banach, 1922). Theorem 2 shows that the recurrence converges to the IFT if we start with locally optimal weights $\mathbf{w}_0 = \mathbf{w}^*(\boldsymbol{\lambda})$, and the Jacobian of the fixed-point operator $\frac{\partial \mathbf{F}}{\partial \mathbf{w}}$ is contractive. We leverage that if an operator U is contractive, then the Neumann series $\sum_{i=0}^{\infty} U^i = (\mathbf{I} - U)^{-1}$.

Theorem 2 (Neumann-SGD). *Given the recurrence from unrolling SGD optimization in Equation 3.6, if $\mathbf{w}_0 = \mathbf{w}^*(\boldsymbol{\lambda})$:*

$$\frac{\partial \mathbf{w}_{i+1}}{\partial \boldsymbol{\lambda}} = - \left(\alpha \sum_{j \leq i} \left[\mathbf{I} - \alpha \frac{\partial^2 \mathcal{L}_{\mathcal{T}}}{\partial \mathbf{w} \partial \mathbf{w}^{\top}} \right]^j \right) \frac{\partial^2 \mathcal{L}_{\mathcal{T}}}{\partial \mathbf{w} \partial \boldsymbol{\lambda}^{\top}} \Big|_{\mathbf{w}^*(\boldsymbol{\lambda})} \quad (3.8)$$

and if $\mathbf{I} - \alpha \frac{\partial^2 \mathcal{L}_{\mathcal{T}}}{\partial \mathbf{w} \partial \mathbf{w}^{\top}}$ is contractive:

$$\lim_{i \rightarrow \infty} \frac{\partial \mathbf{w}_{i+1}}{\partial \boldsymbol{\lambda}} = - \left[\frac{\partial^2 \mathcal{L}_{\mathcal{T}}}{\partial \mathbf{w} \partial \mathbf{w}^{\top}} \right]^{-1} \frac{\partial^2 \mathcal{L}_{\mathcal{T}}}{\partial \mathbf{w} \partial \boldsymbol{\lambda}^{\top}} \Big|_{\mathbf{w}^*(\boldsymbol{\lambda})} \quad (3.9)$$

This result is also shown in Shaban et al. (2019), but they use a different approximation for computing the hypergradient—see Table 3.1. Instead, we use the following best-response Jacobian approximation, where i controls the trade-off between computation and error bounds:

$$\frac{\partial \mathbf{w}^*}{\partial \boldsymbol{\lambda}} \approx - \left(\alpha \sum_{j \leq i} \left[\mathbf{I} - \alpha \frac{\partial^2 \mathcal{L}_{\mathcal{T}}}{\partial \mathbf{w} \partial \mathbf{w}^{\top}} \right]^j \right) \frac{\partial^2 \mathcal{L}_{\mathcal{T}}}{\partial \mathbf{w} \partial \boldsymbol{\lambda}^{\top}} \Big|_{\mathbf{w}^*(\boldsymbol{\lambda})} \quad (3.10)$$

Shaban et al. (2019) use an approximation that scales memory linearly in i , while ours is constant. We save memory because we reuse last \mathbf{w} i times, while Shaban et al. (2019) needs the last i \mathbf{w} 's. Scaling the Hessian by the learning rate α is key for convergence. Our algorithm has the following main advantages relative to other approaches:

- It requires a constant amount of memory, unlike other unrolled differentiation methods (Maclaurin et al., 2015a; Shaban et al., 2019).
- It is more stable than conjugate gradient (Liao et al., 2018).

3.4.3 Scope and Limitations

The assumptions necessary to apply the IFT in our setup are as follows: (1) $\mathcal{L}_V : \mathbf{\Lambda} \times \mathbf{W} \rightarrow \mathbb{R}$ is differentiable, (2) $\mathcal{L}_T : \mathbf{\Lambda} \times \mathbf{W} \rightarrow \mathbb{R}$ is twice differentiable with an invertible Hessian at $\mathbf{w}^*(\boldsymbol{\lambda})$, and (3) $\mathbf{w}^* : \mathbf{\Lambda} \rightarrow \mathbf{W}$ is differentiable.

We need continuous hyperparameters to use gradient-based optimization, but many discrete hyperparameters (e.g., number of hidden units) have continuous relaxations (Maddison et al., 2017; Jang et al., 2016). Also, we can only optimize hyperparameters that change the loss manifold, so our approach is not straightforwardly applicable to optimizer hyperparameters.

To exactly compute hypergradients, we must find $(\boldsymbol{\lambda}', \mathbf{w}')$ such that $\left. \frac{\partial \mathcal{L}_T}{\partial \mathbf{w}} \right|_{\boldsymbol{\lambda}', \mathbf{w}'} = 0$, which we can only solve to a tolerance with an approximate solution denoted $\widehat{\mathbf{w}}^*(\boldsymbol{\lambda})$. Pedregosa (2016) shows results for how an error in the approximate solution affects the inversion.

3.5 Experiments

We first compare the properties of Neumann inverse approximations and conjugate gradient with experiments similar to Liao et al. (2018); Maclaurin et al. (2015a); Shaban et al. (2019); Pedregosa (2016). Then, we demonstrate that our proposed approach can overfit the validation data with small training and validation sets. Finally, we apply our approach to high-dimensional hyperparameter optimization tasks: (1) dataset distillation; (2) learning a data augmentation network; and (3) tuning regularization parameters for an LSTM language model.

Hyperparameter optimization algorithms that are not based on implicit differentiation or differentiation through optimization—such as Jaderberg et al. (2017); Jamieson and Talwalkar (2016); Bergstra and Bengio (2012); Kumar et al. (2018); Li et al. (2016); Snoek et al. (2012)—do not scale to the high-dimensional hyperparameters we use. Thus, we cannot sensibly compare to them for these high-dimensional problems.

3.5.1 Approximate Inversion Algorithms

In Figure 3.3, we investigate how close various approximations are to the true inverse. We calculate the distance between the approximate hypergradient and the true hypergradient. We can only do this for small-scale problems because we need the exact inverse for the true hypergradient. We use a linear network on the Boston housing dataset (Harrison Jr and Rubinfeld, 1978), which makes finding the best-response \mathbf{w}^* and inverse training Hessian feasible.

We measure the cosine similarity, which tells us how accurate the direction is, and the ℓ_2 (Euclidean) distance between the approximate and true hypergradients. The Neumann approximation performs better than CG in cosine similarity if we take enough hyperparameter optimization steps, while CG always performs better for ℓ_2 distance.

In Figure 3.4, we show the inverse Hessian for a fully connected 1-layer neural network on the Boston housing dataset. The true inverse has a dominant diagonal, motivating identity approximations, while using more Neumann terms yields a structure closer to the true inverse.

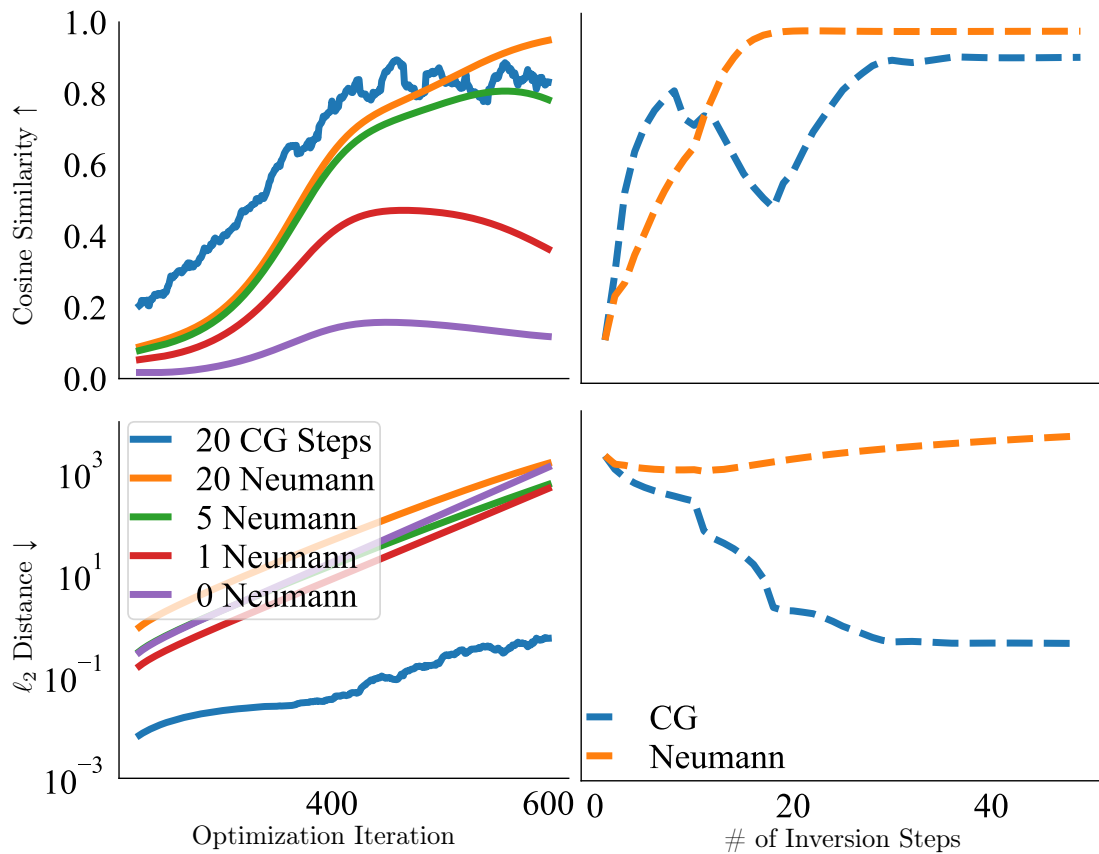


Figure 3.3: Comparing approximate hypergradients for inverse Hessian approximations to true hypergradients. The Neumann scheme can achieve a greater cosine similarity than CG but a larger ℓ_2 distance for equal steps.

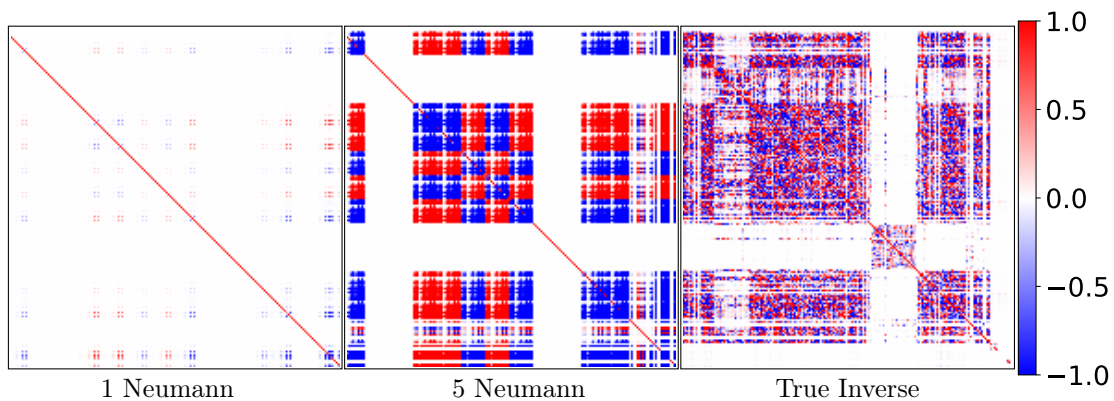


Figure 3.4: Inverse Hessian approximations for a 1-layer, fully-connected neural network on the Boston housing dataset as in Zhang et al. (2018).

3.5.2 Overfitting a Small Validation Set

In Figure 3.5, we check the capacity of our hyperparameter optimization algorithm to overfit the validation data. We use the same restricted dataset as in Franceschi et al. (2017, 2018) of 50 training and validation examples, which allows us to assess hyperparameter optimization performance easily. We tune a separate weight decay hyperparameter for each neural network parameter as in Balaji et al. (2018); Maclaurin et al. (2015a). We show the performance with a linear classifier, AlexNet (Krizhevsky et al., 2012), and ResNet44 (He et al., 2016). For AlexNet, this yields $> 50\,000\,000$ hyperparameters, so we can perfectly classify our validation data by optimizing the hyperparameters.

Algorithm 4 achieves 100% accuracy on the training and validation sets with significantly lower accuracy on the test set (Appendix A.5, Figure A.1), showing that we have a powerful hyperparameter optimization algorithm that can overfit both the training and validation data. The same optimizer is used for weights and hyperparameters in all cases.

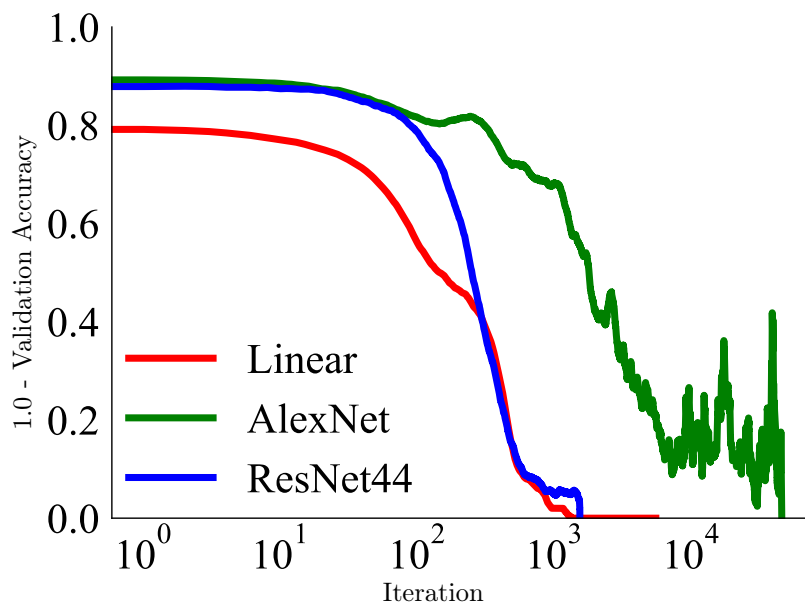


Figure 3.5: Algorithm 4 can overfit a small validation set on CIFAR-10. It optimizes for loss and achieves 100% validation accuracy for standard, large models.

3.5.3 Dataset Distillation

Dataset distillation (Maclaurin et al., 2015a; Wang et al., 2018) aims to learn a small, synthetic training dataset from scratch that condenses the knowledge in the original full-sized training set. The goal is for a model trained on the synthetic data to generalize to the original validation and test sets. Distillation is an interesting benchmark for hyperparameter optimization as it allows us to introduce tens of thousands of hyperparameters and visually inspect what is learned. Here, every pixel value in each synthetic training example is a hyperparameter. We distill MNIST and CIFAR-10/100 (Krizhevsky, 2009), yielding $28 \times 28 \times 10 = 7840$, $32 \times 32 \times 3 \times 10 = 30\,720$, and $32 \times 32 \times 3 \times 100 = 300\,720$ hyperparameters, respectively. All labeled data are in our validation set for these experiments, while our distilled data are in the training set. We visualize the distilled images for each class in Figure 3.6, recovering recognizable digits for MNIST and reasonable color averages for CIFAR-10/100.

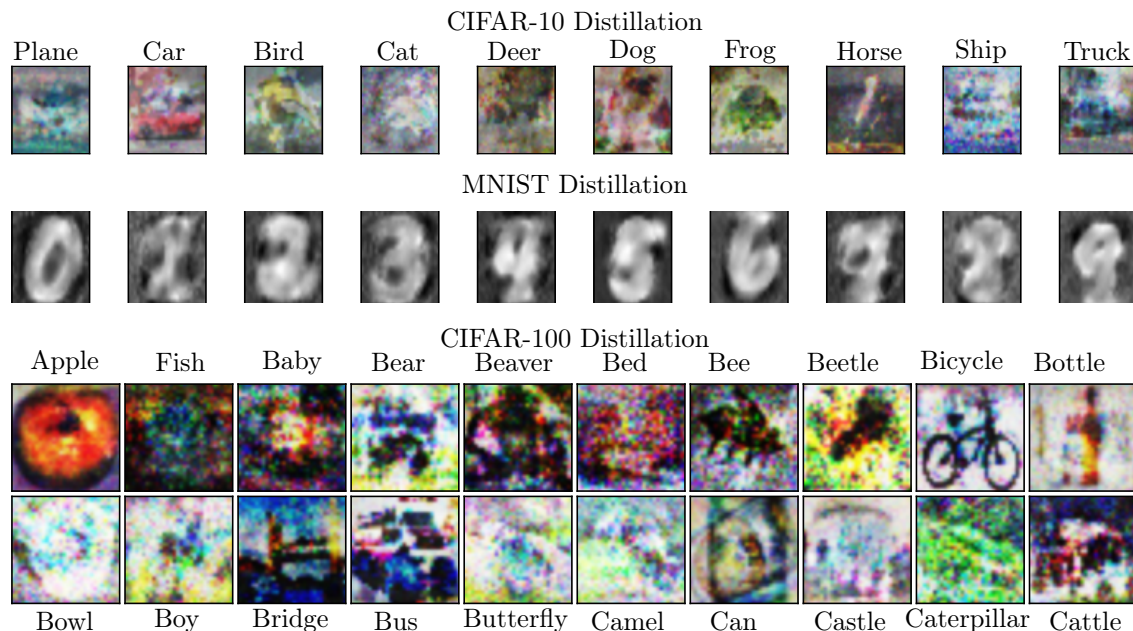


Figure 3.6: Distilled datasets for CIFAR-10, MNIST, and CIFAR-100. For CIFAR-100, we show the first 20 classes—the rest are in Appendix Figure A.2. We learn one distilled image per class. So, after training a logistic regression classifier on the distillation, it generalizes to the rest of the data.

3.5.4 Learned Data Augmentation

Data augmentation is a simple way to introduce invariances to a model—such as scale or contrast invariance—that improve generalization (Cubuk et al., 2018; Xie et al., 2019). Taking advantage of the ability to optimize many hyperparameters, we learn data augmentation from scratch (Figure 3.7).

Specifically, we learn a data augmentation network $\tilde{\mathbf{x}} = \mathbf{f}_{\lambda}(\mathbf{x}, \epsilon)$ that takes a training example \mathbf{x} and noise $\epsilon \sim \mathcal{N}(\mathbf{0}, \mathbf{I})$, and outputs an augmented example $\tilde{\mathbf{x}}$. The noise ϵ allows us to learn stochastic augmentations. We parameterize \mathbf{f} as a U-Net (Ronneberger et al., 2015) with a residual connection from the input to the output, making identity mapping easy to learn. The parameters of the U-Net, λ , are hyperparameters tuned for the validation loss — therefore, we have 6659 hyperparameters. We trained a ResNet18 (He et al., 2016) on CIFAR-10 with augmented examples produced by the U-Net, which is trained simultaneously on the validation set.

The results for the identity and the Neumann inverse approximations are shown in Table 3.3. We omit CG because it performed no better than the identity. Using the data augmentation network improves the validation and test accuracy by 2–3% and produces a smaller variance between multiple random restarts. In Mounsaveng et al. (2019), a different augmentation network architecture is learned with adversarial training.

3.5.5 RNN Hyperparameter Optimization

We also used our proposed algorithm to tune regularization hyperparameters for an LSTM (Hochreiter and Schmidhuber, 1997) trained on the Penn TreeBank (PTB) corpus (Marcus et al., 1993). As in Gal and Ghahramani (2016), we used a 2-layer LSTM with 650 hidden units per layer and 650-dimensional word embeddings. Additional details are provided in Appendix A.5.4.

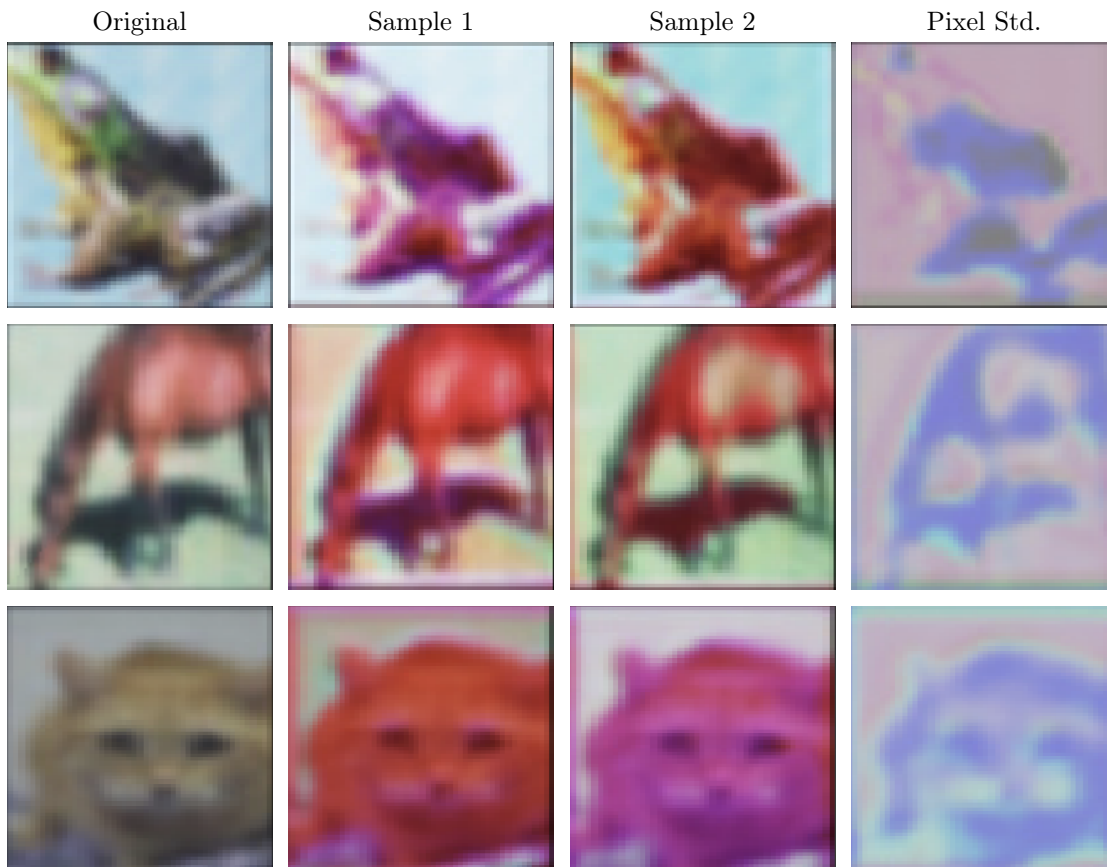


Figure 3.7: Learned data augmentations. The original image is on the left, followed by two augmented samples and the standard deviation of the pixel intensities from the augmentation distribution.

Inverse Approximation	Validation Accuracy \uparrow	Test Accuracy \uparrow
0	92.5 \pm 0.21	92.6 \pm 0.17
3 Neumann steps	95.1 \pm 0.02	94.6 \pm 0.01
3 steps unrolled differentiation	95.0 \pm 0.02	94.7 \pm 0.01
<i>I</i>	94.6 \pm 0.02	94.1 \pm 0.02

Table 3.3: Accuracy of different inverse approximations. Using 0 means no hyperparameter optimization occurs, and the augmentation is initially the identity. The Neumann approach performs similarly to unrolled differentiation (Maclaurin et al., 2015a; Shaban et al., 2019) with equal steps and less memory. Using more terms does better than the identity, and the identity performed better than CG (not shown), which was unstable.

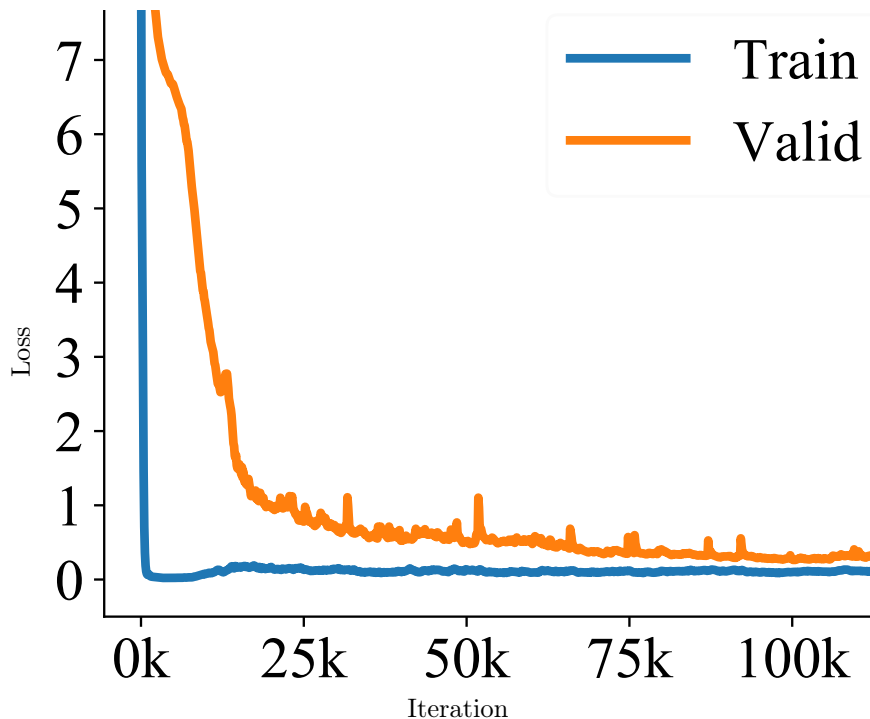


Figure 3.8: Algorithm 4 can overfit a small validation set with an LSTM on PTB.

Overfitting Validation Data. We first verify that our algorithm can overfit the validation set in a small-data setting with 10 training and 10 validation sequences (Figure 3.8). The LSTM architecture we use has 13 280 400 weights, and we tune a separate weight-decay hyperparameter per weight. We overfit the validation set, reaching nearly 0 validation loss.

Large-Scale Hyperparameter Optimization. There are various forms of regularization used for the training of RNNs, including variational dropout (Kingma et al., 2015) on the input, hidden state, and output; embedding dropout that sets rows of the embedding matrix to 0, removing tokens from all sequences in a mini-batch; DropConnect (Wan et al., 2013) on hidden-to-hidden weights; and activation and temporal activation regularization. We tune these 7 hyperparameters simultaneously. Additionally, we experiment with tuning separate dropout/DropConnect rates for each activation/weight, giving 1 691 951 total hyperparameters. To allow gradient-based optimization of dropout rates, we use concrete dropout (Gal et al., 2017).

Instead of using the small dropout initialization as in MacKay et al. (2019a), we use a larger initialization of 0.5. The results for our new initialization without hyperparameter optimization, our method tuning the same hyperparameters as MacKay et al. (2019a) (“Ours”), and our method tuning many more hyperparameters (“Ours, Many”) are shown in Table 3.4. We can tune hyperparameters more quickly and achieve better perplexities than the alternatives.

3.5.6 Effects of Many Hyperparameters

Given the ability to tune high-dimensional hyperparameters and the potential to overfit the validation set, should we reconsider how our training and validation splits are structured? Do the same heuristics apply as with low-dimensional hyperparameters (e.g., use $\sim 10\%$ of the data for validation)?

Method	Validation Loss $\mathcal{L}_V^* \downarrow$	Test Loss \downarrow	Time(s)
Grid Search	97.32	94.58	100k
Random Search	84.81	81.46	100k
Bayesian Opt.	72.13	69.29	100k
STN	70.30	67.68	25k
No hyperparameter optimization	75.72	71.91	18.5k
Ours	69.22	66.40	18.5k
Ours, Many	68.18	66.14	18.5k

Table 3.4: Comparing Hyperparameter Optimization methods for LSTM training on PTB. We tune millions of hyperparameters faster and with memory comparable to competitors that tune a handful. Our method competitively optimizes the same 7 hyperparameters as the baselines of MacKay et al. (2019a) (first four rows). We show a performance boost by tuning millions of hyperparameters introduced with per-unit/weight dropout and DropConnect. “No hyperparameter optimization” shows how our augmented hyperparameter initialization affects training.

In Figure 3.9, we see how splitting our data into training and validation sets of different ratios affects test performance. We show the results of jointly optimizing the neural network weights and hyperparameters, as well as the results of fixing the final optimized hyperparameters and retraining the neural network weights from scratch, which is a common technique for boosting performance (Goodfellow et al., 2016).

We evaluate a high-dimensional regime with a separate weight decay hyperparameter per neural network parameter and a low-dimensional regime with a single global weight decay. We observe that: (1) for a single weight decay, the optimal combination of validation data and weight decay has similar test performance with and without retraining because the optimal amount of validation data is small and (2) for many weight decays, the optimal combination of validation data and weight decay is significantly affected by retraining because the optimal amount of validation data needs to be large to fit our hyperparameters effectively.

For few hyperparameters, our results agree with the standard practice of using 10% of the data for validation and the other 90% for training. For many hyperparameters, our example shows that we may need larger validation partitions for hyperparameter optimization. Retraining our model with all data can be critical if we use a large validation partition to fit the hyperparameters.

3.6 Conclusion

We present a gradient-based hyperparameter optimization algorithm that scales to high-dimensional hyperparameters for modern, deep neural networks. We use the implicit function theorem to formulate the hypergradient as a matrix equation whose bottleneck is inverting the Hessian of the training loss with respect to the neural network parameters. We scale the hypergradient computation to large neural networks by approximately inverting the Hessian, leveraging a relationship with unrolled differentiation. We believe algorithms of this nature provide a path for practical nested optimization, where we have Hessians with a known structure. Examples of this include GANs (Goodfellow et al., 2014), and other multi-agent games (Foerster et al., 2018; Letcher et al., 2018). However, these games have a non-zero direct gradient, which we leverage in the next chapter to create a robust method that circumvents any best-response approximations and scales to (at the time) SOTA architectures.

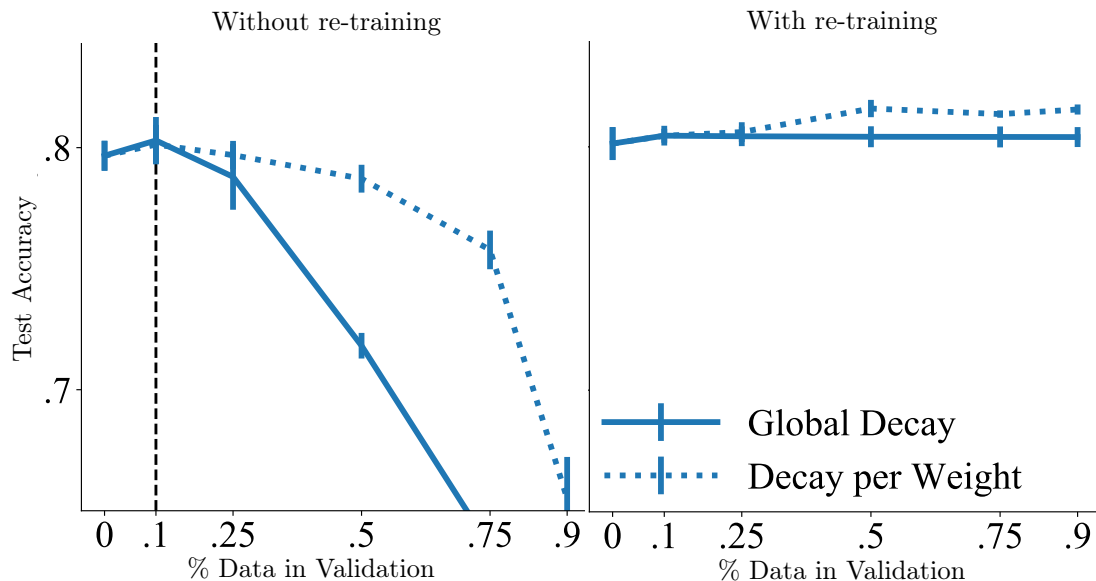


Figure 3.9: Test accuracy of logistic regression on MNIST, with different size validation splits. Solid lines correspond to a single global weight decay (1 hyperparameter), while dotted lines correspond to a separate weight decay per weight (many hyperparameters). The best validation proportion for test performance differs after retraining for many hyperparameters but is similar for few hyperparameters.

Acknowledgements

We thank Chris Pal for recommending we check re-training with all the data, Haoping Xu for discussing experiments on inverse-approximation variants, Roger Grosse for guidance, Cem Anil & Chris Cremer for their feedback on this work, and Xuanyi Dong for noting corrections in the algorithms. Paul Vicol was supported by a JP Morgan AI Fellowship. We also thank anonymous reviewers for their suggestions and everyone else at Vector for helpful discussions and feedback.

My Contributions Towards this Paper As it Pertains to the Thesis

The ideas underlying this project were a collaborative effort from all authors. I ran many of the experiments with much help from Paul Vicol. I also did most of the writing for the paper. This paper has a conference version (Lorraine et al., 2020a) and an arXiv version (Lorraine et al., 2019).

Chapter 4

Complex Momentum for Optimization in Games

We generalize gradient descent with momentum for optimization in differentiable games to have complex-valued momentum. We give theoretical motivation for our method by proving convergence on bilinear zero-sum games for simultaneous and alternating updates. Our method gives real-valued parameter updates, making it a drop-in replacement for standard optimizers. We empirically demonstrate that complex-valued momentum can improve convergence in realistic adversarial games—like generative adversarial networks—by showing that we find better solutions with an almost identical computational cost. We also show a practical complex-valued Adam variant, which we use to train BigGAN to improve inception scores on CIFAR-10.

4.1 Introduction

Gradient-based optimization has been critical for the success of machine learning, updating a single set of parameters to minimize a single loss. A growing number of applications require learning with multiple players, each with parameters and objectives. Common examples are GANs (Goodfellow et al., 2014), hyperparameter optimization (Maclaurin et al., 2015a; Andrychowicz et al., 2016; Fu et al., 2016; Shaban et al., 2019), actor-critic models (Pfau and Vinyals, 2016), curriculum learning (Baker et al., 2019; Balduzzi et al., 2019; Sukhbaatar et al., 2018), adversarial examples (Bose et al., 2020; Yuan et al., 2019), learning models (Rajeswaran et al., 2020; Abachi et al., 2020; Nikishin et al., 2021), domain adversarial adaptation (Acuna et al., 2021), neural architecture search (Elsken et al., 2019), and meta-learning (Finn et al., 2017; Ren et al., 2018a, 2020).

We often want solutions where no player gains from changing their strategy unilaterally, e.g., Nash equilibria (Morgenstern and Von Neumann, 1953) or Stackelberg equilibria (Von Stackelberg, 2010). Classical gradient-based learning often fails to find these equilibria due to rotational dynamics (Berard et al., 2019), or identically zero direct gradients as in Chapters 2 and 3. There are numerous saddle point finding algorithms for zero-sum games (Arrow et al., 1958; Freund and Schapire, 1999).

Gidel et al. (2019) generalize GD with momentum to games, showing that we can use a negative momentum to converge if the eigenvalues of the Jacobian of the gradient vector field have a large imaginary part. We use terminology in Gidel et al. (2019) and say *(purely) cooperative or adversarial games* for games with (purely) real or imaginary eigenvalues. Setups like GANs are not purely adversarial but have both *purely cooperative and adversarial eigenspaces* – i.e., eigenspaces with purely real or imaginary eigenvalues. More generally, we say that an eigenspace is cooperative when the real part of the eigenvalue is larger than the imaginary part and is otherwise adversarial. In cooperative eigenspaces, classical optimization methods perform best, while in adversarial eigenspaces, methods customized for games work best – see Figure 4.5.

We want a method that converges with simultaneous and alternating updates in purely adversarial games – a setup where existing momentum methods fail. Also, we want a method that robustly converges with different mixtures of adversarial and cooperative eigenspaces – see Figure 4.6 – because finding all eigenspaces depends on an eigendecomposition that can be intractable. To solve this, we unify and generalize existing momentum methods (Lucas et al., 2018; Gidel et al., 2019) to recurrently linked momentum – a setup with multiple recurrently linked momentum buffers with potentially negative coefficients – see Figure B.1c.

Selecting two of these recurrently linked buffers with appropriate momentum coefficients can be interpreted as the real and imaginary parts of a single *complex buffer* and *complex momentum coefficient* – see Appendix Figure B.1d. This setup (a) allows us to converge in adversarial games with simultaneous updates, (b) only introduces one new optimizer parameter – the phase or arg of our momentum, (c) allows us to gain intuitions via complex analysis, (d) is trivial to implement in libraries supporting complex arithmetic, and (e) robustly converges for different eigenspace mixtures.

Intuitively, our complex buffer stores historical gradient information, oscillating between adding or subtracting at a frequency dictated by the momentum coefficient. Classical momentum only adds gradients, and negative momentum changes between adding or subtracting each iteration while we oscillate at an arbitrary (fixed) frequency – see Figure 4.2. This reduces rotational dynamics during training by canceling out opposing updates.

Our contributions include:

- Providing generalizations and variants of classical (Polyak, 1964), negative (Gidel et al., 2019), and aggregated (Lucas et al., 2018) momentum for learning in differentiable games.
- Showing our method converges on adversarial games, including bilinear zero-sum games and a Dirac-GAN, with simultaneous and alternating updates.
- Illustrating a robustness during optimization, converging faster and over a larger range of mixtures of cooperative and adversarial games than existing first-order methods.
- Giving a practical extension of our method to a complex-valued Adam (Kingma and Ba, 2014) variant, which we use to train a BigGAN (Brock et al., 2018) on CIFAR-10, improving their inception scores.

Actual JAX implementation: changes in green

```

mass = .8 + .3j
def momentum(step_size, mass):
    ...
    def update(i, g, state):
        x, velocity = state
        velocity = mass * velocity + g
        x=x-jnp.real(step_size(i)*velocity)
        return x, velocity
    ...

```

Figure 4.1: How to modify JAX’s SGD with momentum [here](#) to use complex momentum. The only changes are in green. `jnp.real` gets the real part of `step_size` times the momentum buffer (called `velocity` here). In this case, we use a complex `mass` for our method $\beta = |\beta| \exp(i \arg(\beta)) = 0.9 \exp(i\pi/8) \approx .8 + .3i$.

4.2 Background

Appendix Table B.1 summarizes our notation. Consider the single-objective optimization problem:

$$\boldsymbol{\theta}^* = \underset{\boldsymbol{\theta}}{\operatorname{argmin}} \mathcal{L}(\boldsymbol{\theta}) \quad (4.1)$$

We can find local minima of loss \mathcal{L} using (stochastic) gradient descent with step size α . We denote the loss gradient at parameters $\boldsymbol{\theta}^j$ by $\mathbf{g}^j = \mathbf{g}(\boldsymbol{\theta}^j) = \nabla_{\boldsymbol{\theta}} \mathcal{L}(\boldsymbol{\theta})|_{\boldsymbol{\theta}^j}$.

$$\boldsymbol{\theta}^{j+1} = \boldsymbol{\theta}^j - \alpha \mathbf{g}^j \quad (\text{SGD})$$

Momentum can generalize SGD. For example, Polyak’s Heavy Ball (Polyak, 1964):

$$\boldsymbol{\theta}^{j+1} = \boldsymbol{\theta}^j - \alpha \mathbf{g}^j + \beta (\boldsymbol{\theta}^j - \boldsymbol{\theta}^{j-1}) \quad (4.2)$$

This can be equivalently written with momentum buffer $\boldsymbol{\mu}^j = (\boldsymbol{\theta}^j - \boldsymbol{\theta}^{j-1})/\alpha$.

$$\boldsymbol{\mu}^{j+1} = \beta \boldsymbol{\mu}^j - \mathbf{g}^j, \quad \boldsymbol{\theta}^{j+1} = \boldsymbol{\theta}^j + \alpha \boldsymbol{\mu}^{j+1} \quad (\text{SGDm})$$

SGDm generalizes to aggregated momentum (Lucas et al., 2018), shown in Appendix Algorithm 9.

4.2.1 Game Formulations

Another class of problems is learning in *games*, which includes problems like generative adversarial networks (GANs). As in Chapters 2 and 3, consider 2-player games – with players denoted by A and B – where each player minimizes their loss $\mathcal{L}_A, \mathcal{L}_B$ with their parameters $\boldsymbol{\theta}_A, \boldsymbol{\theta}_B$. If \mathcal{L}_A and \mathcal{L}_B are differentiable in $\boldsymbol{\theta}_A$ and $\boldsymbol{\theta}_B$, we say the game is differentiable. In deep learning, losses are non-convex with many parameters, so we focus on finding local solutions. If $\boldsymbol{\theta}_B^*(\boldsymbol{\theta}_A)$ denotes player B ’s best-response function, then solutions can be defined as:

$$\begin{aligned} \boldsymbol{\theta}_A^* &= \underset{\boldsymbol{\theta}_A}{\operatorname{argmin}} \mathcal{L}_A(\boldsymbol{\theta}_A, \boldsymbol{\theta}_B^*(\boldsymbol{\theta}_A)), \\ \boldsymbol{\theta}_B^*(\boldsymbol{\theta}_A) &= \underset{\boldsymbol{\theta}_B}{\operatorname{argmin}} \mathcal{L}_B(\boldsymbol{\theta}_A, \boldsymbol{\theta}_B) \end{aligned} \quad (4.3)$$

We may be able to approximately find θ_A^* efficiently if we can do SGD on:

$$\mathcal{L}_A^*(\theta_A) = \mathcal{L}_A(\theta_A, \theta_B^*(\theta_A)) \quad (4.4)$$

SGD requires computing $\frac{\partial \mathcal{L}_A^*}{\partial \theta_A}$, which often requires $\frac{\partial \theta_B^*}{\partial \theta_A}$, which we seek to circumvent computing in this chapter. A common optimization algorithm to analyze for finding solutions is simultaneous SGD (SimSGD) – sometimes called gradient descent ascent for zero-sum games – where $\mathbf{g}_A^j = \mathbf{g}_A(\theta_A^j, \theta_B^j)$ and $\mathbf{g}_B^j = \mathbf{g}_B(\theta_A^j, \theta_B^j)$ are estimators for $\nabla_{\theta_A} \mathcal{L}_A|_{\theta_A^j, \theta_B^j}$ and $\nabla_{\theta_B} \mathcal{L}_B|_{\theta_A^j, \theta_B^j}$:

$$\theta_A^{j+1} = \theta_A^j - \alpha \mathbf{g}_A^j, \quad \theta_B^{j+1} = \theta_B^j - \alpha \mathbf{g}_B^j \quad (\text{SimSGD})$$

We simplify the notation with the concatenated or joint-parameters $\omega = [\theta_A, \theta_B] \in \mathbb{R}^d$ and the joint-gradient vector field $\hat{\mathbf{g}}: \mathbb{R}^d \rightarrow \mathbb{R}^d$, which at the j^{th} iteration is the joint-gradient denoted:

$$\hat{\mathbf{g}}^j = \hat{\mathbf{g}}(\omega^j) = \left[\mathbf{g}_A(\omega^j), \mathbf{g}_B(\omega^j) \right] = \left[\mathbf{g}_A^j, \mathbf{g}_B^j \right] \quad (4.5)$$

We extend to n -player games by treating ω and $\hat{\mathbf{g}}$ as concatenations of the players' parameters and loss gradients, allowing for a concise expression of the SimSGD update with momentum:

$$\mu^{j+1} = \beta \mu^j - \hat{\mathbf{g}}^j, \omega^{j+1} = \omega^j + \alpha \mu^{j+1} \quad (\text{SimSGDm})$$

Gidel et al. (2019) show classical momentum choices of $\beta \in [0, 1)$ do not improve convergence rate over SimSGD in some games. Specifically, any non-negative momentum and step size will not converge for purely adversarial games with imaginary eigenvalues. In contrast, negative momentum helps if the Jacobian of the joint-gradient vector field $\nabla_{\omega} \hat{\mathbf{g}}$ has complex eigenvalues. For purely cooperative games – ex., single-objective minimization – $\nabla_{\omega} \hat{\mathbf{g}}$ has real eigenvalues and (if symmetric) can be viewed as the Hessian of a loss, so classical momentum works well.

4.2.2 Limitations of Existing Methods

Higher-order: Methods using higher-order gradients are often harder to parallelize across GPUs (Osawa et al., 2019), get attracted to bad saddle points (Mescheder et al., 2017), require estimators for inverse Hessians (Schäfer and Anandkumar, 2019; Wang et al., 2019b), are complicated to implement, have numerous optimizer parameters, and can be more expensive in iteration and memory cost (Hemmat et al., 2020; Wang et al., 2019b; Schäfer and Anandkumar, 2019; Schäfer et al., 2020; Czarnecki et al., 2020; Zhang et al., 2020a). Instead, we focus on first-order methods.

First-order: Some first-order methods such as extragradient (Korpelevich, 1976) require a second, costly, gradient evaluation per step. Similarly, methods alternating player updates must wait until after the first player's gradient is used to evaluate the second player's gradient. However, many deep learning setups can parallelize the computation of both players' gradients, making alternating updates effectively cost another gradient evaluation. We are interested in convergence speed in the number of gradient queries, so we naturally looked at methods that update with the effective cost of one gradient evaluation – see Appendix Figure B.3. Additionally, simultaneous updates are a standard choice in some settings (Acuna et al., 2021).

Robust convergence: We want our method to converge in purely adversarial games with simultaneous updates – a setup where existing momentum methods fail (Gidel et al., 2019). Furthermore, computing a game’s eigendecomposition is often infeasibly expensive, so we want methods that robustly converge over different mixtures of adversarial and cooperative eigenspaces – see Figure 4.6. We are interested in relevant eigenspace mixtures during GAN training – see Figures 4.7 and B.4.

4.2.3 Coming up with our Method

Combining existing methods: Given the preceding limitations, we would like a robust first-order method using a single, simultaneous gradient evaluation. We looked at combining aggregated (Lucas et al., 2018) with negative (Gidel et al., 2019) momentum by allowing negative coefficients because these methods are first-order and use a single gradient evaluation – see Figure B.1b. Additionally, aggregated momentum provides robustness during optimization by quickly converging on problems with a wide range of conditioning, while negative momentum works in adversarial setups. We hoped to combine their benefits, gaining robustness to different mixtures of adversarial and cooperative eigenspaces. However, with this setup, we could not find solutions that converged with simultaneous updates in purely adversarial games.

Generalize to allow solutions: We generalized the setup to allow recurrent connections between momentum buffers with potentially negative coefficients – see Figure B.1c and Appendix Algorithm 10. Optimizer parameters exist that allow convergence with simultaneous updates in purely adversarial games while being first-order with a single gradient evaluation – see Corollary 1. However, this setup could introduce many optimizer parameters, have unintuitive behavior, and be unsuitable for analysis in general. So, we use a special case of this method to help solve these problems.

A simple solution: With two momentum buffers and correctly chosen recurrent weights, we can conveniently interpret our buffers as the real and imaginary parts of one complex buffer – see Appendix Figure B.1d. This method is (a) capable of converging in purely adversarial games with simultaneous updates – Corollary 1, (b) only introduces one new optimizer parameter – the phase of the momentum coefficient, (c) is tractable to analyze and have intuitions for with Euler’s formula – ex., Equation 4.8, (d) is trivial to implement in libraries supporting complex arithmetic – see Figure 4.1, and (e) can be robust to games with different mixtures of cooperative and adversarial eigenspaces – see Figures 4.5 and 4.6.

4.3 Complex Momentum

We describe our proposed method, where the momentum coefficient $\beta \in \mathbb{C}$, step size $\alpha \in \mathbb{R}$, momentum buffer $\boldsymbol{\mu} \in \mathbb{C}^d$, and player parameters $\boldsymbol{\omega} \in \mathbb{R}^d$. The simultaneous (or Jacobi) update is:

$$\boldsymbol{\mu}^{j+1} = \beta \boldsymbol{\mu}^j - \hat{\boldsymbol{g}}^j, \quad \boldsymbol{\omega}^{j+1} = \boldsymbol{\omega}^j + \Re(\alpha \boldsymbol{\mu}^{j+1}) \quad (\text{SimCM})$$

There are many ways to get a real-valued update from $\boldsymbol{\mu} \in \mathbb{C}$, but we only consider updates equivalent to classical momentum when $\beta \in \mathbb{R}$. The update can use the imaginary part of the momentum buffer, which also works and could yield better solutions. However, we only use the real component of the momentum – $\Re(\boldsymbol{\mu})$ – because this is the simplest setup and is sufficient to work.

Algorithm 7 SimCM Momentum

```

1:  $\beta, \alpha \in \mathbb{C}, \boldsymbol{\mu}^0 \in \mathbb{C}^d, \boldsymbol{\omega}^0 \in \mathbb{R}^d$ 
2: for  $j = 1 \dots N$  do
3:    $\boldsymbol{\mu}^{j+1} = \beta \boldsymbol{\mu}^j - \hat{\boldsymbol{g}}^j$ 
4:    $\boldsymbol{\omega}^{j+1} = \boldsymbol{\omega}^j + \Re(\alpha \boldsymbol{\mu}^{j+1})$ 
5: end for
6: return  $\boldsymbol{\omega}^N$ 

```

We show the **SimCM** update in Algorithm 7 and visualize it in Appendix Figure B.1d. We also show the alternating (or Gauss-Seidel) update, which is common for GAN training:

$$\begin{aligned} \boldsymbol{\mu}_A^{j+1} &= \beta \boldsymbol{\mu}_A^j - \hat{\boldsymbol{g}}_A(\boldsymbol{\omega}^j), \boldsymbol{\theta}_A^{j+1} = \boldsymbol{\theta}_A^j + \Re(\alpha \boldsymbol{\mu}_A^{j+1}) \\ \boldsymbol{\mu}_B^{j+1} &= \beta \boldsymbol{\mu}_B^j - \hat{\boldsymbol{g}}_B(\boldsymbol{\theta}_A^{j+1}, \boldsymbol{\theta}_B^j), \boldsymbol{\theta}_B^{j+1} = \boldsymbol{\theta}_B^j + \Re(\alpha \boldsymbol{\mu}_B^{j+1}) \end{aligned} \quad (\text{AltCM})$$

Generalizing negative momentum: Consider the negative momentum of Gidel et al. (2019): $\boldsymbol{\omega}^{j+1} = \boldsymbol{\omega}^j - \alpha \hat{\boldsymbol{g}}^j + \beta(\boldsymbol{\omega}^j - \boldsymbol{\omega}^{j-1})$. Expanding **SimCM** with $\boldsymbol{\mu}^j = (\boldsymbol{\omega}^j - \boldsymbol{\omega}^{j-1})/\alpha$ for real momentum shows the negative momentum method of Gidel et al. (2019) is a special case of our method:

$$\boldsymbol{\omega}^{j+1} = \boldsymbol{\omega}^j + \Re\left(\alpha \left(\beta(\boldsymbol{\omega}^j - \boldsymbol{\omega}^{j-1})/\alpha - \hat{\boldsymbol{g}}^j\right)\right) \quad (4.6)$$

$$= \boldsymbol{\omega}^j - \alpha \hat{\boldsymbol{g}}^j + \beta(\boldsymbol{\omega}^j - \boldsymbol{\omega}^{j-1}) \quad (4.7)$$

4.3.1 Dynamics of Complex Momentum

For simplicity, we assume NumPy-style (Harris et al., 2020a) component-wise broadcasting for operations like taking the real-part $\Re(\boldsymbol{z})$ of vector $\boldsymbol{z} = [z_1, \dots, z_n] \in \mathbb{C}^n$, with proofs in the Appendix. Expanding the buffer updates with the polar components of β gives intuition for complex momentum:

$$\begin{aligned} \boldsymbol{\mu}^{j+1} = \beta \boldsymbol{\mu}^j - \hat{\boldsymbol{g}}^j &\iff \boldsymbol{\mu}^{j+1} = \beta \left(\beta(\dots) - \hat{\boldsymbol{g}}^{j-1} \right) - \hat{\boldsymbol{g}}^j \iff \\ \boldsymbol{\mu}^{j+1} &= - \sum_{k=0}^{k=j} \beta^k \hat{\boldsymbol{g}}^{j-k} \iff \\ \Re(\boldsymbol{\mu}^{j+1}) &= - \sum_{k=0}^{k=j} \cos(k \arg(\beta)) |\beta|^k \hat{\boldsymbol{g}}^{j-k}, \\ \Im(\boldsymbol{\mu}^{j+1}) &= - \sum_{k=0}^{k=j} \sin(k \arg(\beta)) |\beta|^k \hat{\boldsymbol{g}}^{j-k} \end{aligned} \quad (4.8)$$

The final line is simply by Euler's formula (Equation B.10). Equation 4.8 shows how β controls the momentum buffer $\boldsymbol{\mu}$ by having $|\beta|$ dictate the decay rates of the prior gradient, while $\arg(\beta)$ controls the oscillation frequency between the addition and subtraction of the prior gradients, which we visualize in Figure 4.2.

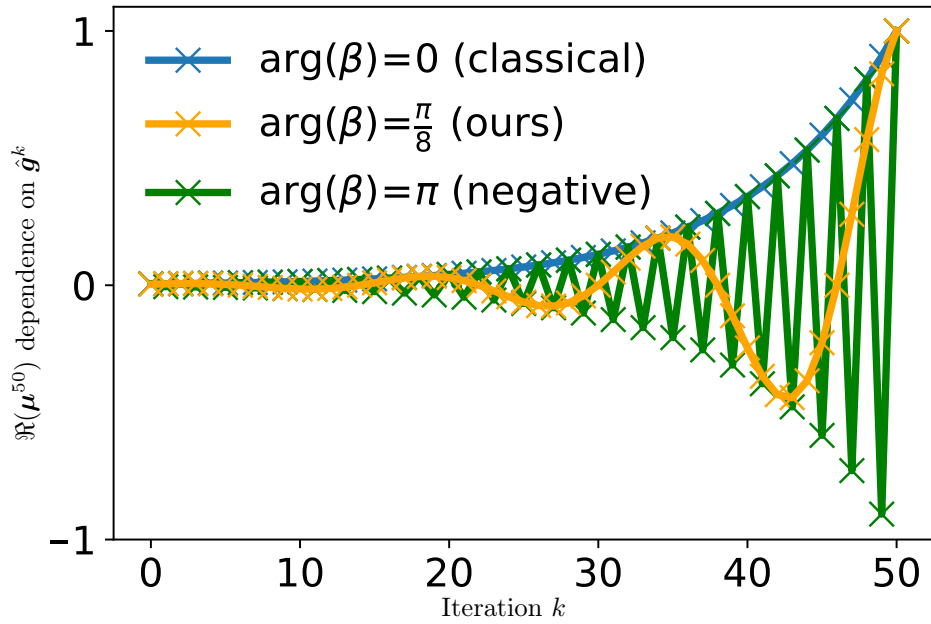


Figure 4.2: We show the real part of our momentum buffer – which dictates the parameter update – at the 50th iteration $\Re(\mu^{50})$ dependence on past gradients \hat{g}^k for $k = 1 \dots 50$. The magnitude of the momentum is fixed at $|\beta| = 0.9$ as in Figure 4.4. Euler’s formula is used in Equation 4.8 to find the dependence or coefficient of \hat{g}^k via $\Re(\mu^{50}) = -\sum_{k=0}^{50} |\beta|^k \cos(k \arg(\beta)) \hat{g}^{j-k}$. Complex momentum allows for smooth changes in the buffer’s dependence on past gradients.

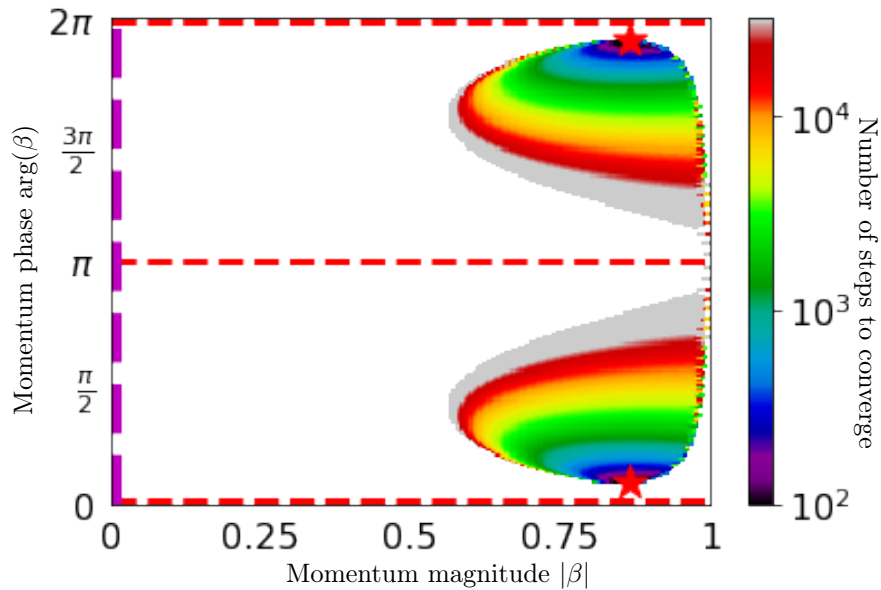


Figure 4.3: We show how many steps simultaneous complex momentum on a Dirac-GAN takes for a set solution distance. We fixed the step size $\alpha = 0.1$ as in Figure 4.4, while varying the phase and magnitude of our momentum $\beta = |\beta| \exp(i \arg(\beta))$. There is a red star at the minimum, dashed red lines at real β , and a magenta line for simultaneous gradient descent. No real-valued β converges for this – or any – α with simultaneous updates (Gidel et al., 2019). Appendix Figure B.3 compares this with alternating updates (AltCM), where negative momentum converges.

Expanding the parameter updates with the Cartesian components of α and β is key for Theorem 3, which characterizes the convergence rate:

$$\begin{aligned}\boldsymbol{\mu}^{j+1} &= \beta \boldsymbol{\mu}^j - \hat{\boldsymbol{g}}^j \iff \\ \Re(\boldsymbol{\mu}^{j+1}) &= \Re(\beta) \Re(\boldsymbol{\mu}^j) - \Im(\beta) \Im(\boldsymbol{\mu}^j) - \Re(\hat{\boldsymbol{g}}^j), \\ \Im(\boldsymbol{\mu}^{j+1}) &= \Im(\beta) \Re(\boldsymbol{\mu}^j) + \Re(\beta) \Im(\boldsymbol{\mu}^j)\end{aligned}\quad (4.9)$$

$$\boldsymbol{\omega}^{j+1} = \boldsymbol{\omega}^j + \Re(\alpha \boldsymbol{\mu}^{j+1}) \iff \boldsymbol{\omega}^{j+1} = \boldsymbol{\omega}^j - \alpha \hat{\boldsymbol{g}}^j + \Re(\alpha \beta) \Re(\boldsymbol{\mu}^j) - \Im(\alpha \beta) \Im(\boldsymbol{\mu}^j) \quad (4.10)$$

So, we can write the next iterate with a fixed-point operator:

$$\left[\Re(\boldsymbol{\mu}^{j+1}), \Im(\boldsymbol{\mu}^{j+1}), \boldsymbol{\omega}^{j+1} \right] = \mathbf{F}_{\alpha, \beta} \left(\left[\Re(\boldsymbol{\mu}^j), \Im(\boldsymbol{\mu}^j), \boldsymbol{\omega}^j \right] \right) \quad (4.11)$$

Equations 4.9 and 4.10 allow us to write the Jacobian of $\mathbf{F}_{\alpha, \beta}$, which can be used to bound convergence rates near fixed points, which we call the Jacobian of the augmented dynamics of buffer $\boldsymbol{\mu}$ and joint-parameters $\boldsymbol{\omega}$ and denote with:

$$\mathbf{J} = \nabla_{[\boldsymbol{\mu}, \boldsymbol{\omega}]} \mathbf{F}_{\alpha, \beta} = \begin{bmatrix} \Re(\beta) \mathbf{I} & -\Im(\beta) \mathbf{I} & -\nabla_{\boldsymbol{\omega}} \hat{\boldsymbol{g}} \\ \Im(\beta) \mathbf{I} & \Re(\beta) \mathbf{I} & \mathbf{0} \\ \Re(\alpha \beta) \mathbf{I} & -\Im(\alpha \beta) \mathbf{I} & \mathbf{I} - \alpha \nabla_{\boldsymbol{\omega}} \hat{\boldsymbol{g}} \end{bmatrix} \quad (4.12)$$

So, for quadratic losses our parameters evolve via:

$$\left[\Re(\boldsymbol{\mu}^{j+1}), \Im(\boldsymbol{\mu}^{j+1}), \boldsymbol{\omega}^{j+1} \right]^\top = \mathbf{J} \left[\Re(\boldsymbol{\mu}^j), \Im(\boldsymbol{\mu}^j), \boldsymbol{\omega}^j \right]^\top \quad (4.13)$$

We bound convergence rates near fixed points by using the spectrum of \mathbf{J} with Theorem 3.

Theorem 3 (Consequence of Prop. 4.4.1 Bertsekas (2008)). *Complex momentum's convergence rate: If the spectral radius $\rho(\nabla \mathbf{F}_{\alpha, \beta}(\boldsymbol{\mu}^*, \boldsymbol{\omega}^*)) < 1$, then, for $[\boldsymbol{\mu}, \boldsymbol{\omega}]$ in a neighborhood of $[\boldsymbol{\mu}^*, \boldsymbol{\omega}^*]$, the distance of $[\boldsymbol{\mu}^j, \boldsymbol{\omega}^j]$ to the stationary point $[\boldsymbol{\mu}^*, \boldsymbol{\omega}^*]$ converges at a linear rate $\mathcal{O}((\rho(\mathbf{J}) + \epsilon)^j)$, $\forall \epsilon > 0$.*

Here, linear convergence means $\lim_{j \rightarrow \infty} \|\boldsymbol{\omega}^{j+1} - \boldsymbol{\omega}^*\| / \|\boldsymbol{\omega}^j - \boldsymbol{\omega}^*\| \in (0, 1)$, where $\boldsymbol{\omega}^*$ is a fixed point. To converge, we select the optimizer parameters α, β so that the augmented dynamics spectral radius $\rho(\mathbf{J}(\alpha, \beta)) < 1$ —with the dependence on α and β now explicit. To easily find convergent parameters, we express $\text{Sp}(\mathbf{J}(\alpha, \beta))$ in terms of the spectrum $\text{Sp}(\nabla_{\boldsymbol{\omega}} \hat{\boldsymbol{g}})$, as in Theorem 3 in Gidel et al. (2019):

$$\mathbf{f}(\text{Sp}(\nabla_{\boldsymbol{\omega}} \hat{\boldsymbol{g}}), \alpha, \beta) = \text{Sp}(\mathbf{J}(\alpha, \beta)) \quad (4.14)$$

We provide a Mathematica command in Appendix B.1.2 for a cubic polynomial characterizing \mathbf{f} with coefficients that are functions of α, β and $\lambda \in \text{Sp}(\nabla_{\boldsymbol{\omega}} \hat{\boldsymbol{g}})$, whose roots are eigenvalues of \mathbf{J} , which we use in subsequent results. O'donoghue and Candes (2015) and Lucas et al. (2018) mention that we often do not know the condition number, eigenvalues – or the mixture of cooperative and adversarial eigenspaces – of a set of functions that we are optimizing, so we try to design algorithms which work over a large range. Sharing this motivation, we consider convergence behavior in games ranging from purely adversarial to cooperative.

In Section 4.4.2 at every non-real β we could select α and $|\beta|$ so Algorithm 7 converges. We define *almost-positive* to mean $\arg(\beta) = \epsilon$ for small ϵ , and show there are almost-positive β which converge.

Corollary 1 (Convergence of Complex Momentum). *There exist $\alpha \in \mathbb{R}, \beta \in \mathbb{C}$ so Algorithm 7 converges for bilinear zero-sum games. More-so, for small ϵ (we show for $\epsilon = \frac{\pi}{16}$), if $\arg(\beta) = \epsilon$ (i.e., almost-positive) or $\arg(\beta) = \pi - \epsilon$ (i.e., almost-negative), then we can select $\alpha, |\beta|$ to converge.*

Why show this? Our result complements Gidel et al. (2019) who show that for all real α, β Algorithm 7 *does not* converge. We include the proof for bilinear zero-sum games, but the result generalizes to some purely adversarial games near fixed points, such as Dirac GANs (Mescheder et al., 2017). The second part of the result shows evidence that there is a sense in which the only β that do not converge are real (with simultaneous updates on purely adversarial games). It also suggests a form of robustness because almost-positive β can approach acceleration in cooperative eigenspaces while converging in adversarial eigenspaces, so almost-positive β may be useful when our games have an uncertain or variable mixture of real and imaginary eigenvalues like GANs. Sections 4.4.2, 4.4.3, and 4.4.4 investigate this further.

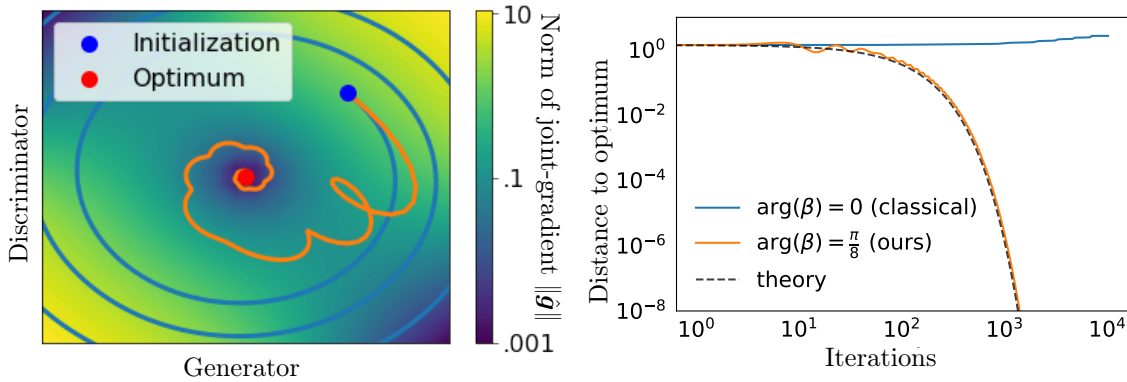


Figure 4.4: Complex momentum helps correct rotational dynamics when training a Dirac-GAN (Mescheder et al., 2018). *Top*: Parameter trajectories with step size $\alpha = 0.1$ and momentum $\beta = 0.9 \exp(i\pi/8)$. We include the classical, real, and positive momentum, which diverges for any α . *Bottom*: The distance to the optimum, which has a convergence rate that matches our prediction with Theorem 3 and Equation 4.14.

4.3.2 What about Acceleration?

With classical momentum, finding the step size α and the momentum β to optimize the convergence rate is tractable if $0 < l \leq L$ and $\text{Sp}(\nabla_{\omega}\hat{g}) \in [l, L]^d$ (Goh, 2017) – that is, we have a l -strongly convex loss and L -Lipschitz loss. The conditioning $\kappa = L/l$ can characterize the problem’s difficulty. Gradient descent with an appropriate α can achieve a convergence rate of $\frac{\kappa-1}{\kappa+1}$, but using momentum with an appropriate (α^*, β^*) can achieve an *accelerated* rate of $\rho^* = \frac{\sqrt{\kappa-1}}{\sqrt{\kappa+1}}$. However, there is no consensus on constraining $\text{Sp}(\nabla_{\omega}\hat{g})$ in games to obtain tractable and useful results. Candidate constraints include monotonic vector fields generalizing notions of convexity or vector fields with bounded eigenvalue norms that capture a kind of sensitivity (Azizian et al., 2020a). Figure 4.7 shows $\text{Sp}(\nabla_{\omega}\hat{g})$ for a GAN, motivating the varying of α and β for each player as in Section 4.4.4.

4.3.3 Implementing Complex Momentum

Complex momentum is trivial to implement with libraries supporting complex arithmetic like JAX (Bradbury et al., 2018) or PyTorch (Paszke et al., 2017). Given an SGD implementation, we often only need to change a few lines of code; see Figure 4.1. In addition, Equations 4.9 and 4.10 can be easily used to implement Algorithm 7 in a library without complex arithmetic. More sophisticated optimizers like Adam can trivially support complex optimizer parameters with real-valued updates, which we explore in Section 4.4.4.

4.3.4 Scope and Limitations

For some games, we need higher-than-first-order information to converge – e.g., pure-response games – because the first-order information for a player is identically zero. So, momentum methods that only use first-order info will generally not converge. However, we can combine the methods with second-order information, as in the prior chapters, using momentum algorithms. The computational cost of complex momentum is almost identical to classical and negative momentum, except we now have a buffer with twice as many real parameters. We require one more optimization hyperparameter than the classical momentum, for which we provide an initial guess in Section 4.4.5.

4.4 Experiments

We investigate complex momentum’s performance in training GANs and games with different cooperative and adversarial eigenspaces mixtures, showing improvements over standard baselines.

Overview: We start with a purely adversarial Dirac-GAN and zero-sum games with known solutions $\omega^* = (\theta_A^*, \theta_B^*)$ and spectrums $\text{Sp}(\nabla_{\omega}\hat{g})$, so we can assess convergence rates. Next, we evaluate GANs that generate 2D distributions because they are simple enough to train with a plain, alternating SGD. Finally, we look at scaling to larger-scale GANs on images with brittle optimization, which requires optimizers like Adam. Complex momentum provides benefits in each setup. We only compare to first-order optimization methods, despite there being various second-order methods due to limitations discussed in Section 4.2.2.

4.4.1 Optimization in Purely Adversarial Games

Here, we consider optimizing the Dirac-GAN objective, which is surprisingly hard and where many classical optimization methods fail, because $\text{Sp}(\nabla_{\omega}\hat{g})$ is imaginary near solutions:

$$\min_x \max_y -\log(1 + \exp(-xy)) - \log(2) \tag{4.15}$$

Figure 4.4 empirically verifies the convergence rates given by Theorem 3 with Equation 4.14, by showing the optimization trajectories with simultaneous updates.

Figure 4.3 shows how the momentum components β affect the convergence rates with simultaneous updates and fixed step size. The best β was almost positive (that is, $\arg(\beta) = \epsilon$ for small ϵ). We repeat this experiment with alternating updates in Appendix Figure B.3, standard in GAN training. There, almost-positive momentum is best (but negative momentum also converges), and the benefit of alternating updates depends on whether we can parallelize player gradient evaluations.

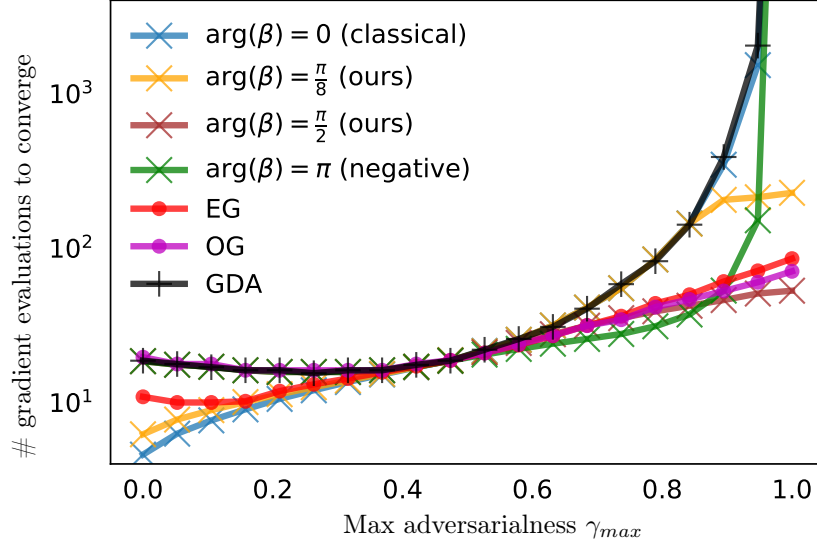


Figure 4.5: We compare first-order methods convergence rates on the game in Equation 4.16, with $\mathbf{A} = \mathbf{B}_1 = \mathbf{B}_2$ diagonal and entries linearly spaced in $[1/4, 4]$. We interpolate from purely cooperative to a mixture of purely cooperative and adversarial eigenspaces in $\text{Sp}(\nabla_{\omega} \hat{g})$ by making γ diagonal with $\gamma_j \sim U[0, \gamma_{max}]$, inducing the j^{th} eigenvalue pair to have $\arg(\lambda_j) \approx \pm \gamma_j \frac{\pi}{2}$. Therefore, γ_{max} controls the largest possible eigenvalue arg or *max adversarialness*. Every method generalizes gradient descent-ascent (GDA) by adding an optimizer parameter, tuned via grid search. **Positive momentum** and **negative momentum** do not converge if there are purely adversarial eigenspaces (i.e., $\gamma_{max} = 1$). **Almost-positive momentum** $\arg(\beta) = \epsilon > 0$ like $\pi/8$ allows us to approach the acceleration of positive momentum if sufficiently cooperative (i.e., $\gamma_{max} < 0.5$), while still converging if there are purely adversarial eigenspaces (i.e., $\gamma_{max} = 1$). Tuning $\arg(\beta)$ with complex momentum performs competitively with **extragradient (EG)**, **optimistic gradient (OG)** for any adversarialness – ex., $\arg(\beta) = \pi/2$ does well if there are purely adversarial eigenspaces (i.e., $\gamma_{max} = 1$).

4.4.2 Adversarialnesses Effect on Convergence

We compare optimization with first-order methods for purely adversarial, cooperative, and mixed games. We use the following game to easily interpolate between these regimes, where if $\gamma = \mathbf{I}$, it is purely adversarial, while if $\gamma = \mathbf{0}$ it is purely cooperative:

$$\min_{\mathbf{x}} \max_{\mathbf{y}} \mathbf{x}^{\top} (\gamma \mathbf{A}) \mathbf{y} + \mathbf{x}^{\top} ((\mathbf{I} - \gamma) \mathbf{B}_1) \mathbf{x} - \mathbf{y}^{\top} ((\mathbf{I} - \gamma) \mathbf{B}_2) \mathbf{y} \quad (4.16)$$

Appendix Figure B.2 explores $\text{Sp}(\mathbf{J})$ in purely adversarial games for various α, β , generalizing Figure 4 in Gidel et al. (2019). At every non-real β —i.e., $\arg(\beta) \neq \pi$ or 0 —we can select convergent $\alpha, |\beta|$.

Figure 4.5 compares the first-order algorithms as we interpolate from purely cooperative games (i.e., minimization) to mixtures of purely adversarial and cooperative eigenspaces because this setup range can occur during GAN training – see Figure 4.7. Our baselines are simultaneous SGD (or gradient descent-ascent (GDA)), extragradient (EG) (Korpelevich, 1976), optimistic gradient (OG) (Chiang et al., 2012; Rakhlin and Sridharan, 2013; Daskalakis et al., 2018), and momentum variants. We additionally *tuned the extrapolation parameters for EG and OG separately* – a nonstandard modification so that EG and OG are competitive with momentum in cooperative eigenspaces; see Appendix Section B.3.3. We show how many gradient evaluations for a set solution distance, and EG costs two evaluations per update. We optimize convergence rates for each game and method by grid search, as is common for optimization parameters in deep learning.

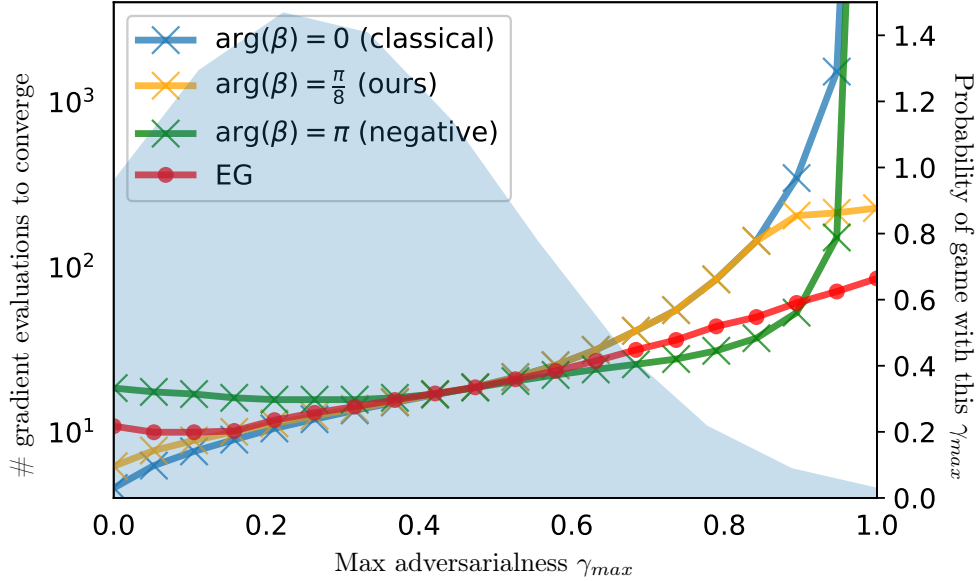


Figure 4.6: We show a setup where almost-positive, complex momentum with $\arg(\beta) = \pi/8$ minimizes risk over gradient evaluations by robustly converging for the distribution of games shown in light blue. We compare with the methods in Figure 4.5. In particular, we believe that this distribution of games may be a useful proxy for what occurs during GAN training. The distribution was calculated during the GAN training in Figure 4.7 by approximating the distribution of γ_{max} in the last 1000 training steps with a truncated Gaussian using the empirical mean and variance. We approximated γ_{max} by looking at the subset of eigenspaces in which the parameters lie and filtering any eigenspaces with a negative real part or where the component of the parameters in that eigenspace was smaller than 10^{-5} for simple visualization.

The x -axis in Figures 4.5 and 4.6 is the *max adversarialness*. Intuitively, this is just a rectangle’s (normalized) width bounding the spectrum in polar coordinates.

Takeaway: In the regime where all eigenspaces are cooperative – i.e., $\gamma_{max} < .5$ or $\max_{\lambda \in \text{Sp}(\nabla_{\omega} \hat{g})} |\Im(\lambda)|/|\Re(\lambda)| < 1$ – the best method is classical, positive momentum. Otherwise, we will benefit from a method to learn in games. If we have purely adversarial eigenspaces – i.e., $\gamma_{max} = 1$ – then GDA, positive and negative momentum fail to converge, while EG, OG, and complex momentum can converge. Choosing any non-real momentum β allows robust convergence for every eigenspace mixture. More so, almost-positive momentum β allows us to approach acceleration when cooperative while still converging if there are purely adversarial eigenspaces.

In games like GANs, our eigendecomposition is infeasible to compute and changes during training – see Appendix Figure B.4 – so we want an optimizer that converges robustly for any potential γ_{max} . A natural goal is to minimize the risk over the possible games of the number of gradient evaluations to converge. Figure 4.6 displays some methods from Figure 4.5 superimposed with a distribution of potential games. **Takeaway:** The best method is complex momentum because most of the game distribution is in cooperative eigenspaces (i.e., $\gamma_{max} < .5$) but could have purely adversarial eigenspaces (i.e., $\gamma_{max} = 1$). Also, we believe that the displayed game distribution could be a reasonable proxy for what is encountered in GAN training.

4.4.3 Training GANs on 2D Distributions

Here, we investigate improving GAN training using alternating gradient descent updates with complex momentum. We examine alternating updates because they are standard in GAN training (Goodfellow et al., 2014; Brock et al., 2018; Wu et al., 2019). We focus on comparisons to positive and negative momentum, the strongest baselines. Note that EG and OG do not have obvious generalizations to alternating updates. We train to generate a 2D mixture of Gaussians because more complicated distributions require more complicated optimizers than SGD. Figure 4.1 shows all the changes necessary to use the JAX momentum optimizer for our updates, with complete details in Appendix B.3.4. We evaluated the log-likelihood of GAN samples under the mixture as an imperfect proxy for matching.

Appendix Figure B.5 shows heatmaps for tuning $\arg(\beta)$ and $|\beta|$ with select step sizes. **Takeaway:** The best momentum was found at the almost-positive $\beta \approx 0.7 \exp(i\pi/8)$ with step size $\alpha = 0.03$, and for each α we tested a broad range of non-real β outperformed any real β . This suggests we can often improve GAN training with alternating updates and complex momentum.

4.4.4 Training BigGAN with a Complex Adam

Here, we investigate improving larger-scale GAN training with complex momentum. However, larger-scale GANs train with more complicated optimizers than gradient descent – like Adam (Kingma and Ba, 2014) – and have notoriously brittle optimization. We looked at training BigGAN (Brock et al., 2018) on CIFAR-10 (Krizhevsky, 2009) but were unable to succeed with optimizers other than (Brock et al., 2018)-supplied setups due to brittle optimization. So, we attempted to change the procedure minimally by taking (Brock et al., 2018)-supplied code [here](#) which was trained with Adam and making only the β_1 parameter – analogous to momentum – complex. The modified complex Adam is shown in Algorithm 8, where the momentum bias correction is removed to match our theory better. It is an open question of how best to carry over the design of Adam (or other optimizers) to the complex setting. Training each BigGAN took 10 hours on an NVIDIA T4 GPU, so Figure B.8 and Table 4.1 took about 1000 and 600 GPU hours, respectively.

Figure B.8 shows a grid search on $\arg(\beta_1)$ and $|\beta_1|$ for a BigGAN trained with Algorithm 8. We only changed β_1 for the discriminator’s optimizer. **Takeaway:** The best momentum was at the almost-positive $\beta_1 \approx 0.8 \exp(i\pi/8)$, whose samples are in Appendix Figure B.7.

Algorithm 8 Complex Adam variant without momentum bias-correction

```

1:  $\beta_1 \in \mathbb{C}, \beta_2 \in [0, 1)$ 
2:  $\alpha \in \mathbb{R}^+, \epsilon \in \mathbb{R}^+$ 
3: for  $j = 1 \dots N$  do
4:    $\boldsymbol{\mu}^{j+1} = \beta_1 \boldsymbol{\mu}^j - \mathbf{g}^j$ 
5:    $\mathbf{v}^{j+1} = \beta_2 \mathbf{v}^j + (1 - \beta_2) (\mathbf{g}^j)^2$ 
6:    $\hat{\mathbf{v}}^{j+1} = \frac{\mathbf{v}^{j+1}}{1 - (\beta_2)^j}$ 
7:    $\boldsymbol{\omega}^{j+1} = \boldsymbol{\omega}^j + \alpha \frac{\Re(\boldsymbol{\mu}^j)}{\sqrt{\hat{\mathbf{v}}^{j+1} + \epsilon}}$ 
8: end for
9: return  $\boldsymbol{\omega}^N$ 

```

Discriminator β_1	CIFAR-10 BigGAN IS for 10 seeds			
	Max	Mean	Median	Std.
0, BigGAN default	9.10	8.93	8.89	0.076
.8 $\exp(i\pi/8)$, ours	9.25(+.15)	8.97(+.04)	8.97(.08)	0.079(.003)
.8	9.05(-.05)	7.19(-1.7)	8.82(.07)	2.753(2.67)

Table 4.1: We display the inception scores (IS) found over 10 runs for training BigGAN on CIFAR-10 with various optimizer settings. We use a complex Adam variant described in Algorithm 8, where we only tuned β_1 for the discriminator. The best parameters found in Appendix Figure B.8 were $\beta_1 = 0.8 \exp(i\pi/8)$, which improved the maximum IS in our runs, as well as the final mean and median IS of the BigGAN authors baseline, which was the SoTA optimizer in this setting to the best of our knowledge. We tested $\beta_1 = 0.8$ to see if the gain was only due to tuning $|\beta_1|$, which occasionally failed and decreased the IS.

We tested the best momentum value over 10 seeds against the author-provided baseline in Appendix Figure B.9, with the results summarized in Table 4.1. **Takeaway:** Our method improves the mean inception score (IS) with a t -test significance of 0.071, which shows the desired phenomena – i.e., complex momentum improving training – with a reasonable significance. Furthermore, the complex momentum improves the best IS found with 9.25(+.15 over author code, +.03 author reported). Brock et al. (2018) reported a single inception score on CIFAR-10 of 9.22, but the best we could reproduce on the seeds with the provided PyTorch code and settings was 9.10.

We trained a real momentum $|\beta_1| = 0.8$ to see if the improvement was solely due to the adjustment of the momentum magnitude. This occasionally failed to train and decreased the best IS over re-runs, showing that we benefit from a non-zero $\arg(\beta_1)$.

4.4.5 A Practical Initial Guess for the Momentum’s Argument

We propose a practical initial guess for our new hyperparameter $\arg(\beta)$. Corollary 1 shows that we can use almost-real momentum coefficients (i.e., $\arg(\beta)$ is near, but not equal to 0). Figure 4.5 shows almost-positive β approach acceleration in cooperative eigenspaces while converging in all eigenspaces. Figure 4.7 shows that GANs can have cooperative and adversarial eigenspaces. Figure 4.6 shows a distribution of games – from GAN training – where almost-positive β robustly converges and minimizes the risk of gradient evaluations. Figures B.5 and B.8 perform a grid search over $\arg(\beta)$ for GANs, finding that almost-positive $\arg(\beta) \approx \pi/8$ works in both cases. Also, by minimally changing $\arg(\beta)$ from 0 to a small ϵ , we can minimally change other hyperparameters in our model, which is useful to adapt existing, brittle setups like in GANs. Based on this, we propose an initial guess of $\arg(\beta) = \epsilon$ for a small $\epsilon > 0$, where $\epsilon = \pi/8$ worked in our GAN experiments.

4.5 Related Work

Accelerated first-order methods: A broad body of work exists using momentum-type methods (Polyak, 1964; Nesterov, 1983, 2013; Maddison et al., 2018), with a recent focus on deep learning (Sutskever et al., 2013; Zhang and Mitliagkas, 2017; Choi et al., 2019; Zhang et al., 2019b; Chen et al., 2020). But these focus on momentum for minimization as opposed to in games.

Learning in games: Various works approximate response-gradients - some by differentiating through optimization (Foerster et al., 2018; Mescheder et al., 2017; Maclaurin et al., 2015a) - or leverage game eigenstructure during optimization (Letcher et al., 2019; Nagarajan et al., 2020; Omidshafiei et al., 2020; Czarnecki et al., 2020; Gidel et al., 2020; Perolat et al., 2020).

First-order methods in games: Zhang et al. (2021a, 2020b); Ibrahim et al. (2020); Bailey et al. (2020); Jin et al. (2020); Azizian et al. (2020a); Nouiehed et al. (2019); Zhang et al. (2020c); Zhang (2023) characterize convergence with various first-order methods. Gidel et al. (2019) is the closest work to ours; showing a negative momentum can help in some games. Zhang and Wang (2020) note the suboptimality of negative momentum in a class of games. Azizian et al. (2020b); Domingo-Enrich et al. (2020) investigate acceleration in some games.

Bilinear zero-sum games: Zhang and Yu (2019) study the convergence of gradient methods in bilinear zero-sum games, extending Gidel et al. (2019), showing we can achieve faster convergence with separate step sizes and momentum for each player or tuning the extragradient step size. Loizou et al. (2020) provide convergence guarantees for games that satisfy a *sufficiently bilinear* condition.

Learning in GANs: Various works make GAN training easier with methods that leverage the structure of the game (Liu et al., 2020; Peng et al., 2020; Albuquerque et al., 2019; Wu et al., 2019; Hsieh et al., 2019). Metz et al. (2016) approximate the discriminator’s response function by differentiating through optimization. Mescheder et al. (2017) find solutions by minimizing the norm of the players’ updates. These methods and various others (Qin et al., 2020; Schäfer et al., 2019; Jolicoeur-Martineau and Mitliagkas, 2019) require higher-order information. Daskalakis et al. (2018); Gidel et al. (2018); Chavdarova et al. (2019) look at first-order methods. Mescheder et al. (2018) explore problems for GAN training convergence and Berard et al. (2019) show that GANs have significant rotations in learning.

4.6 Conclusion

In this chapter, we generalized existing momentum methods for learning in differentiable games by allowing complex momentum with real-valued updates. Our method robustly converges in games with a different range of cooperative and adversarial eigenspace mixtures than existing methods. We also presented a practical generalization of our method to the Adam optimizer, which we used to improve BigGAN training. More generally, we highlight and lay the groundwork for investigating optimizers that work well with various mixtures of cooperative and competitive dynamics in games.

Acknowledgements

Resources used in preparing this research were provided, in part, by the Province of Ontario, the Canadian government through CIFAR, and companies sponsoring the Vector Institute. Paul Vicol was supported by an NSERC PGS-D Scholarship. We thank Guodong Zhang, Guojun Zhang, James Lucas, Romina Abachi, Jonah Phillion, Will Grathwohl, Jakob Foerster, Murat Erdogdu, Ken Jackson, Ioannis Mitliagkis, and Barbara Norton for feedback and discussion.

My Contributions Towards this Paper As it Pertains to the Thesis

I contributed the initial idea to this project, ran all small-scale experiments, collaborated on full-scale experiments, did all the theoretical work, and did most of the writing. This paper was also submitted to arXiv (Lorraine et al., 2021a).

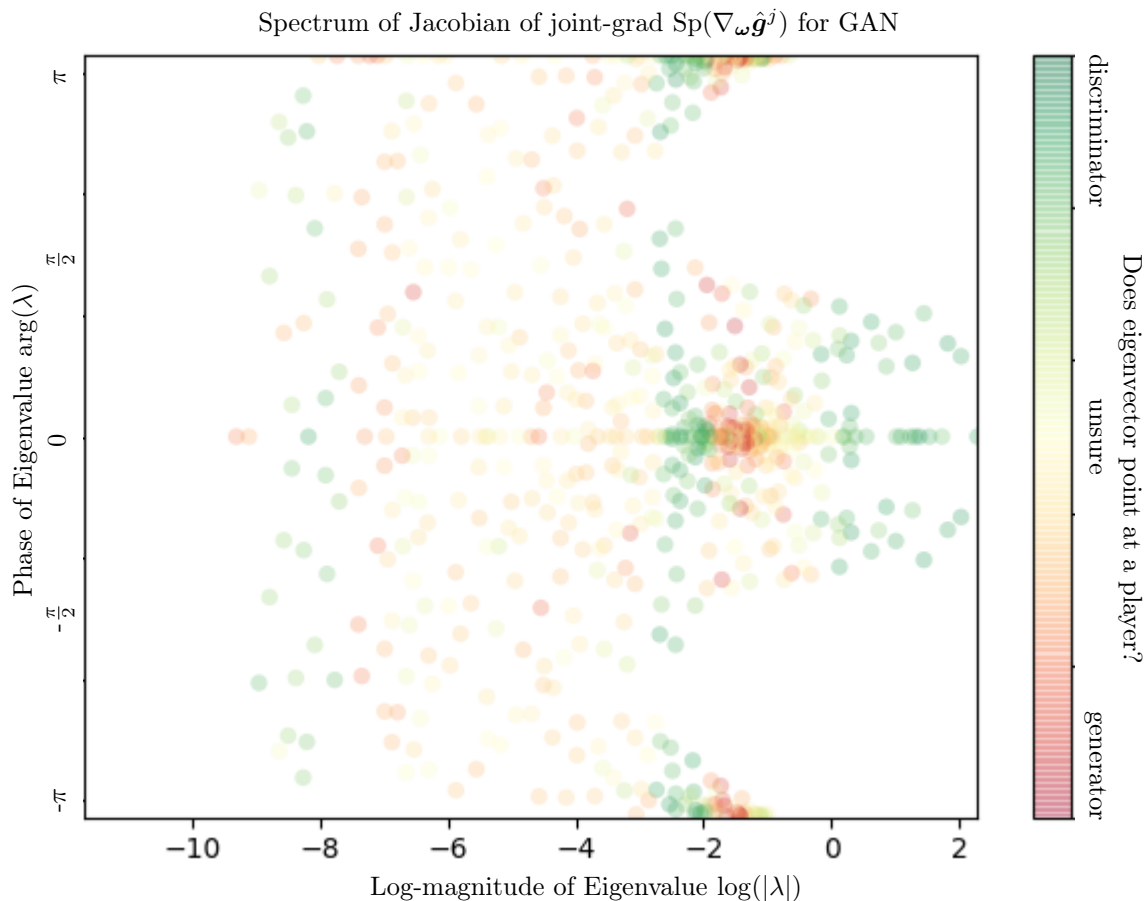


Figure 4.7: A log-polar visualization reveals structure in the spectrum for a GAN at the end of the training on a 2D mixture of Gaussians with a 1-layer discriminator and generator, so the joint-parameters $\omega \in \mathbb{R}^{723}$. Appendix Figure B.4 shows the spectrum through training. There is a mixture of many cooperatives (that is, real or $\arg(\lambda) \approx 0, \pm\pi$) and some adversarial (i.e., imaginary or $\arg(\lambda) \approx \pm\frac{\pi}{2}$) eigenvalues, so – contrary to what the name may suggest – generative adversarial networks are not purely adversarial. We may benefit from optimizers that leverage this structure, such as complex momentum.

Eigenvalues are colored if the associated eigenvector is mostly in one player’s part of the joint-parameter space – see Appendix Figure B.4 for details on this. Many eigenvectors lie mostly in the space of (or point at) one player. The structure of the set of eigenvalues for the discriminator (green) is different from the generator (red), but further investigation of this is an open problem. In particular, this may motivate separate optimizer choices for each player, as in Section 4.4.4.

Chapter 5

Lyapunov Exponents for Diversity in Differentiable Games

Ridge Rider (RR) is a method to find diverse solutions in optimization problems by following eigenvectors of the Hessian (“ridges”). RR is designed for conservative gradient systems (i.e., settings with a single loss/potential function), where it branches at saddles — easy-to-find bifurcations. We generalize RR to nonconservative, multi-agent gradient systems by proposing the Generalized Ridge Rider (GRR) method to find arbitrary bifurcations. We give theoretical motivation for our method by leveraging tools from the field of dynamical systems. We construct novel toy problems where we visualize new phenomena while giving insight into high-dimensional problems of interest. Finally, we empirically evaluate our method by finding diverse solutions to the iterated prisoners’ dilemma and machine learning problems, including generative adversarial networks.

5.1 Introduction

Selecting solutions with desirable properties that an arbitrary (global or local) minimum might not have is often useful. For example, finding solutions in image classification using shapes that generalize more effectively than textures. Important examples of this in single-objective minimization are seeking solutions that generalize to unseen data in supervised learning (Geirhos et al., 2018, 2020), in policy optimization (Cully et al., 2015), and generative models (Song et al., 2020). Many real-world systems are not so simple and instead involve multiple agents, each using a different subset of parameters to minimize their own objective. Some examples are generative adversarial networks (GANs) (Goodfellow et al., 2014; Pfau and Vinyals, 2016), actor-critic models (Pfau and Vinyals, 2016), curriculum learning (Bengio et al., 2009; Baker et al., 2019; Balduzzi et al., 2019; Sukhbaatar et al., 2018), hyperparameter optimization (Domke, 2012; Maclaurin et al., 2015a; Lorraine and Duvenaud, 2017; MacKay et al., 2019a; Raghu et al., 2020; Lorraine et al., 2020b; Raghu et al., 2021a), adversarial examples (Bose et al., 2020; Yuan et al., 2019), learning models (Rajeswaran et al., 2020; Bacon et al., 2019; Nikishin et al., 2021), domain adversarial adaptation (Acuna et al., 2021), neural architecture search (Zoph and Le, 2016; Real et al., 2019; Liu et al., 2018; Grathwohl et al., 2018; Adam and Lorraine, 2019), multi-agent settings (Foerster et al., 2018) and meta-learning (Ren et al., 2018a; Rajeswaran et al., 2019; Ren et al., 2020). In these settings, the aim is to find one equilibrium – of potentially many equilibria – where the agents exhibit some desired behavior.

For example, in the iterated prisoners’ dilemma (Section 5.5), solutions favoring reciprocity over unconditional defection result in higher returns for all agents. In GANs, solutions often generate a subset of the modes of the target distribution (Arjovsky et al., 2017), and in Hanabi, some solutions coordinate better with humans (Hu et al., 2020). Existing methods often find solutions in small subspaces – even after many random restarts, as shown in Table 5.1. By finding a diverse set of equilibria, we may be able to (a) find solutions with a better joint outcome, (b) develop stronger generative models in adversarial learning, or (c) find solutions that coordinate better with humans.

Recently, Ridge Rider (RR) (Parker-Holder et al., 2020a) proposed a method to find diverse solutions in *single-objective* optimization. RR is a branching tree search, which starts at a stationary point and then follows different *eigenvectors of the Hessian* (“ridges”) with negative eigenvalues, moving downhill from saddle point to saddle point. In settings where multiple agents each have their own objective (i.e., games), the relevant generalization of the Hessian — the *game Hessian* (Balduzzi et al., 2018) in Equation 5.6 — is not symmetric. Thus, the game Hessian generally has complex eigenvalues (EVals) with associated complex eigenvectors, making RR not directly applicable.

In this chapter, we generalize RR to multiagent settings using machinery from *dynamical systems*. We connect RR with methods for finding *bifurcation* points, i.e., points where small changes in the initial parameters lead to different optimization dynamics and learning outcomes. We propose novel metrics inspired by *Lyapunov exponents* (Katok and Hasselblatt, 1997) that measure the speed with which learning trajectories separate. These metrics generalize the branching criterion from RR, allowing us to locate a broad class of potential bifurcations and find more diverse behavior. Starting points with rapid trajectory separation can be found via gradient-based optimization by differentiating through the exponent calculation, which is implemented efficiently for large models with Jacobian-vector products. Our contributions include:

- Connections between finding diverse solutions and Lyapunov exponents, allowing us to leverage a broad body of work in dynamical systems.
- Proposing Generalized Ridge Rider (GRR), scaling Ridge Rider (RR) to differentiable games.
- Presenting novel diagnostic problem settings based on high dimensional games like the iterated prisoners dilemma (IPD) and GANs to study various bifurcation types.
- Compared to existing methods, GRR finds diverse solutions in the IPD, spanning cooperation, defection, and reciprocity.
- Lastly, we present larger-scale experiments on GANs — a model class of interest to the machine learning community.

5.2 Background

Appendix Table C.1 summarizes our notation. As before, consider the single-objective problem:

$$\boldsymbol{\theta}^* \in \underset{\boldsymbol{\theta}}{\operatorname{argmin}} \mathcal{L}(\boldsymbol{\theta}) \quad (5.1)$$

Again, we denote the gradient of the loss at parameters $\boldsymbol{\theta}^j$ by $\mathbf{g}^j := \mathbf{g}(\boldsymbol{\theta}^j) := \nabla_{\boldsymbol{\theta}} \mathcal{L}(\boldsymbol{\theta})|_{\boldsymbol{\theta}^j}$. We can locally minimize the loss \mathcal{L} using gradient descent with step size α :

$$\boldsymbol{\theta}^{j+1} = \boldsymbol{\theta}^j - \alpha \mathbf{g}^j \quad (5.2)$$

Due to the potential non-convexity of \mathcal{L} , multiple stationary points can exist, and gradient descent will only find a particular solution based on the initialization $\boldsymbol{\theta}^0$.

5.2.1 Ridge Rider (RR)

Ridge Rider (RR) (Parker-Holder et al., 2020a) finds diverse solutions in single-objective minimization problems. The method first finds a saddle point, either analytically as in tabular reinforcement learning or by minimizing the gradient norm.

Then, RR branches the optimization procedure following different directions (or “ridges”) given by the eigenvectors of the Hessian $\mathcal{H} = \nabla_{\boldsymbol{\theta}} \mathbf{g} = \nabla_{\boldsymbol{\theta}} (\nabla_{\boldsymbol{\theta}} \mathcal{L})$. The complete computation of the eigendecomposition of \mathcal{H} , i.e., its eigenvectors and eigenvalues, is often prohibitively expensive. However, we can efficiently access some of the eigenspaces via Hessian-vector products $\mathcal{H}\mathbf{v} = \nabla_{\boldsymbol{\theta}} ((\nabla_{\boldsymbol{\theta}} \mathcal{L})\mathbf{v})$ (Pearlmutter, 1994; Abadi et al., 2015; Paszke et al., 2017; Bradbury et al., 2018).

5.2.2 Optimization in Games

Instead of simply optimizing a single loss, optimization in games involves multiple agents, each with a loss function that can depend on other agents. Again, we look at 2-player games with players (denoted by A and B) who want to minimize their loss – $\mathcal{L}_A(\boldsymbol{\theta}_A, \boldsymbol{\theta}_B)$ or $\mathcal{L}_B(\boldsymbol{\theta}_A, \boldsymbol{\theta}_B)$ – with their parameters – $\boldsymbol{\theta}_A$ or $\boldsymbol{\theta}_B$.

$$\boldsymbol{\theta}_A^* \in \underset{\boldsymbol{\theta}_A}{\operatorname{argmin}} \mathcal{L}_A(\boldsymbol{\theta}_A, \boldsymbol{\theta}_B^*), \boldsymbol{\theta}_B^* \in \underset{\boldsymbol{\theta}_B}{\operatorname{argmin}} \mathcal{L}_B(\boldsymbol{\theta}_A^*, \boldsymbol{\theta}_B) \quad (5.3)$$

One of the simplest optimization methods is to find local solutions simply by following the players’ gradients, but this is often unstable (Bailey et al., 2020). Here, $\mathbf{g}_A^j = \mathbf{g}_A(\boldsymbol{\theta}_A^j, \boldsymbol{\theta}_B^j)$ is an estimator for $\nabla_{\boldsymbol{\theta}_A} \mathcal{L}_A|_{\boldsymbol{\theta}_A^j, \boldsymbol{\theta}_B^j}$ with \mathbf{g}_B^j defined analogously, and the simultaneous gradient update is:

$$\boldsymbol{\theta}_A^{j+1} = \boldsymbol{\theta}_A^j - \alpha \mathbf{g}_A^j, \quad \boldsymbol{\theta}_B^{j+1} = \boldsymbol{\theta}_B^j - \alpha \mathbf{g}_B^j \quad (\text{SimSGD})$$

Again, we denote the concatenation of all players’ parameters (or joint-parameters) $\boldsymbol{\omega} = [\boldsymbol{\theta}_A, \boldsymbol{\theta}_B] \in \mathbb{R}^d$ and the joint-gradient vector field $\hat{\mathbf{g}} : \mathbb{R}^d \rightarrow \mathbb{R}^d$, denoted at the j^{th} iteration by:

$$\hat{\mathbf{g}}^j = \hat{\mathbf{g}}(\boldsymbol{\omega}^j) = \left[\mathbf{g}_A(\boldsymbol{\omega}^j), \mathbf{g}_B(\boldsymbol{\omega}^j) \right] = \left[\mathbf{g}_A^j, \mathbf{g}_B^j \right] \quad (5.4)$$

We write the next iterate in SimSGD with the fixed-point operator \mathbf{F} :

$$\omega^{j+1} = \mathbf{F}_{SGD}(\omega^j) = \omega^j - \alpha \hat{\mathbf{g}}^j \quad (5.5)$$

As in Chapter 4, the Jacobian of the fixed-point operator \mathbf{F} – denoted \mathbf{J} – is useful for analysis, including bounding convergence rates near fixed-points (Bertsekas, 2008) and finding points where local changes to parameters cause convergence to qualitatively different solutions (Hale and Koçak, 2012). The Jacobian of the fixed-point operator crucially depends on the Jacobian of the joint-gradient $\hat{\mathbf{g}}$, which is called the *game Hessian* (Letcher et al., 2019) because it generalizes the Hessian:

$$\hat{\mathcal{H}} := \nabla_{\omega} \hat{\mathbf{g}} = \begin{bmatrix} \nabla_{\theta_A}^2 \mathcal{L}_A & \nabla_{\theta_A} \nabla_{\theta_B} \mathcal{L}_A \\ \nabla_{\theta_B} \nabla_{\theta_A} \mathcal{L}_B^\top & \nabla_{\theta_B}^2 \mathcal{L}_B \end{bmatrix} \quad (5.6)$$

$$\mathbf{J}_{SGD} := \nabla_{\omega} \mathbf{F}_{SGD}(\omega) = \mathbf{I} - \alpha \hat{\mathcal{H}} \quad (5.7)$$

Figure 5.2 shows a game with a solution we can only converge to using an appropriate optimizer. Thus, we must incorporate information about the optimizer to generalize RR, which we do by using the (largest) eigenvalues/vectors of \mathbf{J} instead of the (most negative) eigenvalues/vectors of $\hat{\mathcal{H}}$.

The crucial difference between optimization with a single and multiple objectives is as follows: In single-objective optimization, following the gradient forms trajectories from a conservative vector field because $\hat{\mathcal{H}} = \mathcal{H}$ is the Hessian of the loss, which is symmetric and has real eigenvalues. However, in games with multiple objectives, $\hat{\mathcal{H}}$ can be non-symmetric and have complex eigenvalues, resulting in a nonconservative vector field from optimization, opening the door to many new phenomena.

5.3 Methods for Generalizing RR

Here, we present two key contributions for generalizing RR to games. We first connect diversity in optimization to the concept of bifurcations, where a small change in the parameters causes a large change in the optimization trajectories. Second, we introduce Lyapunov exponents (Katok and Hasselblatt, 1997) and easy-to-optimize variants to find these bifurcations.

5.3.1 Connecting Diversity and Bifurcations

In dynamical systems, *bifurcations* are regions of the parameter space where small perturbations result in qualitatively different optimization trajectories. In general, a dynamical system can contain various bifurcation types. In contrast, saddle points (and their separatrix) are the only relevant bifurcation type in conservative gradient vector fields. Consequently, their eigenvectors play a key role in the shape of the phase portraits, which are geometric representations of the underlying dynamics. In particular, the negative eigenvectors are orthogonal to separatrices (Tabor, 1989), boundaries between regions in our system with different dynamical behavior, thus providing directions to move in for finding different solutions. This perspective provides a novel view of RR, which branches at saddle points, the relevant class of bifurcation points in single-loss optimization.

However, in the literature on dynamical systems, many bifurcation types have been studied (Katok and Hasselblatt, 1997). This inspires generalizing RR to nonconservative gradient fields (e.g., multi-agent settings) where various bifurcations occur. See Figure 5.2 for a *Hopf bifurcation* (Hale and Koçak, 2012) or Figure 5.7 for various others.

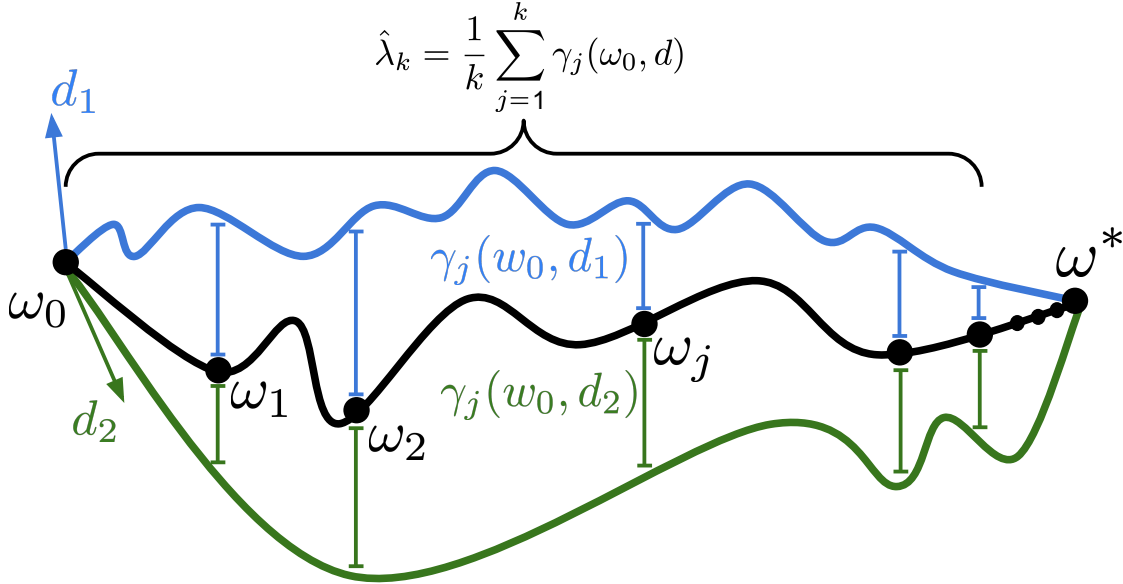


Figure 5.1: Visualization of the components to a Lyapunov exponent $\hat{\lambda}_k(\omega_0, \mathbf{d})$ described in Equations 5.8, 5.9, which measures how quickly trajectories separate starting at a point ω_0 in direction \mathbf{d} . Here, the optimization trajectory iterates ω_j accumulate at a fixed-point ω^* . We show two displacements – \mathbf{d}_1 and \mathbf{d}_2 – resulting in separate “perturbed” trajectories as shown in blue and green. We measure the separation rate between the true and perturbed trajectories at the j^{th} optimizer iteration with the Lyapunov term $\gamma_j(\omega_0, \mathbf{d})$. The exponent $\hat{\lambda}_k(\omega_0, \mathbf{d})$ is the average of the first k terms. See Figure 5.6 for actual trajectories on a toy problem used in an exponent calculation.

5.3.2 Lyapunov Exponents for Bifurcations

Using tools from dynamical systems research, we look at how to find general bifurcation points. Our objectives are inspired by the Lyapunov exponent, which measures asymptotic separation rates of optimization trajectories for small perturbations. We use a similar quantity but for finite-length trajectories. Given a k -step trajectory generated by our fixed-point operator \mathbf{F} – i.e., optimizer – with initialization ω_0 and Jacobian at iteration j of \mathbf{J}^j , we measure the separation rate for an initial normalized displacement \mathbf{d} with:

$$\hat{\lambda}_k(\omega_0, \mathbf{d}) = \frac{1}{k} \sum_{j=1}^k \gamma_j(\omega_0, \mathbf{d}), \quad (5.8)$$

$$\text{where } \gamma_j(\omega_0, \mathbf{d}) := \log \left(\mathbf{d}^\top \left(\mathbf{J}^{j-1}(\omega_0) \right)^\top \mathbf{J}^{j-1}(\omega_0) \mathbf{d} \right) \quad (5.9)$$

We call γ_j the j^{th} *Lyapunov term*. When $k = 0$, the $\hat{\lambda}$ are called the *local Lyapunov exponents*, while as $k \rightarrow \infty$ they are called the *(global) Lyapunov exponents* (Wolff, 1992). We denote this as the *k-step or truncated Lyapunov exponent*. Figure 5.1 visualizes the exponents’ calculation, providing additional intuition. In the future, we suppress the dependency of \mathbf{J}^{j-1} on ω_0 to simplify notation.

Within a basin of attraction to a given fixed-point, the global Lyapunov exponent is constant (Katok and Hasselblatt, 1997). Intuitively, this is because an arbitrarily high number of Lyapunov terms near the fixed-point dominate the average defining the exponent in Equation 5.8. This property prevents us from optimizing the global exponent using gradients, making it a poor bifurcation objective. As such, our interest in the truncated exponent is motivated from multiple directions:

1. Non-zero gradient signals for finding bifurcations
2. Computationally tractability
3. A better separation rate description for the finite trajectories used in practice

However, unlike the global exponent, the truncated version has less theoretical results. In more than one dimension, the k -step Lyapunov exponent depends on the perturbation direction \mathbf{d} (Tabor, 1989). We look at using the direction for maximal separation — i.e., the *max k -step Lyapunov exponent*:

$$\hat{\lambda}_k^{\max}(\boldsymbol{\omega}_0) = \max_{\mathbf{d}, \|\mathbf{d}\|=1} \hat{\lambda}_k(\boldsymbol{\omega}_0, \mathbf{d}) \quad (5.10)$$

For dynamical systems with basins of attraction to fixed points, common in optimization, the max exponent is the largest on the boundary between basins, motivating maximizing the max exponent to find bifurcations. The max exponent can be evaluated by finding the largest eigenvalue of an average of Jacobians over the optimization steps (Katok and Hasselblatt, 1997):

$$\mathbf{J}^\dagger = \frac{1}{k} \sum_{j=1}^k \left(\mathbf{J}^{j-1} \right)^\top \left(\mathbf{J}^{j-1} \right), \quad (5.11)$$

$$\hat{\lambda}_k^{\max}(\boldsymbol{\omega}_0) = \max_{\lambda \in \text{Sp}(\mathbf{J}^\dagger)} |\lambda| \quad (5.12)$$

Importantly, in higher dimensions, an eigenvalue dominates the spectrum of \mathbf{J} after many steps (Loreto et al., 1996; Kachman et al., 2017).

We note some practical points for computing these exponents: When $k = 1$, the maximum exponent is the maximum eigenvalue of \mathbf{J}^0 . As $k \rightarrow \infty$ and our fixed-point operator converges to a fixed-point $\boldsymbol{\omega}^*$, the maximum exponent is the maximum eigenvalue of \mathbf{J} at $\boldsymbol{\omega}^*$. Calculating $\hat{\lambda}_k^{\max}$ is easiest when $k = 1$ or $k \rightarrow \infty$, e.g., by power iteration on the relevant \mathbf{J} . For intermediary k , directly using leading eigenvalues of \mathbf{J}^\dagger can often involve re-evaluating the entire optimization trajectory. Instead, it can be easier to work with bounds. A simple lower bound is formed by using the leading eigenvector in any single step, or an upper bound by using the leading eigenvector in each step, which are tight as $k \rightarrow \infty$ (Loreto et al., 1996). We investigate these strategies in Appendix Figure C.2.

We aim to obtain many qualitatively different solutions from a single starting point, which motivates the simultaneous optimization of the exponents corresponding to multiple different directions. Relatedly, the sum of positive global Lyapunov exponents estimates the Kolmogorov–Sinai or metric entropy by Pesin’s theorem (Pesin, 1977). We use this to motivate different performance metrics in Section 5.4.2.

5.4 Proposed Algorithms

Having given an overview of the key mathematical concepts, we now present our overall algorithm. First, we introduce a general branching-tree search framework to find diverse solutions in differentiable games. Next, we present our method – Generalized Ridge Rider (GRR) – which implements this framework using truncated Lyapunov exponents (Equation 5.10) as the branching criterion. Lastly, we highlight the differences between GRR and RR.

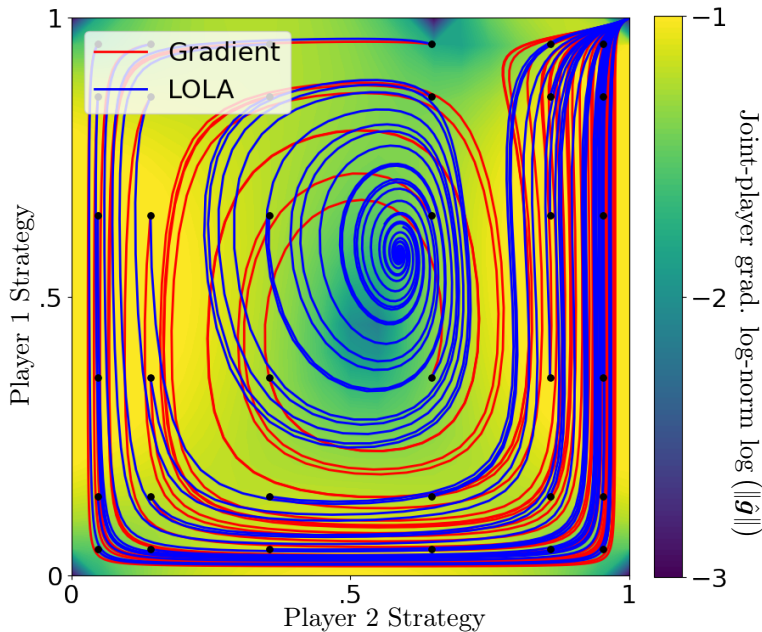


Figure 5.2: The phase portrait for two standard optimization algorithms on the mixed small IPD and Matching Pennies problem. We show the trajectories following the gradient with SimSGD in red and LOLA (Foerster et al., 2018) – a method for learning in games – in blue. All SimSGD initializations find only the solution on the top right because the center solution has imaginary eigenvalues, while LOLA finds all solutions. For comparisons on more test problems, see Appendix Figure C.1.

5.4.1 Branching Optimization Tree Searches

Our framework is a generalized version of RR and contains the following components:

1. A method for finding a suitable *starting point* for our branching process - see Figure 5.6.
2. A process for selecting *branching directions* (or perturbations) from a given branching point - see Figure 5.4.
3. A prescription for how to *continue the optimization process* along a given branch after the initial perturbation.
4. A re-branching decision rule, i.e., when to return to step 2. This was important in RR because optimizers in high-dimensional non-convex machine learning problems often finish at saddle points (Yao et al., 2020).
5. Lastly, a metric to rank the different solutions.

We visualize this process in Figure 5.3. RR is an instance of this general process where each component is suitable for single-objective optimization. In the next section, we present another instance of this method, designed for game optimization. We include a more detailed description of branching tree searches in Appendix Algorithm 13, highlighting the important changes compared to RR.

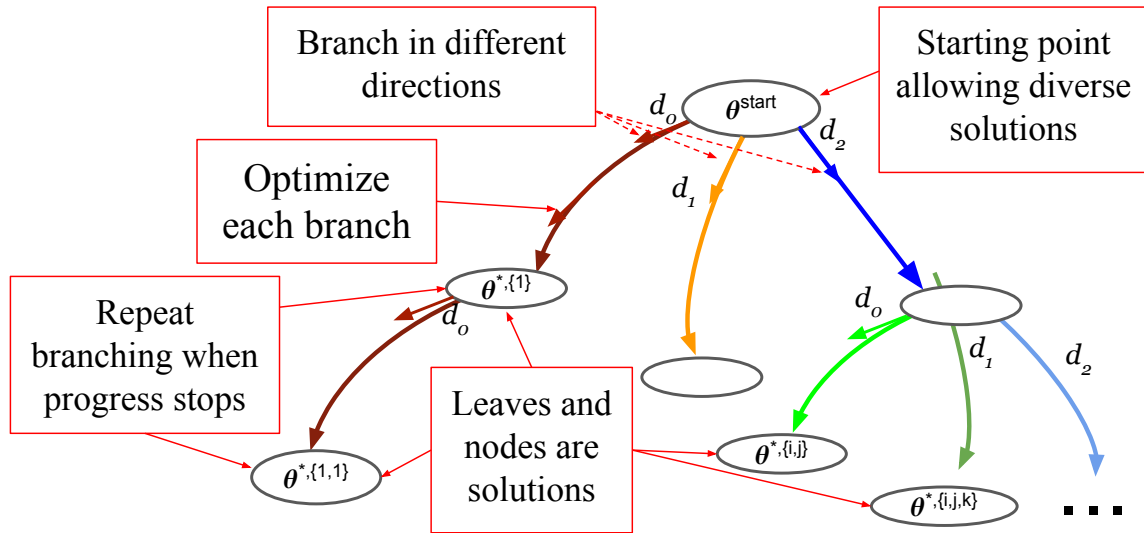


Figure 5.3: A visualization of branching optimization tree search with components: (1) selecting the starting point, (2) creating branches, (3) optimizing each branch, and (4) choosing when to re-branch.

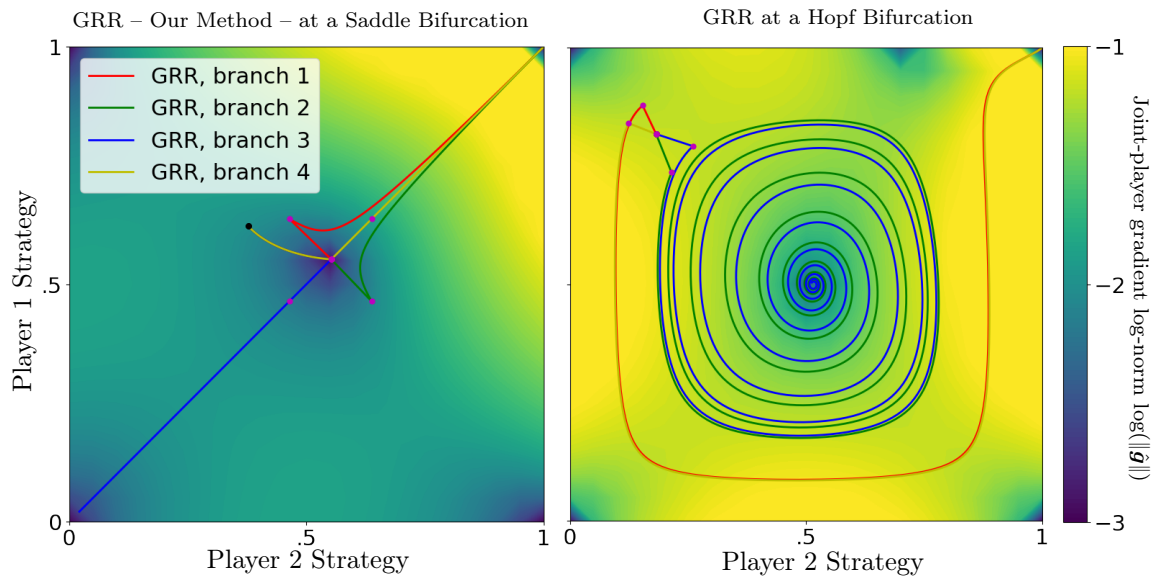


Figure 5.4: We show branching at different bifurcations obtained by optimizing a Lyapunov exponent as shown in Figure 5.6. In each setup, we have two eigenvectors that branch in opposite directions, giving four paths displayed in different colors. The steps with the eigenvector have magenta circles marking boundaries. *Left*: In the small IPD, finding, then branching at a saddle – where the joint-player gradient log-norm $\log(\|\hat{g}\|)$ is 0 – allows us to find defect-defect and tit-for-tat solutions. *Right*: In the Mixed Problem of Small IPD and Matching Pennies, branching at the Hopf bifurcation allows us to find both solutions. There are no saddle points near the bifurcation, so RR’s starting point does not allow branching to find both solutions.

5.4.2 Generalized Ridge Rider (GRR)

Starting point: Motivated by Section 5.3.2, we look at optimizing the maximal k -step Lyapunov exponent from Equation 5.10 to obtain our starting point:

$$\mathcal{L}(\omega_0) = -\hat{\lambda}_k^{\max}(\omega_0) = -\max_{\mathbf{d}, \|\mathbf{d}\|=1} \hat{\lambda}_k(\omega_0, \mathbf{d}) \quad (5.13)$$

However, using a single exponent only guarantees trajectory separation in a single direction. If we want to branch across multiple bifurcations in different directions, we need an objective using exponents in multiple directions. We look at the simple objective choice by adding exponents:

$$\mathcal{L}_n^{\text{sum}}(\omega_0) = -\max_{\mathbf{d}_1, \dots, \mathbf{d}_n} \sum_{l=1}^n \hat{\lambda}_k(\omega_0, \mathbf{d}_l), \quad (5.14)$$

$$\text{such that } \|\mathbf{d}_l\| = 1, \mathbf{d}_l^\top \mathbf{d}_m = 0 \text{ for all } l, m \in 1, \dots, n, l \neq m \quad (5.15)$$

Intuitively, the constraint guarantees that we have different directions to separate in by making them orthogonal. It is straightforward to evaluate this objective by evaluating the top- n eigenvalues of the matrix from Equation 5.11. More generally, various functions of the k -step exponents in different directions form reasonable objectives more amenable to optimization. Specifically, we also look at:

$$\mathcal{L}_n^{\min}(\omega_0) = -\max_{\mathbf{d}_1, \dots, \mathbf{d}_n} \min_{l=1 \dots n} \hat{\lambda}_k(\omega_0, \mathbf{d}_l) \quad (5.16)$$

$$\text{such that } \|\mathbf{d}_l\| = 1, \mathbf{d}_l^\top \mathbf{d}_m = 0 \text{ for all } l, m \in 1, \dots, n, l \neq m \quad (5.17)$$

Branching the parameter optimization: We must choose which direction to branch in; our procedure for evaluating Lyapunov exponent objectives creates natural candidates. Specifically, evaluating the maximum exponent involves finding the direction maximizing trajectory separation, which we re-use for branching. Notably, this is the most negative eigenvalue of the Hessian if we start at a saddle point and use SGD when calculating the trajectories, generalizing the choice from RR. We can move in a positive and negative direction for each eigenvector, giving two branches.

Also, we must choose how far to move in each direction. If we move too far, we may leap into entirely different parts of the parameter space – e.g., missing interesting regions and recovering similar solution modes. If we are not exactly at a bifurcation – only near it – then we may need to move some minimum distance to cross the separatrix and find a new solution. We look at two simple strategies to move sufficiently far. First, we try to take a single step with the normalized exponent direction. Second, we look at taking small steps in the exponent direction until the alignment with the joint-gradient flips, generalizing RR’s “riding a ridge” (following an eigenvector of the Hessian) while it is a descent direction.

Optimizing each branch: For game optimization, the stability properties of the solutions can crucially depend on the optimizer choice (Gidel et al., 2019). One should choose an optimizer suited to the problem. In our experiments, we use Learning with Opponent Learning Awareness (LOLA) (Foerster et al., 2018), which can converge to periodic solutions and is attracted to high-welfare solutions in the IPD. In Section 5.6.1, we compare the finding of diverse solutions using LOLA with simultaneous SGD (SimSGD) – a method that works well for single-objective optimization but cannot find periodic solutions. Appendix C.1 summarizes other optimizer choices.

Rebranching: In single-objective optimization in machine learning, our optimizer often finishes at a high-dimensional saddle (Yao et al., 2020), making rebranching important. RR rebranches at the saddle in negative eigenvector directions to find critical points until we have fewer negative eigenvectors. In our setup, we are interested in rebranching if our optimizer finishes at a point where the eigenvalues of the Jacobian of the fixed-point operator \mathbf{J} are greater than 1. Figure 4.7 shows eigenvalues of \mathbf{J} larger than 1 at the end of GAN training.

5.4.3 Comparing GRR and RR

RR is a branching optimization search specifically for single-objective optimization – which is less general than optimization in games – so it can simplify GRR. For example, nonconservative systems have more bifurcation types than conservative ones. If we are only concerned with saddle bifurcations, we can just find a saddle stationary point by minimizing the gradient norm. We know this (relatively) easy-to-find stationary point lies on the separatrix. However, Hopf bifurcations are not necessarily near stationary points. Thus, minimizing gradient norms generally does not work, while optimizing a Lyapunov exponent does (Figure 5.2).

Although finding a separatrix with Lyapunov exponents in a single-objective setting might be overkill, we take some lessons from GRR back to RR. It is useful to view RR as a method to find bifurcations and branch across them. This motivates ways to sort between different stationary points to start at – an open problem from RR. For example, we use the point with the highest Kolmogorov-Sinai entropy (Pesin, 1977). This is roughly the (negative) sum of negative eigenvalues at stationary points. Another limitation of RR is effectively estimating the most negative eigenvalues of the Hessian. It is often simpler – in computation and implementation – to estimate the leading eigenvalues of the Jacobian of the fixed-point operator \mathbf{J} instead of the most negative eigenvalues of the Hessian $\hat{\mathcal{H}}$. Section 5.6.2 shows that our method reduces Hessian-vector product evaluations when estimating eigenvectors in setups from RR.

5.5 Experimental Setting

We experimentally investigate GRR on various problems summarized in this section and described in detail in Appendix C.3.1, chosen because they cover various dynamics and bifurcation types. Some are standard benchmarks, while others – i.e., Random Subspaces – are novel. We also summarize our gradient computation for these problems.

The **Iterated Prisoners’ Dilemma (IPD)** is the discounted, infinitely iterated Prisoner’s Dilemma (Poundstone, 1993). Each agent’s policy conditions on the actions in the prior time step, so there are 5 parameters for each agent – the probability of cooperating initially and given both agents’ preceding actions. There are multiple relevant equilibria in the IPD, including *unconditional* defection (DD), leading to the worst-case joint outcome, and *tit-for-tat* (TT), where agents initially cooperate, then copy the opponents’ action, giving a higher reward. We turn the IPD into a differentiable game by calculating the analytical expected return as a function of the two agents’ joint policy.

The **Small IPD** is a two-parameter simplification of IPD, which has both the DD and TT equilibria, allowing us to visualize the optimization difficulties of the full-scale IPD. However, unlike the full-scale IPD, the game Hessian has strictly real eigenvalues and, thus, conservative dynamics.

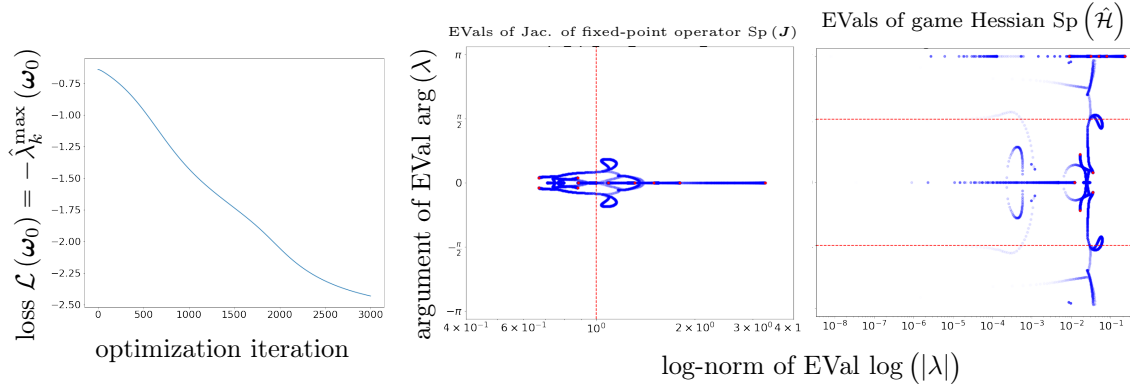


Figure 5.5: We display gradient descent optimization on the 1-step maximum Lyapunov exponent objective (Equation 5.13) on the IPD. **Takeaway:** We effectively reduce our loss and correspondingly increase the maximum eigenvalue of J . *Left:* We display our loss – i.e., the negative Lyapunov exponent objective – as optimization progresses. *Middle:* We visualize the spectrum of the Jacobian of our fixed-point operator in log-polar coordinates as optimization progresses. The spectrum is shown with a scatterplot in blue, with a progressively larger alpha at each iteration. The final spectrum is shown in red. A vertical red line is shown where the eigenvalue norm is equal to 1, signifying the cutoff between the (locally) convergent and divergent eigenspaces. We effectively maximize the norm of the largest eigenvalue. *Right:* We display the spectrum of the game Hessian. A horizontal red line is shown where the real part of the eigenvalue transitions from negative to positive, signifying the cutoff between (locally) convergent and divergent eigenspaces under gradient flow. Log-polar coordinates are required to see the structure in the spectrum.

Matching Pennies is a 2-parameter version of rock-paper-scissors. This problem’s game Hessian has purely imaginary eigenvalues, unlike the small IPD, but only a single solution. Thus, it is a poor diagnostic for diverse solutions but a useful test for probing nonconservative behavior.

Mixing Small IPD and Matching Pennies interpolates between the Small IPD and Matching Pennies games with an interpolation factor $\tau \in [0, 1]$ as in Equation C.1. This problem has two solutions – one where both players cooperate and one where both players select actions uniformly, with a Hopf bifurcation separating these.

We use a **Generative Adversarial Network (GAN)** setup from Metz et al. (2016); Balduzzi et al. (2018); Letcher et al. (2018), where the task is to learn a Gaussian mixture distribution using GANs. The data is sampled from a multimodal distribution to investigate the tendency to collapse on a subset of modes during training.

We construct **Random Subspace IPD/GANs** for more complicated diagnostics by optimizing higher-dimensional problems in a random subspace to see how robustly we can find bifurcations with the exponents. For each player, we select a random direction to optimize by sampling a vector \mathbf{v} with entries from $U[0, 1]$ and normalizing it. We also select a random offset \mathbf{b} from an appropriate initialization for the higher-dimensional problem. So, the first player controls the x coordinate and optimizes the loss $\mathcal{L}_A(\mathbf{v}_A x + \mathbf{b}_A, \mathbf{v}_B y + \mathbf{b}_B)$, while the second player controls the y coordinate and optimizes $\mathcal{L}_B(\mathbf{v}_A x + \mathbf{b}_A, \mathbf{v}_B y + \mathbf{b}_B)$.

We apply our method in **single-objective problems** to find bifurcations. There are various relevant problems in machine learning, but we focus on comparisons with RRs eigenvector estimation in MNIST classification.

To **optimizing the starting point objective**, we use automatic differentiation libraries (such as Jax (Bradbury et al., 2018) or PyTorch (Paszke et al., 2017)) to compute gradients through methods that calculate our Lyapunov exponent-inspired objectives. The scalability of this approach depends on the implementation of our exponent calculation, which can depend on estimating the top eigenvalues of the positive semi-definite (PSD) symmetric matrix in Equation 5.11. In simple settings, we can differentiate by calculating the full spectrum via `jax.linalg.numpy.eigh`; we investigate this in the toy experiment in Section 5.6.1 and IPD in Section 5.6.2. However, in machine learning, the matrix of Equation 5.11 is typically too large for the full spectrum. Directly estimating the top eigenvalues with an iterative method allows us to differentiate through them. We differentiate through `jax.numpy.linalg.eigh` in Figure 5.6 and investigate using power iteration with Hessian-vector products in Appendix Figure C.2.

5.6 Experimental Results

First, in Section 5.6.1, we use diagnostic problems to demonstrate and ablate the key parts of our algorithms – i.e., optimizers, starting points, and branching. Next, in Section 5.6.2, we scale GRR to larger-scale problem settings by (a) demonstrating that we improve RR’s eigenvector estimation for neural network classifiers and (b) calculating Lyapunov exponents for GANs.

5.6.1 Diagnostic Experiments

Optimizer Choice

Here, we show a system with complex eigenvectors showing (a) the importance of selecting a convergent optimizer in GRR and (b) an example task where RR cannot be applied. Figure 5.2 shows the phase portrait for the baseline methods in our Mixed Problem. LOLA (and other game optimizers) can find both solutions while naïvely following the gradient always finds a single solution.

Starting Point Selection

Figure 5.6 shows optimization of the maximum 10-step Lyapunov exponent on the Mixed Problem, where we find bifurcations with gradient-based optimization. Figure C.2 contrasts different direction choices for the exponent calculation. Re-estimating the top eigenvectors at each iteration performs best, although simpler methods can also work. Appendix Figure C.3 shows the maximum k -step exponent for multiple numbers of steps k , showing that a moderate number of steps – e.g., 10 – allows us to find bifurcations. Appendix Figure C.8 shows different Lyapunov exponent objectives that seek trajectory divergence in multiple directions. We find bifurcations while guaranteeing trajectory separation in every direction.

Impact of inner optimizer choices on bifurcation structure: Appendix Figure C.4 contrasts the exponents for LOLA and SimSGD, showing we find optimizer-dependent bifurcations. Appendix Figure C.5 investigates the impact of optimization-algorithm parameter choices on the bifurcation structure. If the step size is too large, the optimizer does not converge, resulting in bifurcations between complicated limit cycle trajectories (Strogatz, 2018), making GRR difficult to apply.

Starting points on single-objective problems: Appendix Figure C.6 shows our method in single-objective problems and finds bifurcations in the same setup as RR. Appendix Figure C.7 shows the logistic map, giving intuition for our method on a canonical example for bifurcations.

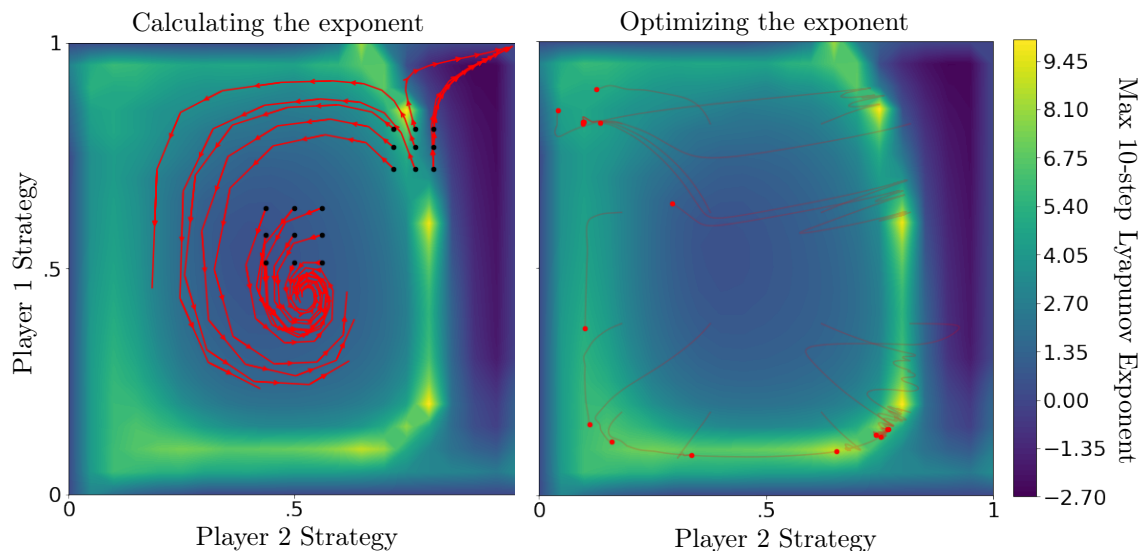


Figure 5.6: We show the calculation and optimization of a maximum 10-step Lyapunov exponent from Equation 5.10 on the mixed small IPD and Matching Pennies problem. Gradient-based optimization of this objective effectively finds the bifurcation. *Left*: We show a heatmap of the exponent and visualize the calculation of each exponent in two regions. This involves simulating the 10-step trajectories shown in red, starting at the black points, and then finding a direction that maximizes trajectory separation. We use the exponent to find bifurcations – in this case, between the solution in the top right and the center. *Right*: We show optimization trajectories for gradient ascent on the exponent for a grid of initializations. The optimization procedure finds large exponent locations for various starting points, with the final iterate shown by red circles.

Branching at Bifurcations

In Figure 5.4, we demonstrate branching at bifurcations to find multiple solutions to toy problems. This shows an explicit example of where RR’s starting point does not work, but GRR’s does. The small IPD has a saddle bifurcation, while the Mixed Problem has a Hopf bifurcation.

A Range of Complicated Toy Problems

In Figure 5.7, we calculate Lyapunov exponents on problems with more complicated dynamics by taking the high-dimensional IPD and GAN problems and selecting a random subspace to optimize. We effectively highlight bifurcations in this setup.

5.6.2 Scaling the Results

Optimizing Lyapunov Exponents on IPD

Here, we investigate our ability to use gradient-based optimizers on Lyapunov exponents in the IPD. Figure 5.5 shows the feasibility of using gradient descent to tune the 1-step maximum Lyapunov exponent. Appendix Figure C.11 optimizes an objective using multiple exponents, showing that we effectively optimize multiple exponents, which gives trajectory separation in multiple directions. Appendix Figure C.12 compares objectives using multiple exponents, showing that using the minimum of the top n exponents gives trajectory separation in all n directions, unlike the naïve choice of optimizing their sum. The sum of exponents finds solutions that separate extremely fast in the top directions while (slowly) converging in the bottom directions. In contrast, the minimum of the exponents does not allow for convergence in the bottom directions. Appendix Figure C.13 compares optimizing the k -step maximum Lyapunov exponent for variable k , showing that we effectively minimize multi-step exponents in higher-dimensional problems if required.

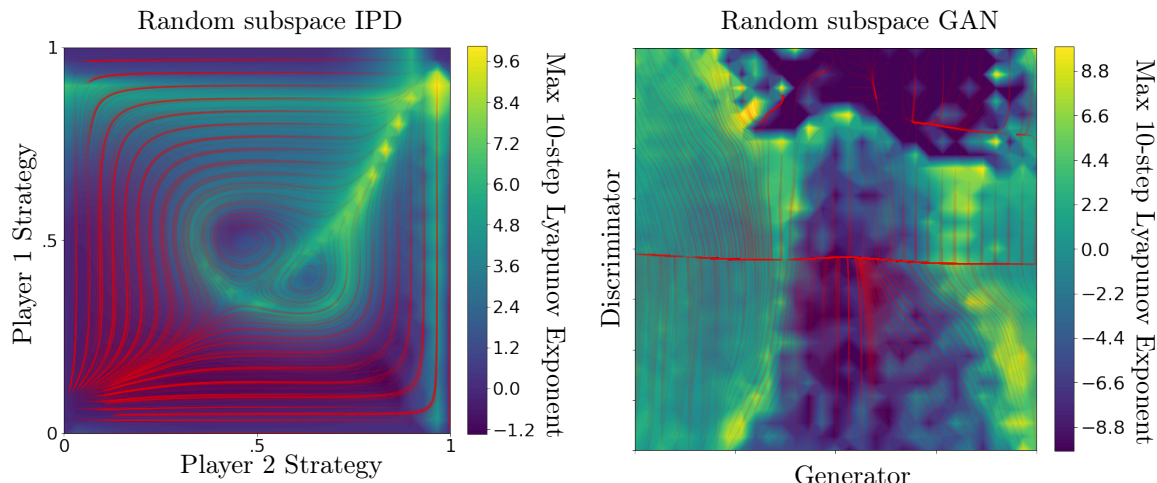


Figure 5.7: We show the Lyapunov exponent heatmap (as in Figure 5.6) on more complicated toy problems to see how robustly we can find different bifurcations. The exponent peaks near where the trajectories (shown in red) separate, showing that we find various bifurcations. See Appendix Figure C.10 for other sampled subspaces. Section 5.5 describes how we construct these examples by taking higher-dimensional problems and optimizing them in a random subspace. *Left*: An IPD subspace with multiple Hopf bifurcations. *Right*: A GAN subspace with various bifurcations.

GRR Applied to the IPD

Here, we use our method on the IPD, where existing methods have difficulty finding diverse solutions. There are two solution modes: ones where both agents defect and cooperate, respectively. Table 5.1 compares our method with the baselines of the following gradients and LOLA, each run with random initializations. Our method finds both solution modes, unlike existing approaches. Using the maximum Lyapunov exponent as our objective was sufficient, which only guarantees separation in 1 direction. Similarly, we found that using a 1-step or local Lyapunov exponent objective was sufficient, though we may require more steps to find bifurcations in other problems.

Improving RR’s Eigenvector Estimation

We investigate efficiently finding the most negative eigenvectors in RR by estimating the largest eigenvalues/vectors of the Jacobian of our fixed-point operator, where RR measures the most negative eigenvalues/vectors of the Hessian. We measure efficiency by comparing the number of Hessian-vector product (HVP) evaluations, which dominate the cost of eigenvector estimation. Table 5.2 shows how many HVP evaluations to reach different MNIST classifier accuracies by following eigenvectors. Our method can more efficiently use HVP evaluations than the RR method because we simply do power iteration on the fixed-point operator Jacobian.

We stress that this problem is not designed to train a single strong classifier; it is easy to just train our network by following the gradient to 100% train accuracy. This problem was selected from RR’s experiments because it requires us to estimate negative eigenvectors accurately and efficiently many times. A downstream use of this is training an ensemble of classifiers for generalization.

Search Strategy	P1 loss \mathcal{L}_A min, max	(P)layer 1 Strategy Distribution: min, max				
		$p(C_0)$	$p(C CC)$	$p(C CD)$	$p(C DC)$	$p(C DD)$
Us: Lyap init, EVec branch, SimSGD	1.000, 2.000	.003, .999	.032, .999	.004, .884	.001, .912	.000, .013
Us: Lyap init, EVec branch, LOLA	1.000, 2.000	.002, .999	.063, .993	.001, .910	.000, .922	.005, .103
20 Random init, SimSGD	1.997, 1.998	.043, .194	.142, .480	.041, .143	.055, .134	.001, .001
20 Random init, LOLA	1.000, 1.396	.000, 1.00	.093, 1.00	.000, .966	.057, 1.00	.000, .947
1 Random init, EVec branch, SimSGD	2.000, 2.000	.001, .003	.027, .030	.003, .007	.008, .009	.000, .000

Table 5.1: We show strategies for finding diverse solutions to the iterated prisoner’s dilemma (IPD). **Takeaway:** Our method finds solutions in both loss modes, while existing approaches of using random initializations, then following the gradient or using LOLA do not find diverse solutions. The IPD has two solution modes – i.e., solutions where both agents defect with a loss of 2 and where both agents cooperate with a loss of 1 (like tit-for-tat). We assess which modes were found by showing (P)layer 1’s strategy, which is the chance of cooperating given both players’ last action – ex., $p(C|DC)$ is the chance if previously P1 (*D*)efected and P2 (*C*)ooperated. We compare GRR flavors with just following gradients via SimSGD and LOLA (Foerster et al., 2018) from random (initializations). We compare with 20 random initializations because GRR follows at most 20 branches due to having 10 eigenvectors in 2 directions (+/-). GRR only branches in directions where eigenvalues of the Jacobian of the fixed-point operator are greater than 1 (i.e., trajectories locally diverge) as visualized in Figure 5.5 (middle). We look at the impact of starting at an approximate bifurcation in GRR by branching on the eigenvectors at a random init. Each branch finds the same solution if the maximum Lyapunov exponent is not tuned.

Number of HVP Evaluations	MNIST Accuracy	
	Our Method	RR’s Method
10 000	19%(+8%)	11%
100 000	89%(+6%)	83%
1 000 000	93%(+2%)	91%

Table 5.2: We show how many HVP evaluations to reach different MNIST classifier accuracies by following eigenvectors, repeating the experiment in RR’s Figure 4. We aim not to train a single strong classifier but to test our ability to follow negative eigenvectors efficiently – see Section 5.6.2.

Calculating Lyapunov Exponents for GANs

Here, we scale our exponent calculations to machine learning models where the (game) Hessian is so large that we cannot materialize it and only use Hessian-vector products. Specifically, we use the GAN described in Section 5.5. We look at calculating our exponent for various hyperparameters and random re-starts. We evaluate the quality of using our exponent to find diverse solutions with the log probability of samples from an ensemble of GANs from the top 5 optimization branches. Table 5.3 shows the mean and standard deviation (over 10 random restarts) of the maximum 10-step Lyapunov exponent and the resulting ensemble’s log probability. Each GAN was trained for 10 000 updates, so evaluating ensembles costs approximately 50 000 evaluations of both players’ gradients. In contrast, each exponent costs less than 1000 evaluations of both gradients to compute.

This shows that we effectively scale our exponent calculation to larger models of interest from machine learning. We find that a large (mean) exponent may align with regions where we can branch to train the strongest ensemble of GANs.

Initial scale, step size	Max Lyapunov Coefficient	Ensemble log prob
0.001, 1.0	0.952 ± 0.834	$-16\,342 \pm 817$
0.1, 1.0	6.485 ± 1.155	$-13\,691 \pm 1317$
10.0, 1.0	0.053 ± 0.128	$-46\,659 \pm 26\,793$
0.001, 0.1	0.849 ± 0.765	$-12\,321 \pm 126$
0.1, 0.1	6.571 ± 0.953	$-10\,846 \pm 256$
10.0, 0.1	-0.012 ± 0.014	$-23\,459 \pm 12\,693$

Table 5.3: We display the mean and standard deviation (over 10 random restarts) of the maximum 10-step Lyapunov exponent and the log probability of an ensemble of 5 GANs obtained by branching in the top 5 directions at the initialization. We show that the better-performing ensembles also have higher Lyapunov coefficients and demonstrate that our exponent calculation is scalable to larger problems. The best GANs log probability from the best ensemble was $-12\,861 \pm 356$, which is worse than the ensemble’s performance of $-10\,846 \pm 256$. This indicates that each GAN may be learning a different part of the data distribution, with samples shown in Appendix Figure C.9.

5.7 Conclusion

This chapter introduces Generalized Ridge Rider (GRR), an extension of the Ridge Rider (RR) algorithm to settings with multiple losses. In these settings, we showed that a broader class of bifurcation points needs to be considered and that GRR indeed discovers them in various problems. Experimentally, we isolate each component of GRR, demonstrating their effectiveness, and show that – in contrast to baseline methods – GRR can obtain a diversity of qualitatively different solutions in multi-agent settings such as the iterated prisoner’s dilemma. We also provide empirical justification for our method using tools from the dynamical systems literature, allowing us to find arbitrary bifurcations. This hints at a multitude of approaches and tools from dynamical systems that can be used for understanding game dynamics and learning diversity.

Acknowledgements

The Province of Ontario, the Canadian government through CIFAR, and companies sponsoring the Vector Institute provided resources used in preparing this chapter. We would also like to thank C. Daniel Freeman, Herve Jégou, Noam Brown, and David Acuna for feedback on this work and acknowledge the Python community (Van Rossum and Drake Jr, 1995; Oliphant, 2007) for developing the tools that enabled this work, including NumPy (Oliphant, 2006; Van Der Walt et al., 2011; Harris et al., 2020b), Matplotlib (Hunter, 2007) and SciPy (Jones et al., 2001).

My Contributions Towards this Paper As it Pertains to the Thesis

I contributed the initial idea to this project, ran all the experiments, and did most of the writing.

Chapter 6

Discussion and Concluding Remarks

This thesis introduces new methods for scalable nested optimization in various relevant problems within machine learning. First, we give methods based on hypernetworks and implicit differentiation for computing the best-response Jacobian, which we used to calculate approximate hypergradients for large-scale hyperparameter optimization. Next, we augmented classical first-order optimization methods to reduce rotational dynamics when applied to nested optimization problems. Finally, we generalize an algorithm that branches gradient-based optimization at bifurcations to work with nonconservative dynamics often present in nested optimization.

6.1 Summary of Chapters

In Chapter 2, we address tuning hyperparameters using gradient-based optimization by replacing the training optimization loop with a differentiable hypernetwork. We presented a simple and scalable method that jointly optimizes both hyperparameters and hypernetwork weights.

In Chapter 3, we present a gradient-based hyperparameter optimization algorithm that scales to high-dimensional hyperparameters the size of modern, deep neural networks. We use the implicit function theorem to formulate the hypergradient whose bottleneck is inverting the training loss Hessian with respect to the neural network parameters. We approximate inverse-Hessian-vector products using a relationship with unrolled differentiation.

In Chapter 4, we generalize existing momentum methods for learning in differentiable games by allowing complex momentum with real-valued updates. Our method robustly converges in games with a different range of eigenspace mixtures than existing methods. We also presented a practical generalization of our method to the Adam optimizer, which we used to improve BigGAN training.

In Chapter 5, we introduce Generalized Ridge Rider, an extension of the Ridge Rider algorithm to settings with multiple losses. In these settings, we showed that a broader class of bifurcation points needs to be considered and that GRR indeed discovers them in various problems. We also provide an empirical justification for our method using tools from the dynamical systems literature, allowing us to find arbitrary bifurcations. Experimentally, GRR obtains various solutions in multi-agent settings, such as the iterated prisoner’s dilemma.

6.2 Limitations and Future Directions

6.2.1 Hyperparameter Optimization Through Hypernetworks

Limitations

The most scalable architecture proposed in this work is a linear hypernetwork, which will not scale when the output weights are the size of modern neural networks. We look at smarter factorized networks in non-thesis research [MacKay et al. \(2019a\)](#) that scale to large modern networks. Another limitation is that it is difficult to set the scale of the hyperparameters sampled during training, which is again partially resolved by adaptive scales in non-thesis research [MacKay et al. \(2019a\)](#). Unlike Bayesian optimization, this method does not facilitate uncertainty-aware exploration and requires a differentiable validation loss. A further limitation is that this method relies on sampling hyperparameters, which will not scale for ultra-large hyperparameter regimes, i.e., hundreds of thousands to millions of hyperparameters.

Future directions

Future directions could include combining this amortized optimization framework into other nested optimization setups besides hyperparameter optimization – ex., meta-learning schemes like MAML ([Finn et al., 2017](#)) or (small-scale) GANs. Alternatively, we could combine these methods with other strategies for approximating the best-response, like unrolled or implicit differentiation. Furthermore, optimizing thousands of hyperparameters raises the question of *hyper-regularization*, or regularization of hyperparameters. We could also look for improved ways to formulate hypernetwork training, as in [Bae and Grosse \(2020\)](#).

6.2.2 Optimizing Millions of Hyperparameters by Implicit Differentiation

Limitations

For implicit differentiation, we can only optimize hyperparameters that change the loss manifold, so our approach is not straightforwardly applicable to optimizer hyperparameters. Also, we need continuous hyperparameters to use gradient-based optimization, but many discrete hyperparameters (e.g., number of hidden units) have continuous relaxations ([Maddison et al., 2017](#); [Jang et al., 2016](#)). We cannot exactly compute the hypergradients since we must find (λ', \mathbf{w}') such that $\frac{\partial \mathcal{L}_T}{\partial \mathbf{w}}|_{\lambda', \mathbf{w}'} = 0$, which we can only solve to a tolerance with an approximate solution denoted $\widehat{\mathbf{w}}^*(\lambda)$. Some hyperparameters fail when we retrain the model with the final fixed value. Furthermore, this method does not facilitate uncertainty-aware exploration. Unlike Bayesian optimization, we also require a differentiable validation loss, which can directly optimize validation objectives such as accuracy. We also observed that the introduction of millions of hyperparameters can easily overfit the validation dataset. Some noisy hyperparameters, such as the continuous relaxation of discrete parameters as in [MacKay et al. \(2019a\)](#), did not work robustly with this method – perhaps due to a higher sensitivity to noise. It would be better to investigate the effects of stochasticity in our results, for example, when we should compare to CG or re-sample batches in our hypergradient evaluation. As such, this does not scale to settings such as generating the code for our model as a hyperparameter as in [Zhang et al. \(2023a\)](#).

Future directions

We believe algorithms of this nature provide a path for practical nested optimization, where we have Hessians with a known structure. We seek to understand why some hyperparameters fail to retrain, which is partially solved in the non-thesis work of [Vicol et al. \(2022a\)](#). Since naïvely introducing hyperparameters causes validation overfitting, we should find useful ways to introduce many hyperparameters. Further, we should investigate useful cross-validation data splits when using many hyperparameters and when we want to retrain with the final hyperparameters. Investigating other matrix-inversion methods besides the Neumann series could also be fruitful.

6.2.3 Complex Momentum for Optimization in Games

Limitations

Our method stores real and imaginary components in the momentum buffer μ , so we use more memory than standard momentum. Our method is more challenging to analyze, as our augmented dynamics requires wielding the roots of a cubic instead of a quadratic. Our method introduces a new hyperparameter – the imaginary components or \arg of β – that needs to be tuned. For some games, we need higher-order information than first-order to converge – ex., pure-response games ([Lorraine et al., 2020a](#)) – because the first-order information for a player is identically zero. So, momentum methods that only use first-order info, like the direct gradient, will not generally converge.

Future directions

We should consider which kind of spectrum gradient optimization induces in nested optimization setups of interest, such as GANs, to guide our algorithm design. Furthermore, we should find useful approximations of these empirical spectrums that are tractable to analyze yet still provide useful results. We should also look to get a closed-form solution for the optimal learning rate and momentum as a function of the spectrum so that we can tightly bound the convergence rates for our method. Additionally, we should explore other, more general recurrently linked momentum setups to see which achieves the best convergence rates on spectrums of interest.

6.2.4 Lyapunov Exponents for Diversity in Differentiable Games

Limitations

Our method does not have guarantees if our optimization process does not converge – ex., when the learning rate is too high, when there is stochasticity, or when we have solutions as the parameters tend to infinity. Furthermore, our approaches to estimating the exponent involve simulating trajectories for a finite horizon, which we must tune. If the horizon is too long, our gradients become too sharp and have a limited signal, while if the horizon is too short, we may not find bifurcations. Further, instead of approximating the maximum eigenvalue of the sum of Jacobians in optimization trajectories, we tractably approximate the maximum eigenvalue for each Jacobian. We approximate the maximum eigenvalue via a power iteration. We also do gradient descent on our approximate Lyapunov exponent, which finds approximate solutions, and it is unclear how far we have to move in each direction to move across the bifurcation. Further, scaling to large-scale setups like GANs proves challenging, especially when optimizing the exponent. We should find strong use cases for which we want to find diverse solutions in nested optimization setups.

Future directions

This work hints at many approaches and tools from dynamical systems that can be used to understand game dynamics and learning diversity. We should also look for more use cases where we care about finding multiple solutions to the nested optimization. Using objectives wielding more elements of the Lyapunov spectrum may also be useful for finding regions where we can branch across bifurcations in multiple directions. Finding uses of Lyapunov exponent optimization may be helpful in other problems, e.g., augmented influence functions, where removing a data point changes our optimization trajectory instead of just the converged value.

Appendix A

Optimizing Millions of Hyperparameters by Implicit Differentiation

A.1 Extended Background

This section outlines our notation (Table A.1) and the proposed algorithm. Here, we assume that we have access to a finite dataset $\mathcal{D} = \{(\mathbf{x}_i, \mathbf{y}_i) \mid i = 1 \dots n\}$, with n examples drawn from the distribution $p(\mathbf{x}, \mathbf{y})$ with support \mathcal{P} . We denote the input and target domains by \mathcal{X} and \mathcal{Y} , respectively. Assume $\mathbf{y} : \mathcal{X} \rightarrow \mathcal{Y}$ is a function and we wish to learn $\hat{\mathbf{y}} : \mathcal{X} \times \mathbf{W} \rightarrow \mathcal{Y}$ with a neural network parameterized by $\mathbf{w} \in \mathbf{W}$, so that $\hat{\mathbf{y}}$ is close to \mathbf{y} . We measure how close a predicted value is to a target with the prediction loss $\mathcal{L} : \mathcal{Y} \times \mathcal{Y} \rightarrow \mathbb{R}$. Our goal is to minimize the expected prediction loss or population risk: $\operatorname{argmin}_{\mathbf{w}} \mathbb{E}_{\mathbf{x} \sim p(\mathbf{x})} [\mathcal{L}(\hat{\mathbf{y}}(\mathbf{x}, \mathbf{w}), \mathbf{y}(\mathbf{x}))]$. Since we only have access to a finite number of samples, we minimize the empirical risk: $\operatorname{argmin}_{\mathbf{w}} \frac{1}{n} \sum_{\mathbf{x}, \mathbf{y} \in \mathcal{D}} \mathcal{L}(\hat{\mathbf{y}}(\mathbf{x}, \mathbf{w}), \mathbf{y}(\mathbf{x}))$.

Due to a limited size dataset \mathcal{D} , there may be a significant difference between the minimizer of the empirical risk and the population risk. We can estimate this difference by partitioning our dataset into training and validation datasets— $\mathcal{D}_{train}, \mathcal{D}_{valid}$. We find the minimizer on the training dataset \mathcal{D}_{train} and estimate its performance on the population risk by evaluating the empirical risk over the validation dataset \mathcal{D}_{valid} . We modify the empirical training risk to decrease our population risk, parameterized by $\boldsymbol{\lambda} \in \boldsymbol{\Lambda}$. These parameters for generalization are called hyperparameters. We call the modified empirical training risk our training loss for simplicity and denote it $\mathcal{L}_T(\boldsymbol{\lambda}, \mathbf{w})$. Our empirical validation risk is called validation loss for simplicity and is denoted by $\mathcal{L}_V(\boldsymbol{\lambda}, \mathbf{w})$. Often, the validation loss does not directly depend on the hyperparameters, and we have $\mathcal{L}_V(\mathbf{w})$.

The population risk is estimated by plugging the training loss minimizer $\mathbf{w}^*(\boldsymbol{\lambda}) = \operatorname{argmin}_{\mathbf{w}} \mathcal{L}_T(\boldsymbol{\lambda}, \mathbf{w})$ into the validation loss for the estimated population risk $\mathcal{L}_V^*(\boldsymbol{\lambda}) = \mathcal{L}_V(\boldsymbol{\lambda}, \mathbf{w}^*(\boldsymbol{\lambda}))$. We want our hyperparameters to minimize the estimated population risk: $\boldsymbol{\lambda}^* = \operatorname{argmin}_{\boldsymbol{\lambda}} \mathcal{L}_V^*(\boldsymbol{\lambda})$. We can create a third partition of our dataset \mathcal{D}_{test} to assess if we overfit the validation dataset \mathcal{D}_{valid} with our hyperparameters $\boldsymbol{\lambda}$. A citation for this thesis is included at [Lorraine \(2024\)](#).

A.2 Extended Related Work

Black-box optimization methods such as random search (Bergstra and Bengio, 2012) or Bayesian optimization (Mockus, 1998; Shahriari et al., 2015) have been deployed for hyperparameter optimization (HPO). Beyond black-box methods, other works further use the problem structure, e.g., are compute-environment-aware Ginsbourger et al. (2010), compute-budget-aware (Lam et al., 2016), multi-task (Swersky et al., 2013), like transfer-learning (Golovin et al., 2017) or multi-fidelity (Klein et al., 2017), iterative-optimization-aware (Li et al., 2017), online (Jaderberg et al., 2017), or multi-objective (Daulton et al., 2022). However, these methods (a) still rely on practitioners to design a search space, which includes selecting which parameters can be optimized and specifying bounds on these parameters, and (b) typically struggle in the initial search phase ($< 2^d$ queries for d -dimensional hyperparameters). We further detail a few notable cases:

Independent hyperparameter optimization: A simple class of hyperparameter optimization algorithms involves making several independent hyperparameter selections and training the model to completion. Popular examples include grid search and random search (Bergstra and Bengio, 2012). Since each hyperparameter selection is independent, these algorithms are trivial to parallelize.

Global hyperparameter optimization: Some hyperparameter optimization algorithms try to find a globally optimal hyperparameter setting, which can be important if the loss is non-convex. A simple example is random search, while a more sophisticated example is Bayesian optimization (Moćkus, 1975; Snoek et al., 2012; Kandasamy et al., 2019). These HO algorithms often involve reinitializing the hyperparameter and weights on each optimization iteration. This allows global optimization at the cost of expensive retraining weights or hyperparameters.

Local hyperparameter optimization: Other hyperparameter optimization algorithms only try to find a locally optimal hyperparameter setting. Often, these algorithms maintain a current estimate of the best combination of hyperparameters and weights. The hyperparameter is adjusted by a small amount on each optimization iteration, which allows us to avoid excessive retraining of the weights on each update. This is because the new optimal weights are close to the old optimal weights because of a small change in the hyperparameters.

Learned proxy function based hyperparameter optimization: Many hyperparameter optimization algorithms try to learn a proxy function for optimization. The proxy function is used to estimate the loss for a hyperparameter selection. We could learn a proxy function for global or local hyperparameter optimization. We can learn a useful proxy function on any node in our computational graph, including the optimized weights. For example, we could learn how optimized weights change with respect to hyperparameters (Lorraine and Duvenaud, 2017), how the optimized predictions change with respect to the hyperparameters (MacKay et al., 2019a), or how the optimized validation loss changes with respect to the hyperparameters as in Bayesian optimization. As in Bayesian optimization, it is possible to do gradient descent on the proxy function to find new hyperparameters to query. Alternatively, we could use a non-differentiable proxy function to get cheap estimates of the validation loss like SMASH (Brock et al., 2017) for architecture choices.

Table A.1: Notation For Optimizing Millions of Hyperparameters by Implicit Differentiation

HO	Hyperparameter optimization
NN	Neural network
IFT	Implicit Function Theorem
HVP / JVP	Hessian/Jacobian-vector product
λ, \mathbf{w}	Hyperparameters and neural network parameters/weights
n, m	Hyperparameter and neural network parameter dimensionality
$\Lambda \subseteq \mathbb{R}^n, \mathbf{W} \subseteq \mathbb{R}^m$	Hyperparameters and neural network parameter domains
λ', \mathbf{w}'	Arbitrary, fixed hyperparameters and weights
$\mathcal{L}_T(\lambda, \mathbf{w}), \mathcal{L}_V(\lambda, \mathbf{w})$	Training loss & validation loss
$\mathbf{w}^*(\lambda)$	Best-response of the weights to the hyperparameters
$\widehat{\mathbf{w}}^*(\lambda)$	Approximate best-response of the weights to the hyperparameters
$\mathcal{L}_V^*(\lambda) = \mathcal{L}_V(\lambda, \mathbf{w}^*(\lambda))$	The validation loss with best-responding weights
Red	(Approximate) Validation loss with best-responding weights
$\mathbf{W}^* = \mathbf{w}^*(\Lambda)$	The domain of best-responding weights
λ^*	The optimal hyperparameters
\mathbf{x}, \mathbf{y}	An input and its associated target
\mathcal{X}, \mathcal{Y}	The input and target domains, respectively.
\mathcal{D}	A data matrix consisting of tuples of inputs and targets
$\mathbf{y}(\mathbf{x}, \mathbf{w})$	A predicted target for a input data and weights
$\frac{\partial \mathcal{L}_V}{\partial \lambda}, \frac{\partial \mathcal{L}_V}{\partial \mathbf{w}}$	The (validation loss hyperparameter / parameter) direct gradient
Green	(Approximations to) The validation loss direct gradient.
$\frac{\partial \mathbf{w}^*}{\partial \lambda}$	The best-response Jacobian
Blue	(Approximate) (Jacobian of the) best-response of the weights to the hyperparameters
$\frac{\partial \mathcal{L}_V}{\partial \mathbf{w}} \frac{\partial \mathbf{w}^*}{\partial \lambda}$	The indirect gradient
$\frac{\partial \mathcal{L}_V^*}{\partial \lambda}$	Hypergradient: sum of validation losses direct and indirect gradient
$\left[\frac{\partial^2 \mathcal{L}_T}{\partial \mathbf{w} \partial \mathbf{w}^\top} \right]^{-1}$	The training Hessian inverse
Magenta	(Approximations to) The training Hessian inverse
$\frac{\partial \mathcal{L}_V}{\partial \mathbf{w}} \left[\frac{\partial^2 \mathcal{L}_T}{\partial \mathbf{w} \partial \mathbf{w}^\top} \right]^{-1}$	The vector - Inverse Hessian product.
Orange	(Approximations to) The vector - Inverse Hessian product.
$\frac{\partial^2 \mathcal{L}_T}{\partial \mathbf{w} \partial \lambda^\top}$	The training mixed partial derivatives
\mathbf{I}	The identity matrix

A.3 Implicit Function Theorem

Theorem (Augustin-Louis Cauchy, Implicit Function Theorem). Let $\frac{\partial \mathcal{L}_T}{\partial \mathbf{w}}(\boldsymbol{\lambda}, \mathbf{w}) : \boldsymbol{\Lambda} \times \mathbf{W} \rightarrow \mathbf{W}$ be a continuously differentiable function. Fix a point $(\boldsymbol{\lambda}', \mathbf{w}')$ with $\frac{\partial \mathcal{L}_T}{\partial \mathbf{w}}(\boldsymbol{\lambda}', \mathbf{w}') = 0$. If the Jacobian $J_{\mathbf{w}}^{\frac{\partial \mathcal{L}_T}{\partial \mathbf{w}}}(\boldsymbol{\lambda}', \mathbf{w}')$ is invertible, there exists an open set $U \subseteq \boldsymbol{\Lambda}$ containing $\boldsymbol{\lambda}'$ such that there exists a continuously differentiable function $\mathbf{w}^* : U \rightarrow \mathbf{W}$ such that:

$$\mathbf{w}^*(\boldsymbol{\lambda}') = \mathbf{w}' \text{ and } \forall \boldsymbol{\lambda} \in U, \frac{\partial \mathcal{L}_T}{\partial \mathbf{w}}(\boldsymbol{\lambda}, \mathbf{w}^*(\boldsymbol{\lambda})) = 0$$

Moreover, the partial derivatives of \mathbf{w}^* in U are given by the matrix product:

$$\frac{\partial \mathbf{w}^*}{\partial \boldsymbol{\lambda}}(\boldsymbol{\lambda}) = - \left[J_{\mathbf{w}}^{\frac{\partial \mathcal{L}_T}{\partial \mathbf{w}}}(\boldsymbol{\lambda}, \mathbf{w}^*(\boldsymbol{\lambda})) \right]^{-1} J_{\boldsymbol{\lambda}}^{\frac{\partial \mathcal{L}_T}{\partial \mathbf{w}}}(\boldsymbol{\lambda}, \mathbf{w}^*(\boldsymbol{\lambda}))$$

Typically the IFT is presented with $\frac{\partial \mathcal{L}_T}{\partial \mathbf{w}} = f$, $\mathbf{w}^* = g$, $\boldsymbol{\Lambda} = \mathbb{R}^m$, $\mathbf{W} = \mathbb{R}^n$, $\boldsymbol{\lambda} = x$, $\mathbf{w} = y$, $\boldsymbol{\lambda}' = a$, $\mathbf{w}' = b$.

A.4 Proofs

Lemma (1). If the recurrence given by unrolling SGD optimization in Equation 3.6 has a fixed point \mathbf{w}_∞ (i.e., $0 = \frac{\partial \mathcal{L}_T}{\partial \mathbf{w}}|_{\boldsymbol{\lambda}, \mathbf{w}_\infty(\boldsymbol{\lambda})}$), then:

$$\frac{\partial \mathbf{w}_\infty}{\partial \boldsymbol{\lambda}} = - \left[\frac{\partial^2 \mathcal{L}_T}{\partial \mathbf{w} \partial \mathbf{w}^\top} \right]^{-1} \frac{\partial^2 \mathcal{L}_T}{\partial \mathbf{w} \partial \boldsymbol{\lambda}^\top} \Big|_{\mathbf{w}_\infty(\boldsymbol{\lambda})}$$

Proof.

$$\begin{aligned} \Rightarrow \frac{\partial}{\partial \boldsymbol{\lambda}} \left(\frac{\partial \mathcal{L}_T}{\partial \mathbf{w}} \Big|_{\boldsymbol{\lambda}, \mathbf{w}_\infty(\boldsymbol{\lambda})} \right) &= 0 && \text{given} \\ \Rightarrow \left(\frac{\partial^2 \mathcal{L}_T}{\partial \mathbf{w} \partial \boldsymbol{\lambda}^\top} I + \frac{\partial^2 \mathcal{L}_T}{\partial \mathbf{w} \partial \mathbf{w}^\top} \frac{\partial \mathbf{w}_\infty}{\partial \boldsymbol{\lambda}} \right) \Big|_{\boldsymbol{\lambda}, \mathbf{w}_\infty(\boldsymbol{\lambda})} &= 0 && \text{chain rule through } |_{\boldsymbol{\lambda}, \mathbf{w}_\infty(\boldsymbol{\lambda})} \\ \Rightarrow \frac{\partial^2 \mathcal{L}_T}{\partial \mathbf{w} \partial \mathbf{w}^\top} \frac{\partial \mathbf{w}_\infty}{\partial \boldsymbol{\lambda}} \Big|_{\boldsymbol{\lambda}, \mathbf{w}_\infty(\boldsymbol{\lambda})} &= - \frac{\partial^2 \mathcal{L}_T}{\partial \mathbf{w} \partial \boldsymbol{\lambda}^\top} \Big|_{\boldsymbol{\lambda}, \mathbf{w}_\infty(\boldsymbol{\lambda})} && \text{re-arrange terms} \\ \Rightarrow \frac{\partial \mathbf{w}_\infty}{\partial \boldsymbol{\lambda}} \Big|_{\boldsymbol{\lambda}} &= - \left[\frac{\partial^2 \mathcal{L}_T}{\partial \mathbf{w} \partial \mathbf{w}^\top} \right]^{-1} \frac{\partial^2 \mathcal{L}_T}{\partial \mathbf{w} \partial \boldsymbol{\lambda}^\top} \Big|_{\boldsymbol{\lambda}} && \text{left-multiply by } \left[\frac{\partial^2 \mathcal{L}_T}{\partial \mathbf{w} \partial \mathbf{w}^\top} \right]^{-1} \Big|_{\boldsymbol{\lambda}, \mathbf{w}_\infty(\boldsymbol{\lambda})} \end{aligned}$$

□

Lemma (2). Given the recurrence from unrolling SGD optimization in Equation 3.6 we have:

$$\frac{\partial \mathbf{w}_{i+1}}{\partial \boldsymbol{\lambda}} = - \sum_{j \leq i} \left(\prod_{k < j} I - \frac{\partial^2 \mathcal{L}_T}{\partial \mathbf{w} \partial \mathbf{w}^\top} \Big|_{\boldsymbol{\lambda}, \mathbf{w}_{i-k}(\boldsymbol{\lambda})} \right) \frac{\partial^2 \mathcal{L}_T}{\partial \mathbf{w} \partial \boldsymbol{\lambda}^\top} \Big|_{\boldsymbol{\lambda}, \mathbf{w}_{i-j}(\boldsymbol{\lambda})}$$

Proof.

$$\begin{aligned}
\frac{\partial \mathbf{w}_{i+1}}{\partial \boldsymbol{\lambda}} \Big|_{\boldsymbol{\lambda}} &= \frac{\partial}{\partial \boldsymbol{\lambda}} \left(\mathbf{w}_i(\boldsymbol{\lambda}) - \frac{\partial \mathcal{L}_T}{\partial \mathbf{w}} \Big|_{\boldsymbol{\lambda}, \mathbf{w}_i(\boldsymbol{\lambda})} \right) && \text{take derivative with respect to } \boldsymbol{\lambda} \\
&= \frac{\partial \mathbf{w}_i}{\partial \boldsymbol{\lambda}} \Big|_{\boldsymbol{\lambda}} - \frac{\partial}{\partial \boldsymbol{\lambda}} \left(\frac{\partial \mathcal{L}_T}{\partial \mathbf{w}} \Big|_{\boldsymbol{\lambda}, \mathbf{w}_i(\boldsymbol{\lambda})} \right) && \text{chain rule} \\
&= \frac{\partial \mathbf{w}_i}{\partial \boldsymbol{\lambda}} \Big|_{\boldsymbol{\lambda}} - \left(\frac{\partial^2 \mathcal{L}_T}{\partial \mathbf{w} \partial \mathbf{w}^\top} \frac{\partial \mathbf{w}_i}{\partial \boldsymbol{\lambda}} + \frac{\partial^2 \mathcal{L}_T}{\partial \mathbf{w} \partial \boldsymbol{\lambda}^\top} \right) \Big|_{\boldsymbol{\lambda}, \mathbf{w}_i(\boldsymbol{\lambda})} && \text{chain rule through } \Big|_{\boldsymbol{\lambda}, \mathbf{w}_i(\boldsymbol{\lambda})} \\
&= -\frac{\partial^2 \mathcal{L}_T}{\partial \mathbf{w} \partial \boldsymbol{\lambda}^\top} \Big|_{\boldsymbol{\lambda}, \mathbf{w}_i(\boldsymbol{\lambda})} + \left(I - \frac{\partial^2 \mathcal{L}_T}{\partial \mathbf{w} \partial \mathbf{w}^\top} \right) \frac{\partial \mathbf{w}_i}{\partial \boldsymbol{\lambda}} \Big|_{\boldsymbol{\lambda}, \mathbf{w}_i(\boldsymbol{\lambda})} && \text{re-arrange terms} \\
&= -\frac{\partial^2 \mathcal{L}_T}{\partial \mathbf{w} \partial \boldsymbol{\lambda}^\top} \Big|_{\boldsymbol{\lambda}, \mathbf{w}_i(\boldsymbol{\lambda})} + \left(I - \frac{\partial^2 \mathcal{L}_T}{\partial \mathbf{w} \partial \mathbf{w}^\top} \right) \Big|_{\boldsymbol{\lambda}, \mathbf{w}_i(\boldsymbol{\lambda})} \cdot \\
&\quad \left(\left(I - \frac{\partial^2 \mathcal{L}_T}{\partial \mathbf{w} \partial \mathbf{w}^\top} \right) \frac{\partial \mathbf{w}_{i-1}}{\partial \boldsymbol{\lambda}} - \frac{\partial^2 \mathcal{L}_T}{\partial \mathbf{w} \partial \boldsymbol{\lambda}^\top} \right) \Big|_{\boldsymbol{\lambda}, \mathbf{w}_{i-1}(\boldsymbol{\lambda})} && \text{expand } \frac{\partial \mathbf{w}_i}{\partial \boldsymbol{\lambda}} \\
&= -\frac{\partial^2 \mathcal{L}_T}{\partial \mathbf{w} \partial \boldsymbol{\lambda}^\top} \Big|_{\boldsymbol{\lambda}, \mathbf{w}_i(\boldsymbol{\lambda})} - \left(I - \frac{\partial^2 \mathcal{L}_T}{\partial \mathbf{w} \partial \mathbf{w}^\top} \Big|_{\boldsymbol{\lambda}, \mathbf{w}_i(\boldsymbol{\lambda})} \right) \frac{\partial^2 \mathcal{L}_T}{\partial \mathbf{w} \partial \boldsymbol{\lambda}^\top} \Big|_{\boldsymbol{\lambda}, \mathbf{w}_{i-1}(\boldsymbol{\lambda})} + \\
&\quad \left[\prod_{k < 2} I - \frac{\partial^2 \mathcal{L}_T}{\partial \mathbf{w} \partial \mathbf{w}^\top} \Big|_{\boldsymbol{\lambda}, \mathbf{w}_{i-k}(\boldsymbol{\lambda})} \right] \frac{\partial \mathbf{w}_{i-1}}{\partial \boldsymbol{\lambda}} \Big|_{\boldsymbol{\lambda}} && \text{re-arrange terms} \\
&= \dots \\
\text{So, } \frac{\partial \mathbf{w}_{i+1}}{\partial \boldsymbol{\lambda}} &= - \sum_{j \leq i} \left[\prod_{k < j} I - \frac{\partial^2 \mathcal{L}_T}{\partial \mathbf{w} \partial \mathbf{w}^\top} \Big|_{\boldsymbol{\lambda}, \mathbf{w}_{i-k}(\boldsymbol{\lambda})} \right] \frac{\partial^2 \mathcal{L}_T}{\partial \mathbf{w} \partial \boldsymbol{\lambda}^\top} \Big|_{\boldsymbol{\lambda}, \mathbf{w}_{i-j}(\boldsymbol{\lambda})} && \text{telescope the recurrence}
\end{aligned}$$

□

Theorem (Neumann-SGD). Given the recurrence from unrolling SGD optimization in Equation 3.6, if $\mathbf{w}_0 = \mathbf{w}^*(\boldsymbol{\lambda})$:

$$\frac{\partial \mathbf{w}_{i+1}}{\partial \boldsymbol{\lambda}} = - \left(\sum_{j \leq i} \left[I - \frac{\partial^2 \mathcal{L}_T}{\partial \mathbf{w} \partial \mathbf{w}^\top} \right]^j \right) \frac{\partial^2 \mathcal{L}_T}{\partial \mathbf{w} \partial \boldsymbol{\lambda}^\top} \Big|_{\mathbf{w}^*(\boldsymbol{\lambda})}$$

and if $I - \frac{\partial^2 \mathcal{L}_T}{\partial \mathbf{w} \partial \mathbf{w}^\top}$ is contractive:

$$\lim_{i \rightarrow \infty} \frac{\partial \mathbf{w}_{i+1}}{\partial \boldsymbol{\lambda}} = - \left[\frac{\partial^2 \mathcal{L}_T}{\partial \mathbf{w} \partial \mathbf{w}^\top} \right]^{-1} \frac{\partial^2 \mathcal{L}_T}{\partial \mathbf{w} \partial \boldsymbol{\lambda}^\top} \Big|_{\mathbf{w}^*(\boldsymbol{\lambda})}$$

Proof.

$$\begin{aligned}
& \lim_{i \rightarrow \infty} \frac{\partial \mathbf{w}_{i+1}}{\partial \boldsymbol{\lambda}} \Big|_{\boldsymbol{\lambda}} && \text{take } \lim_{i \rightarrow \infty} \\
& = \lim_{i \rightarrow \infty} \left(- \sum_{j \leq i} \left[\prod_{k < j} I - \frac{\partial^2 \mathcal{L}_{\mathcal{T}}}{\partial \mathbf{w} \partial \mathbf{w}^{\top}} \Big|_{\boldsymbol{\lambda}, \mathbf{w}_{i-k}(\boldsymbol{\lambda})} \right] \frac{\partial^2 \mathcal{L}_{\mathcal{T}}}{\partial \mathbf{w} \partial \boldsymbol{\lambda}^{\top}} \Big|_{\boldsymbol{\lambda}, \mathbf{w}_{i-j}(\boldsymbol{\lambda})} \right) && \text{by Lemma 2} \\
& = - \lim_{i \rightarrow \infty} \left(\sum_{j \leq i} \left[\prod_{k < j} I - \frac{\partial^2 \mathcal{L}_{\mathcal{T}}}{\partial \mathbf{w} \partial \mathbf{w}^{\top}} \right] \frac{\partial^2 \mathcal{L}_{\mathcal{T}}}{\partial \mathbf{w} \partial \boldsymbol{\lambda}^{\top}} \right) \Big|_{\boldsymbol{\lambda}, \mathbf{w}^*(\boldsymbol{\lambda})} && \mathbf{w}_0 = \mathbf{w}^*(\boldsymbol{\lambda}) = \mathbf{w}_i \\
& = - \lim_{i \rightarrow \infty} \left(\sum_{j \leq i} \left[I - \frac{\partial^2 \mathcal{L}_{\mathcal{T}}}{\partial \mathbf{w} \partial \mathbf{w}^{\top}} \right]^j \right) \frac{\partial^2 \mathcal{L}_{\mathcal{T}}}{\partial \mathbf{w} \partial \boldsymbol{\lambda}^{\top}} \Big|_{\boldsymbol{\lambda}, \mathbf{w}^*(\boldsymbol{\lambda})} && \text{simplify} \\
& = - \left[I - \left(I - \frac{\partial^2 \mathcal{L}_{\mathcal{T}}}{\partial \mathbf{w} \partial \mathbf{w}^{\top}} \right) \right]^{-1} \frac{\partial^2 \mathcal{L}_{\mathcal{T}}}{\partial \mathbf{w} \partial \boldsymbol{\lambda}^{\top}} \Big|_{\boldsymbol{\lambda}, \mathbf{w}^*(\boldsymbol{\lambda})} && \text{contractive \& Neumann series} \\
& = - \left[\frac{\partial^2 \mathcal{L}_{\mathcal{T}}}{\partial \mathbf{w} \partial \mathbf{w}^{\top}} \right]^{-1} \frac{\partial^2 \mathcal{L}_{\mathcal{T}}}{\partial \mathbf{w} \partial \boldsymbol{\lambda}^{\top}} \Big|_{\boldsymbol{\lambda}, \mathbf{w}^*(\boldsymbol{\lambda})} && \text{simplify}
\end{aligned}$$

□

A.5 Experiments

We use PyTorch (Paszke et al., 2017) as our computational framework. All experiments were performed on NVIDIA TITAN Xp GPUs.

For all CNN experiments, we use the following optimization setup: for the neural network weights we use Adam (Kingma and Ba, 2014) with a learning rate of $1e-4$. For the hyperparameters, we use RMSprop (Hinton et al., 2012) with a learning rate of $1e-2$.

A.5.1 Overfitting a Small Validation Set

We see our algorithm’s ability to overfit the validation data (see Fig. A.1). We use 50 training input and 50 validation input with the standard testing partition for both MNIST and CIFAR-10. We check performance with logistic regression (Linear), a 1-layer fully-connected neural network with as many hidden units as input size (ex., $28 \times 28 = 784$, or $32 \times 32 \times 3 = 3072$), LeNet (LeCun et al., 1998), AlexNet (Krizhevsky et al., 2012), and ResNet44 (He et al., 2016). In all examples, we can achieve 100% training and validation accuracy, while the testing accuracy is significantly lower.

A.5.2 Dataset Distillation

With MNIST, we use the entire validation dataset, while for CIFAR, we use 300 data points.

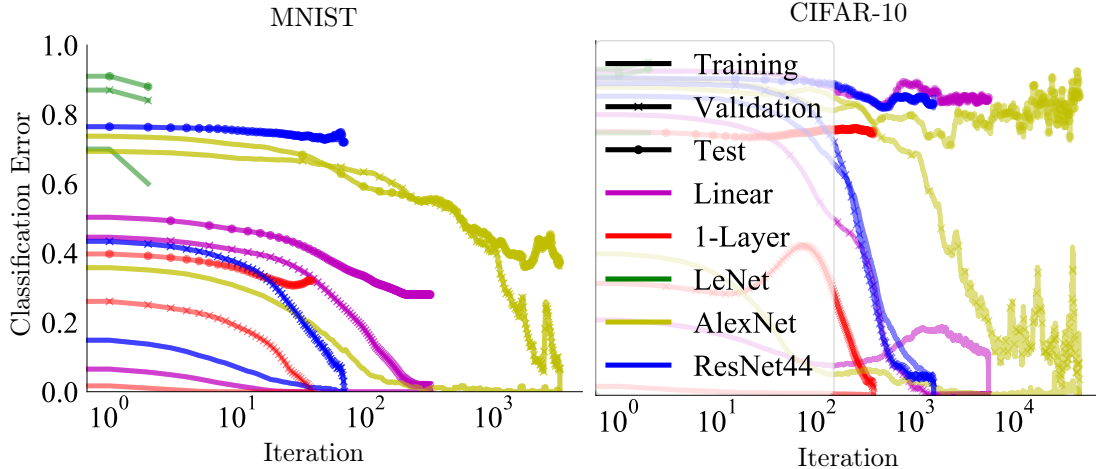


Figure A.1: Overfitting validation data. Algorithm 4 can overfit the validation dataset. We use 50 training input and 50 validation input with the standard testing partition for both MNIST and CIFAR-10. We check the performance with logistic regression (Linear), a fully connected 1-layer neural network with as many hidden units as input size (ex., $28 \times 28 = 784$, or $32 \times 32 \times 3 = 3072$), LeNet (LeCun et al., 1998), AlexNet (Krizhevsky et al., 2012), and ResNet44 (He et al., 2016). Separate lines are plotted for the training, validation, and testing errors. In all examples, we achieve 100% training and validation accuracy, while testing accuracy is significantly lower.

A.5.3 Learned Data Augmentation

Augmentation Network Details: Data augmentation can be framed as an image-to-image transformation problem. Inspired by this, we use a U-Net (Ronneberger et al., 2015) as the data augmentation network. To allow stochastic transformations, we provide random noise by concatenating a noise channel into the input image so that the resulting input has 4 channels. We evaluated the accuracy for training, validation, and testing with an average of 10 augmented samples.

A.5.4 RNN Hyperparameter Optimization

We base our implementation on the AWD-LSTM codebase.¹ Similar to Gal and Ghahramani (2016), we used a 2-layer LSTM with 650 hidden units per layer and 650-dimensional word embeddings.

Overfitting Validation Data: We used a subset of 10 training sequences and 10 validation sequences and tuned separate weight decays per parameter. The LSTM architecture we use has 13 280 400 weights and thus an equal number of weight decay hyperparameters.

Optimization Details: For the large-scale experiments, we follow the training setup proposed in Merity et al. (2018): for the neural network weights, we use SGD with learning rate 30 and gradient clipping to magnitude 0.25. The learning rate was decayed by a factor of 4 based on the non-monotonic criterion introduced by Merity et al. (2018) (i.e., when the validation loss fails to decrease for 5 epochs). We used Adam with learning rate 0.001 to optimize the hyperparameters. We trained on sequences of length 70 in mini-batches of size 40.

¹<https://github.com/salesforce/awd-lstm-lm>

CIFAR-100 Distillation

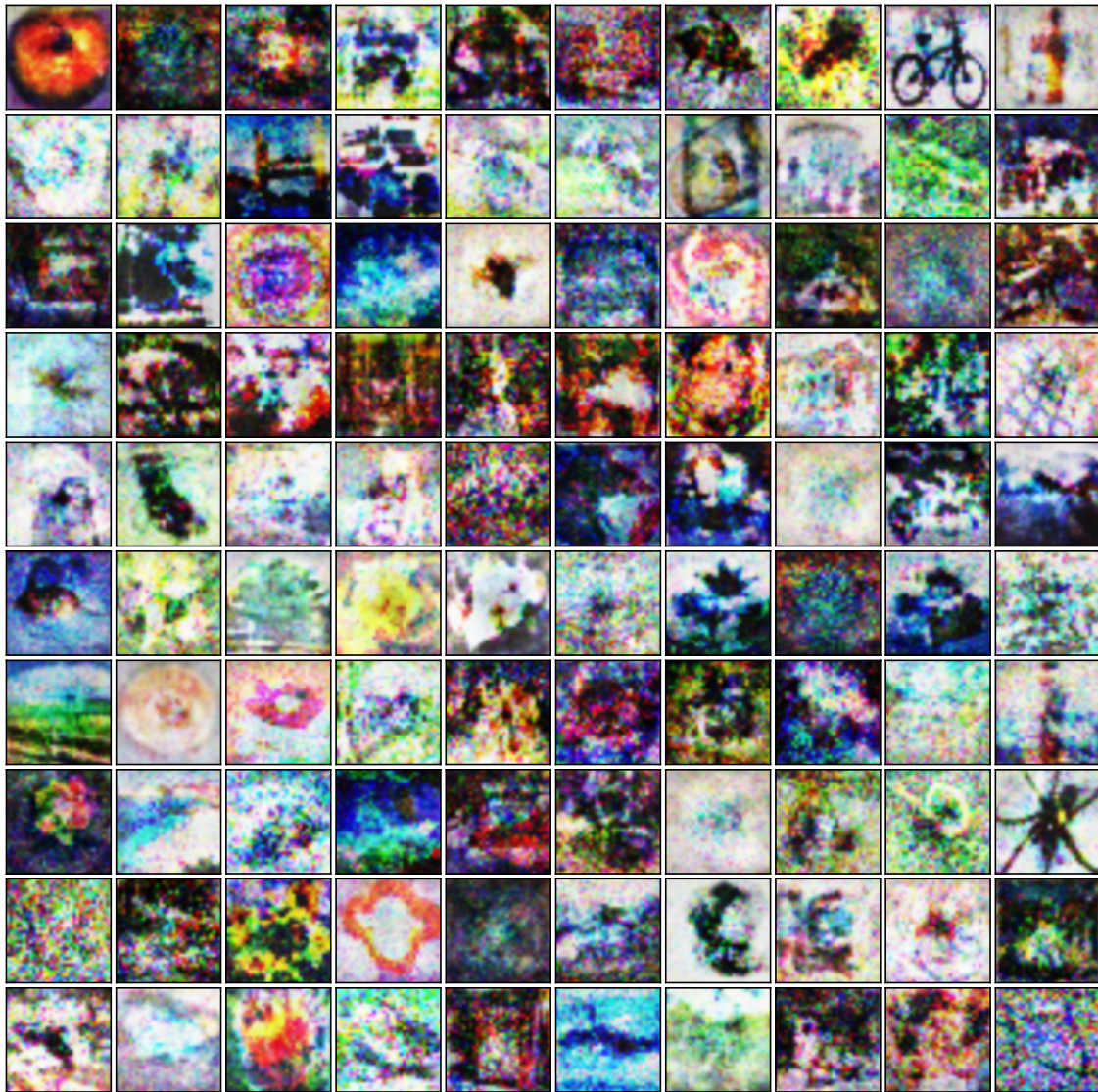


Figure A.2: The complete dataset distillation for CIFAR-100. Referenced in Fig. 3.6.

Appendix B

Complex Momentum for Optimization in Games

B.1 Supporting Results

First, some basic results about complex numbers that are used:

$$z = \Re(z) + i\Im(z) = |z| \exp(i \arg(z)) \quad (\text{B.1})$$

$$\bar{z} = \Re(z) - i\Im(z) = |z| \exp(-i \arg(z)) \quad (\text{B.2})$$

$$\exp(iz) + \exp(-iz) = 2 \cos(z) \quad (\text{B.3})$$

$$\overline{z_1 z_2} = \bar{z}_1 \bar{z}_2 \quad (\text{B.4})$$

$$1/2(z + \bar{z}) = \Re(z) \quad (\text{B.5})$$

$$\Re(z_1 z_2) = \Re(z_1) \Re(z_2) - \Im(z_1) \Im(z_2) \quad (\text{B.6})$$

$$z_1 + z_2 = (\Re(z_1) + \Re(z_2)) + i(\Im(z_1) + \Im(z_2)) \quad (\text{B.7})$$

$$z_1 z_2 = (\Re(z_1) \Re(z_2) - \Im(z_1) \Im(z_2)) + i(\Im(z_1) \Re(z_2) + \Re(z_1) \Im(z_2)) \quad (\text{B.8})$$

$$z_1 z_2 = |z_1| |z_2| \exp(i(\arg(z_1) + \arg(z_2))) \quad (\text{B.9})$$

$$z^k = |z|^k \exp(i \arg(z) k) = |z|^k (\cos(k \arg(z)) + i \sin(k \arg(z))) \quad (\text{B.10})$$

This Lemma shows how we expand the complex-valued momentum buffer $\boldsymbol{\mu}$ into its Cartesian components as in Equation 4.9.

Lemma B.1.1.

$$\begin{aligned} \boldsymbol{\mu}^{j+1} &= \beta \boldsymbol{\mu}^j - \hat{\boldsymbol{g}}^j \iff \\ \Re(\boldsymbol{\mu}^{j+1}) &= \Re(\beta) \Re(\boldsymbol{\mu}^j) - \Im(\beta) \Im(\boldsymbol{\mu}^j) - \Re(\hat{\boldsymbol{g}}^j), \Im(\boldsymbol{\mu}^{j+1}) = \Im(\beta) \Re(\boldsymbol{\mu}^j) + \Re(\beta) \Im(\boldsymbol{\mu}^j) - \Im(\hat{\boldsymbol{g}}^j) \end{aligned}$$

Proof.

$$\begin{aligned}
\boldsymbol{\mu}^{j+1} &= \beta \boldsymbol{\mu}^j - \hat{\boldsymbol{g}}^j \\
\iff \boldsymbol{\mu}^{j+1} &= (\Re(\beta) + i\Im(\beta)) \left(\Re(\boldsymbol{\mu}^j) + i\Im(\boldsymbol{\mu}^j) \right) - \left(\Re(\hat{\boldsymbol{g}}^j) + i\Im(\hat{\boldsymbol{g}}^j) \right) \\
\iff \boldsymbol{\mu}^{j+1} &= \left(\Re(\beta) \Re(\boldsymbol{\mu}^j) - \Im(\beta) \Im(\boldsymbol{\mu}^j) \right) + \\
&\quad i \left(\Im(\beta) \Re(\boldsymbol{\mu}^j) + \Re(\beta) \Im(\boldsymbol{\mu}^j) \right) - \left(\Re(\hat{\boldsymbol{g}}^j) + i\Im(\hat{\boldsymbol{g}}^j) \right) \\
\iff \boldsymbol{\mu}^{j+1} &= \left(\Re(\beta) \Re(\boldsymbol{\mu}^j) - \Im(\beta) \Im(\boldsymbol{\mu}^j) - \Re(\hat{\boldsymbol{g}}^j) \right) + \\
&\quad i \left(\Im(\beta) \Re(\boldsymbol{\mu}^j) + \Re(\beta) \Im(\boldsymbol{\mu}^j) - \Im(\hat{\boldsymbol{g}}^j) \right) \\
\iff \Re(\boldsymbol{\mu}^{j+1}) &= \Re(\beta) \Re(\boldsymbol{\mu}^j) - \Im(\beta) \Im(\boldsymbol{\mu}^j) - \Re(\hat{\boldsymbol{g}}^j), \\
\Im(\boldsymbol{\mu}^{j+1}) &= \Im(\beta) \Re(\boldsymbol{\mu}^j) + \Re(\beta) \Im(\boldsymbol{\mu}^j) - \Im(\hat{\boldsymbol{g}}^j)
\end{aligned}$$

□

We further assume $\Im(\hat{\boldsymbol{g}}^j)$ is 0 - i.e., our gradients are real-valued. This Lemma decomposes the joint-parameters $\boldsymbol{\omega}$ at the next iterate as a linear combination of the joint-parameters, joint-gradient, and Cartesian components of the momentum-buffer at the current iterate as in Equation 4.10.

Lemma B.1.2.

$$\boldsymbol{\omega}^{j+1} = \boldsymbol{\omega}^j + \Re(\alpha \boldsymbol{\mu}^{j+1}) \iff \boldsymbol{\omega}^{j+1} = \boldsymbol{\omega}^j - \Re(\alpha) \hat{\boldsymbol{g}}^j + \Re(\alpha\beta) \Re(\boldsymbol{\mu}^j) - \Im(\alpha\beta) \Im(\boldsymbol{\mu}^j)$$

Proof.

$$\begin{aligned}
&\Re(\alpha \boldsymbol{\mu}^{j+1}) \\
&= \left(\Re(\alpha) \Re(\boldsymbol{\mu}^{j+1}) - \Im(\alpha) \Im(\boldsymbol{\mu}^{j+1}) \right) \\
&= \left(\Re(\alpha) \left(\Re(\beta) \Re(\boldsymbol{\mu}^j) - \Im(\beta) \Im(\boldsymbol{\mu}^j) - \Re(\hat{\boldsymbol{g}}^j) \right) - \Im(\alpha) \left(\Im(\beta) \Re(\boldsymbol{\mu}^j) + \Re(\beta) \Im(\boldsymbol{\mu}^j) \right) \right) \\
&= -\Re(\alpha) \hat{\boldsymbol{g}}^j + \left(\Re(\alpha) \left(\Re(\beta) \Re(\boldsymbol{\mu}^j) - \Im(\beta) \Im(\boldsymbol{\mu}^j) \right) - \Im(\alpha) \left(\Im(\beta) \Re(\boldsymbol{\mu}^j) + \Re(\beta) \Im(\boldsymbol{\mu}^j) \right) \right) \\
&= -\Re(\alpha) \hat{\boldsymbol{g}}^j + \left(\Re(\alpha) \Re(\beta) - \Im(\alpha) \Im(\beta) \right) \Re(\boldsymbol{\mu}^j) - \left(\Re(\alpha) \Im(\beta) + \Im(\alpha) \Re(\beta) \right) \Im(\boldsymbol{\mu}^j) \\
&= -\Re(\alpha) \hat{\boldsymbol{g}}^j + \Re(\alpha\beta) \Re(\boldsymbol{\mu}^j) - \Im(\alpha\beta) \Im(\boldsymbol{\mu}^j)
\end{aligned}$$

Thus,

$$\boldsymbol{\omega}^{j+1} = \boldsymbol{\omega}^j + \Re(\alpha \boldsymbol{\mu}^{j+1}) \iff \boldsymbol{\omega}^{j+1} = \boldsymbol{\omega}^j - \Re(\alpha) \hat{\boldsymbol{g}}^j + \Re(\alpha\beta) \Re(\boldsymbol{\mu}^j) - \Im(\alpha\beta) \Im(\boldsymbol{\mu}^j)$$

□

B.1.1 Theorem 3 Proof Sketch

Theorem 3 (Consequence of Prop. 4.4.1 Bertsekas (2008)). *Complex momentum's convergence rate: If the spectral radius $\rho(\nabla F_{\alpha,\beta}(\mu^*, \omega^*)) < 1$, then, for $[\mu, \omega]$ in a neighborhood of $[\mu^*, \omega^*]$, the distance of $[\mu^j, \omega^j]$ to the stationary point $[\mu^*, \omega^*]$ converges at a linear rate $\mathcal{O}((\rho(\mathbf{J}) + \epsilon)^j)$, $\forall \epsilon > 0$.*

Proof. We reproduce the proof quadratic games, which is simple case of the well-known method from Polyak (1964) for analyzing the convergence of iterative methods. Bertsekas (2008) generalizes this result from quadratic games to when we are sufficiently close to any stationary point.

For quadratic games, we have that $\hat{g}^j = (\nabla_{\omega} \hat{g})^\top \omega^j$. By Lemma B.1.1 and B.1.2 we have:

$$\begin{pmatrix} \Re(\mu^{j+1}) \\ \Im(\mu^{j+1}) \\ \omega^{j+1} \end{pmatrix} = \mathbf{J} \begin{pmatrix} \Re(\mu^j) \\ \Im(\mu^j) \\ \omega^j \end{pmatrix} \quad (\text{B.11})$$

By telescoping the recurrence for the j^{th} augmented parameters:

$$\begin{pmatrix} \Re(\mu^j) \\ \Im(\mu^j) \\ \omega^j \end{pmatrix} = \mathbf{J}^j \begin{pmatrix} \Re(\mu^0) \\ \Im(\mu^0) \\ \omega^0 \end{pmatrix} \quad (\text{B.12})$$

We can compare μ^j with the value it converges to μ^* which exists if \mathbf{J} is contractive. We do the same with ω . Because $\mu^* = \mathbf{J}\mu^* = \mathbf{J}^j\mu^*$:

$$\begin{pmatrix} \Re(\mu^j) - \Re(\mu^*) \\ \Im(\mu^j) - \Im(\mu^*) \\ \omega^j - \omega^* \end{pmatrix} = \mathbf{J}^j \begin{pmatrix} \Re(\mu^0) - \Re(\mu^*) \\ \Im(\mu^0) - \Im(\mu^*) \\ \omega^0 - \omega^* \end{pmatrix} \quad (\text{B.13})$$

By taking norms:

$$\left\| \begin{pmatrix} \Re(\mu^j) - \Re(\mu^*) \\ \Im(\mu^j) - \Im(\mu^*) \\ \omega^j - \omega^* \end{pmatrix} \right\|_2 = \left\| \mathbf{J}^j \begin{pmatrix} \Re(\mu^0) - \Re(\mu^*) \\ \Im(\mu^0) - \Im(\mu^*) \\ \omega^0 - \omega^* \end{pmatrix} \right\|_2 \quad (\text{B.14})$$

$$\implies \left\| \begin{pmatrix} \Re(\mu^j) - \Re(\mu^*) \\ \Im(\mu^j) - \Im(\mu^*) \\ \omega^j - \omega^* \end{pmatrix} \right\|_2 \leq \|\mathbf{J}^j\|_2 \left\| \begin{pmatrix} \Re(\mu^0) - \Re(\mu^*) \\ \Im(\mu^0) - \Im(\mu^*) \\ \omega^0 - \omega^* \end{pmatrix} \right\|_2 \quad (\text{B.15})$$

With Lemma 11 from Foucart (2012), we have there exists a matrix norm $\forall \epsilon > 0$ such that:

$$\|\mathbf{J}^j\| \leq (\rho(\mathbf{J}) + \epsilon)^j \quad (\text{B.16})$$

We have a finite-dimensional space norm equivalence. So, for all norms $\|\cdot\|$, $\exists C \geq B > 0$ such that:

$$B\|\mathbf{J}^j\| \leq \|\mathbf{J}^j\|_2 \leq C\|\mathbf{J}^j\| \quad (\text{B.17})$$

Combining Equations B.16) and B.17 we have:

$$\left\| \begin{pmatrix} \Re(\boldsymbol{\mu}^j) - \Re(\boldsymbol{\mu}^*) \\ \Im(\boldsymbol{\mu}^j) - \Im(\boldsymbol{\mu}^*) \\ \boldsymbol{\omega}^j - \boldsymbol{\omega}^* \end{pmatrix} \right\|_2 \leq C(\rho(\mathbf{J}) + \epsilon)^j \left\| \begin{pmatrix} \Re(\boldsymbol{\mu}^0) - \Re(\boldsymbol{\mu}^*) \\ \Im(\boldsymbol{\mu}^0) - \Im(\boldsymbol{\mu}^*) \\ \boldsymbol{\omega}^0 - \boldsymbol{\omega}^* \end{pmatrix} \right\|_2 \quad (\text{B.18})$$

So, we have:

$$\left\| \begin{pmatrix} \Re(\boldsymbol{\mu}^j) - \Re(\boldsymbol{\mu}^*) \\ \Im(\boldsymbol{\mu}^j) - \Im(\boldsymbol{\mu}^*) \\ \boldsymbol{\omega}^j - \boldsymbol{\omega}^* \end{pmatrix} \right\|_2 = \mathcal{O}\left((\rho(\mathbf{J}) + \epsilon)^j\right) \quad (\text{B.19})$$

Thus, we converge linearly with a rate of $\mathcal{O}(\rho(\mathbf{J}) + \epsilon)$. \square

B.1.2 Characterizing the Augmented Dynamics Eigenvalues

Here, we present polynomials whose roots are the eigenvalues of the Jacobian of our augmented dynamics $\text{Sp}(\mathbf{J})$, given the eigenvalues of the Jacobian of the joint-gradient vector field $\text{Sp}(\nabla_{\boldsymbol{\omega}} \hat{\mathbf{g}})$.

We use a similar decomposition as Gidel et al. (2019).

We expand $\nabla_{\boldsymbol{\omega}} \hat{\mathbf{g}} = \mathbf{P}\mathbf{T}\mathbf{P}^{-1}$ where \mathbf{T} is upper-triangular and λ_i is an eigenvalue of $\nabla_{\boldsymbol{\omega}} \hat{\mathbf{g}}$.

$$\mathbf{T} = \begin{bmatrix} \lambda_1 & * & \dots & * \\ 0 & \dots & \dots & \dots \\ \dots & \dots & \dots & * \\ 0 & \dots & 0 & \lambda_d \end{bmatrix} \quad (\text{B.20})$$

We then break up into components for each eigenvalue, giving us submatrices $\mathbf{R}_k \in \mathbb{C}^{3 \times 3}$:

$$\mathbf{J}_k := \begin{bmatrix} \Re(\beta) & -\Im(\beta) & -\lambda_k \\ \Im(\beta) & \Re(\beta) & 0 \\ \Re(\alpha\beta) & -\Im(\alpha\beta) & 1 - \Re(\alpha)\lambda_k \end{bmatrix} \quad (\text{B.21})$$

We can get the characteristic polynomial of \mathbf{J}_k with the following Mathematica command, where we use substitute the symbols $r + iu = \lambda_k$, $a = \Re(\beta)$, $b = \Im(\beta)$, $c = \Re(\alpha)$, and $d = \Im(\alpha)$.

`CharacteristicPolynomial[{{a, -b, -(r + u I)}, {b, a, 0}, {a c - b d, -(b c + a d), 1 - c (r + u I)}}, x]`

The command gives us the polynomial associated with the eigenvalue $\lambda_k = r + iu$:

$$p_k(x) = -a^2x + a^2 + acrx + iacux + 2ax^2 - 2ax - b^2x + b^2 + bdrx + ibdux - crx^2 - icux^2 - x^3 + x^2 \quad (\text{B.22})$$

Consider the case where λ_k is imaginary – i.e., $r = 0$ – which is true in all purely adversarial and bilinear zero-sum games. Then (B.22) simplifies to:

$$p_k(x) = -a^2x + a^2 + iacux + 2ax^2 - 2ax - b^2x + b^2 + ibdux - icux^2 - x^3 + x^2 \quad (\text{B.23})$$

Our complex λ_k come in conjugate pairs where $\lambda_k = u_k i$ and $\bar{\lambda}_k = -u_k i$. Equation B.23 has the same roots for λ_k and $\bar{\lambda}_k$, which can be verified by writing the roots with the cubic formula. This corresponds to spiraling around the solution in either a clockwise or counterclockwise direction. Thus, we restrict ourselves to analyzing λ_k where u_k is positive without loss of generality.

If we make the step size α real – i.e., $d = 0$ – then Equation B.23 simplifies to:

$$p_k(x) = x \left(-a^2 + iacu - 2a - b^2 \right) + a^2 + x^2 (2a - icu + 1) + b^2 - x^3 \quad (\text{B.24})$$

Using a heuristic from single-objective optimization, we look at making step size proportional to the inverse of the magnitude of eigenvalue k – i.e., $\alpha_k = \frac{\alpha'}{|\lambda_k|} = \frac{\alpha'}{u_k}$. With this, (B.24) simplifies to:

$$p_k(x) = x \left(-a^2 + ia\alpha' - 2a - b^2 \right) + a^2 + x^2 (2a - i\alpha' + 1) + b^2 - x^3 \quad (\text{B.25})$$

Notably, in Equation B.25 there is no dependence on the components of imaginary eigenvalue $\lambda_k = r + iu = 0 + iu$, by selecting a α that is proportional to the eigenvalues inverse magnitude. We can further simplify with $a^2 + b^2 = |\beta|^2$:

$$p_k(x) = x \left(\Re(\beta) (i\alpha' - 2) - |\beta|^2 \right) + x^2 (2\Re(\beta) - i\alpha' + 1) + |\beta|^2 - x^3 \quad (\text{B.26})$$

We could expand this in polar form for β by noting $\Re(\beta) = |\beta| \cos(\arg(\beta))$:

$$p_k(x) = x \left(|\beta| \cos(\arg(\beta)) (i\alpha' - 2) - |\beta|^2 \right) + x^2 \left(2|\beta| \cos(\arg(\beta)) - i\alpha' + 1 \right) + |\beta|^2 - x^3 \quad (\text{B.27})$$

We can simplify further by considering an imaginary β – i.e., $\Re(\beta) = 0$ or $\cos(\arg(\beta)) = 0$:

$$p_k(x) = |\beta|^2 - x|\beta|^2 - x^2 (i\alpha' - 1) - x^3 \quad (\text{B.28})$$

The roots of these polynomials can be trivially evaluated numerically or symbolically with the by plugging in β, α , and λ_k then using the cubic formula. This section can be easily modified for the eigenvalues of the augmented dynamics for variants of complex momentum by defining the appropriate \mathbf{J} and modifying the Mathematica command to get the characteristic polynomial for each component, which can be evaluated if it is a sufficiently low degree using known formulas.

B.1.3 Convergence Bounds

Corollary 1 (Convergence of Complex Momentum). *There exist $\alpha \in \mathbb{R}, \beta \in \mathbb{C}$ so Algorithm 7 converges for bilinear zero-sum games. More-so, for small ϵ (we show for $\epsilon = \frac{\pi}{16}$), if $\arg(\beta) = \epsilon$ (i.e., almost-positive) or $\arg(\beta) = \pi - \epsilon$ (i.e., almost-negative), then we can select $\alpha, |\beta|$ to converge.*

Proof. Note that Theorem 3 bounds the convergence rate of Algorithm 7 by $\text{Sp}(\mathbf{J})$. Also, Equation B.24 gives a formula for 3 eigenvalues in $\text{Sp}(\mathbf{J})$ given α, β , and an eigenvalue $\lambda \in \text{Sp}(\nabla_{\omega} \hat{\mathbf{g}})$. The formula outputs a cubic polynomial whose roots are eigenvalues of $\text{Sp}(\mathbf{J})$, which can be trivially evaluated with the cubic formula.

We denote the k^{th} eigenspace of $\text{Sp}(\nabla_{\omega} \hat{\mathbf{g}})$ with eigenvalue $\lambda_k = ic_k$ and $|c_1| \leq \dots \leq |c_n|$, because bilinear zero-sum games have purely imaginary eigenvalues due to $\nabla_{\omega} \hat{\mathbf{g}}$ being antisymmetric. Eigenvalues come in a conjugate pairs, where $\bar{\lambda}_k = i(-c_k)$

If we select momentum coefficient $\beta = |\beta| \exp(i \arg(\beta))$ and step size $\alpha_k = \frac{\alpha'_k}{|c_k|}$, and use that $\lambda \in \text{Sp}(\nabla_{\omega} \hat{g})$ are imaginary, then – as shown in Appendix Section B.1.2 – (B.24) simplifies to:

$$p_k(x) = x \left(|\beta| \cos(\arg(\beta)) (i\alpha'_k - 2) - |\beta|^2 \right) + x^2 \left(2|\beta| \cos(\arg(\beta)) - i\alpha'_k + 1 \right) + |\beta|^2 - x^3 \quad (\text{B.29})$$

So, with these parameter selections, the convergence rate of Algorithm 7 in the k^{th} eigenspace is bounded by the largest root of Equation B.29.

Note that if we find a separate α'_k that converges in each eigenspace k , then selected the smallest α'_k converges in every eigenspace because the convergence rate in eigenspace k is a convex function of α that equals 1 when $\alpha = 0$ and is minimized when $\alpha > 0$.

First, consider $\arg(\beta) = \pi - \epsilon$, where $\epsilon = \frac{\pi}{16}$. We select $\alpha'_k = 0.75$ (equivalently, $\alpha_k = \frac{0.75}{|c_k|}$) and $|\beta| = 0.986$ via grid search. Using the cubic formula on the associated $p(x)$ from Equation B.29, the maximum magnitude root has size $\approx 0.9998 < 1$, so this selection converges in the k^{th} eigenspace. So, selecting:

$$\hat{\alpha} \leq \min_k \alpha_k \quad (\text{B.30})$$

$$= \min_k \frac{0.75}{c_k} \quad (\text{B.31})$$

$$= \frac{0.75}{\max_k c_k} \quad (\text{B.32})$$

$$= \frac{0.75}{\|\nabla_{\omega} \hat{g}\|_2} \quad (\text{B.33})$$

with $\beta = 0.986 \exp(i(\pi - \epsilon))$ will converge in each eigenspace.

Now, consider $\arg(\beta) = \epsilon = \frac{\pi}{16}$ with $\alpha'_k = 0.025$ and $|\beta| = 0.9$. Using the cubic formula on the associated $p(x)$ from Equation B.29 the maximum magnitude root has size $\approx 0.973 < 1$, so this selection converges in the k^{th} eigenspace. So, selecting:

$$\hat{\alpha} \leq \min_k \alpha_k \quad (\text{B.34})$$

$$= \min_k \frac{0.025}{c_k} \quad (\text{B.35})$$

$$= \frac{0.025}{\max_k c_k} \quad (\text{B.36})$$

$$= \frac{0.025}{\|\nabla_{\omega} \hat{g}\|_2} \quad (\text{B.37})$$

with $\beta = 0.9 \exp(i\epsilon)$ will converge in each eigenspace.

Thus, for any of the $\arg(\beta)$ choices, we can select $\hat{\alpha}, |\beta|$ that converges in every eigenspace and thus converges. □

In the preceding proof, our prescribed $\hat{\alpha}$ depends on the largest norm eigenvalue of $\text{Sp}(\nabla_{\omega} \hat{g})$, due to our selections of $\hat{\alpha} \propto \frac{1}{\|\nabla_{\omega} \hat{g}\|_2}$. In practice, we may not have access to the largest norm eigenvalue of $\text{Sp}(\nabla_{\omega} \hat{g})$. Nevertheless, this shows that a parameter selection converges, even if it may be difficult to find. Often, in convex optimization we describe the choices of α, β in terms of the largest and smallest norm eigenvalues of $\text{Sp}(\nabla_{\omega} \hat{g})$ (i.e., the Hessian of the loss) (Boyd et al., 2004).

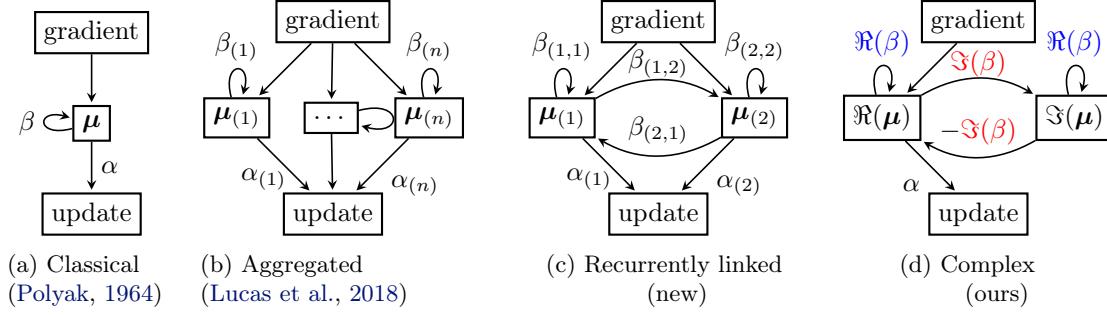


Figure B.1: We show computational diagrams for momentum variants simultaneously updating all players parameters, which update the momentum buffers $\boldsymbol{\mu}$ at iteration $j+1$ with coefficient β via $\boldsymbol{\mu}^{j+1} = (\beta\boldsymbol{\mu}^j - \text{gradient})$. Our parameter update is a linear combination of momentum buffers weighted by step sizes α . (a) Classical momentum (Polyak, 1964; Sutskever et al., 2013), with a single buffer and coefficient $\beta \in [0, 1)$. (b) Aggregated momentum (Lucas et al., 2018) adds multiple buffers with different coefficients. (c) Recurrently linked momentum adds cross-buffer coefficients and updates the buffers with $\boldsymbol{\mu}_{(k)}^{j+1} = \left(\sum_l \beta_{(l,k)} \boldsymbol{\mu}_{(l)}^j - \text{gradient}\right)$. We allow $\beta_{(l,k)}$ to be negative as negative momentum (Gidel et al., 2019) for solutions with simultaneous updates in adversarial games. (d) Complex momentum is a special case of recurrently linked momentum with two buffers and $\beta_{(1,1)} = \beta_{(2,2)} = \Re(\beta)$, $\beta_{(1,2)} = -\beta_{(2,1)} = \Im(\beta)$. Analyzing other recurrently linked momentum setups is an open problem.

B.2 Algorithms

Here, we include additional algorithms that may be useful to some readers. Algorithm 9 show aggregated momentum (Lucas et al., 2018). Algorithm 10 shows the recurrently linked momentum that generalizes and unifies aggregated momentum with negative momentum (Gidel et al., 2019). Algorithm 11 shows our algorithm with alternating updates, which we use for training GANs. Algorithm 12 shows our method with all real-valued objects if one wants to implement complex momentum in a library that does not support complex arithmetic.

Algorithm 9 Aggregated momentum

- 1: Select number of buffers $K \in \mathbb{N}$
 - 2: Select $\beta_{(k)} \in [0, 1)$ for $k = 1 \dots K$
 - 3: Select $\alpha_{(k)} \in \mathbb{R}^+$ for $k = 1 \dots K$
 - 4: Initialize $\boldsymbol{\mu}_{(k)}^0$ for $k = 1 \dots K$
 - 5: **for** $j = 1 \dots N$ **do**
 - 6: **for** $k = 1 \dots K$ **do**
 - 7: $\boldsymbol{\mu}_{(k)}^{j+1} = \beta_{(k)} \boldsymbol{\mu}_{(k)}^j - \hat{\boldsymbol{g}}^j$
 - 8: **end for**
 - 9: $\boldsymbol{\omega}^{j+1} = \boldsymbol{\omega}^j + \sum_{k=1}^K \alpha_{(k)} \boldsymbol{\mu}_{(k)}^{j+1}$
 - 10: **end for**
 - 11: **return** $\boldsymbol{\omega}_N$
-

Algorithm 10 Recurrently linked momentum

```

1: Select number of buffers  $K \in \mathbb{N}$ 
2: Select  $\beta_{(l,k)} \in \mathbb{R}$  for  $l = 1 \dots K$  and  $k = 1 \dots K$ 
3: Select  $\alpha_{(k)} \in \mathbb{R}^+$  for  $k = 1 \dots K$ 
4: Initialize  $\boldsymbol{\mu}_{(k)}^0$  for  $k = 1 \dots K$ 
5: for  $j = 1 \dots N$  do
6:   for  $k = 1 \dots K$  do
7:      $\boldsymbol{\mu}_{(k)}^{j+1} = \sum_l \beta_{(l,k)} \boldsymbol{\mu}_{(l)}^j - \hat{\boldsymbol{g}}^j$ 
8:   end for
9:    $\boldsymbol{\omega}^{j+1} = \boldsymbol{\omega}^j + \sum_{k=1}^K \alpha_{(k)} \boldsymbol{\mu}_{(k)}^{j+1}$ 
10: end for
11: return  $\boldsymbol{\omega}_N$ 

```

Algorithm 11 (AltCM) Momentum

```

1: Select  $\beta \in \mathbb{C}, \alpha \in \mathbb{R}^+$ 
2: Initialize  $\boldsymbol{\mu}_A^0, \boldsymbol{\mu}_B^0$ 
3: for  $j = 1 \dots N$  do
4:    $\boldsymbol{\mu}_A^{j+1} = \beta \boldsymbol{\mu}_A^j - \boldsymbol{g}_A^j$ 
5:    $\boldsymbol{\theta}_A^{j+1} = \boldsymbol{\theta}_A^j + \Re(\alpha \boldsymbol{\mu}_A^{j+1})$ 
6:    $\boldsymbol{\mu}_B^{j+1} = \beta \boldsymbol{\mu}_B^j - \boldsymbol{g}_B(\boldsymbol{\theta}_A^{j+1}, \boldsymbol{\theta}_B^j)$ 
7:    $\boldsymbol{\theta}_B^{j+1} = \boldsymbol{\theta}_B^j + \Re(\alpha \boldsymbol{\mu}_B^{j+1})$ 
8: end for
9: return  $\boldsymbol{\omega}_N$ 

```

Algorithm 12 (SimCM) Complex Momentum - \mathbb{R} valued

```

1: Select  $\Re(\beta), \Im(\beta), \Re(\alpha), \Im(\alpha) \in \mathbb{R}$ 
2: Select  $\Re(\beta), \Im(\beta), \Re(\alpha), \Im(\alpha) \in \mathbb{R}$ 
3: Initialize  $\Re(\boldsymbol{\mu}^0), \Im(\boldsymbol{\mu}^0)$ 
4: for  $j = 1 \dots N$  do
5:    $\Re(\boldsymbol{\mu}^{j+1}) = \Re(\beta) \Re(\boldsymbol{\mu}^j) - \Im(\beta) \Im(\boldsymbol{\mu}^j) - \hat{\boldsymbol{g}}^j$ 
6:    $\Im(\boldsymbol{\mu}^{j+1}) = \Re(\beta) \Im(\boldsymbol{\mu}^j) + \Im(\beta) \Re(\boldsymbol{\mu}^j)$ 
7:    $\boldsymbol{\omega}^{j+1} = \boldsymbol{\omega}^j - \Re(\alpha) \hat{\boldsymbol{g}}^j + \Re(\alpha\beta) \Re(\boldsymbol{\mu}^j) - \Im(\alpha\beta) \Im(\boldsymbol{\mu}^j)$ 
8: end for
9: return  $\boldsymbol{\omega}_N$ 

```

B.2.1 Complex Momentum in PyTorch

Our method can be easily implemented in PyTorch 1.6+ by using complex tensors. The only necessary change to the SGD with momentum optimizer is extracting the real-component from momentum buffer as with JAX – see [here](#).

In older versions of Pytorch, we can use a tensor to represent the momentum buffer $\boldsymbol{\mu}$, step size α , and momentum coefficient β . Specifically, we represent the real and imaginary components of the complex number independently. Then, we redefine the operations `__add__` and `__mult__` to satisfy the rules of complex arithmetic – i.e., Equations B.7 and B.8.

B.3 Experiments

B.3.1 Computing Infrastructure and Runtime

We do our computing in CPU for the purely adversarial experiments in Sections 4.4.1 and 4.4.2. Training each 2D GAN in Section 4.4.3 takes 2 hours and we can train 10 simultaneously on an NVIDIA T4 GPU. Training each CIFAR GAN in Section 4.4.4 takes 10 hours, and we can only train 1 model per NVIDIA T4 GPU.

B.3.2 Optimization in Purely Adversarial Games

We include the alternating update version of Figure 4.3 in Appendix Figure B.3, which allows us to contrast simultaneous and alternating updates. With alternating updates on a Dirac-GAN for $\alpha = 0.1$ the best momentum coefficient β was complex, but we could converge with real, negative momentum. Simultaneous updates may be a competitive choice with alternating updates, if alternating updates cost two gradient evaluations per step, which is common in deep learning setups.

B.3.3 Adversarialnesses Effect on Convergence

We include the extragradient (EG) update with extrapolation parameter α' and step size α :

$$\begin{aligned}\omega^{j+\frac{1}{2}} &= \omega^j - \alpha' \hat{g}^j \\ \omega^{j+1} &= \omega^j - \alpha \hat{g}^{j+\frac{1}{2}}\end{aligned}\tag{EG}$$

and the optimistic gradient (OG) update with extrapolation parameter α' and step size α :

$$\omega^{j+1} = \omega^j - 2\alpha \hat{g}^j + \alpha' \hat{g}^{j-1}\tag{OG}$$

EG and OG are often used with $\alpha = \alpha'$. However, we found that this constraint crippled these methods in cooperative games (that is, minimization). As such, we tune the extrapolation parameter α' separately from the step size α , so EG and OG were competitive baselines.

We include Figure B.4, which shows a GANs spectrum throughout training and elaborates on Figure 4.7. This shows many real and imaginary eigenvalues, so GAN training is neither purely cooperative nor adversarial. In addition, the structure of the set of eigenvalues for the discriminator differs from the generator, which may motivate separate optimizer choices. The structure between the players persists through training, but the eigenvalues grow in magnitude and spread out their phases. This indicates how adversarial the game is can change during training.

B.3.4 Training GANs on 2D Distributions

For 2D distributions, the data is generated by sampling from a mixture of 8 Gaussian distributions distributed uniformly around the unit circle.

For the GAN, we use a fully connected network with 4 ReLU (Hahnloser et al., 2000) layers with 256 hidden units. We chose this architecture to be the same as Gidel et al. (2019). Our noise source for the generator is a 4D Gaussian. We trained the models for 100 000 iterations. The performance of the optimizer settings is evaluated by computing the negative log-likelihood of a batch of 100 000 generated 2D samples.

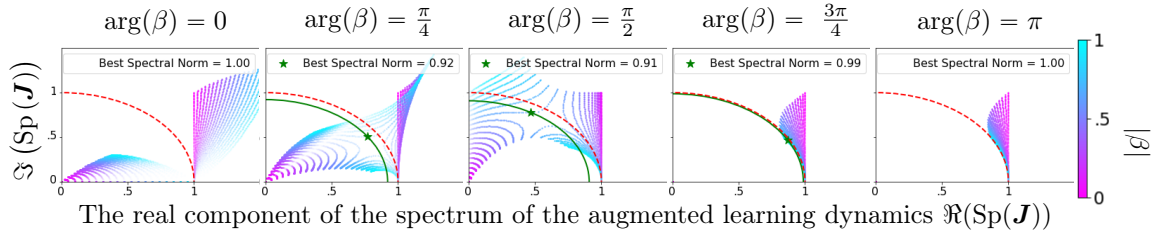


Figure B.2: The spectrum of the augmented learning dynamics \mathbf{J} is shown, whose spectral norm is the convergence rate in Theorem 3. Each image is a different momentum phase $\arg(\beta)$ for a range of $\alpha, |\beta| \in [0, 1]$. The opacity of an eigenvalue is the step size α , and the color corresponds to the magnitude of the momentum $|\beta|$. A red unit circle shows where all eigenvalues must lie to converge for a fixed α, β . If the max eigenvalue norm < 1 , we draw a green circle whose radius is our convergence rate and a green star at the associated eigenvalue. In particular, at every non-real β we can select $\alpha, |\beta|$ for convergence. The eigenvalues are symmetric on the x -axis, and the eigenvalues near $\Re(\lambda) = 1$ dictate convergence rate. The eigenvalues near the center are due to state augmentation, are of small magnitude, and do not impact the convergence rate. Simultaneous gradient descent corresponds to the magenta values where $|\beta| = 0$.

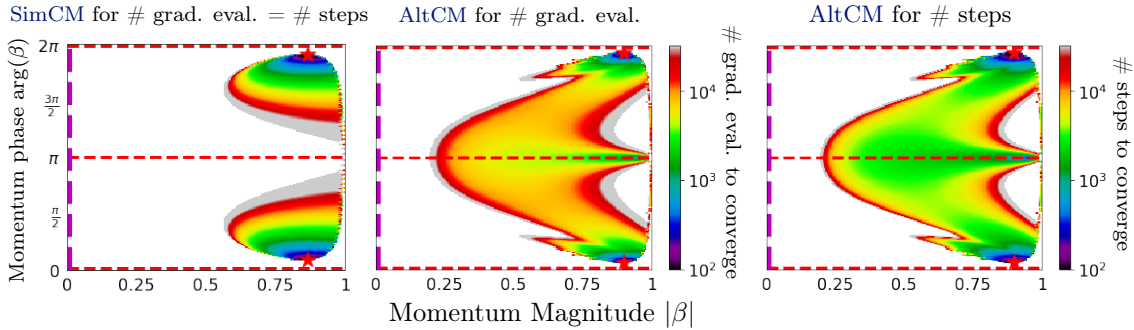


Figure B.3: We show many steps and gradient evaluations both simultaneous and alternating complex momentum take on a Dirac-GAN take for a set solution distance. We fix the step size $\alpha = 0.1$ as in Figure 4.4, while varying the phase and magnitude of our momentum $\beta = |\beta| \exp(i \arg(\beta))$. There is a red star at the optima, dashed red lines at real β , and a dashed magenta line for simultaneous or alternating gradient descent. We only display color for convergent setups. *Left*: Simultaneous complex momentum (SimCM). This is the same as in Figure 4.3, which we repeat to contrast with alternating updates. No real-valued β converges for this – or any – α with simultaneous updates (Gidel et al., 2019). Simultaneous updates can parallelize gradient computation for all players at each step, thus costing only one gradient evaluation per step for many deep learning setups. The best convergence rate per step and gradient evaluation is ≈ 0.955 . *Middle*: Alternating complex momentum (AltCM), where we show how many gradient evaluations – as opposed to steps – to reach a set solution distance. Alternating updates are bottlenecked by waiting for the first player’s update to compute the second player’s update, effectively costing two gradient evaluations per step for many deep learning setups. As shown by Gidel et al. (2019), negative momentum can converge here, but the best momentum is still complex. Also, alternating updates can make the momentum phase $\arg(\beta)$ choice less sensitive to our convergence. The best convergence rate per gradient evaluation is ≈ 0.965 . *Right*: AltCM, where we show how many steps it takes to reach a set solution distance. The best convergence rate per step is ≈ 0.931 . **Takeaway**: If we can parallelize the computation of the gradients of both players, we can benefit from SimCM. However, if we cannot, then AltCM can converge more quickly for a wider set of optimizer parameters. In any case, the best solution uses a complex momentum β for this α .

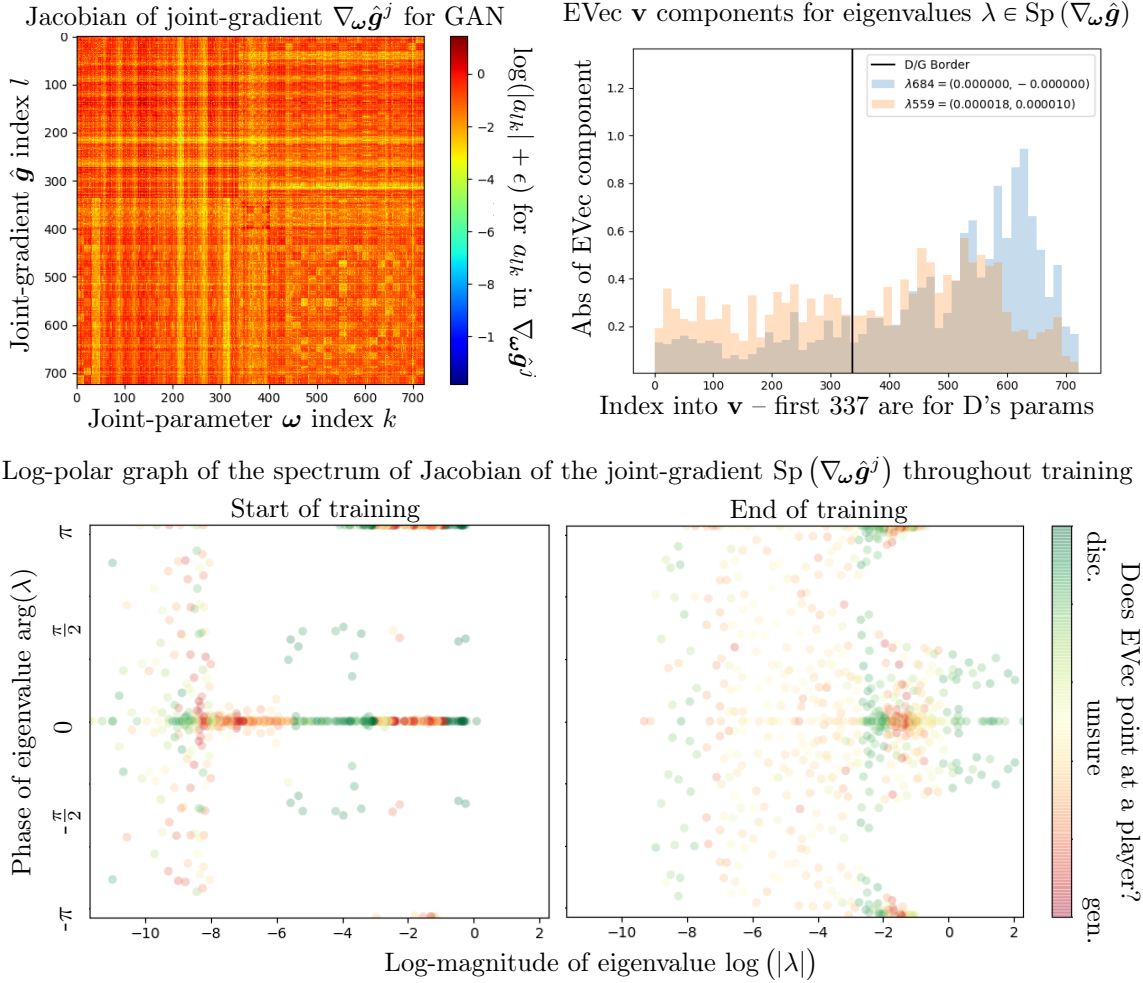


Figure B.4: These plots investigate the spectrum of the Jacobian of the joint-gradient for the GAN in Figure 4.7 through training. The spectrum is key for bounding convergence rates in optimization. *Top left:* The Jacobian $\nabla_{\omega} \hat{g}$ for a GAN on a 2D mixture of Gaussians with a two-layer, fully-connected 16 hidden unit discriminator (D) and generator (G) at the end of training. In the concatenated parameters $\omega \in \mathbb{R}^{723}$, the first 337 are for D, while the last 386 are for G. We display the log of the absolute value of each component plus $\epsilon = 10^{-10}$. The upper left and lower right quadrants are the Hessian of D’s and G’s losses, respectively.

Top Right: We visualize two randomly sampled eigenvectors from $\nabla_{\omega} \hat{g}$. The first part of the parameters is for the discriminator, while the second is for the generator. Given an eigenvalue with eigenvector \mathbf{v} , we approximate the attribution of eigenvectors to players by calculating how much of it lies in the parameter space of D with $\frac{\|\mathbf{v}_{1:D}\|_1}{\|\mathbf{v}\|_1} = \frac{\|\mathbf{v}_{1:337}\|_1}{\|\mathbf{v}\|_1}$. If this ratio is close to 1 (or 0) and say *the eigenvector mostly points at D (or G)*. The blue eigenvector mostly points to G, while the orange eigenvector is unclear. Finding useful ways to attribute eigenvalues to players is an open problem.

Bottom: The spectrum of the Jacobian of the joint-gradient $\text{Sp}(\nabla_{\omega} \hat{g}^j)$ is shown in log-polar coordinates because it is difficult to see structure when graphing in Cartesian (i.e., \Re and \Im) coordinates, due to eigenvalues spanning orders of magnitude, while being positive and negative. The end of training is when we stop making progress on the log-likelihood. We have imaginary eigenvalues at $\arg(\lambda) = \pm\pi/2$, positive eigenvalues at $\arg(\lambda) = 0$, and negative eigenvalues at $\arg(\lambda) = \pm\pi$.

Takeaway: A banded structure for the coloring of the eigenvalues persists through training. We may want different optimizer parameters for the discriminator and generator due to asymmetry in their associated eigenvalues. Furthermore, the magnitude of the eigenvalues increases during training, and the args spread out, indicating that the game can change the eigenstructure near the solutions.

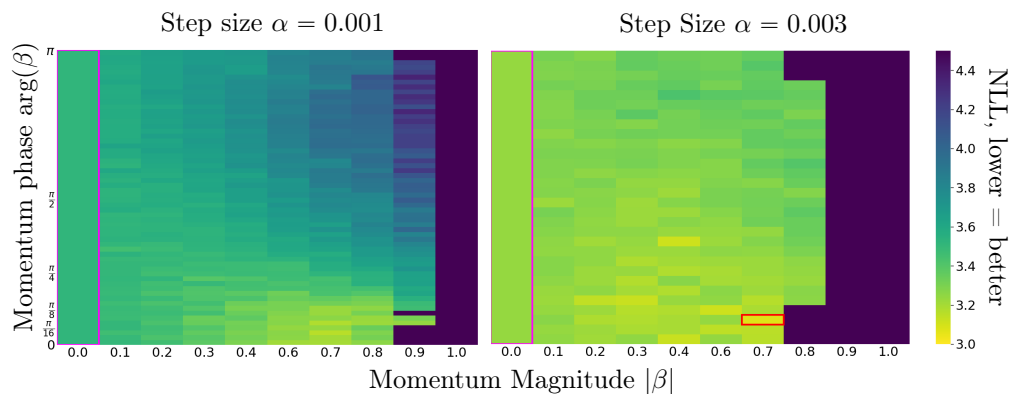


Figure B.5: Heatmaps of the negative log-likelihood (NLL) for tuning $\arg(\beta)$, $|\beta|$ with various fixed α on a 2D mixture of Gaussians GAN. We highlight the best performing cell in red, which had $\arg(\beta) \approx \pi/8$. Runs equivalent to alternating SGD are shown in a magenta box. We compare to negative momentum with alternating updates as in Gidel et al. (2019) in the top row with $\arg(\beta) = \pi$. *Left*: Tuning the momentum with $\alpha = 0.001$. *Right*: Tuning the momentum with $\alpha = 0.003$.

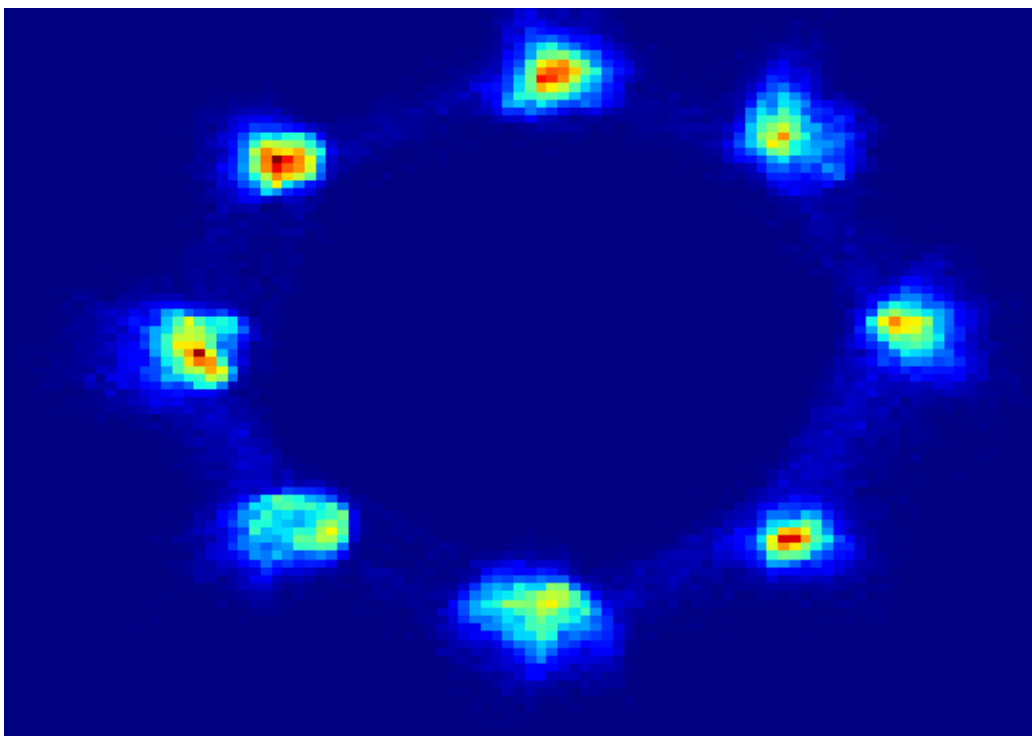


Figure B.6: The mixture of Gaussian samples from the GAN with the best hyperparameters from Figure B.5.



Figure B.7: Class-conditional CIFAR-10 samples from the GAN with the best hyperparameters from Figure B.8.

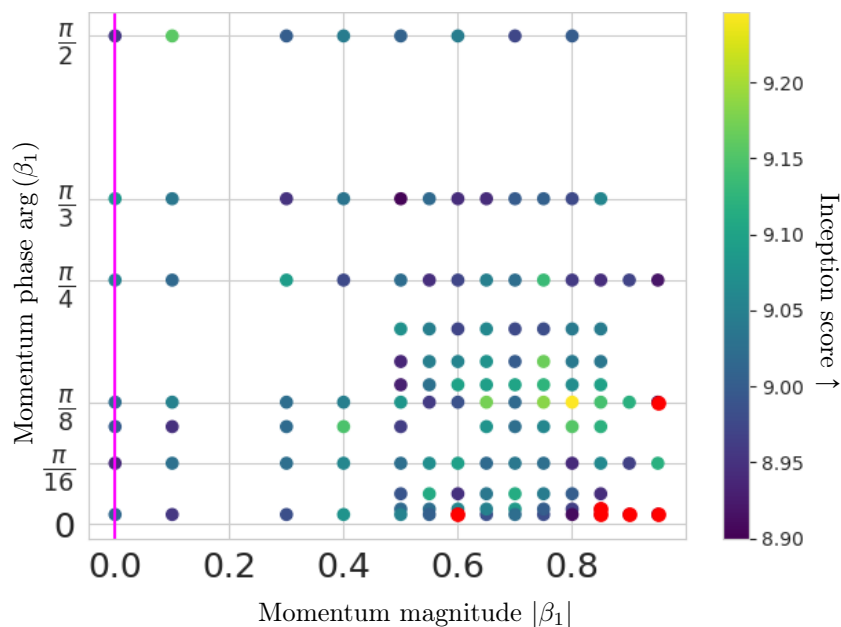


Figure B.8: The inception score for a grid search on $\arg(\beta_1)$ and $|\beta_1|$ for training BigGAN on CIFAR-10 with the Adam variant in Algorithm 8. The β_1 is complex for the discriminator, while the generator's optimizer is fixed to the defaults supplied by the author. Red points are runs that failed to train to the minimum inception score in the color bar. The vertical magenta line denotes runs equivalent to alternating SGD. Negative momentum did not train for any magnitude of momentum $|\beta_1| > .5$, so we did not display it for more resolution near the values of interest.

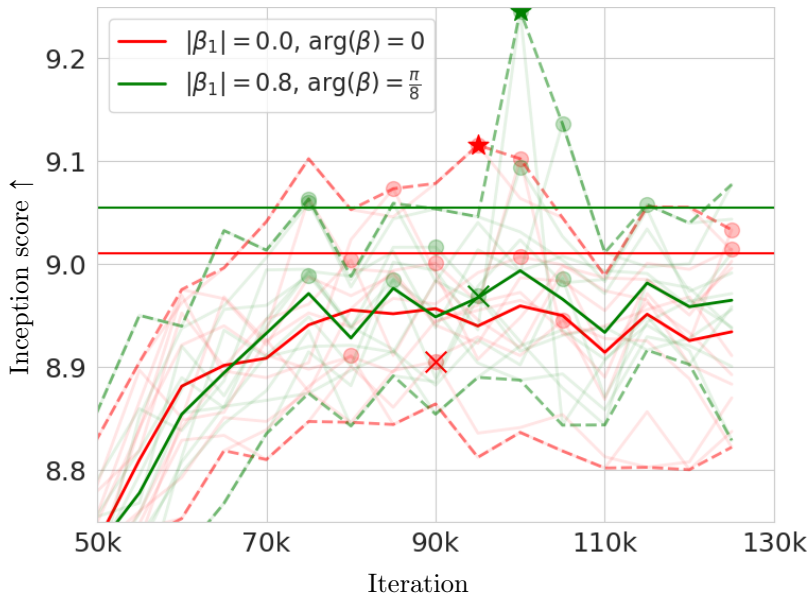


Figure B.9: We compare the best optimization parameters from grid search Figure B.8 for our complex Adam variant (i.e., Algorithm 8) shown in green, with the author provided values shown in red for the CIFAR-10 BigGAN over 10 seeds. A star is displayed at the best inception score for all runs, a cross is at the worst inception score for all runs, and a circle is at the best inception score for each run. Dashed lines are shown at the max/min inception score over all runs at each iteration, low-alpha lines for each runs inception score, and solid lines for the average inception score over all seeds at each iteration. The results are summarized in Table 4.1.

Table B.1: Notation for Complex Momentum for Optimization in Games

SGD	Stochastic Gradient Descent
CM	Complex Momentum
SGDm, SimSGDm, with momentum
SimSGD, SimCM	Simultaneous ...
AltSGD, AltCM	Alternating ...
GAN	Generative Adversarial Network
EG, OG	Extragradient and Optimistic Gradient
IS	Inception Score (Salimans et al., 2016)
$:=$	Defined to be equal to
$x, y, z, \dots \in \mathbb{C}$	Scalars
$\mathbf{x}, \mathbf{y}, \mathbf{z}, \dots \in \mathbb{C}^n$	Vectors
$\mathbf{X}, \mathbf{Y}, \mathbf{Z}, \dots \in \mathbb{C}^{n \times n}$	Matrices
\mathbf{X}^\top	The transpose of matrix \mathbf{X}
\mathbf{I}	The identity matrix
$\Re(z), \Im(z)$	The real or imaginary component of $z \in \mathbb{C}$
i	The imaginary unit. $z \in \mathbb{C} \implies z = \Re(z) + i\Im(z)$
\bar{z}	The complex conjugate of $z \in \mathbb{C}$
$ z := \sqrt{z\bar{z}}$	The magnitude or modulus of $z \in \mathbb{C}$
$\arg(z)$	The argument or phase of $z \in \mathbb{C} \implies z = z \exp(i \arg(z))$
$z \in \mathbb{C}$ is <i>almost-positive</i>	$\arg(z) = \epsilon$ for small ϵ respectively
A, B	A symbol for the outer/inner players
$d_A, d_B \in \mathbb{N}$	The number of weights for the outer/inner players
$\boldsymbol{\theta}$	A symbol for the parameters or weights of a player
$\boldsymbol{\theta}_A \in \mathbb{R}^{d_A}, \boldsymbol{\theta}_B \in \mathbb{R}^{d_B}$	The outer/inner parameters or weights
$\mathcal{L} : \mathbb{R}^n \rightarrow \mathbb{R}$	A symbol for a loss
$\mathcal{L}_A(\boldsymbol{\theta}_A, \boldsymbol{\theta}_B), \mathcal{L}_B(\boldsymbol{\theta}_A, \boldsymbol{\theta}_B)$	The outer/inner losses – $\mathbb{R}^{d_A+d_B} \mapsto \mathbb{R}$
$\mathbf{g}_A(\boldsymbol{\theta}_A, \boldsymbol{\theta}_B), \mathbf{g}_B(\boldsymbol{\theta}_A, \boldsymbol{\theta}_B)$	Gradient of outer/inner losses w.r.t. their weights in \mathbb{R}^{d_A/d_B}
$\boldsymbol{\theta}_B^*(\boldsymbol{\theta}_A) := \operatorname{argmin}_{\boldsymbol{\theta}_B} \mathcal{L}_B(\boldsymbol{\theta}_A, \boldsymbol{\theta}_B)$	The best-response of the inner player to the outer player
$\mathcal{L}_A^*(\boldsymbol{\theta}_A) := \mathcal{L}_A(\boldsymbol{\theta}_A, \boldsymbol{\theta}_B^*(\boldsymbol{\theta}_A))$	The outer loss with a best-responding inner player
$\boldsymbol{\theta}_A^* := \operatorname{argmin}_{\boldsymbol{\theta}_A} \mathcal{L}_A^*(\boldsymbol{\theta}_A)$	Outer optimal weights with a best-responding inner player
$d := d_A + d_B$	The combined number of weights for both players
$\boldsymbol{\omega} := [\boldsymbol{\theta}_A, \boldsymbol{\theta}_B] \in \mathbb{R}^d$	A concatenation of the outer/inner weights
$\hat{\boldsymbol{\omega}} := [\mathbf{g}_A(\boldsymbol{\omega}), \mathbf{g}_B(\boldsymbol{\omega})] \in \mathbb{R}^d$	A concatenation of the outer/inner gradients
$\boldsymbol{\omega}^0 = [\boldsymbol{\theta}_A^0, \boldsymbol{\theta}_B^0] \in \mathbb{R}^d$	The initial parameter values
j	An iteration number
$\hat{\boldsymbol{g}}^j := \hat{\boldsymbol{g}}(\boldsymbol{\omega}^j) \in \mathbb{R}^d$	The joint-gradient vector field at weights $\boldsymbol{\omega}^j$
$\nabla_{\boldsymbol{\omega}} \hat{\boldsymbol{g}}^j := \nabla_{\boldsymbol{\omega}} \hat{\boldsymbol{g}} _{\boldsymbol{\omega}^j} \in \mathbb{R}^{d \times d}$	The Jacobian of the joint-gradient $\hat{\boldsymbol{g}}$ at weights $\boldsymbol{\omega}^j$
$\alpha \in \mathbb{C}$	The step size or learning rate
$\beta \in \mathbb{C}$	The momentum coefficient
$\beta_1 \in \mathbb{C}$	The first momentum parameter for Adam
$\boldsymbol{\mu} \in \mathbb{C}^d$	The momentum buffer
$\lambda \in \mathbb{C}$	Notation for an arbitrary eigenvalue
$\operatorname{Sp}(\mathbf{M}) \in \mathbb{C}^n$	The spectrum – or set of eigenvalues – of $\mathbf{M} \in \mathbb{R}^{n \times n}$
<i>Purely adversarial/cooperative game</i>	$\operatorname{Sp}(\nabla_{\boldsymbol{\omega}} \hat{\boldsymbol{g}})$ is purely real/imaginary
$\rho(\mathbf{M}) := \max_{z \in \operatorname{Sp}(\mathbf{M})} z $	The spectral radius in \mathbb{R}^+ of $\mathbf{M} \in \mathbb{R}^{n \times n}$
$\mathbf{F}_{\alpha, \beta}([\boldsymbol{\mu}, \boldsymbol{\omega}])$	Fixed point op. for CM, or augmented learning dynamics
$\mathbf{J} := \nabla_{[\boldsymbol{\mu}, \boldsymbol{\omega}]} \mathbf{F}_{\alpha, \beta} \in \mathbb{R}^{3d \times 3d}$	Jacobian of the augmented learning dynamics in Corollary 3
$\alpha^*, \beta^* := \operatorname{argmin}_{\alpha, \beta} \rho(\mathbf{J}(\alpha, \beta))$	The optimal step size and momentum coefficient
$\rho^* := \rho(\mathbf{R}(\alpha^*, \beta^*))$	The optimal spectral radius or convergence rate
$\kappa := \frac{\max \operatorname{Sp}(\nabla_{\boldsymbol{\omega}} \mathbf{g})}{\min \operatorname{Sp}(\nabla_{\boldsymbol{\omega}} \mathbf{g})}$	Condition number, for convex single-objective optimization
$\sigma_{\min}^2(\mathbf{M}) := \max \operatorname{Sp}(\mathbf{M}^\top \mathbf{M})$	The minimum singular value of a matrix \mathbf{M}

Appendix C

Lyapunov Exponents for Diversity in Differentiable Games

C.1 Related Work

The material from Chapter 5 is primarily from Lorraine et al. (2022b), with a prior workshop submission of Lorraine et al. (2021b) and an arXiv submission of Lorraine et al. (2021c).

Diversity in machine learning: Finding diverse solutions is often desirable in machine learning, for example, improving performance for model ensembles (Hansen and Salamon, 1990), with canonical approaches directly optimizing for negative correlation amongst model predictions (Liu and Yao, 1999). In recent times, these ideas have begun to re-emerge, improving ensemble performance (Sinha et al., 2021; Ross et al., 2020; Mariet and Sra, 2016), robustness (Pang et al., 2019; Cully et al., 2015) and boosting exploration in reinforcement learning (Lehman and Stanley, 2008; Eysenbach et al., 2019; Parker-Holder et al., 2020b; Pugh et al., 2016).

Many of these approaches seek diverse solutions by following gradients of an altered, typically multi-objective loss function. In contrast, the recent *Ridge Rider* (RR) (Parker-Holder et al., 2020a) algorithm searches for diverse solutions by following eigenvectors of the Hessian with respect to the original loss function, producing orthogonal (loss reducing) search directions.

Finding solutions in games: There are first-order methods for finding solutions in games (Zhang et al., 2021b) including alternating updates (Zhang et al., 2022), extragradient (Korpelevich, 1976; Azizian et al., 2020c), optimistic gradient (Rakhlin and Sridharan, 2013; Daskalakis et al., 2018), negative momentum (Gidel et al., 2019; Zhang and Wang, 2021), complex momentum (Lorraine et al., 2022c), and iterate averaging (Gidel et al., 2018). There are also higher-order methods such as consensus optimization (Mescheder et al., 2017), symplectic gradient adjustment (SGA) (Letcher et al., 2019), local symplectic surgery (LSS) (Mazumdar et al., 2019), competitive gradient descent (CGD) (Schäfer and Anandkumar, 2019), follow-the-ridge (Wang et al., 2019b). Recently, Vicol et al. (2022a) looked at the effects of overparameterization while doing online learning in games.

Diversity in multi-agent RL: In recent times, a series of works have explored the benefit of diversity in competitive (Balduzzi et al., 2019; Garnelo et al., 2021; Vinyals et al., 2019) and cooperative (Yang et al., 2020; Lupu et al., 2021) multi-agent RL. However, once again, these approaches all consider augmented loss functions. Instead, we take inspiration from RR and extend it to the multi-agent setting.

Table C.1: Notation for Lyapunov Exponents for Diversity in Differentiable Games

RR	Ridge Rider
IPD	Iterated Prisoners' Dilemma
GAN	Generative Adversarial Network
LOLA	Learning with Opponent Learning Awareness
EVec, EVal	Shorthand for Eigenvector or Eigenvalue
SGD	Stochastic Gradient Descent
SimSGD	Simultaneous SGD
$:=$	Defined to be equal to
$x, y, z, \dots \in \mathbb{C}$	Scalars
$\mathbf{x}, \mathbf{y}, \mathbf{z}, \dots \in \mathbb{C}^n$	Vectors
$\mathbf{X}, \mathbf{Y}, \mathbf{Z}, \dots \in \mathbb{C}^{n \times n}$	Matrices
\mathbf{X}^\top	The transpose of matrix \mathbf{X}
\mathbf{I}	The identity matrix
$\Re(z), \Im(z)$	The real or imaginary component of $z \in \mathbb{C}$
i	The imaginary unit. $z \in \mathbb{C} \implies z = \Re(z) + i\Im(z)$
\bar{z}	The complex conjugate of $z \in \mathbb{C}$
$ z := \sqrt{z\bar{z}}$	The magnitude or modulus of $z \in \mathbb{C}$
$\arg(z)$	The argument or phase of $z \in \mathbb{C} \implies z = z \exp(i \arg(z))$
A, B	A symbol for the outer/inner players
$d_A, d_B \in \mathbb{N}$	The number of weights for the outer/inner players
$\boldsymbol{\theta}$	A symbol for the parameters or weights of a player
$\boldsymbol{\theta}_A \in \mathbb{R}^{d_A}, \boldsymbol{\theta}_B \in \mathbb{R}^{d_B}$	The outer/inner parameters or weights
$\mathcal{L} : \mathbb{R}^n \rightarrow \mathbb{R}$	A symbol for a loss
$\mathcal{L}_A(\boldsymbol{\theta}_A, \boldsymbol{\theta}_B), \mathcal{L}_B(\boldsymbol{\theta}_A, \boldsymbol{\theta}_B)$	The outer/inner losses – $\mathbb{R}^{d_A+d_B} \mapsto \mathbb{R}$
$\mathbf{g}_A(\boldsymbol{\theta}_A, \boldsymbol{\theta}_B), \mathbf{g}_B(\boldsymbol{\theta}_A, \boldsymbol{\theta}_B)$	Gradient of outer/inner losses w.r.t. their weights in \mathbb{R}^{d_A/d_B}
$\boldsymbol{\theta}_B^*(\boldsymbol{\theta}_A) := \operatorname{argmin}_{\boldsymbol{\theta}_B} \mathcal{L}_B(\boldsymbol{\theta}_A, \boldsymbol{\theta}_B)$	The best-response of the inner player to the outer player
$\mathcal{L}_A^*(\boldsymbol{\theta}_A) := \mathcal{L}_A(\boldsymbol{\theta}_A, \boldsymbol{\theta}_B^*(\boldsymbol{\theta}_A))$	The outer loss with a best-responding inner player
$\boldsymbol{\theta}_A^* := \operatorname{argmin}_{\boldsymbol{\theta}_A} \mathcal{L}_A^*(\boldsymbol{\theta}_A)$	Outer optimal weights with a best-responding inner player
$d := d_A + d_B$	The combined number of weights for both players
$\boldsymbol{\omega} := [\boldsymbol{\theta}_A, \boldsymbol{\theta}_B] \in \mathbb{R}^d$	A concatenation of the outer/inner weights
$\hat{\mathbf{g}}(\boldsymbol{\omega}) := [\mathbf{g}_A(\boldsymbol{\omega}), \mathbf{g}_B(\boldsymbol{\omega})] \in \mathbb{R}^d$	A concatenation of the outer/inner gradients
$\boldsymbol{\omega}^0 = [\boldsymbol{\theta}_A^0, \boldsymbol{\theta}_B^0] \in \mathbb{R}^d$	The initial parameter values
j	An iteration number
$\hat{\mathbf{g}}^j := \hat{\mathbf{g}}(\boldsymbol{\omega}^j) \in \mathbb{R}^d$	The joint-gradient vector field at weights $\boldsymbol{\omega}^j$
$\nabla_{\boldsymbol{\omega}} \hat{\mathbf{g}}^j := \nabla_{\boldsymbol{\omega}} \hat{\mathbf{g}} _{\boldsymbol{\omega}^j} \in \mathbb{R}^{d \times d}$	The Jacobian of the joint-gradient $\hat{\mathbf{g}}$ at weights $\boldsymbol{\omega}^j$
\mathcal{H}	The game Hessian
$\alpha \in \mathbb{C}$	The step size or learning rate
$\lambda \in \mathbb{C}, e$	Notation for an arbitrary Eval
$\operatorname{Sp}(\mathbf{M}) \in \mathbb{C}^n$	The spectrum – or set of eigenvalues – of $\mathbf{M} \in \mathbb{R}^{n \times n}$
$\rho(\mathbf{M}) := \max_{z \in \operatorname{Sp}(\mathbf{M})} z $	The spectral radius in \mathbb{R}^+ of $\mathbf{M} \in \mathbb{R}^{n \times n}$
$\mathbf{F}(\boldsymbol{\omega})$	Fixed-point operator for our optimization
\mathbf{J}	The Jacobian of the fixed-point operator
\mathbf{d}	A displacement for a Lyapunov exponent
$\gamma_j(\boldsymbol{\omega}_0, \mathbf{d}) := \log(\mathbf{d}^\top (\mathbf{J}^j(\boldsymbol{\omega}_0))^\top \mathbf{J}^j(\boldsymbol{\omega}_0) \mathbf{d})$	A Lyapunov term for a Lyapunov exponent
$\hat{\lambda}_k(\boldsymbol{\omega}_0, \mathbf{d}) = \frac{1}{k} \sum_{j=0}^k \gamma_j(\boldsymbol{\omega}_0, \mathbf{d})$	A k -step Lyapunov exponent
$\hat{\lambda}_k^{max}(\boldsymbol{\omega}_0) = \max_{\mathbf{d}, \ \mathbf{d}\ =1} \hat{\lambda}_k(\boldsymbol{\omega}_0, \mathbf{d})$	The max k -step Lyapunov exponent
$\mathcal{L}(\boldsymbol{\omega}_0)$	A starting point loss using Lyapunov exponents
$\mathcal{L}_n^{\text{sum}}(\boldsymbol{\omega}_0)$	A loss using the sum of top n exponents
$\mathcal{L}_n^{\text{min}}(\boldsymbol{\omega}_0)$	A loss using the min of top n exponents

Tree searches in MDP: Tree searches are a classic technique for planning and control in discrete Markov Decision Processes (MDP). The branch locations and the possible branch choices are provided in these settings. All that remains is to choose which to explore. There is much interest in performing these searches ranging from depth/breadth-first search, A* (Hart et al., 1968), to more sophisticated methods such as Monte Carlo Tree Search (Abramson, 2014) potentially with learned value functions (Silver et al., 2016). Searching in continuous action spaces was explored in Moerland et al. (2018); Kim et al. (2020); Mao et al. (2020). All of these methods search in the agents’ action space, and we employ them to find agent parameters.

Rapidly-exploring random tree builds a space-filling tree to cover a continuous optimization space (LaValle et al., 1998; LaValle and Kuffner Jr, 2001). Unlike RR-based methods, the branching points are not determined by the underlying properties of the loss landscape (e.g., only at saddles or bifurcation). This technique is commonly used in robotic motion planning (Rodriguez et al., 2006).

Branching in evolutionary optimization: Designing optimization algorithms in a multimodal loss landscape is a focus of the evolutionary optimization community (Singh and Deb, 2006; Wong, 2015), which implicitly build a tree of candidate solutions. Evolutionary algorithms designed to encourage diversity have been explored in the context of multi-player games (Balduzzi et al., 2019; Vinyals et al., 2019; Arulkumaran et al., 2019) by encouraging agent populations to learn different strategies that perform well against other agents, resulting in a growing collection of strategies.

Bifurcations: This work builds on the previous workshop submission of Lorraine et al. (2022b). The works of Zeeman (1980); Yang et al. (2018); Chotibut et al. (2020); Piliouras (2020); Leonardos and Piliouras (2020); Bielawski et al. (2021) leverage the bifurcations for learning in games. Yang et al. (2018) introduces hysteresis and optimal control mechanisms to control equilibrium selection and improve social welfare. We do not focus on maximizing social welfare but on finding multiple solutions. Chotibut et al. (2020) studies the properties of bifurcations in routing games, showing various analyses for social cost. Piliouras (2020) combines catastrophe theory with mechanism design to destabilize inefficient solutions. Leonardos and Piliouras (2020) studies how changing an exploration parameter in multi-agent learning can affect equilibrium selection. Our work focuses on connecting bifurcations with finding diverse solutions in optimization with Ridge Rider and finding those bifurcations - potentially with gradient-based methods.

Lyapunov exponents: The works of Cheung and Piliouras (2019); Cheung and Tao (2020); Sato et al. (2002) use Lyapunov exponents when learning in games. Cheung and Piliouras (2019) shows that some learning algorithms are Lyapunov chaotic in the payoff space. Our work focuses on using Lyapunov exponent variants to identify bifurcations (which are used to find diverse solutions in optimization) and potentially using optimization methods on the exponent.

Separatrices: The works of Panageas and Piliouras (2016); Zhang and Hofbauer (2015); Nagarajan et al. (2020) look at computing separatrices in games used for various purposes. Nagarajan et al. (2020) finds the shape of separatrices using invariant functions with online learning dynamics.

C.2 Proposed Algorithms

C.2.1 Branching Optimization Tree Searches

Algorithm 13 Branching Optimization Tree Search – important changes from RR to GRR in red

```

1: Input: FindStartingPoint, ChooseBranch, SplitBranch, EndRide, Optimize, VerifySolution,
   ContinueBranching
2: Select optimization parameters  $\alpha$ 
3: Find starting parameters  $\omega^{\text{start}} = \text{FindStartingPoint}(\alpha)$ 
4: Initialize a branch  $\psi^{\text{init}} = \text{InitBranch}(\omega^{\text{start}}, \alpha)$ 
5: Initialize the set of branches  $\mathcal{B} = \text{SplitBranch}(\psi^{\text{init}})$ 
6: Initialize the set of solutions  $\mathcal{S} = \emptyset$ 
7: while Branches  $\mathcal{B}$  non-empty do
8:    $\psi, \mathcal{B} = \text{ChooseBranch}(\mathcal{B})$ 
9:    $\omega^* = \text{Optimize}(\psi, \omega, \psi, \alpha)$  # Optimize our parameters
10:  if VerifySolution( $\omega^*$ ) then
11:     $\mathcal{S} = \mathcal{S} \cup \{\omega^*\}$ 
12:  end if
13:  Make new branch to split  $\psi' = \text{copy}(\psi)$ 
14:  Store the optimized parameters  $\psi'.\text{parameters} = \omega^*$ 
15:  if ContinueBranching( $\psi'$ ) then
16:     $\mathcal{B} = \mathcal{B} \cup \text{SplitBranch}(\psi')$ 
17:  end if
18: end while
19: return  $\mathcal{S}$ 

```

C.3 Experiments

C.3.1 Test Problems

Iterated Prisoners' Dilemma (IPD): This game is an infinite sequence of the Prisoner's Dilemma, where the future payoff is discounted by $\gamma \in [0, 1)$. In other words, the rewards sequences r_j for each player were summed through $\sum_{j=0}^{\infty} \gamma^j r_j$. Each agent is conditioned on the actions in the prior state (s). Thus, there are 5 parameters for each agent i : $P^i(C|s)$ is the probability of cooperating in the start state $s_0 = \emptyset$ or in the state $s_t = (a_{t-1}^1, a_{t-1}^2)$ for $t > 0$. There are two Nash equilibria we care about: Defect-Defect (DD), where agents are selfish (resulting in poor reward), and tit-for-tat (TT), where agents initially cooperate, then copy the opponents' action (resulting in higher reward).

Small IPD: This is a 2-parameter simplification of IPD, which allows DD and TT Nash equilibria. We fix the strategy if our opponent defects, to defect with high probability. We also constrain the probability of cooperating to depend only on whether the opponent cooperates, and in the initial state, we assume our opponent cooperated. This game allows us to visualize some optimization difficulties for the full-scale IPD. However, the game Hessian has strictly real eigenvalues, unlike the full-scale IPD. See Figure 5.2 top for a visualization of the strategy space.

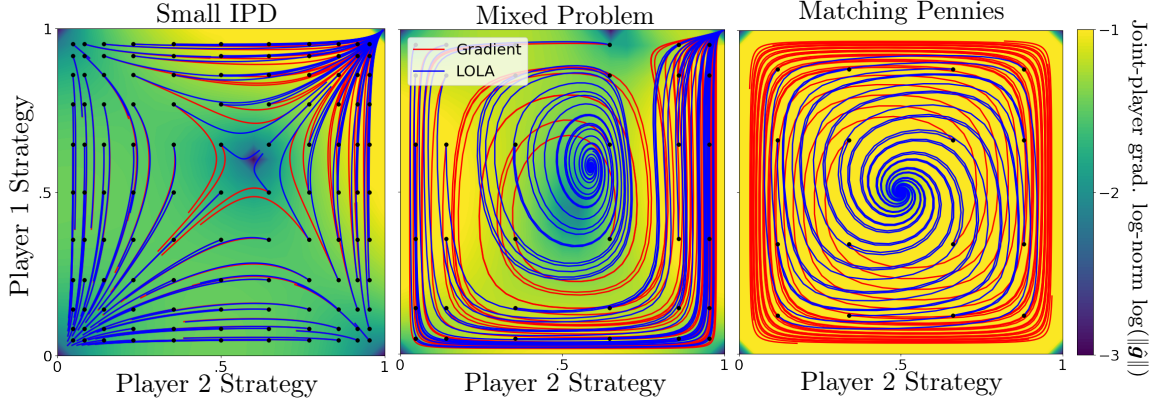


Figure C.1: This shows the phase portrait for two standard optimization algorithms on various problems. Following the gradient is shown in red, while LOLA – a method for learning in games – is shown in blue. *Left:* The small IPD has solutions in the top right and bottom left. *Middle:* Matching Pennies, which has a single solution in the middle. Following the gradient does not find this solution because it has imaginary eigenvalues, so we must use a method like LOLA. *Right:* A mixture of small IPD and Matching Pennies. Following the gradient only finds the solution in the top right because the center solution has imaginary eigenvalues; LOLA can find either solution. **Takeaway:** The mixture game has a range of phenomena, including an imaginary eigenvalue solution, a real eigenvalue solution, and a Hopf bifurcation. We may want to use a method for learning in games to converge robustly to different solutions.

Matching Pennies: This is a simplified 2-parameter version of rock-paper-scissors, where each player selects to cooperate or defect. This game has a Nash equilibrium, in which players select their actions uniformly. Notably, this problem’s game Hessian has purely imaginary eigenvalues, so following the gradient does not converge to solutions, and we need a method for learning in games like LOLA. Also, this game only has one solution. Thus, it is a poor fit for evaluating RR, which finds diverse solutions. See Figure 5.2, bottom for a visualization of the strategy space.

Mixing Small IPD and Matching Pennies: This game interpolates between the Small IPD and Matching Pennies games, with the loss for player j :

$$\mathcal{L}_{\text{mix},P_j,\tau} = \tau \mathcal{L}_{\text{smallIPD},P_j} + (1 - \tau) \mathcal{L}_{\text{matchingPennies},P_j} \quad (\text{C.1})$$

This problem has two solutions: one where both players cooperate and one where both players select actions uniformly. The uniform action solution has imaginary eigenvalues, so it is only stable under a method for learning in games, while the both cooperate solution has real eigenvalues. There is a Hopf bifurcation that separates these solutions. See Figure 5.2 for standard methods on this problem and Appendix Figure C.1 to contrast this problem with Small IPD or Matching Pennies.

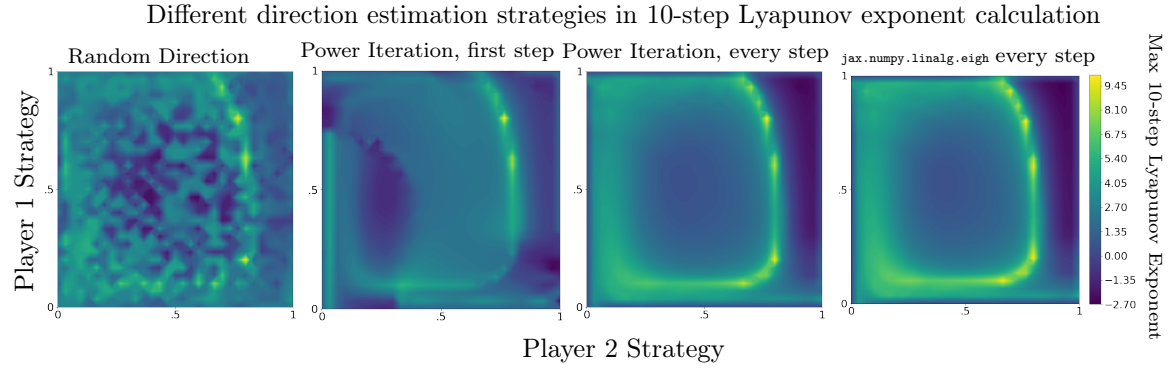


Figure C.2: We compare different methods for choosing a direction in the max 10-step Lyapunov exponent calculation on the Mixed Objective. **Takeaway:** Re-estimating the top eigenvectors at each iteration performs best but is most expensive. *Left:* We uniformly sample a random normalized direction for our displacement \mathbf{d} at each exponent calculation, which does not clearly show the bifurcation. *Middle:* We perform 10 steps of power iteration to tune \mathbf{d} . First, we tune the displacement only at the first iteration, which shows the bifurcation. Next, we tune the displacement at every iteration in the exponent calculation, which shows the bifurcation more clearly. *Right:* We use `jax.numpy.linalg.eigh` to tune \mathbf{d} , which also clearly shows the bifurcation.

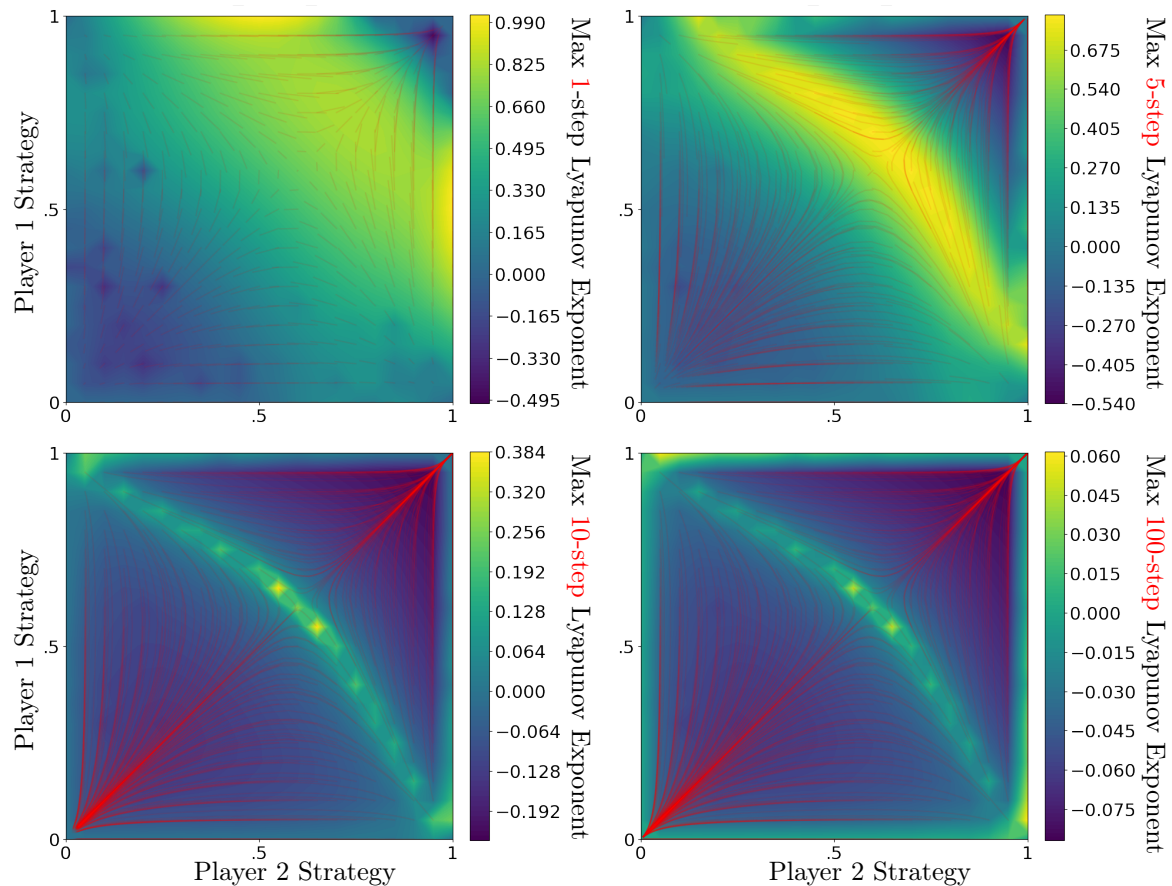


Figure C.3: We show the k -step Lyapunov exponent calculation for various k on the small IPD. The k -step optimization trajectories used for calculating the exponent are shown in red, allowing us to see the horizon over which the associated exponent measures separation. **Takeaway:** We can effectively find bifurcations with a k -step exponent for various k . Using only 1-step does not show the bifurcation, while using more does. As k gets larger, the scale of the gradients changes, causing difficult optimization in the limit – note the changing color bar scale.

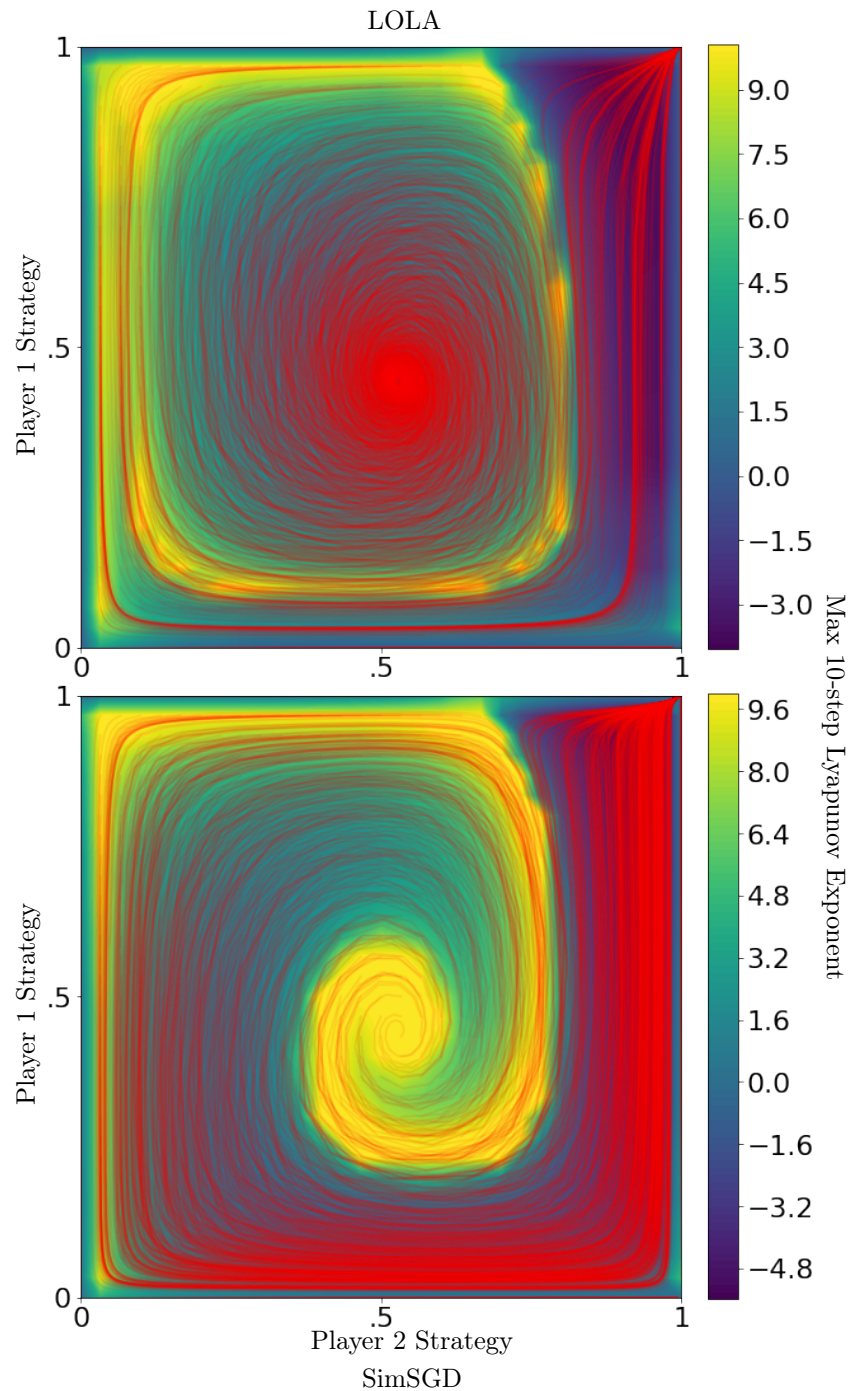


Figure C.4: We contrast the max 20-step Lyapunov exponent calculations between LOLA and SimSGD. The 20-step optimization trajectories used for calculating the exponent are shown in red, allowing us to see the trajectories in which the associated exponent measures separation. **Takeaway:** We can find optimizer-dependent bifurcations with our method. *Top:* 10 steps from the optimization with LOLA at each point where we calculate an exponent for the heatmap. *Bottom:* The same visualization as the top, except with a SimSGD optimizer.

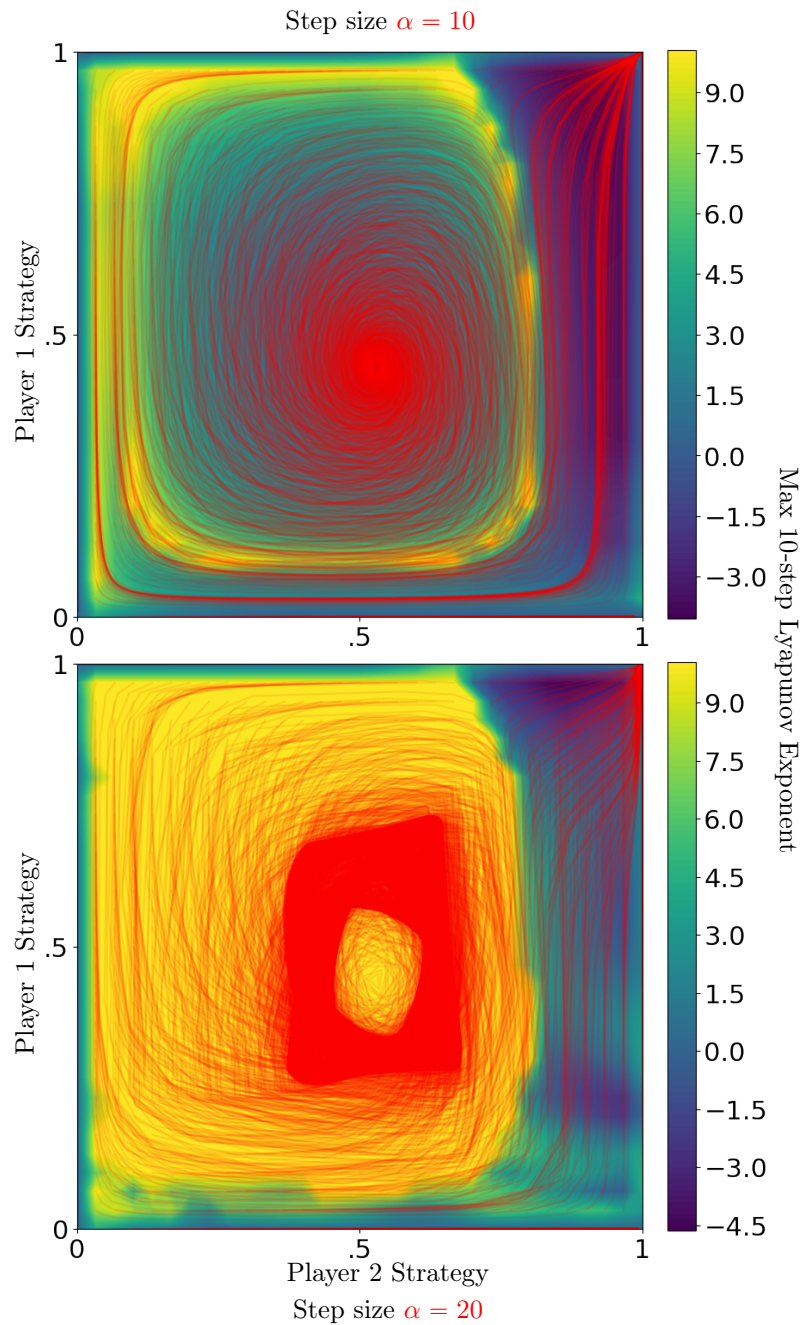


Figure C.5: We investigate the impact of optimization algorithm parameters on the 10-step max Lyapunov exponent calculation with LOLA. The 10-step optimization trajectories used for calculating the exponent are shown in red, allowing us to see the trajectories in which the associated exponent measures separation. **Takeaway:** If the step size is too large, the optimizer does not converge to solutions, resulting in limit cycles. *Top:* 10 steps from the optimization with a step size of $\alpha = 10$ at each point where we calculate an exponent for the heatmap. *Bottom:* The same visualization as the top, except with a step size of $\alpha = 20$. Optimization trajectories only converge at the solution in the top right. In the center, the trajectories accumulate in a limit cycle, rotating around the solution.

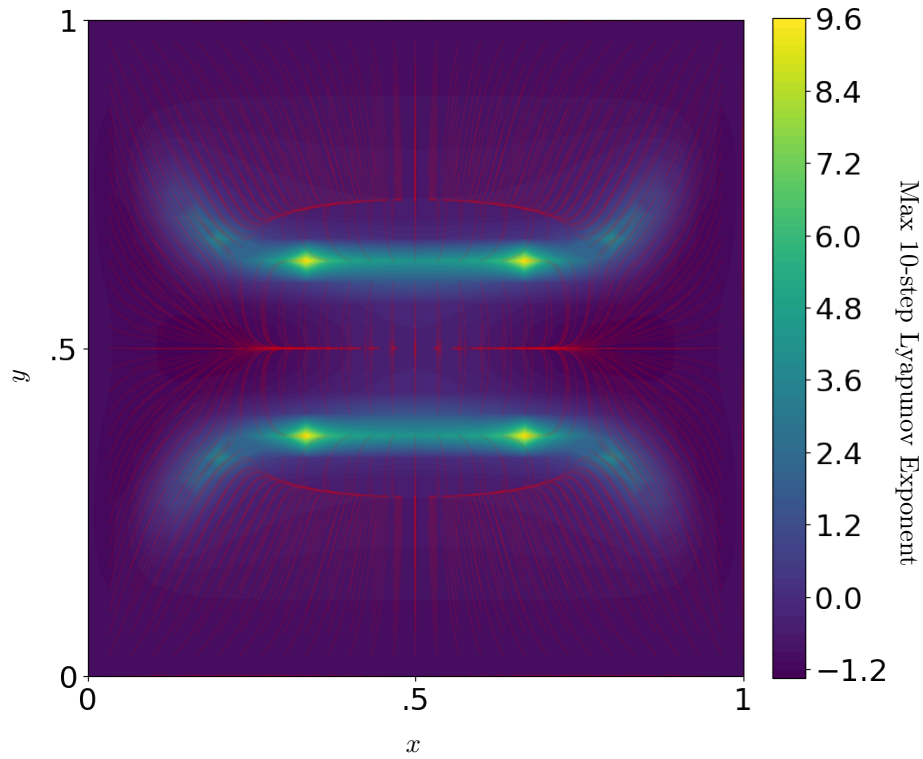


Figure C.6: We investigate finding bifurcations with a 10-step max Lyapunov exponent on a single-objective optimization problem from RR. The optimization trajectories used for the calculation of the exponent are shown in red, allowing us to verify where the bifurcations are. **Takeaway:** Our method effectively highlights bifurcations in RRs example.

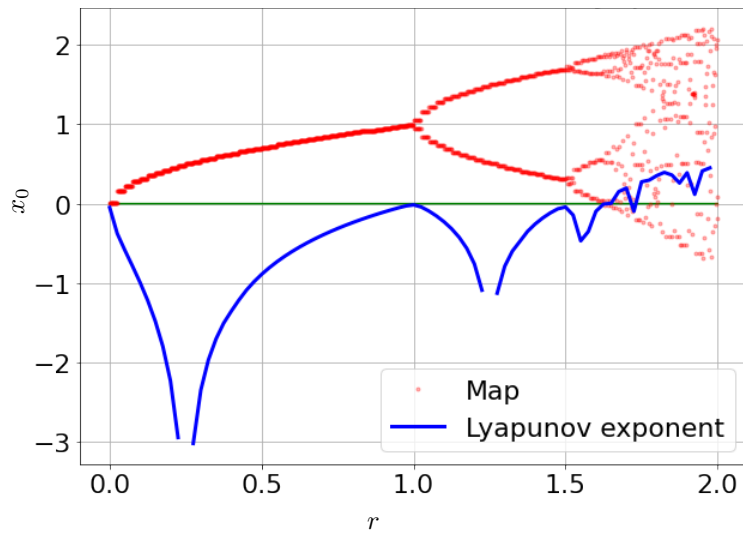


Figure C.7: We display the Lyapunov exponent on the logistic map: $x(t+1) = x(t) + r + x(t)^2$. **Takeaway:** Intuition for Lyapunov exponents on a canonical 1-dimensional example for bifurcations.

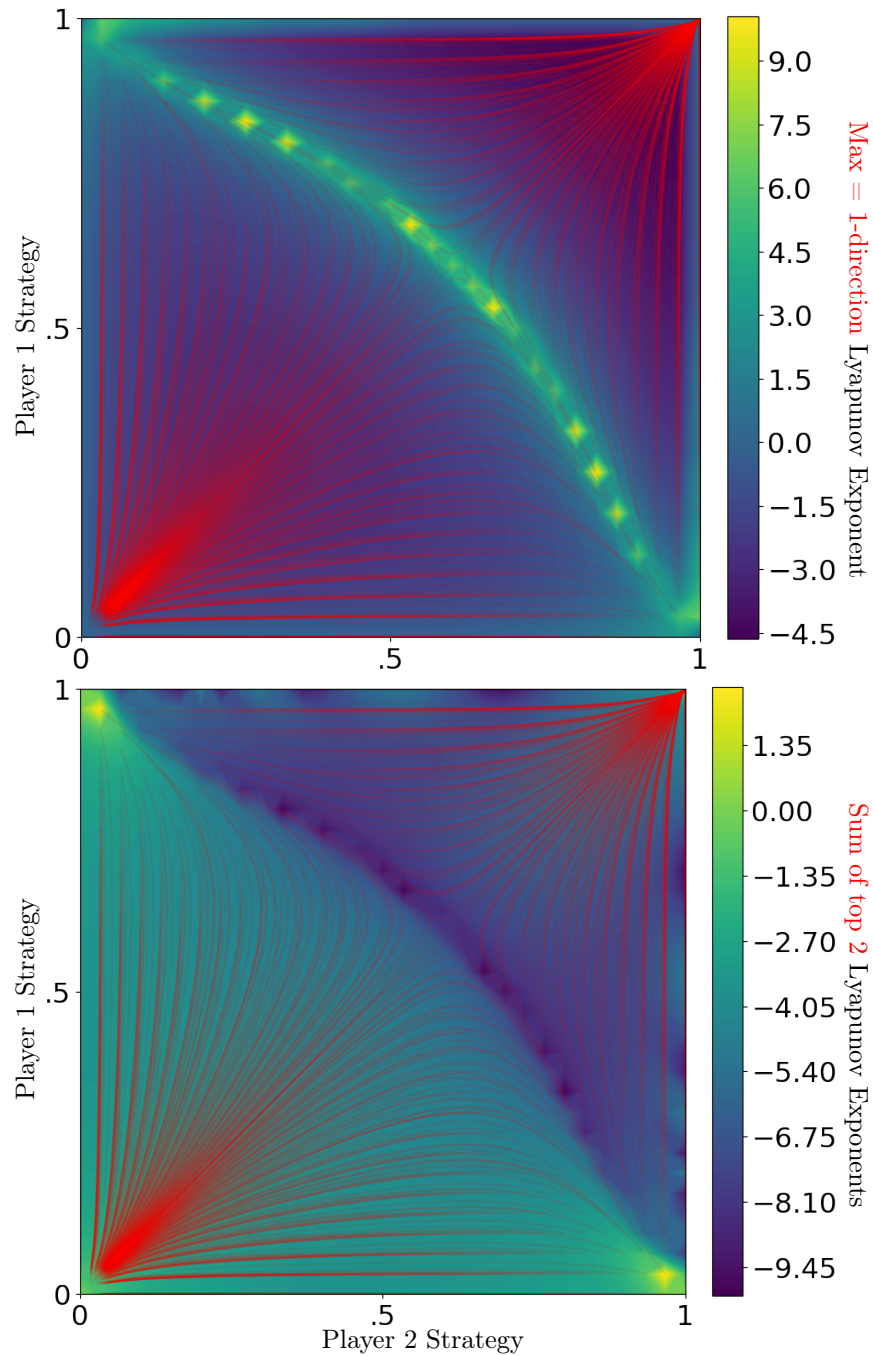


Figure C.8: We compare different 10-step Lyapunov exponent objectives trying to guarantee divergence in multiple directions on the small IPD. The optimization trajectories used for the exponent calculation are shown in red, allowing us to see the trajectories for the associated objective. **Takeaway:** We can find bifurcations while guaranteeing trajectory separation in every direction. Local maxima – not saddles – allow trajectory separation in all directions here. *Top:* The max 10-step Lyapunov exponent. *Bottom:* The sum of the top two 10-step Lyapunov exponents.

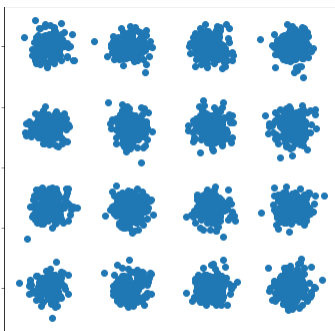


Figure C.9: Ground truth samples for our Mixture of Gaussian experiments.

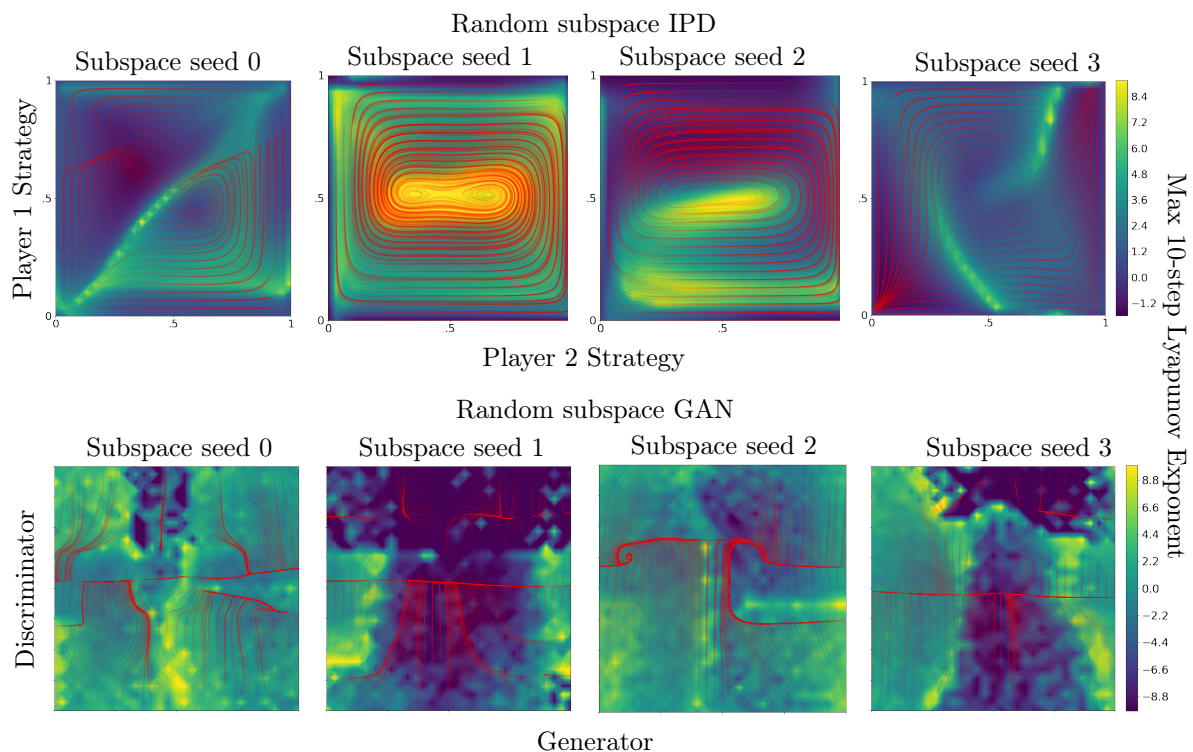


Figure C.10: This reproduces Figure 5.7 with more random subspaces. The optimization trajectories used for the exponent calculation are shown in red, allowing us to see the trajectories the associated exponent measures separation over. **Takeaway:** The exponent is peaked near where trajectories separate for each subspace, showing that these strategies can find various bifurcations. We display the Lyapunov exponent calculation – as in Figure 5.6 – on more complicated toy problems to see how robustly we can find different bifurcations. Section 5.5 describes how we construct these examples by taking higher-dimensional problems and optimizing them in a random subspace. *Top:* Different IPD subspaces: we effectively highlight bifurcations – i.e., regions where trajectory behavior qualitatively changes. *Bottom:* Different GAN subspaces: we can find bifurcations, but the highlighted structure is less crisp in this more complicated and stochastic toy example.

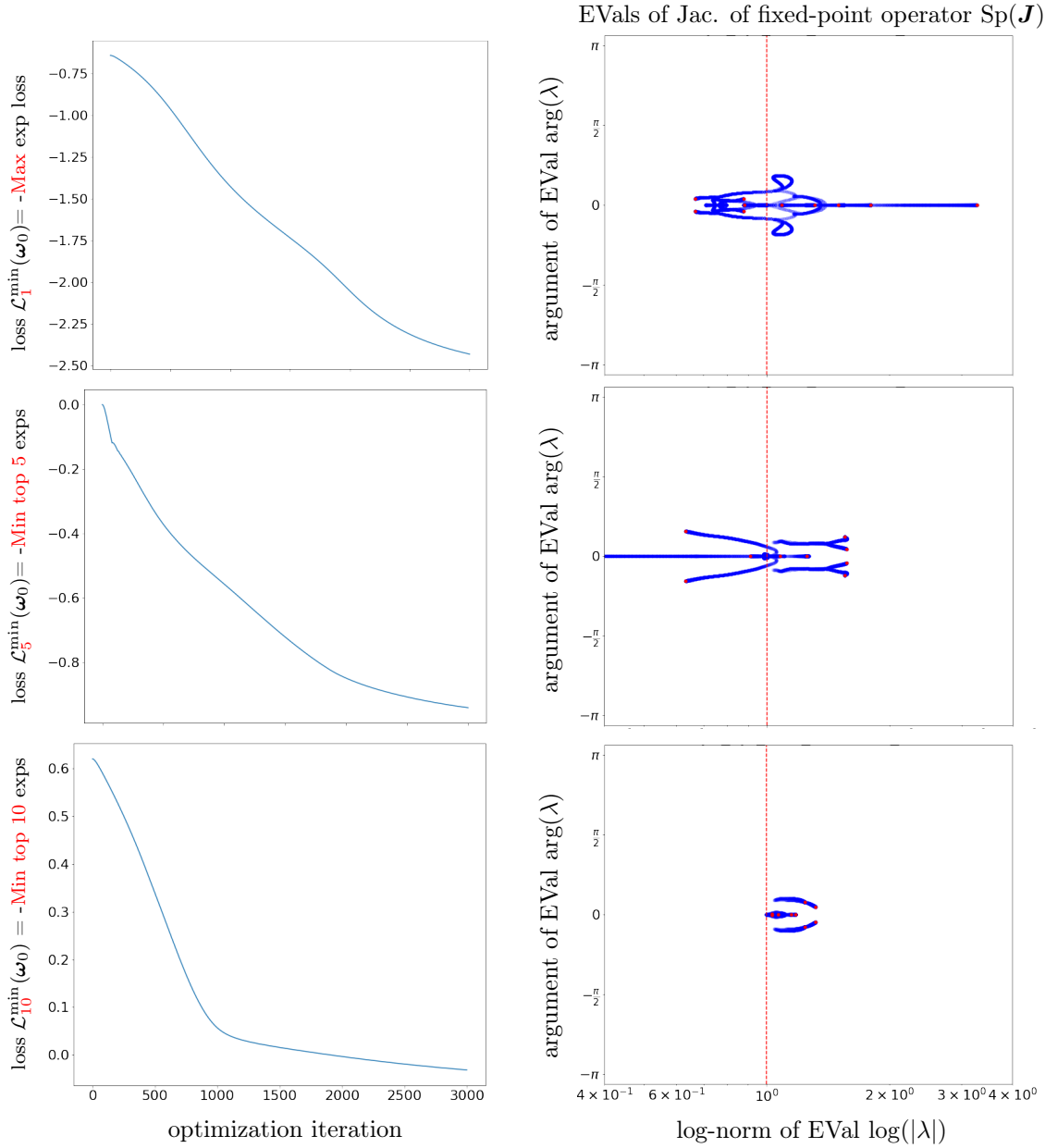


Figure C.11: We compare the optimization for different losses using the local Lyapunov exponent with varying numbers of exponents. **Takeaway:** We can effectively optimize multiple exponents, which give trajectory separation in multiple directions. Our objective is the minimum of the top n local Lyapunov exponents, with a different n 's optimization trajectory shown in each row. To review this visualization also in Figure 5.5: The spectrum is shown with a scatterplot in blue and a progressively larger alpha at each iteration. The final spectrum is shown in red. For the Jacobian of the fixed-point operator \mathbf{J} , a vertical red line is shown where the eigenvalue norm equals 1, signifying the cutoff between (locally) convergent and divergent eigenspaces. *Top:* Optimizing the max local Lyapunov exponent from Figure 5.5, where the largest eigenvalue is effectively maximized. *Middle:* Optimizing the top 5 local exponents, where we find 5 moderately divergent directions instead of 1 extremely divergent direction as in the top. *Bottom:* Optimizing the top 10 local exponents results in trajectory separation in all directions. We study different objectives of the top n exponents in Appendix Figure C.12, and study non-local k -step exponents in Appendix Figure C.13.

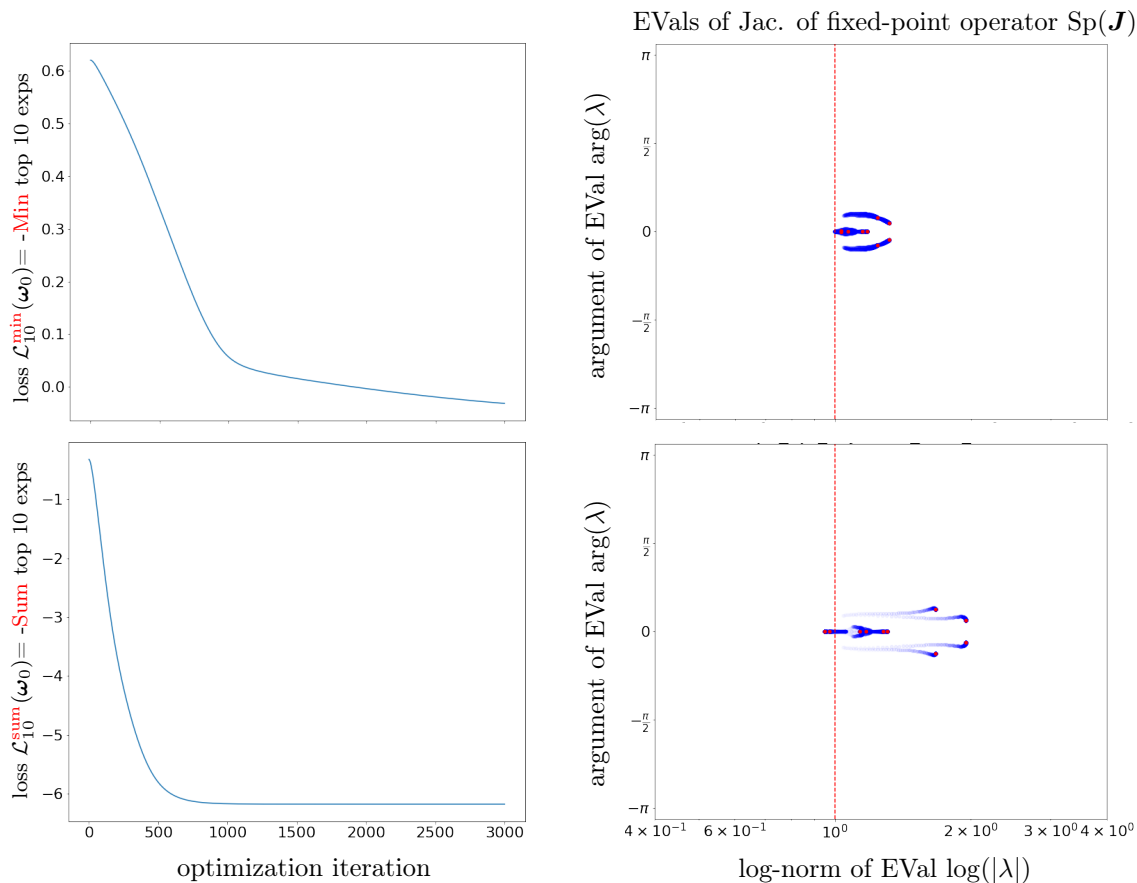


Figure C.12: We compare the optimization for different losses using the top 10 local Lyapunov exponents. **Takeaway:** Using the minimum of the top exponents is a strong method to guarantee separation in many directions. This visualizes the same aspects as Figure 5.5: The spectrum is shown with a scatterplot in blue and a progressively larger alpha at each iteration. The final spectrum is shown in red. For the Jacobian of the fixed-point operator \mathbf{J} , a vertical red line is shown where the eigenvalue norm equals 1, signifying the cutoff between (locally) convergent and divergent eigenspaces. *Top:* To guarantee trajectory separation in all directions, we optimize the minimum of the top exponents. At the end of the training, all eigenvalues of \mathbf{J} are greater than 1, signifying local trajectory separation in all directions. *Bottom:* We optimize the sum of the top 10 exponents, which does not guarantee trajectory separation in every direction. Our optimizer is happy with solutions diverging rapidly in the top directions while converging (slowly) in the bottom directions.

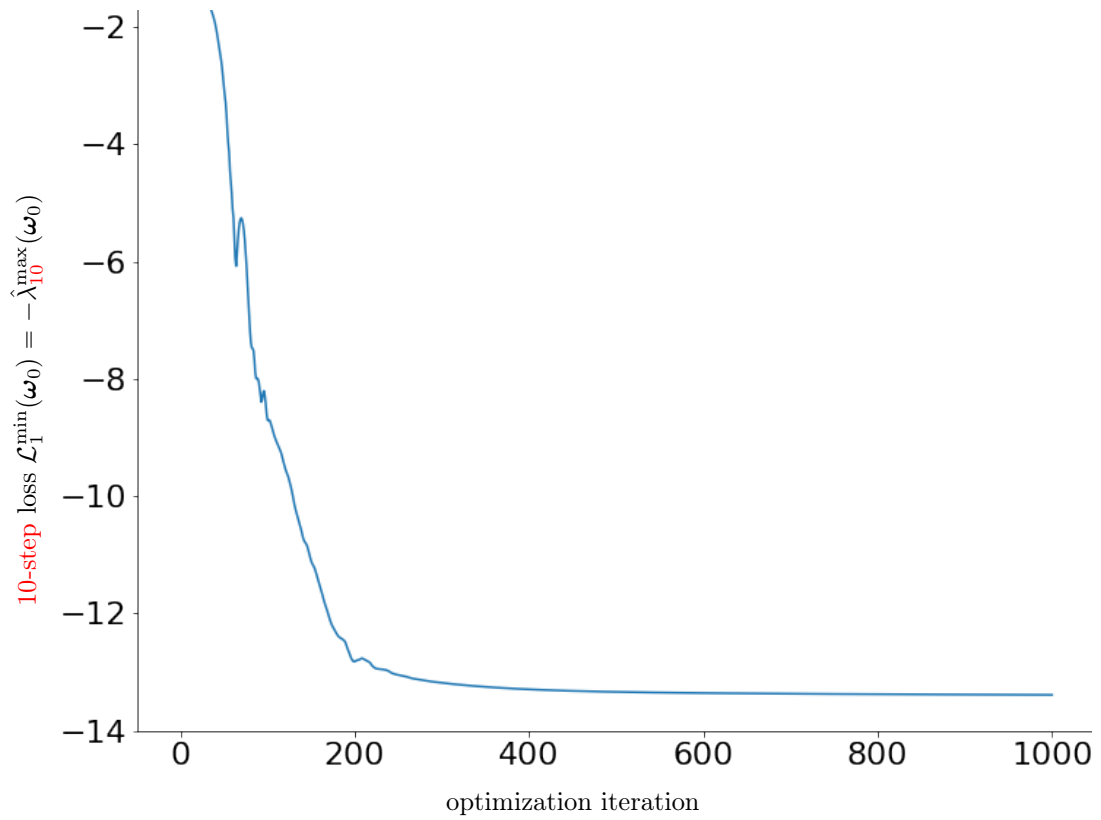


Figure C.13: We investigate optimizing a loss of the max k -step Lyapunov exponent for $k > 1$. **Takeaway:** We effectively minimize multi-step exponents in higher-dimensional problems if required, extending the visualization in Figure 5.5.

Bibliography

- Dougal Maclaurin, David Duvenaud, and Ryan Adams. Gradient-based hyperparameter optimization through reversible learning. In *International Conference on Machine Learning*, pages 2113–2122, 2015a. [Cited on pages 1, 12, 17, 22, 23, 25, 27, 29, 33, 46, and 49]
- Marcin Andrychowicz, Misha Denil, Sergio Gomez, Matthew W Hoffman, David Pfau, Tom Schaul, Brendan Shillingford, and Nando De Freitas. Learning to learn by gradient descent by gradient descent. In *Advances in Neural Information Processing Systems*, pages 3981–3989, 2016. [Cited on pages 1, 23, and 33]
- Jie Fu, Hongyin Luo, Jiashi Feng, Kian Hsiang Low, and Tat-Seng Chua. DrMAD: Distilling reverse-mode automatic differentiation for optimizing hyperparameters of deep neural networks. In *International Joint Conference on Artificial Intelligence*, pages 1469–1475, 2016. [Cited on pages 1, 23, and 33]
- Amirreza Shaban, Ching-An Cheng, Nathan Hatch, and Byron Boots. Truncated back-propagation for bilevel optimization. In *International Conference on Artificial Intelligence and Statistics*, pages 1723–1732, 2019. [Cited on pages 1, 17, 18, 22, 23, 24, 25, 29, and 33]
- Ian Goodfellow, Jean Pouget-Abadie, Mehdi Mirza, Bing Xu, David Warde-Farley, Sherjil Ozair, Aaron Courville, and Yoshua Bengio. Generative adversarial nets. In *Advances in neural information processing systems*, pages 2672–2680, 2014. [Cited on pages 1, 23, 31, 33, 45, and 49]
- David Pfau and Oriol Vinyals. Connecting generative adversarial networks and actor-critic methods. *arXiv preprint arXiv:1610.01945*, 2016. [Cited on pages 1, 33, and 49]
- Bowen Baker, Ingmar Kanitscheider, Todor Markov, Yi Wu, Glenn Powell, Bob McGrew, and Igor Mordatch. Emergent tool use from multi-agent autotutorials. In *International Conference on Learning Representations*, 2019. [Cited on pages 1, 33, and 49]
- David Balduzzi, Marta Garnelo, Yoram Bachrach, Wojciech Czarnecki, Julien Perolat, Max Jaderberg, and Thore Graepel. Open-ended learning in symmetric zero-sum games. In *International Conference on Machine Learning*, pages 434–443. PMLR, 2019. [Cited on pages 1, 33, 49, 92, and 94]
- Sainbayar Sukhbaatar, Zeming Lin, Ilya Kostrikov, Gabriel Synnaeve, Arthur Szlam, and Rob Fergus. Intrinsic motivation and automatic curricula via asymmetric self-play. In *International Conference on Learning Representations*, 2018. [Cited on pages 1, 33, and 49]

- Avishek Joey Bose, Gauthier Gidel, Hugo Berrard, Andre Cianflone, Pascal Vincent, Simon Lacoste-Julien, and William L Hamilton. Adversarial example games. *arXiv preprint arXiv:2007.00720*, 2020. [Cited on pages 1, 33, and 49]
- Xiaoyong Yuan, Pan He, Qile Zhu, and Xiaolin Li. Adversarial examples: Attacks and defenses for deep learning. *IEEE Transactions on Neural Networks and Learning Systems*, 30(9):2805–2824, 2019. [Cited on pages 1, 33, and 49]
- Aravind Rajeswaran, Igor Mordatch, and Vikash Kumar. A game theoretic framework for model based reinforcement learning. *arXiv preprint arXiv:2004.07804*, 2020. [Cited on pages 1, 33, and 49]
- Romina Abachi, Mohammad Ghavamzadeh, and Amir-massoud Farahmand. Policy-aware model learning for policy gradient methods. *arXiv preprint arXiv:2003.00030*, 2020. [Cited on pages 1 and 33]
- Evgenii Nikishin, Romina Abachi, Rishabh Agarwal, and Pierre-Luc Bacon. Control-oriented model-based reinforcement learning with implicit differentiation. *arXiv preprint arXiv:2106.03273*, 2021. [Cited on pages 1, 33, and 49]
- David Acuna, Guojun Zhang, Marc T Law, and Sanja Fidler. f-domain-adversarial learning: Theory and algorithms for unsupervised domain adaptation with neural networks, 2021. URL <https://openreview.net/forum?id=WqXAKcwfZtI>. [Cited on pages 1, 33, 36, and 49]
- Thomas Elsken, Jan Hendrik Metzen, and Frank Hutter. Neural architecture search: A survey. *The Journal of Machine Learning Research*, 20(1):1997–2017, 2019. [Cited on pages 1 and 33]
- Chelsea Finn, Pieter Abbeel, and Sergey Levine. Model-agnostic meta-learning for fast adaptation of deep networks. In *International Conference on Machine Learning*, pages 1126–1135, 2017. [Cited on pages 1, 15, 17, 22, 33, and 66]
- Mengye Ren, Eleni Triantafillou, Sachin Ravi, Jake Snell, Kevin Swersky, Joshua B Tenenbaum, Hugo Larochelle, and Richard S Zemel. Meta-learning for semi-supervised few-shot classification. *arXiv preprint arXiv:1803.00676*, 2018a. [Cited on pages 1, 33, and 49]
- Mengye Ren, Eleni Triantafillou, Kuan-Chieh Wang, James Lucas, Jake Snell, Xaq Pitkow, Andreas S Tolias, and Richard Zemel. Flexible few-shot learning with contextual similarity. *arXiv preprint arXiv:2012.05895*, 2020. [Cited on pages 1, 33, and 49]
- Aniruddh Raghu, Maithra Raghu, Simon Kornblith, David Duvenaud, and Geoffrey Hinton. Teaching with commentaries. *arXiv preprint arXiv:2011.03037*, 2020. [Cited on pages 1 and 49]
- Heinrich Von Stackelberg. *The theory of the market economy*. William Hodge, 1952. [Cited on page 1]
- Paul Vicol, Jonathan P Lorraine, Fabian Pedregosa, David Duvenaud, and Roger B Grosse. On implicit bias in overparameterized bilevel optimization. In *International Conference on Machine Learning*, pages 22234–22259. PMLR, 2022a. [Cited on pages 2, 4, 8, 19, 67, and 92]
- Hugo Berard, Gauthier Gidel, Amjad Almahairi, Pascal Vincent, and Simon Lacoste-Julien. A closer look at the optimization landscapes of generative adversarial networks. In *International Conference on Learning Representations*, 2019. [Cited on pages 2, 33, and 47]

- Jonas Moćkus. On Bayesian methods for seeking the extremum. In *Optimization Techniques IFIP Technical Conference*, pages 400–404, 1975. [Cited on pages 2, 12, 18, and 70]
- Jasper Snoek, Hugo Larochelle, and Ryan Adams. Practical Bayesian optimization of machine learning algorithms. In *Advances in Neural Information Processing Systems*, pages 2951–2959, 2012. [Cited on pages 2, 9, 12, 18, 25, and 70]
- Nikhil Mehta, Jonathan Lorraine, Steve Masson, Ramanathan Arunachalam, Zaid Pervaiz Bhat, James Lucas, and Arun George Zachariah. Improving hyperparameter optimization with checkpointed model weights. *arXiv preprint arXiv:2406.18630*, 2024a. [Cited on page 4]
- Nikhil Mehta, Jonathan Lorraine, Steve Masson, Zaid Arunachalam, Ramanathan Pervaiz Bhat, James Lucas, and Arun George Zachariah. Improving hyperparameter optimization with checkpointed model weights. In *In Submission to Advances in Neural Information Processing Systems (NeurIPS)*, 2024b. [Cited on page 4]
- Juhan Bae, Wu Lin, Jonathan Lorraine, and Roger Grosse. Training data attribution via approximate unrolled differentiation. *arXiv preprint arXiv:2405.12186*, 2024. [Cited on page 4]
- Kevin Xie, Jonathan Lorraine, Tianshi Cao, Jun Gao, James Lucas, Antonio Torralba, Antonio Torralba, Sanja Fidler, and Xiaohui Zeng. Latte3d: Large-scale amortized text-to-enhanced3d synthesis. *arXiv preprint arXiv:2403.15385*, 2024. [Cited on page 4]
- Derek Lim, Haggai Maron, Marc T. Law, Jonathan Lorraine, and James Lucas. Graph metanetworks for processing diverse neural architectures. In *The International Conference on Learning Representations (ICLR)*, 2024. [Cited on page 4]
- Derek Lim, Haggai Maron, Marc T Law, Jonathan Lorraine, and James Lucas. Graph metanetworks for processing diverse neural architectures. *arXiv preprint arXiv:2312.04501*, 2023. [Cited on page 4]
- Michael Zhang, Nishkrit Desai, Juhan Bae, Jonathan Lorraine, and Jimmy Ba. Using large language models for hyperparameter optimization. In *Advances in Neural Information Processing Systems (NeurIPS) 2023 Foundation Models for Decision Making Workshop*, 2023a. [Cited on pages 4 and 66]
- Michael R Zhang, Nishkrit Desai, Juhan Bae, Jonathan Lorraine, and Jimmy Ba. Using large language models for hyperparameter optimization. *arXiv preprint arXiv:2312.04528*, 2023b. [Cited on page 4]
- Jonathan Lorraine, Kevin Xie, Xiaohui Zeng, Chen-Hsuan Lin, Towaki Takikawa, Nicholas Sharp, Tsung-Yi Lin, Ming-Yu Liu, Sanja Fidler, and James Lucas. Att3d: Amortized text-to-3d object synthesis. In *Proceedings of the IEEE/CVF International Conference on Computer Vision*, pages 17946–17956, 2023a. [Cited on page 4]
- Jonathan Lorraine, Kevin Xie, Xiaohui Zeng, Chen-Hsuan Lin, Towaki Takikawa, Nicholas Sharp, Tsung-Yi Lin, Ming-Yu Liu, Sanja Fidler, and James Lucas. Att3d: Amortized text-to-3d object synthesis. *arXiv preprint arXiv:2306.07349*, 2023b. [Cited on page 4]
- Jonathan Lorraine, Nihesh Anderson, Chansoo Lee, Quentin De Laroussilhe, and Mehadi Hassen. Task selection for automl system evaluation. *arXiv preprint arXiv:2208.12754*, 2022a. [Cited on page 4]

- Paul Vicol, Jonathan Lorraine, Fabian Pedregosa, David Duvenaud, and Roger Grosse. On implicit bias in overparameterized bilevel optimization, 2022b. [Cited on page 4]
- Paul Vicol, Jonathan Lorraine, David Duvenaud, and Roger Grosse. Implicit regularization in overparameterized bilevel optimization. In *ICML 2021 Beyond First Order Methods Workshop*, 2021. [Cited on page 4]
- Jack Richter-Powell, Jonathan Lorraine, and Brandon Amos. Input convex gradient networks. *arXiv preprint arXiv:2111.12187*, 2021. [Cited on page 4]
- Aniruddh Raghu, Jonathan Lorraine, Simon Kornblith, Matthew McDermott, and David K Duvenaud. Meta-learning to improve pre-training. *Advances in Neural Information Processing Systems*, 34, 2021a. [Cited on pages 4 and 49]
- Aniruddh Raghu, Jonathan Lorraine, Simon Kornblith, Matthew McDermott, and David Duvenaud. Meta-learning to improve pre-training. *arXiv preprint arXiv:2111.01754*, 2021b. [Cited on page 4]
- Jonathan Lorraine and Safwan Hossain. Jacnet: Learning functions with structured jacobians. In *ICML INNF Workshop*, 2019. [Cited on page 4]
- Matthew MacKay, Paul Vicol, Jon Lorraine, David Duvenaud, and Roger Grosse. Self-tuning networks: Bilevel optimization of hyperparameters using structured best-response functions. In *International Conference on Learning Representations*, 2019a. [Cited on pages 4, 6, 9, 10, 14, 22, 30, 31, 49, 66, and 70]
- Matthew MacKay, Paul Vicol, Jon Lorraine, David Duvenaud, and Roger Grosse. Self-tuning networks: Bilevel optimization of hyperparameters using structured best-response functions. *arXiv preprint arXiv:1903.03088*, 2019b. [Cited on page 4]
- George Adam and Jonathan Lorraine. Understanding neural architecture search techniques. *arXiv preprint arXiv:1904.00438*, 2019. [Cited on pages 4 and 49]
- Jonathan Lorraine and David Duvenaud. Hyperparameter optimization with hypernets. In *31st Conference on Neural Information Processing Systems (NIPS 2017), Workshop on Meta-learning*, Long Beach, USA, 2017. [Cited on pages 6, 16, 22, 49, and 70]
- Juhan Bae and Roger B Grosse. Delta-stn: Efficient bilevel optimization for neural networks using structured response jacobians. *Advances in Neural Information Processing Systems*, 33:21725–21737, 2020. [Cited on pages 6 and 66]
- Lisha Li, Kevin Jamieson, Giulia DeSalvo, Afshin Rostamizadeh, and Ameet Talwalkar. Hyperband: A novel bandit-based approach to hyperparameter optimization. *arXiv preprint arXiv:1603.06560*, 2016. [Cited on pages 8, 12, and 25]
- Kevin Swersky, Jasper Snoek, and Ryan Prescott Adams. Freeze-thaw bayesian optimization. *arXiv preprint arXiv:1406.3896*, 2014. [Cited on page 8]
- David Ha, Andrew Dai, and Quoc V. Le. Hypernetworks. *arXiv preprint arXiv:1609.09106*, 2016. [Cited on page 8]

- Andrew Brock, Theodore Lim, JM Ritchie, and Nick Weston. Smash: One-shot model architecture search through hypernetworks. *arXiv preprint arXiv:1708.05344*, 2017. [Cited on pages 9, 12, and 70]
- Carl Edward Rasmussen and Christopher KI Williams. *Gaussian processes for machine learning*, volume 1. MIT press Cambridge, 2006. [Cited on page 9]
- Brandon Amos. Tutorial on amortized optimization for learning to optimize over continuous domains. *arXiv e-prints*, pages arXiv–2202, 2022. [Cited on page 12]
- James Requeima, Jonathan Gordon, John Bronskill, Sebastian Nowozin, and Richard E Turner. Fast and flexible multi-task classification using conditional neural adaptive processes. *Advances in Neural Information Processing Systems*, 32, 2019. [Cited on page 12]
- Neale Ratzlaff and Li Fuxin. Hypergan: A generative model for diverse, performant neural networks. In *International Conference on Machine Learning*, pages 5361–5369. PMLR, 2019. [Cited on page 12]
- Jonathan Pilault, Amine Elhattami, and Christopher Pal. Conditionally adaptive multi-task learning: Improving transfer learning in nlp using fewer parameters & less data. *arXiv preprint arXiv:2009.09139*, 2020. [Cited on page 12]
- Yi Tay, Zhe Zhao, Dara Bahri, Donald Metzler, and Da-Cheng Juan. Hypergrid transformers: Towards a single model for multiple tasks. In *International Conference on Learning Representations*, 2020. [Cited on page 12]
- Andrei A Rusu, Dushyant Rao, Jakub Sygnowski, Oriol Vinyals, Razvan Pascanu, Simon Osindero, and Raia Hadsell. Meta-learning with latent embedding optimization. *arXiv preprint arXiv:1807.05960*, 2018. [Cited on page 12]
- James Bergstra and Yoshua Bengio. Random search for hyper-parameter optimization. *Journal of Machine Learning Research*, 13(Feb):281–305, 2012. [Cited on pages 12, 25, and 70]
- Jasper Snoek, Michael Gelbart, et al. Spearmint: A software package for bayesian optimization. <https://github.com/HIPS/Spearmint>, 2019. [Cited on page 12]
- Stamatios-Aggelos N Alexandropoulos, Christos K Aridas, Sotiris B Kotsiantis, and Michael N Vrahatis. Multi-objective evolutionary optimization algorithms for machine learning: A recent survey. *Approximation and Optimization: Algorithms, Complexity and Applications*, pages 35–55, 2019. [Cited on page 12]
- Max Jaderberg, Valentin Dalibard, Simon Osindero, Wojciech M Czarnecki, Jeff Donahue, Ali Razavi, Oriol Vinyals, Tim Green, Iain Dunning, Karen Simonyan, et al. Population based training of neural networks. *arXiv preprint arXiv:1711.09846*, 2017. [Cited on pages 12, 25, and 70]
- Justin Domke. Generic methods for optimization-based modeling. In *Artificial Intelligence and Statistics*, pages 318–326, 2012. [Cited on pages 12, 17, 18, 22, 23, and 49]
- Luca Franceschi, Michele Donini, Paolo Frasconi, and Massimiliano Pontil. Forward and reverse gradient-based hyperparameter optimization. In *Proceedings of the 34th International Conference on Machine Learning*, volume 70 of *Proceedings of Machine Learning Research*, pages 1165–1173. PMLR, 2017. [Cited on pages 12, 13, 17, 23, and 27]

- Yann LeCun, Léon Bottou, Yoshua Bengio, Patrick Haffner, et al. Gradient-based learning applied to document recognition. *Proceedings of the IEEE*, 86(11):2278–2324, 1998. [Cited on pages 13, 74, and 75]
- Vinod Nair and Geoffrey E. Hinton. Rectified linear units improve restricted boltzmann machines. In *Proceedings of the 27th international conference on machine learning (ICML-10)*, pages 807–814, 2010. [Cited on page 13]
- Dougal Maclaurin, David Duvenaud, and Ryan P. Adams. Autograd: Effortless gradients in numpy. ICML 2015 AutoML Workshop, 2015b. [Cited on page 13]
- Diederik Kingma and Jimmy Ba. Adam: A method for stochastic optimization. *arXiv preprint arXiv:1412.6980*, 2014. [Cited on pages 13, 34, 45, and 74]
- Jonathan Lorraine and David Duvenaud. Stochastic hyperparameter optimization through hypernetworks. *arXiv preprint arXiv:1802.09419*, 2018. [Cited on page 16]
- Jürgen Schmidhuber. *Evolutionary principles in self-referential learning, or on learning how to learn: The meta-meta-... hook*. PhD thesis, Technische Universität München, 1987. [Cited on page 17]
- Yoshua Bengio. Gradient-based optimization of hyperparameters. *Neural Computation*, 12(8): 1889–1900, 2000. [Cited on pages 17, 21, and 22]
- Luca Franceschi, Paolo Frasconi, Saverio Salzo, Riccardo Grazi, and Massimiliano Pontil. Bilevel programming for hyperparameter optimization and meta-learning. In *International Conference on Machine Learning*, pages 1563–1572, 2018. [Cited on pages 17, 23, and 27]
- Aravind Rajeswaran, Chelsea Finn, Sham Kakade, and Sergey Levine. Meta-learning with implicit gradients. *arXiv preprint arXiv:1909.04630*, 2019. [Cited on pages 17, 21, and 49]
- Hanxiao Liu, Karen Simonyan, and Yiming Yang. Darts: Differentiable architecture search. *arXiv preprint arXiv:1806.09055*, 2018. [Cited on pages 17, 22, and 49]
- Edward Grefenstette, Brandon Amos, Denis Yarats, Phu Mon Htut, Artem Molchanov, Franziska Meier, Douwe Kiela, Kyunghyun Cho, and Soumith Chintala. Generalized inner loop meta-learning. *arXiv preprint arXiv:1910.01727*, 2019. [Cited on page 17]
- Akshay Mehra and Jihun Hamm. Penalty method for inversion-free deep bilevel optimization. *arXiv preprint arXiv:1911.03432*, 2019. [Cited on page 17]
- Jan Kukačka, Vladimir Golkov, and Daniel Cremers. Regularization for deep learning: A taxonomy. *arXiv preprint arXiv:1710.10686*, 2017. [Cited on page 17]
- Tongzhou Wang, Jun-Yan Zhu, Antonio Torralba, and Alexei A Efros. Dataset distillation. *arXiv preprint arXiv:1811.10959*, 2018. [Cited on pages 17 and 27]
- Mengye Ren, Wenyan Zeng, Bin Yang, and Raquel Urtasun. Learning to reweight examples for robust deep learning. In *International Conference on Machine Learning*, pages 4331–4340, 2018b. [Cited on pages 17 and 22]

- Tae-Hoon Kim and Jonghyun Choi. ScreenerNet: Learning self-paced curriculum for deep neural networks. *arXiv preprint arXiv:1801.00904*, 2018. [Cited on page 17]
- Jiong Zhang, Hsiang-fu Yu, and Inderjit Dhillon. AutoAssist: A framework to accelerate training of deep neural networks. *arXiv preprint arXiv:1905.03381*, 2019a. [Cited on page 17]
- Ekin D Cubuk, Barret Zoph, Dandelion Mane, Vijay Vasudevan, and Quoc V Le. Autoaugment: Learning augmentation policies from data. *arXiv preprint arXiv:1805.09501*, 2018. [Cited on pages 17 and 28]
- Qizhe Xie, Zihang Dai, Eduard Hovy, Minh-Thang Luong, and Quoc V Le. Unsupervised data augmentation. *arXiv preprint arXiv:1904.12848*, 2019. [Cited on pages 17 and 28]
- Kirthevasan Kandasamy, Karun Raju Vysyaraju, Willie Neiswanger, Biswajit Paria, Christopher R Collins, Jeff Schneider, Barnabas Poczos, and Eric P Xing. Tuning hyperparameters without grad students: Scalable and robust Bayesian optimisation with Dragonfly. *arXiv preprint arXiv:1903.06694*, 2019. [Cited on pages 18 and 70]
- Renjie Liao, Yuwen Xiong, Ethan Fetaya, Lisa Zhang, KiJung Yoon, Xaq Pitkow, Raquel Urtasun, and Richard Zemel. Reviving and improving recurrent back-propagation. In *International Conference on Machine Learning*, pages 3088–3097, 2018. [Cited on pages 18, 21, 22, and 25]
- Barak A Pearlmutter. Fast exact multiplication by the hessian. *Neural computation*, 6(1):147–160, 1994. [Cited on pages 20 and 51]
- Bruce Christianson. Reverse accumulation and implicit functions. *Optimization Methods and Software*, 9(4):307–322, 1998. [Cited on page 21]
- Jan Larsen, Lars Kai Hansen, Claus Svarer, and M Ohlsson. Design and regularization of neural networks: The optimal use of a validation set. In *Neural Networks for Signal Processing VI. Proceedings of the 1996 IEEE Signal Processing Society Workshop*, pages 62–71, 1996. [Cited on pages 21 and 22]
- Peter Ochs, René Ranftl, Thomas Brox, and Thomas Pock. Bilevel optimization with nonsmooth lower level problems. In *International Conference on Scale Space and Variational Methods in Computer Vision*, pages 654–665, 2015. [Cited on page 21]
- Yuanhao Wang, Guodong Zhang, and Jimmy Ba. On solving minimax optimization locally: A follow-the-ridge approach. *arXiv preprint arXiv:1910.07512*, 2019a. [Cited on page 21]
- Kwonjoon Lee, Subhransu Maji, Avinash Ravichandran, and Stefano Soatto. Meta-learning with differentiable convex optimization. In *Proceedings of the IEEE Conference on Computer Vision and Pattern Recognition*, pages 10657–10665, 2019. [Cited on page 21]
- Ahmad Beirami, Meisam Razaviyayn, Shahin Shahrampour, and Vahid Tarokh. On optimal generalizability in parametric learning. In *Advances in Neural Information Processing Systems*, pages 3455–3465, 2017. [Cited on page 21]
- Pang Wei Koh and Percy Liang. Understanding black-box predictions via influence functions. In *Proceedings of the 34th International Conference on Machine Learning-Volume 70*, pages 1885–1894. JMLR. org, 2017. [Cited on page 21]

- Jelena Luketina, Mathias Berglund, Klaus Greff, and Tapani Raiko. Scalable gradient-based tuning of continuous regularization hyperparameters. In *International Conference on Machine Learning*, pages 2952–2960, 2016. [Cited on pages 21 and 22]
- Fabian Pedregosa. Hyperparameter optimization with approximate gradient. In *International Conference on Machine Learning*, pages 737–746, 2016. [Cited on pages 21 and 25]
- Shaojie Bai, J Zico Kolter, and Vladlen Koltun. Deep equilibrium models. *arXiv preprint arXiv:1909.01377*, 2019. [Cited on page 21]
- Naman Agarwal, Brian Bullins, and Elad Hazan. Second-order stochastic optimization for machine learning in linear time. *The Journal of Machine Learning Research*, 18(1):4148–4187, 2017. [Cited on page 22]
- James Martens and Roger Grosse. Optimizing neural networks with Kronecker-factored approximate curvature. In *International Conference on Machine Learning*, pages 2408–2417, 2015. [Cited on page 22]
- Yogesh Balaji, Swami Sankaranarayanan, and Rama Chellappa. Metareg: Towards domain generalization using meta-regularization. In *Advances in Neural Information Processing Systems*, pages 998–1008, 2018. [Cited on pages 22 and 27]
- Ira Shavitt and Eran Segal. Regularization learning networks: Deep learning for tabular datasets. In *Advances in Neural Information Processing Systems*, pages 1379–1389, 2018. [Cited on page 22]
- Alex Nichol, Joshua Achiam, and John Schulman. On first-order meta-learning algorithms. *arXiv preprint arXiv:1803.02999*, 2018. [Cited on page 22]
- Lars Mescheder, Sebastian Nowozin, and Andreas Geiger. The numerics of gans. In *Advances in Neural Information Processing Systems*, pages 1825–1835, 2017. [Cited on pages 22, 36, 41, 46, 47, and 92]
- Yuhuai Wu, Mengye Ren, Renjie Liao, and Roger Grosse. Understanding short-horizon bias in stochastic meta-optimization. *arXiv preprint arXiv:1803.02021*, 2018. [Cited on page 23]
- David Balduzzi, Sebastien Racaniere, James Martens, Jakob Foerster, Karl Tuyls, and Thore Graepel. The mechanics of n-player differentiable games. In *International Conference on Machine Learning*, pages 363–372, 2018. [Cited on pages 23, 50, and 59]
- Stefan Banach. Sur les opérations dans les ensembles abstraits et leur application aux équations intégrales. *Fundamenta Mathematicae*, 3:133–181, 1922. [Cited on page 24]
- C Maddison, A Mnih, and Y Teh. The concrete distribution: A continuous relaxation of discrete random variables. In *International Conference on Learning Representations*, 2017. [Cited on pages 25 and 66]
- Eric Jang, Shixiang Gu, and Ben Poole. Categorical reparameterization with Gumbel-softmax. *arXiv preprint arXiv:1611.01144*, 2016. [Cited on pages 25 and 66]
- Kevin Jamieson and Ameet Talwalkar. Non-stochastic best arm identification and hyperparameter optimization. In *Artificial Intelligence and Statistics*, pages 240–248, 2016. [Cited on page 25]

- Manoj Kumar, George E Dahl, Vijay Vasudevan, and Mohammad Norouzi. Parallel architecture and hyperparameter search via successive halving and classification. *arXiv preprint arXiv:1805.10255*, 2018. [Cited on page 25]
- David Harrison Jr and Daniel L Rubinfeld. Hedonic housing prices and the demand for clean air. *Journal of Environmental Economics and Management*, 5(1):81–102, 1978. [Cited on page 25]
- Guodong Zhang, Shengyang Sun, David Duvenaud, and Roger Grosse. Noisy natural gradient as variational inference. In *International Conference on Machine Learning*, pages 5847–5856, 2018. [Cited on page 26]
- Alex Krizhevsky, Ilya Sutskever, and Geoffrey E Hinton. ImageNet classification with deep convolutional neural networks. In *Advances in Neural Information Processing Systems*, pages 1097–1105, 2012. [Cited on pages 27, 74, and 75]
- Kaiming He, Xiangyu Zhang, Shaoqing Ren, and Jian Sun. Deep residual learning for image recognition. In *Conference on Computer Vision and Pattern Recognition*, pages 770–778, 2016. [Cited on pages 27, 28, 74, and 75]
- Alex Krizhevsky. Learning multiple layers of features from tiny images, 2009. [Cited on pages 27 and 45]
- Olaf Ronneberger, Philipp Fischer, and Thomas Brox. U-Net: Convolutional networks for biomedical image segmentation. In *International Conference on Medical Image Computing and Computer-Assisted Intervention*, pages 234–241, 2015. [Cited on pages 28 and 75]
- Saypraseuth Mounsaveng, David Vazquez, Ismail Ben Ayed, and Marco Pedersoli. Adversarial learning of general transformations for data augmentation. *International Conference on Learning Representations*, 2019. [Cited on page 28]
- Sepp Hochreiter and Jürgen Schmidhuber. Long short-term memory. *Neural Computation*, 9(8):1735–1780, 1997. [Cited on page 28]
- Mitchell P Marcus, Mary Ann Marcinkiewicz, and Beatrice Santorini. Building a large annotated corpus of English: The Penn Treebank. *Computational Linguistics*, 19(2):313–330, 1993. [Cited on page 28]
- Yarin Gal and Zoubin Ghahramani. A theoretically grounded application of dropout in recurrent neural networks. In *Advances in Neural Information Processing Systems*, pages 1027–1035, 2016. [Cited on pages 28 and 75]
- Durk P Kingma, Tim Salimans, and Max Welling. Variational dropout and the local reparameterization trick. In *Advances in Neural Information Processing Systems*, pages 2575–2583, 2015. [Cited on page 30]
- Li Wan, Matthew Zeiler, Sixin Zhang, Yann Le Cun, and Rob Fergus. Regularization of neural networks using Dropconnect. In *International Conference on Machine Learning*, pages 1058–1066, 2013. [Cited on page 30]
- Yarin Gal, Jiri Hron, and Alex Kendall. Concrete dropout. In *Advances in Neural Information Processing Systems*, pages 3581–3590, 2017. [Cited on page 30]

- Ian Goodfellow, Yoshua Bengio, and Aaron Courville. *Deep Learning*. MIT Press, 2016. <http://www.deeplearningbook.org>. [Cited on page 31]
- Jakob Foerster, Richard Y Chen, Maruan Al-Shedivat, Shimon Whiteson, Pieter Abbeel, and Igor Mordatch. Learning with opponent-learning awareness. In *International Conference on Autonomous Agents and MultiAgent Systems*, pages 122–130, 2018. [Cited on pages 31, 46, 49, 55, 57, and 63]
- Alistair Letcher, Jakob Foerster, David Balduzzi, Tim Rocktäschel, and Shimon Whiteson. Stable opponent shaping in differentiable games. *arXiv preprint arXiv:1811.08469*, 2018. [Cited on pages 31 and 59]
- Jonathan Lorraine, Paul Vicol, and David Duvenaud. Optimizing millions of hyperparameters by implicit differentiation. In *International Conference on Artificial Intelligence and Statistics*, pages 1540–1552. PMLR, 2020a. [Cited on pages 32 and 67]
- Jonathan Lorraine, Paul Vicol, and David Duvenaud. Optimizing millions of hyperparameters by implicit differentiation. *arXiv preprint arXiv:1911.02590*, 2019. [Cited on page 32]
- Oskar Morgenstern and John Von Neumann. *Theory of Games and Economic Behavior*. Princeton University Press, 1953. [Cited on page 33]
- Heinrich Von Stackelberg. *Market Structure and Equilibrium*. Springer Science & Business Media, 2010. [Cited on page 33]
- Kenneth Joseph Arrow, Hirofumi Azawa, Leonid Hurwicz, and Hirofumi Uzawa. *Studies in Linear and Non-Linear Programming*, volume 2. Stanford University Press, 1958. [Cited on page 33]
- Yoav Freund and Robert E Schapire. Adaptive game playing using multiplicative weights. *Games and Economic Behavior*, 29(1-2):79–103, 1999. [Cited on page 33]
- Gauthier Gidel, Reyhane Askari Hemmat, Mohammad Pezeshki, Rémi Le Priol, Gabriel Huang, Simon Lacoste-Julien, and Ioannis Mitliagkas. Negative momentum for improved game dynamics. In *The 22nd International Conference on Artificial Intelligence and Statistics*, pages 1802–1811. PMLR, 2019. [Cited on pages 33, 34, 36, 37, 38, 39, 40, 41, 43, 47, 57, 80, 83, 85, 86, 88, and 92]
- James Lucas, Shengyang Sun, Richard Zemel, and Roger Grosse. Aggregated momentum: Stability through passive damping. In *International Conference on Learning Representations*, 2018. [Cited on pages 34, 35, 37, 40, and 83]
- Boris T Polyak. Some methods of speeding up the convergence of iteration methods. *USSR Computational Mathematics and Mathematical Physics*, 4(5):1–17, 1964. [Cited on pages 34, 35, 46, 79, and 83]
- Andrew Brock, Jeff Donahue, and Karen Simonyan. Large scale gan training for high fidelity natural image synthesis. In *International Conference on Learning Representations*, 2018. [Cited on pages 34, 45, and 46]
- Kazuki Osawa, Yohei Tsuji, Yuichiro Ueno, Akira Naruse, Rio Yokota, and Satoshi Matsuoka. Large-scale distributed second-order optimization using Kronecker-factored approximate curvature for deep convolutional neural networks. In *Proceedings of the IEEE/CVF Conference on Computer Vision and Pattern Recognition*, pages 12359–12367, 2019. [Cited on page 36]

- Florian Schäfer and Anima Anandkumar. Competitive gradient descent. In *Advances in Neural Information Processing Systems*, pages 7623–7633, 2019. [Cited on pages 36 and 92]
- Yuanhao Wang, Guodong Zhang, and Jimmy Ba. On solving minimax optimization locally: A follow-the-ridge approach. In *International Conference on Learning Representations*, 2019b. [Cited on pages 36 and 92]
- Reyhane Askari Hemmat, Amartya Mitra, Guillaume Lajoie, and Ioannis Mitliagkas. LEAD: Least-action dynamics for min-max optimization. *arXiv preprint arXiv:2010.13846*, 2020. [Cited on page 36]
- Florian Schäfer, Anima Anandkumar, and Houman Owhadi. Competitive mirror descent. *arXiv preprint arXiv:2006.10179*, 2020. [Cited on page 36]
- Wojciech Marian Czarnecki, Gauthier Gidel, Brendan Tracey, Karl Tuyls, Shayegan Omidshafiei, David Balduzzi, and Max Jaderberg. Real world games look like spinning tops. *arXiv preprint arXiv:2004.09468*, 2020. [Cited on pages 36 and 46]
- Guojun Zhang, Kaiwen Wu, Pascal Poupart, and Yaoliang Yu. Newton-type methods for minimax optimization. *arXiv preprint arXiv:2006.14592*, 2020a. [Cited on page 36]
- GM Korpelevich. The extragradient method for finding saddle points and other problems. *Matecon*, 12:747–756, 1976. [Cited on pages 36, 43, and 92]
- Charles R Harris, K Jarrod Millman, Stéfan J van der Walt, Ralf Gommers, Pauli Virtanen, David Cournapeau, Eric Wieser, Julian Taylor, Sebastian Berg, Nathaniel J Smith, et al. Array programming with numpy. *Nature*, 585(7825):357–362, 2020a. [Cited on page 38]
- D Bertsekas. *Nonlinear Programming*. Athena Scientific, 2008. [Cited on pages 40, 52, and 79]
- Brendan O’donoghue and Emmanuel Candes. Adaptive restart for accelerated gradient schemes. *Foundations of computational mathematics*, 15(3):715–732, 2015. [Cited on page 40]
- Lars Mescheder, Andreas Geiger, and Sebastian Nowozin. Which training methods for gans do actually converge? In *International Conference on Machine Learning (ICML)*, pages 3481–3490. PMLR, 2018. [Cited on pages 41 and 47]
- Gabriel Goh. Why momentum really works. *Distill*, 2(4):e6, 2017. [Cited on page 41]
- Waïss Azizian, Ioannis Mitliagkas, Simon Lacoste-Julien, and Gauthier Gidel. A tight and unified analysis of gradient-based methods for a whole spectrum of differentiable games. In *International Conference on Artificial Intelligence and Statistics*, pages 2863–2873. PMLR, 2020a. [Cited on pages 41 and 47]
- James Bradbury, Roy Frostig, Peter Hawkins, Matthew James Johnson, Chris Leary, Dougal Maclaurin, George Necula, Adam Paszke, Jake VanderPlas, Skye Wanderman-Milne, et al. Jax: composable transformations of python+ numpy programs, 2018. [Cited on pages 42, 51, and 60]
- Adam Paszke, Sam Gross, Soumith Chintala, Gregory Chanan, Edward Yang, Zachary DeVito, Zeming Lin, Alban Desmaison, Luca Antiga, and Adam Lerer. Automatic differentiation in PyTorch, 2017. [Cited on pages 42, 51, 60, and 74]

- Chao-Kai Chiang, Tianbao Yang, Chia-Jung Lee, Mehrdad Mahdavi, Chi-Jen Lu, Rong Jin, and Shenghuo Zhu. Online optimization with gradual variations. In *Conference on Learning Theory*, pages 6–1. JMLR Workshop and Conference Proceedings, 2012. [Cited on page 43]
- Alexander Rakhlin and Karthik Sridharan. Optimization, learning, and games with predictable sequences. In *Proceedings of the 26th International Conference on Neural Information Processing Systems*, pages 3066–3074, 2013. [Cited on pages 43 and 92]
- Constantinos Daskalakis, Andrew Ilyas, Vasilis Syrgkanis, and Haoyang Zeng. Training GANs with Optimism. In *International Conference on Learning Representations (ICLR 2018)*, 2018. [Cited on pages 43, 47, and 92]
- Yan Wu, Jeff Donahue, David Balduzzi, Karen Simonyan, and Timothy Lillicrap. Logan: Latent optimisation for generative adversarial networks. *arXiv preprint arXiv:1912.00953*, 2019. [Cited on pages 45 and 47]
- Yurii E Nesterov. A method for solving the convex programming problem with convergence rate $o(1/k^2)$. In *Dokl. Akad. Nauk SSSR*, volume 269, pages 543–547, 1983. [Cited on page 46]
- Yurii Nesterov. *Introductory lectures on convex optimization: A basic course*, volume 87. Springer Science & Business Media, 2013. [Cited on page 46]
- Chris J Maddison, Daniel Paulin, Yee Whye Teh, Brendan O’Donoghue, and Arnaud Doucet. Hamiltonian descent methods. *arXiv preprint arXiv:1809.05042*, 2018. [Cited on page 46]
- Ilya Sutskever, James Martens, George Dahl, and Geoffrey Hinton. On the importance of initialization and momentum in deep learning. In *International Conference on Machine Learning*, pages 1139–1147, 2013. [Cited on pages 46 and 83]
- Jian Zhang and Ioannis Mitliagkas. Yellowfin and the art of momentum tuning. *arXiv preprint arXiv:1706.03471*, 2017. [Cited on page 46]
- Dami Choi, Christopher J Shallue, Zachary Nado, Jaehoon Lee, Chris J Maddison, and George E Dahl. On empirical comparisons of optimizers for deep learning. *arXiv preprint arXiv:1910.05446*, 2019. [Cited on page 46]
- Michael R Zhang, James Lucas, Geoffrey Hinton, and Jimmy Ba. Lookahead optimizer: k steps forward, 1 step back. *arXiv preprint arXiv:1907.08610*, 2019b. [Cited on page 46]
- Ricky TQ Chen, Dami Choi, Lukas Balles, David Duvenaud, and Philipp Hennig. Self-tuning stochastic optimization with curvature-aware gradient filtering. *arXiv preprint arXiv:2011.04803*, 2020. [Cited on page 46]
- Alistair Letcher, David Balduzzi, Sébastien Racaniere, James Martens, Jakob N Foerster, Karl Tuyls, and Thore Graepel. Differentiable game mechanics. *Journal of Machine Learning Research*, 20(84):1–40, 2019. [Cited on pages 46, 52, and 92]
- Sai Ganesh Nagarajan, David Balduzzi, and Georgios Piliouras. From chaos to order: Symmetry and conservation laws in game dynamics. In *International Conference on Machine Learning*, pages 7186–7196. PMLR, 2020. [Cited on pages 46 and 94]

- Shayegan Omidshafiei, Karl Tuyls, Wojciech M Czarnecki, Francisco C Santos, Mark Rowland, Jerome Connor, Daniel Hennes, Paul Muller, Julien Pérolat, Bart De Vylder, et al. Navigating the landscape of multiplayer games. *Nature Communications*, 11(1):1–17, 2020. [Cited on page 46]
- Gauthier Gidel, David Balduzzi, Wojciech Marian Czarnecki, Marta Garnelo, and Yoram Bachrach. Minimax theorem for latent games or: How I learned to stop worrying about mixed-Nash and love neural nets. *arXiv preprint arXiv:2002.05820*, 2020. [Cited on page 46]
- Julien Perolat, Remi Munos, Jean-Baptiste Lespiau, Shayegan Omidshafiei, Mark Rowland, Pedro Ortega, Neil Burch, Thomas Anthony, David Balduzzi, Bart De Vylder, et al. From poincaré recurrence to convergence in imperfect information games: Finding equilibrium via regularization. *arXiv preprint arXiv:2002.08456*, 2020. [Cited on page 46]
- Guodong Zhang, Yuanhao Wang, Laurent Lessard, and Roger Grosse. Don’t fix what ain’t broke: Near-optimal local convergence of alternating gradient descent-ascent for minimax optimization. *arXiv preprint arXiv:2102.09468*, 2021a. [Cited on page 47]
- Guodong Zhang, Xuchao Bao, Laurent Lessard, and Roger Grosse. A unified analysis of first-order methods for smooth games via integral quadratic constraints. *arXiv preprint arXiv:2009.11359*, 2020b. [Cited on page 47]
- Adam Ibrahim, Waiss Azizian, Gauthier Gidel, and Ioannis Mitliagkas. Linear lower bounds and conditioning of differentiable games. In *International Conference on Machine Learning*, pages 4583–4593. PMLR, 2020. [Cited on page 47]
- James P Bailey, Gauthier Gidel, and Georgios Piliouras. Finite regret and cycles with fixed step-size via alternating gradient descent-ascent. In *Conference on Learning Theory*, pages 391–407. PMLR, 2020. [Cited on pages 47 and 51]
- Chi Jin, Praneeth Netrapalli, and Michael Jordan. What is local optimality in nonconvex-nonconcave minimax optimization? In *International Conference on Machine Learning*, pages 4880–4889. PMLR, 2020. [Cited on page 47]
- Maher Nouiehed, Maziar Sanjabi, Tianjian Huang, Jason D Lee, and Meisam Razaviyayn. Solving a class of non-convex min-max games using iterative first order methods. *Advances in Neural Information Processing Systems*, 32:14934–14942, 2019. [Cited on page 47]
- Guojun Zhang, Pascal Poupart, and Yaoliang Yu. Optimality and stability in non-convex smooth games. *arXiv e-prints*, pages arXiv–2002, 2020c. [Cited on page 47]
- Guodong Zhang. *Deep Learning Dynamics: From Minimization to Games*. PhD thesis, University of Toronto (Canada), 2023. [Cited on page 47]
- Guodong Zhang and Yuanhao Wang. On the suboptimality of negative momentum for minimax optimization. *arXiv preprint arXiv:2008.07459*, 2020. [Cited on page 47]
- Waïss Azizian, Damien Scieur, Ioannis Mitliagkas, Simon Lacoste-Julien, and Gauthier Gidel. Accelerating smooth games by manipulating spectral shapes. *arXiv preprint arXiv:2001.00602*, 2020b. [Cited on page 47]

- Carles Domingo-Enrich, Fabian Pedregosa, and Damien Scieur. Average-case acceleration for bilinear games and normal matrices. *arXiv preprint arXiv:2010.02076*, 2020. [Cited on page 47]
- Guojun Zhang and Yaoliang Yu. Convergence of gradient methods on bilinear zero-sum games. In *International Conference on Learning Representations*, 2019. [Cited on page 47]
- Nicolas Loizou, Hugo Berard, Alexia Jolicoeur-Martineau, Pascal Vincent, Simon Lacoste-Julien, and Ioannis Mitliagkas. Stochastic Hamiltonian gradient methods for smooth games. In *International Conference on Machine Learning*, pages 6370–6381. PMLR, 2020. [Cited on page 47]
- Mingrui Liu, Youssef Mroueh, Jerret Ross, Wei Zhang, Xiaodong Cui, Payel Das, and Tianbao Yang. Towards better understanding of adaptive gradient algorithms in generative adversarial nets. In *International Conference on Learning Representations*, 2020. URL <https://openreview.net/forum?id=SJxIm0VtwH>. [Cited on page 47]
- Wei Peng, Yu-Hong Dai, Hui Zhang, and Lizhi Cheng. Training GANs with centripetal acceleration. *Optimization Methods and Software*, 35(5):955–973, 2020. [Cited on page 47]
- Isabela Albuquerque, João Monteiro, Thang Doan, Breandan Considine, Tiago Falk, and Ioannis Mitliagkas. Multi-objective training of generative adversarial networks with multiple discriminators. In *International Conference on Machine Learning*, pages 202–211. PMLR, 2019. [Cited on page 47]
- Ya-Ping Hsieh, Chen Liu, and Volkan Cevher. Finding mixed Nash equilibria of generative adversarial networks. In *International Conference on Machine Learning*, pages 2810–2819. PMLR, 2019. [Cited on page 47]
- Luke Metz, Ben Poole, David Pfau, and Jascha Sohl-Dickstein. Unrolled generative adversarial networks. *arXiv preprint arXiv:1611.02163*, 2016. [Cited on pages 47 and 59]
- Chongli Qin, Yan Wu, Jost Tobias Springenberg, Andrew Brock, Jeff Donahue, Timothy P Lillicrap, and Pushmeet Kohli. Training generative adversarial networks by solving ordinary differential equations. *arXiv preprint arXiv:2010.15040*, 2020. [Cited on page 47]
- Florian Schäfer, Hongkai Zheng, and Anima Anandkumar. Implicit competitive regularization in GANs. *arXiv preprint arXiv:1910.05852*, 2019. [Cited on page 47]
- Alexia Jolicoeur-Martineau and Ioannis Mitliagkas. Connections between support vector machines, Wasserstein distance and gradient-penalty GANs. *arXiv preprint arXiv:1910.06922*, 2019. [Cited on page 47]
- Gauthier Gidel, Hugo Berard, Gaëtan Vignoud, Pascal Vincent, and Simon Lacoste-Julien. A variational inequality perspective on generative adversarial networks. In *International Conference on Learning Representations*, 2018. [Cited on pages 47 and 92]
- Tatjana Chavdarova, Gauthier Gidel, Francois Fleuret, and Simon Lacoste-Julien. Reducing noise in GAN training with variance reduced extragradient. In *Proceedings of the International Conference on Neural Information Processing Systems*, 2019. [Cited on page 47]
- Jonathan Lorraine, David Acuna, Paul Vicol, and David Duvenaud. Complex momentum for learning in games. *arXiv preprint arXiv:2102.08431*, 2021a. [Cited on page 47]

- Robert Geirhos, Patricia Rubisch, Claudio Michaelis, Matthias Bethge, Felix A Wichmann, and Wieland Brendel. Imagenet-trained cnns are biased towards texture; increasing shape bias improves accuracy and robustness. In *ICLR*, 2018. [Cited on page 49]
- Robert Geirhos, Jörn-Henrik Jacobsen, Claudio Michaelis, Richard Zemel, Wieland Brendel, Matthias Bethge, and Felix A Wichmann. Shortcut learning in deep neural networks. *Nature Machine Intelligence*, 2(11):665–673, 2020. [Cited on page 49]
- Antoine Cully, Jeff Clune, Danesh Tarapore, and Jean-Baptiste Mouret. Robots that can adapt like animals. *Nature*, 521(7553):503–507, 2015. [Cited on pages 49 and 92]
- Yang Song, Jascha Sohl-Dickstein, Diederik P Kingma, Abhishek Kumar, Stefano Ermon, and Ben Poole. Score-based generative modeling through stochastic differential equations. In *ICLR*, 2020. [Cited on page 49]
- Yoshua Bengio, Jérôme Louradour, Ronan Collobert, and Jason Weston. Curriculum learning. In *International Conference on Machine Learning*, pages 41–48. ACM, 2009. [Cited on page 49]
- Jonathan Lorraine, Paul Vicol, and David Duvenaud. Optimizing millions of hyperparameters by implicit differentiation. In *International Conference on Artificial Intelligence and Statistics (AISTATS)*, pages 1540–1552, 2020b. [Cited on page 49]
- Pierre-Luc Bacon, Florian Schäfer, Clement Gehring, Animashree Anandkumar, and Emma Brunskill. A Lagrangian method for inverse problems in reinforcement learning. *lis.csail.mit.edu/pubs*, 2019. [Cited on page 49]
- Barret Zoph and Quoc V Le. Neural architecture search with reinforcement learning. *arXiv preprint arXiv:1611.01578*, 2016. [Cited on page 49]
- Esteban Real, Alok Aggarwal, Yanping Huang, and Quoc V Le. Regularized evolution for image classifier architecture search. In *AAAI Conference on Artificial Intelligence*, volume 33, pages 4780–4789, 2019. [Cited on page 49]
- Will Grathwohl, Elliot Creager, Seyed Kamyar Seyed Ghasemipour, and Richard Zemel. Gradient-based optimization of neural network architecture, 2018. [Cited on page 49]
- Martin Arjovsky, Soumith Chintala, and Léon Bottou. Wasserstein generative adversarial networks. In *International Conference on Machine Learning (ICML)*, pages 214–223, 2017. [Cited on page 50]
- Hengyuan Hu, Adam Lerer, Alex Peysakhovich, and Jakob Foerster. “Other-Play” for zero-shot coordination. In *International Conference on Machine Learning (ICML)*, pages 4399–4410, 2020. [Cited on page 50]
- Jack Parker-Holder, Luke Metz, Cinjon Resnick, Hengyuan Hu, Adam Lerer, Alistair Letcher, Alexander Peysakhovich, Aldo Pacchiano, and Jakob Foerster. Ridge Rider: Finding diverse solutions by following eigenvectors of the Hessian. In *Advances in Neural Information Processing Systems (NeurIPS)*, pages 753–765, 2020a. [Cited on pages 50, 51, and 92]
- Anatole Katok and Boris Hasselblatt. *Introduction to the Modern Theory of Dynamical Systems*. Cambridge University Press, 1997. [Cited on pages 50, 52, 53, and 54]

- Martín Abadi, Ashish Agarwal, Paul Barham, Eugene Brevdo, Zhifeng Chen, Craig Citro, Greg S. Corrado, Andy Davis, Jeffrey Dean, Matthieu Devin, Sanjay Ghemawat, Ian Goodfellow, Andrew Harp, Geoffrey Irving, Michael Isard, Yangqing Jia, Rafal Jozefowicz, Lukasz Kaiser, Manjunath Kudlur, Josh Levenberg, Dandelion Mané, Rajat Monga, Sherry Moore, Derek Murray, Chris Olah, Mike Schuster, Jonathon Shlens, Benoit Steiner, Ilya Sutskever, Kunal Talwar, Paul Tucker, Vincent Vanhoucke, Vijay Vasudevan, Fernanda Viégas, Oriol Vinyals, Pete Warden, Martin Wattenberg, Martin Wicke, Yuan Yu, and Xiaoqiang Zheng. TensorFlow: Large-scale machine learning on heterogeneous systems, 2015. URL <https://www.tensorflow.org/>. [Cited on page 51]
- Jack K Hale and Hüseyin Koçak. *Dynamics and Bifurcations*, volume 3. Springer Science & Business Media, 2012. [Cited on page 52]
- Michael Tabor. *Chaos and Integrability in Nonlinear Dynamics: An Introduction*. Wiley-Interscience, 1989. [Cited on pages 52 and 54]
- Rodney CL Wolff. Local Lyapunov exponents: Looking closely at chaos. *Journal of the Royal Statistical Society*, 1992. [Cited on page 53]
- Vittorio Loreto, Giovanni Paladin, Michele Pasquini, and Angelo Vulpiani. Characterization of chaos in random maps. *Physica A: Statistical Mechanics and its Applications*, 232(1-2):189–200, 1996. [Cited on page 54]
- Tal Kachman, Shmuel Fishman, and Avy Soffer. Numerical implementation of the multiscale and averaging methods for quasi periodic systems. *Computer Physics Communications*, 221:235–245, 2017. [Cited on page 54]
- Yakov Borisovich Pesin. Characteristic Lyapunov exponents and smooth ergodic theory. *Uspekhi Matematicheskikh Nauk*, 1977. [Cited on pages 54 and 58]
- Zhewei Yao, Amir Gholami, Kurt Keutzer, and Michael W Mahoney. PyHessian: Neural networks through the lens of the Hessian. In *IEEE International Conference on Big Data (Big Data)*, pages 581–590, 2020. [Cited on pages 55 and 58]
- William Poundstone. *Prisoner’s Dilemma/John Von Neumann, Game Theory and the Puzzle of the Bomb*. Anchor Press, 1993. [Cited on page 58]
- Steven H Strogatz. *Nonlinear Dynamics and Chaos with Student Solutions Manual: With Applications to Physics, Biology, Chemistry, and Engineering*. CRC Press, 2018. [Cited on page 60]
- Guido Van Rossum and Fred L Drake Jr. *Python reference manual*. Centrum voor Wiskunde en Informatica Amsterdam, 1995. [Cited on page 64]
- Travis E Oliphant. Python for scientific computing. *Computing in Science & Engineering*, 9(3): 10–20, 2007. [Cited on page 64]
- Travis E Oliphant. *A guide to NumPy*, volume 1. Trelgol Publishing USA, 2006. [Cited on page 64]
- Stefan Van Der Walt, S Chris Colbert, and Gael Varoquaux. The NumPy array: A structure for efficient numerical computation. *Computing in Science & Engineering*, 13(2):22–30, 2011. [Cited on page 64]

- Charles R Harris, K Jarrod Millman, Stéfan J van der Walt, Ralf Gommers, Pauli Virtanen, David Cournapeau, Eric Wieser, Julian Taylor, Sebastian Berg, Nathaniel J Smith, et al. Array programming with NumPy. *Nature*, 585(7825):357–362, 2020b. [Cited on page 64]
- John D Hunter. Matplotlib: A 2D graphics environment. *Computing in Science & Engineering*, 9(3): 90–95, 2007. [Cited on page 64]
- Eric Jones, Travis Oliphant, Pearu Peterson, et al. SciPy: Open source scientific tools for Python, 2001. [Cited on page 64]
- Jonathan Lorraine. *Scalable Nested Optimization for Deep Learning*. PhD thesis, University of Toronto (Canada), 2024. [Cited on page 69]
- Jonas Mockus. The application of bayesian methods for seeking the extremum. *Towards global optimization*, 2:117, 1998. [Cited on page 70]
- Bobak Shahriari, Kevin Swersky, Ziyu Wang, Ryan P Adams, and Nando De Freitas. Taking the human out of the loop: A review of bayesian optimization. *Proceedings of the IEEE*, 104(1): 148–175, 2015. [Cited on page 70]
- David Ginsbourger, Rodolphe Le Riche, and Laurent Carraro. Kriging is well-suited to parallelize optimization. In *Computational intelligence in expensive optimization problems*, pages 131–162. Springer, 2010. [Cited on page 70]
- Remi Lam, Karen Willcox, and David H Wolpert. Bayesian optimization with a finite budget: An approximate dynamic programming approach. *Advances in Neural Information Processing Systems*, 29, 2016. [Cited on page 70]
- Kevin Swersky, Jasper Snoek, and Ryan P Adams. Multi-task bayesian optimization. *Advances in neural information processing systems*, 26, 2013. [Cited on page 70]
- Daniel Golovin, Benjamin Solnik, Subhdeep Moitra, Greg Kochanski, John Karro, and David Sculley. Google vizio: A service for black-box optimization. In *Proceedings of the 23rd ACM SIGKDD international conference on knowledge discovery and data mining*, pages 1487–1495, 2017. [Cited on page 70]
- Aaron Klein, Stefan Falkner, Simon Bartels, Philipp Hennig, and Frank Hutter. Fast bayesian optimization of machine learning hyperparameters on large datasets. In *Artificial intelligence and statistics*, pages 528–536. PMLR, 2017. [Cited on page 70]
- Lisha Li, Kevin Jamieson, Giulia DeSalvo, Afshin Rostamizadeh, and Ameet Talwalkar. Hyperband: A novel bandit-based approach to hyperparameter optimization. *The journal of machine learning research*, 18(1):6765–6816, 2017. [Cited on page 70]
- Samuel Daulton, David Eriksson, Maximilian Balandat, and Eytan Bakshy. Multi-objective bayesian optimization over high-dimensional search spaces. In *Uncertainty in Artificial Intelligence*, pages 507–517. PMLR, 2022. [Cited on page 70]
- Geoffrey Hinton, Nitish Srivastava, and Kevin Swersky. Neural networks for machine learning. Lecture 6a. Overview of mini-batch gradient descent, 2012. [Cited on page 74]

- Stephen Merity, Nitish Shirish Keskar, and Richard Socher. Regularizing and optimizing LSTM language models. *International Conference on Learning Representations*, 2018. [Cited on page 75]
- Tim Salimans, Ian Goodfellow, Wojciech Zaremba, Vicki Cheung, Alec Radford, and Xi Chen. Improved techniques for training GANs. In *Advances in Neural Information Processing Systems*, pages 2234–2242, 2016. [Cited on page 91]
- Simon Foucart. Matrix norm and spectral radius. <https://www.math.drexel.edu/~foucart/TeachingFiles/F12/M504Lect6.pdf>, 2012. Accessed: 2020-05-21. [Cited on page 79]
- Stephen Boyd, Stephen P Boyd, and Lieven Vandenberghe. *Convex Optimization*. Cambridge university press, 2004. [Cited on page 82]
- Richard HR Hahnloser, Rahul Sarpeshkar, Misha A Mahowald, Rodney J Douglas, and H Sebastian Seung. Digital selection and analogue amplification coexist in a cortex-inspired silicon circuit. *Nature*, 405(6789):947–951, 2000. [Cited on page 85]
- Jonathan Lorraine, Paul Vicol, Jack Parker-Holder, Tal Kachman, Luke Metz, and Jakob Foerster. Lyapunov exponents for diversity in differentiable games. In *Proceedings of the 21st International Conference on Autonomous Agents and Multiagent Systems*, pages 842–852, 2022b. [Cited on pages 92 and 94]
- Jonathan Lorraine, Jack Parker-Holder, Paul Vicol, Aldo Pacchiano, Luke Metz, Tal Kachman, and Jakob Foerster. Using bifurcations for diversity in differentiable games. In *ICML 2021 Beyond First Order Methods Workshop*, 2021b. [Cited on page 92]
- Jonathan Lorraine, Paul Vicol, Jack Parker-Holder, Tal Kachman, Luke Metz, and Jakob Foerster. Lyapunov exponents for diversity in differentiable games. *arXiv preprint arXiv:2112.14570*, 2021c. [Cited on page 92]
- Lars Kai Hansen and Peter Salamon. Neural network ensembles. *IEEE Transactions on Pattern Analysis and Machine Intelligence*, 1990. [Cited on page 92]
- Yong Liu and Xin Yao. Ensemble learning via negative correlation. *Neural Networks*, 12(10):1399 – 1404, 1999. [Cited on page 92]
- Samarth Sinha, Homanga Bharadhwaj, Anirudh Goyal, Hugo Larochelle, Animesh Garg, and Florian Shkurti. Diversity inducing information bottleneck in model ensembles. *AAAI*, 2021. [Cited on page 92]
- Andrew Slavin Ross, Weiwei Pan, Leo A. Celi, and Finale Doshi-Velez. Ensembles of locally independent prediction models. In *The Thirty-Fourth AAAI Conference on Artificial Intelligence, AAAI*, 2020. [Cited on page 92]
- Zelda Mariet and Suvrit Sra. Diversity networks: Neural network compression using determinantal point processes. In *International Conference on Learning Representations (ICLR)*, May 2016. [Cited on page 92]
- Tianyu Pang, Kun Xu, Chao Du, Ning Chen, and Jun Zhu. Improving adversarial robustness via promoting ensemble diversity. In *International Conference on Machine Learning (ICML)*, 2019. [Cited on page 92]

- Joel Lehman and Kenneth O. Stanley. Exploiting open-endedness to solve problems through the search for novelty. In *Proceedings of the Eleventh International Conference on Artificial Life (Alife XI)*. MIT Press, 2008. [Cited on page 92]
- Benjamin Eysenbach, Abhishek Gupta, Julian Ibarz, and Sergey Levine. Diversity is all you need: Learning skills without a reward function. In *International Conference on Learning Representations (ICLR)*, 2019. [Cited on page 92]
- Jack Parker-Holder, Aldo Pacchiano, Krzysztof M Choromanski, and Stephen J Roberts. Effective diversity in population based reinforcement learning. *Advances in Neural Information Processing Systems*, 33:18050–18062, 2020b. [Cited on page 92]
- Justin K. Pugh, Lisa B. Soros, and Kenneth O. Stanley. Quality diversity: A new frontier for evolutionary computation. *Frontiers in Robotics and AI*, 3:40, 2016. [Cited on page 92]
- Guodong Zhang, Xuchan Bao, Laurent Lessard, and Roger Grosse. A unified analysis of first-order methods for smooth games via integral quadratic constraints. *Journal of Machine Learning Research*, 22(103):1–39, 2021b. [Cited on page 92]
- Guodong Zhang, Yuanhao Wang, Laurent Lessard, and Roger B Grosse. Near-optimal local convergence of alternating gradient descent-ascent for minimax optimization. In *International Conference on Artificial Intelligence and Statistics*, pages 7659–7679. PMLR, 2022. [Cited on page 92]
- Waïss Azizian, Ioannis Mitliagkas, Simon Lacoste-Julien, and Gauthier Gidel. A tight and unified analysis of gradient-based methods for a whole spectrum of differentiable games. In *International Conference on Artificial Intelligence and Statistics (AISTATS)*, 2020c. [Cited on page 92]
- Guodong Zhang and Yuanhao Wang. On the suboptimality of negative momentum for minimax optimization. In *International Conference on Artificial Intelligence and Statistics*, pages 2098–2106. PMLR, 2021. [Cited on page 92]
- Jonathan P Lorraine, David Acuna, Paul Vicol, and David Duvenaud. Complex momentum for optimization in games. In *International Conference on Artificial Intelligence and Statistics*, pages 7742–7765. PMLR, 2022c. [Cited on page 92]
- Eric V Mazumdar, Michael I Jordan, and S Shankar Sastry. On finding local Nash equilibria (and only local Nash equilibria) in zero-sum games. *arXiv preprint arXiv:1901.00838*, 2019. [Cited on page 92]
- Marta Garnelo, Wojciech Marian Czarnecki, Siqi Liu, Dhruva Tirumala, Junhyuk Oh, Gauthier Gidel, Hado van Hasselt, and David Balduzzi. Pick your battles: Interaction graphs as population-level objectives for strategic diversity. In *Proceedings of the 20th International Conference on Autonomous Agents and MultiAgent Systems (AAMA)*, pages 1501–1503, 2021. [Cited on page 92]
- Oriol Vinyals, Igor Babuschkin, Wojciech M Czarnecki, Michaël Mathieu, Andrew Dudzik, Junyoung Chung, David H Choi, Richard Powell, Timo Ewalds, Petko Georgiev, et al. Grandmaster level in StarCraft II using multi-agent reinforcement learning. *Nature*, 575, 2019. [Cited on pages 92 and 94]

- Yaodong Yang, Ying Wen, Jun Wang, Liheng Chen, Kun Shao, David Mguni, and Weinan Zhang. Multi-agent determinantal q-learning. In *International Conference on Machine Learning (ICML)*, 2020. [Cited on page 92]
- Andrei Lupu, Hengyuan Hu, and Jakob Foerster. Trajectory diversity for zero-shot coordination. In *Proceedings of the 20th International Conference on Autonomous Agents and MultiAgent Systems*, 2021. [Cited on page 92]
- Peter Hart, Nils Nilsson, and Bertram Raphael. A formal basis for the heuristic determination of minimum cost paths. *IEEE Transactions on Systems Science and Cybernetics*, 4(2):100–107, 1968. [Cited on page 94]
- Bruce Abramson. *The Expected-Outcome Model of Two-Player Games*. Morgan Kaufmann, 2014. [Cited on page 94]
- David Silver, Aja Huang, Chris J Maddison, Arthur Guez, Laurent Sifre, George Van Den Driessche, Julian Schrittwieser, Ioannis Antonoglou, Veda Panneershelvam, Marc Lanctot, et al. Mastering the game of Go with deep neural networks and tree search. *Nature*, 2016. [Cited on page 94]
- Thomas M Moerland, Joost Broekens, Aske Plaat, and Catholijn M Jonker. A0c: Alpha zero in continuous action space. *arXiv preprint arXiv:1805.09613*, 2018. [Cited on page 94]
- Beomjoon Kim, Kyungjae Lee, Sungbin Lim, Leslie Kaelbling, and Tomás Lozano-Pérez. Monte Carlo tree search in continuous spaces using Voronoi optimistic optimization with regret bounds. In *Proceedings of the AAAI Conference on Artificial Intelligence*, 2020. [Cited on page 94]
- Weichao Mao, Kaiqing Zhang, Qiaomin Xie, and Tamer Basar. Poly-hoot: Monte-carlo planning in continuous space mdps with non-asymptotic analysis. *Advances in Neural Information Processing Systems*, 33, 2020. [Cited on page 94]
- Steven M LaValle et al. Rapidly-exploring random trees: A new tool for path planning. *Technical Report, Iowa State University, USA*, 1998. [Cited on page 94]
- Steven M LaValle and James J Kuffner Jr. Randomized kinodynamic planning. *The International Journal of Robotics Research*, 2001. [Cited on page 94]
- Samuel Rodriguez, Xinyu Tang, Jyh-Ming Lien, and Nancy M Amato. An obstacle-based rapidly-exploring random tree. In *IEEE International Conference on Robotics and Automation (ICRA)*, 2006. [Cited on page 94]
- Gulshan Singh and Kalyanmoy Deb. Comparison of multi-modal optimization algorithms based on evolutionary algorithms. In *Proceedings of the 8th Annual Conference on Genetic and Evolutionary Computation*, pages 1305–1312, 2006. [Cited on page 94]
- Ka-Chun Wong. Evolutionary multimodal optimization: A short survey, 2015. [Cited on page 94]
- Kai Arulkumaran, Antoine Cully, and Julian Togelius. Alphastar: An evolutionary computation perspective. In *Proceedings of the Genetic and Evolutionary Computation Conference Companion*, 2019. [Cited on page 94]

- E Christopher Zeeman. Population dynamics from game theory. In *Global Theory of Dynamical Systems*, pages 471–497. Springer, 1980. [Cited on page 94]
- Ger Yang, David Basanta, and Georgios Piliouras. Bifurcation mechanism design—from optimal flat taxes to better cancer treatments. *Games*, 9(2):21, 2018. [Cited on page 94]
- Thiparat Chotibut, Fryderyk Falniowski, Michał Misiurewicz, and Georgios Piliouras. The route to chaos in routing games: When is price of anarchy too optimistic? *Advances in Neural Information Processing Systems (NeurIPS)*, 2020. [Cited on page 94]
- Georgios Piliouras. Catastrophe by design in population games: Destabilizing wasteful locked-in technologies. In *Web and Internet Economics: 16th International Conference (WINE)*, page 473, 2020. [Cited on page 94]
- Stefanos Leonardos and Georgios Piliouras. Exploration-exploitation in multi-agent learning: Catastrophe theory meets game theory. *arXiv preprint arXiv:2012.03083*, 2020. [Cited on page 94]
- Jakub Bielawski, Thiparat Chotibut, Fryderyk Falniowski, Grzegorz Kosiorowski, Michał Misiurewicz, and Georgios Piliouras. Follow-the-regularized-leader routes to chaos in routing games. *arXiv preprint arXiv:2102.07974*, 2021. [Cited on page 94]
- Yun Kuen Cheung and Georgios Piliouras. Vortices instead of equilibria in minmax optimization: Chaos and butterfly effects of online learning in zero-sum games. In *Conference on Learning Theory*, 2019. [Cited on page 94]
- Yun Kuen Cheung and Yixin Tao. Chaos of learning beyond zero-sum and coordination via game decompositions. In *International Conference on Learning Representations (ICLR)*, 2020. [Cited on page 94]
- Yuzuru Sato, Eizo Akiyama, and J Doyne Farmer. Chaos in learning a simple two-person game. *Proceedings of the National Academy of Sciences*, 99(7):4748–4751, 2002. [Cited on page 94]
- Ioannis Panageas and Georgios Piliouras. Average case performance of replicator dynamics in potential games via computing regions of attraction. In *Proceedings of the 2016 ACM Conference on Economics and Computation*, pages 703–720, 2016. [Cited on page 94]
- Boyu Zhang and Josef Hofbauer. Equilibrium selection via replicator dynamics in 2x2 coordination games. *International Journal of Game Theory*, 44(2):433–448, 2015. [Cited on page 94]